MRC | Mammalian Genetics Unit

Characterisation of *pitch*: an early onset model of sensorineural deafness

A thesis presented for the degree of Doctor of Philosophy (D.Phil)

Wolfson College, Oxford

Leanne Jane Carrott

Mammalian Genetics Unit, MRC Harwell

Department of Biochemistry, University of Oxford

Supervisors: Dr Michael Bowl (MGU, MRC Harwell)

Professor Steve Brown (MGU, MRC Harwell)

Professor Jonathan Hodgkin (Biochemistry, Oxford)

Trinity term 2014

Word count: 39,890

Characterisation of *pitch*: an early onset model of sensorineural deafness

Leanne Carrott

Wolfson College, Oxford
Mammalian Genetics Unit, MRC Harwell
Department of Biochemistry, University of Oxford

A thesis presented for D.Phil, Trinity term, 2014.

Abstract

At MRC Harwell n-ethyl-n-nitrosourea (ENU) mutagenesis coupled with auditory phenotyping is utilised to generate new mouse models of hearing loss. This approach identified *pitch*, an autosomal recessive model of early-onset, sensorineural deafness (+90dB). Mapping studies identified a 1.6Mb critical region comprising a novel deafness locus on chromosome 9 and prioritised candidate gene sequencing identified a coding mutation in *Neuroplastin* (*Nptn*).

This thesis details experiments to investigate the role of Neuroplastin in the auditory pathway. Complementation studies using a second nonsense allele ($Nptn^{Y219X}$) confirmed *Neuroplastin* as the causative gene in *pitch*. Modelling of $Nptn^{pitch}$ *in silico* suggested that the *pitch* mutation is likely harmful to protein function and *in vitro* studies using Nptn-tagged constructs revealed that the *pitch* mutation affected protein processing, and was thus likely a loss-of-function mutation. Expression studies identified that the 65kDa Nptn isoform, Np65, is expressed in the inner hair cells (IHCs) and outer hair cells (OHCs) of the cochlea in wild type mice. However, Np65 is absent in the cochleae of $Nptn^{pitch/pitch}$ animals. Inner ear morphology appears grossly normal in $Nptn^{pitch/pitch}$ mice at postnatal day (P)16, even though a severe auditory deficit is already present at this age. Electrophysiological studies suggest that whilst the IHCs of $Nptn^{pitch/pitch}$ mice begin to mature normally, their maturation arrests shortly after the onset of hearing. Immunolabelling of the auditory ribbon synapse identified an increased number of mismatched pre-synaptic ribbons (RIBEYE) and post-synaptic densities (GluR2) in $Nptn^{pitch/pitch}$ compared to wild type controls.

In conclusion, my studies demonstrate that Np65 regulates the physiological and morphological differentiation of cochlear inner hair cells at the onset of hearing and as such coordinates one of the most distinctive functional refinements of the mammalian auditory system. These data also confirm that *Nptn* is a new deafness-related gene.

Acknowledgements

First and foremost I would like to extend my gratitude to my supervisors Dr Michael Bowl and Professor Steve Brown for their continued support, wisdom and guidance throughout the last three and a half years. I would also like to thank all of the members of the Deafness laboratory, both past and present, at MRC Harwell for making the past 4 years a thoroughly enjoyable experience. Particular thanks go to Andy Parker, Sue Morse, Carlos Aguilar and Jo Dorning, all of whom helped to shape the *pitch* project into the story in this thesis. I'm also extremely grateful to Philomena Mburu, Jeremy Sanderson and Andy Parker who took the time to proof-read the first drafts of my chapters.

At MRC Harwell we are very lucky to have access to have an abundance of core service groups who facilitate our work. I would like to thank the staff in Ward 4 and Ward 6 of the Mary Lyon Centre who have maintained my colonies and facilitated my experiments. Particularly, I'd like to thank Sara Wells, Lucie Visor and Michelle Stewart, without whom I could not have completed this project. I would also like to thank the Histology and Necropsy core services, and Jeremy Sanderson, the manager of the Bio-imaging facility.

I would like to thank Dr Dan Jagger, Dr Jakob Neef and Dr Tobias Moser for welcoming me into their respective laboratories and expanding my technical capabilities. I would also love to thank Dr Walter Marcotti, Dr Stuart Johnson and Dr Alun Barnard for their experimental contributions to the *pitch* project, and Walter for his continued input and support.

Outside of the lab I have a large network of family and friends who have supported me. I'd like to thank my parents, Ian and Tracy Carrott, and my Nan, Audrey Hogan, for their unconditional support. I'd like to thank my sister Rachael for showing me what's really important in life and having excellent taste in music. In my extended family, I'd also like to thank Mike and Beth Sayce who've supported my studies from afar. I'd like to thank my childhood friends Chris Bleach, Keri Hore and Kim Walker for never allowing the physical distance between us to dampen our friendships. Rowing has been a massive part of my life in Oxford and I would like to thank everyone at WCBC and OUWLRC who's made the last couple of years the best in my life, particularly Chris O'Hara, Nicky Huskens, Becky Lane, Jo Green and Jim Kirkbride. I would like to thank my brilliant friends from MedSci at Oxford: Hayley Lees, Raffaella Facchini, Emma Dixon, Johnny Beale and Jimmy Allen. Finally, I would like to thank my incredible partner Drew Sayce for his love, understanding and superb washing up skills. One day we'll get a dishwasher.

I would like to thank the Medical Research Council for funding this research.

Table of Contents

List of Figures

List of Tables

List of Abbreviations

3D	Three-dimensional
AA	Amino acid
AB	Avidin-Biotin solution
ABR	Auditory-evoked brainstem response
AC	Air conductance
AHL	Age-related hearing loss
AMPA	α-Amino-3-hydroxy-5-methyl-4-isoxazolepropionic acid
BC	Bone conductance
BEEM	Better electron microscopy
BMI	Body mass index
BX	Backcross
CAM	Cell adhesion molecule
cDNA	Complimentary DNA
COME	Chronic otitis media with effusion
CPD	Critical point dried
CPHI	Communicative Profile for the Hearing Impaired
CSF	Cerebrospinal fluid
DAB	3-3'diaminobenzidine
DAPI	4',6-diamidino-2-phenylindole
dd	Double deionised
DMEM	Dulbecco's modified eagle medium
DNA	Deoxyribonucleic acid
dsDNA	Double stranded DNA
E	Embryonic day
ECL	Enhanced chemiluminescence
EDTA	Ethylenediaminetetraacetic acid

ENU	n-ethyl-n-nitrosourea
EP	Endocochlear potential
ER	Endoplasmic reticulum
ERAD	ER associated degradation
ERG	Electroretinography
ES cells	Embryonic stem cell
FCS	Foetal calf serum
FESA	Frozen embryo and sperm archive
FGFR	Fibroblast growth factor receptor
G	Generation
GABA	γ-Aminobutyric acid
GWA	Genome-wide association
H&E	Haematoxylin and Eosin
HHIE	Hearing Handicap Inventory for the Elderly
HRP	Horse radish peroxidase
Ig	Immunoglobulin
IHC	Inner hair cell
IMPC	International Mouse Phenotyping Consortium
INL	Inner nuclear layer
IP	Intraperitoneal
IPL	Inner plexiform layer
IQ	Intelligence quotient
KO	Knock out
LB	Luria-Bertani
LTD	Long term depression
LTP	Long term potentiation
MCT	Monocarboxylate transporter

MET	Mechano-electrical transduction
METH	Methamphetamine
mGluR	Metabotropic glutamate receptor
MIP	Maximum intensity projection
MLC	The Mary Lyon Centre, MRC Harwell
mRNA	Messenger RNA
nCAM	Neural cell adhesion molecule
NEB	New England Biosystems
NHS	National Health Service
OHC	Outer hair cell
OM	Otitis media
ONL	Outer nuclear layer
OPL	Outer plexiform layer
P	Postnatal day
PBS	Phosphate-buffered saline
PBS-T	0.1% PBS-Tween
PCP	Phencyclidine
PCR	Polymerase chain reaction
PDI	Protein disulphide-isomerase
PEI	Polyethylenimine
Pen/Strep	Penicillin/Streptavidin solution
PFA	Paraformaldehyde
PMTs	Photomultiplier tubes
PSD	Post-synaptic density
qPCR	Quantitative PCR
qRT-PCR	Quantitative reverse transcription PCR
RAOM	Recurrent acute otitis media

RER	Rough endoplasmic reticulum
RIN	RNA Integrity Number
RNA	Ribonucleic acid
RP	Retinitis pigmentosa
RQ	Relative quantity
RRP	Readily releasable pool
rs	Reference SNP
SAGE	Serial analysis of gene expression
SDM	Site directed mutagenesis
SEM	Scanning electron microscopy
SF	Super family
SGNs	Spiral ganglion neurons
SNP	Single nucleotide polymorphism
SOC	Super optimal broth with catabolite repression
SRP	Secondarily releasable pool
ssDNA	Single strand DNA
SSRI	Selective serotonin reuptake inhibitor
TAA	Tumour associated antigen
TAE	Tris-acetate EDTA
TBS-T	Tris-buffered saline-Tween
TDT	Tucker Davies Technology
TE	Tris-EDTA
TEM	Transmission electron microscopy
UPR	Unfolded protein response
UV	Ultraviolet light
VEGF	Vascular epithelial growth factor
WT	Wild type

Chapter 1. Introduction

Hearing loss has multiple known causes, both genetic and environmental, and depending on the causative mechanism the timeline for onset of symptoms varies from birth to old age. From a clinical perspective hearing loss is defined as the inability to partially or completely perceive sound and the clinical terminology "hearing loss" is often used interchangeably with terms such as deafness, hearing impaired, auditory impaired and hard of hearing.

Approximately 1 in 1600 children in the UK are born with moderate to profound hearing loss as a consequence of a genetic mutation (Action-on-Hearing-Loss, 2011). As of June 2014, 143 loci have been associated with non-syndromic deafness in the human genome. However, only 89 causative genes have currently been identified (Van Camp and Smith, 2014). Through studying mutations that cause deafness it has been possible to start piecing together the molecular basis of hearing. However, with causative genes not yet identified for nearly half of the known deafness loci there is still a lot to learn about the genetics of hearing and hearing loss.

Through expanding our knowledge of the auditory pathway it is hoped that more effective and convenient therapeutics can be developed, improving the lives of those who live with hearing impairment. At the present time hearing loss is a significant economic burden across the globe. Otitis media (OM), also known as 'glue ear', is the leading cause of physician visits in childhood (Grevers, 2010) and treatment including surgery to insert tympanostomy tubes is estimated to cost in excess of $5 billion in the United States each year (Schraff, 2008). Recurrent or chronic OM often leads to increased parental absenteeism and loss of earnings, however these costs are hard to quantify (Grevers, 2010). Referral for cochlea implant insertion is becoming much more common for early-onset and congenitally deaf patients; however this technology is expensive, costing in the region of $40,000 per implant and inaccessible to those in lower economically developed nations or those without health insurance in countries lacking nationalised health care systems (ASHA, 2014).In the

UK, the National Health Service (NHS) spends an estimated £29.2 million per annum providing the newborn hearing screening programme, and the biennial replacement of hearing aids for paediatric patients is estimated to cost the NHS around £4 million pounds per year (Ladapo et al., 2008). In 2007 the NHS was spending an estimated £120 million per year on services to modernise hearing aids for people with AHL and this amount is likely to increase in the future with an aging population (Davis et al., 2007).

Hearing loss is not only a financial burden, but also a personal and social burden. In addition to auditory symptoms, people with hearing impairment have a high incidence of self-reported depression and anxiety. Hearing loss can often lead to reduced social interaction and participation limitation due to communication difficulties (Chisolm et al., 2004). For the congenitally deaf this problem is often exacerbated by the prevalence of "home-signing" or non-standard sign languages developed within families to communicate. This often means without audiological assistance they are unable to communicate outside of their home environments, even with other auditory impaired individuals. It has been reported that those suffering from presbycusis often delay getting assistance for around 10 years after the onset of hearing impairment (Davis et al., 2007), with reasons such as embarrassment, denial of hearing loss or inconvenience often cited (ASHA, 2014). This delay is thought to make adapting to the technology harder than if installed in the early stages of hearing loss and extends periods of social inactivity and reduced participation. Measurement of psychosocial parameters, using tests such as the Hearing Handicap Inventory for the Elderly (HHIE) and the Communicative Profile for the Hearing Impaired (CPHI), have successfully shown that treatment with hearing aids improves social interaction, levels of perceived disability and depressive feelings a short period of time after installation (Newman and Weinstein, 1988, Humes et al., 2001). This improvement isn't just reported by those suffering from hearing loss, but also those they live with and share close relationships with.

In order to improve treatment of hearing loss and lessen the socio-economic burden associated with auditory impairment, it is essential to identify the molecular mechanisms underpinning the auditory pathway. Identification of loci or genes related to hearing in humans traditionally relied on identifying genes in a mouse model and confirming this gene as containing a causative variant in consanguineous families reporting familial deafness, for examples see (Ali Mosrati et al., 2013, Veske et al., 1996, Guilford et al., 1994). Recent innovations are paving the way for easier identification of genes associated with disease. In particular the development of affordable high-throughput assays which utilise hundreds of thousands of single nucleotide polymorphism (SNPs) variants across the genome, have made it relatively inexpensive, quicker and easier to map disease loci, such as loci linked to hearing loss.

Linkage analysis is commonly employed to identify hearing loss genes or loci in family studies. Linkage analysis utilises the principles of recombination to determine the location of disease causing genes relative to known genetic markers. Chromosomes are inherited in pairs, one maternal and one paternal. Whilst the genes are in the same location on each parental chromosome, the DNA sequences differ between individuals, allowing for determination of the parental origin of particular sequences of DNA (Twyman, 2003). During meiosis chromosomes exchange regions, in a process known as recombination. Recombination is more likely to occur between DNA sequences which are further from each other on the chromosome, leading to the presence of both maternal and paternal alleles between these DNA sequences (Alberts, 2008). In contrast DNA sequences that are very close to each other will rarely experience recombination (Twyman, 2003). In order to identify disease causing genes, recombination is measured across the genome against a panel of genetic markers. Markers which are in close proximity to the gene of interest have a very low incidence of recombination and are determined to be genetically linked (Ferreira, 2004). The regions around linked markers are selected for further investigation, allowing for identification of the disease causing gene. Linkage analysis has been successfully employed in family studies, however for

identification of disease genes of weaker effect, linkage disequilibrium association mapping, known as association studies, are thought to be a more powerful tool (Ott et al., 2011). Linkage disequilibrium is the non-random correlation of genetic markers or alleles from single ancestral chromosomes, where association of alleles is seen more or less frequently than would be expected in a population (Reich et al., 2001). Association studies utilise SNP panel arrays to genotype across hundreds and thousands of SNPs in large populations (both control and disease) and genotypes are inferred between neighbouring loci with strong linkage disequilibrium (Manolio, 2010). If a variant is found to be more frequent in the population with the disease, this variant is found to be associated with the disease (Hirschhorn et al., 2002).

Genome wide association (GWA) studies are becoming more popular in the auditory field as a discovery tool, identifying candidate genes and novel susceptibility locus for hearing impairment (Rye et al., 2012, Allen et al., 2013). In mice, many GWA studies to identify auditory genes have found associations with reported or novel deafness genes/loci, however these studies commonly fail to meet genome wide significance (Johnson et al., 2008, Zheng et al., 2009). Ohmen et al. (2014) undertook a recent meta-analysis which suggests that even with large numbers of mice these studies are often underpowered for whole genome analysis. However, by combining 5 cohorts from previous GWA studies and using a random effects model to correct for population size and backgrounds, they were able to identify 4 novel AHL loci that were not detectable in the individual study pools. In human populations Girotto et al. (2011) reported a GWA study in which they identified hundreds of SNPs with suggestive p values, however none of these associations reached genome wide significance. Further data published by Girotto et al. (2014), using an additional cohort of 493 subjects collected from the Silk Road, was used to replicate associations in a shortlist of 19 candidate genes taken from their 2011 study. Twelve of these genes were subsequently shown to be expressed in the (mouse) ear and 9 genes showed nominally significant association in the new cohort. Genotype to audiometric phenotype analysis (using three genotypes of the most strongly

associated variants in each gene) confirmed that 7 of these genes showed audiometric differences between genotypes, thereby proving their role in the auditory system. Whilst GWA studies are a useful tool for identifying new candidates for disease, their failure to meet genome wide significance means they rely heavily on mouse models to validate their findings.

While there are many benefits to treating hearing loss; social, economic and emotional, the limitations of our current knowledge of the auditory system prevent the development of more targeted, non-surgical therapeutics. The focus of my thesis studies are to characterise a genetic model of early-onset deafness known as *pitch*. By understanding the mechanism through which deafness is caused in *pitch,* I hope to further elucidate the genetic pathways and mechanisms associated with normal hearing.

1.1. Structure of the mammalian ear

The mammalian ear is divided into three compartments: the outer, middle and inner ear (see Figure 1). Sound waves enter the outer ear at the pinna/auricle (the fleshy external part of the ear), travel down the external auditory canal and contact the lateral tympanic membrane causing small vibrations. The middle ear is an air filled chamber containing the medial tympanic membrane and the ossicular bones, which transmit the tympanic membrane vibrations to the inner ear. The inner ear is a fluid filled structure combining the cochlea and vestibular apparatus, which are responsible for transduction of sound and balance respectively. Each part of the ear plays a distinct and essential role in the eventual perception of sound.

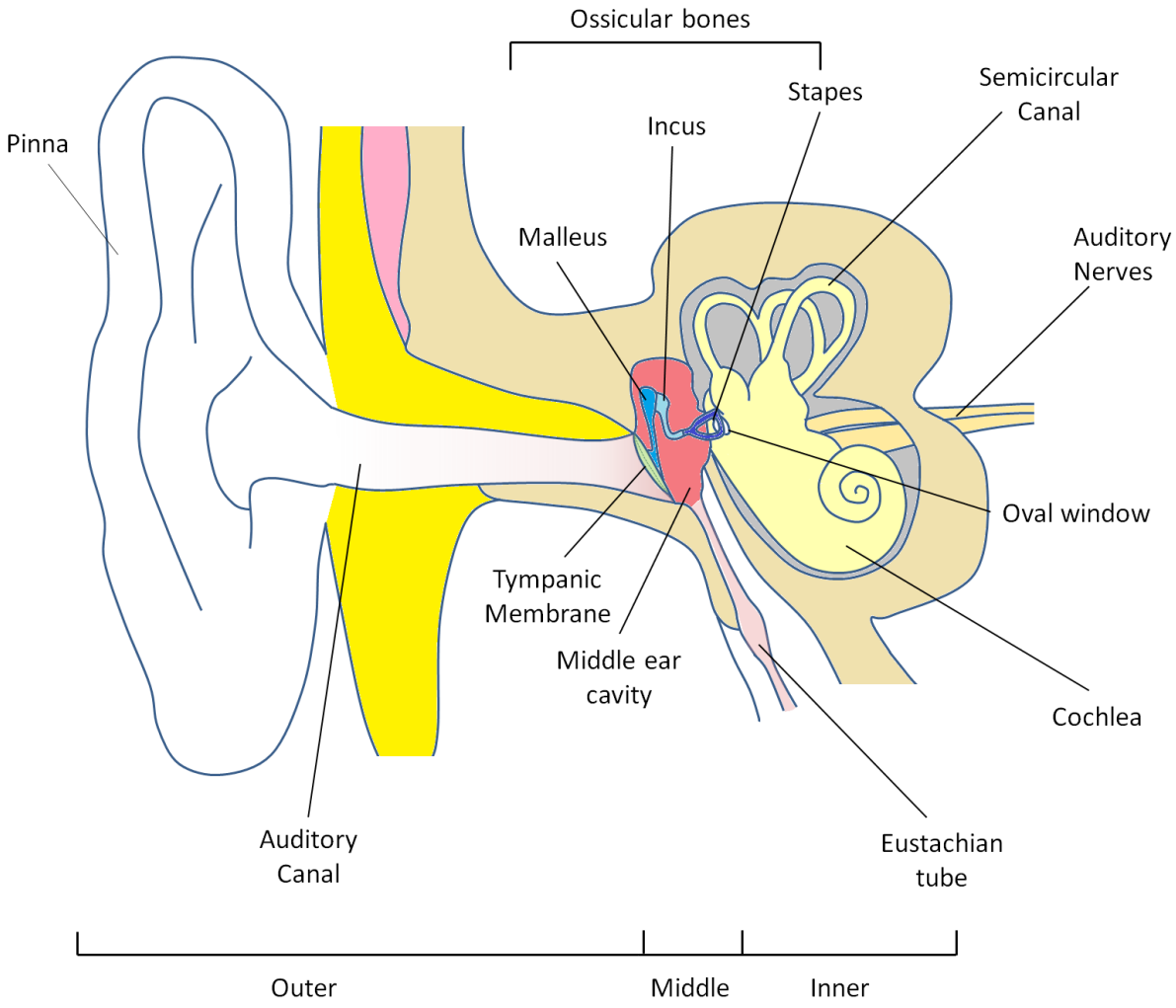

Figure 1. Overview of the outer, middle and inner ear.

The outer ear is composed of the pinna (auricle), the auditory canal and the lateral wall of the tympanic membrane, which spans the diameter of the auditory canal and separates the outer ear from the middle ear cavity. The middle ear cavity contains the ossicular bones (the Malleus, Incus and Stapes) and is connected to the nasopharynx via the Eustachian tube. The footplate of the stapes bone rests on the oval window of the inner ear. The inner ear comprises the vestibular apparatus (semi-circular canals, saccule and utricle) which are responsible for balance and the cochlea, which is responsible for auditory transduction. The cochlear and vestibular (auditory) nerves extend from the inner ear to the auditory cortex.

1.1.1. The outer ear

The outer ear is the 'external' part of the auditory apparatus. Sound waves travel down the external auditory canal, reaching the tympanic membrane at the end of the canal (Figure 1). The tympanic membrane, composed of collagenous fibres, stretches tight across the full diameter of the auditory canal and is colloquially named the 'ear drum'. Sound waves cause the tight surface of the tympanic

membrane to vibrate, and these vibrations are then transmitted mechanically to the middle ear (Emslie-Smith and Bell, 1988).

1.1.2. The middle ear

The mammalian middle ear is an air filled cavity between the tympanic membrane and the inner ear, connected to the nasopharynx via the Eustachian tube, which allows for ventilation and pressure equalisation (Carola et al., 1992). The middle ear essentially acts as an acoustic transformer, converting the sound waves of the ear canal into a mechanical signal to be deciphered by the inner ear. It contains three ossicles, which form a chain to mechanically transfer vibrations of the tympanic membrane to the oval window of the inner ear (Emslie-Smith and Bell, 1988). The three ossicles are named the malleus, incus and stapes, but are also known colloquially as the hammer, anvil and stirrup, due to their respective shapes (Figure 1).

1.1.3. The inner ear

The inner ear is composed of two functionally distinct compartments: the vestibular apparatus and the cochlea. The cochlea is responsible for auditory transduction, whilst the vestibular organs are responsible for the perception of orientation and movement required for maintaining balance.

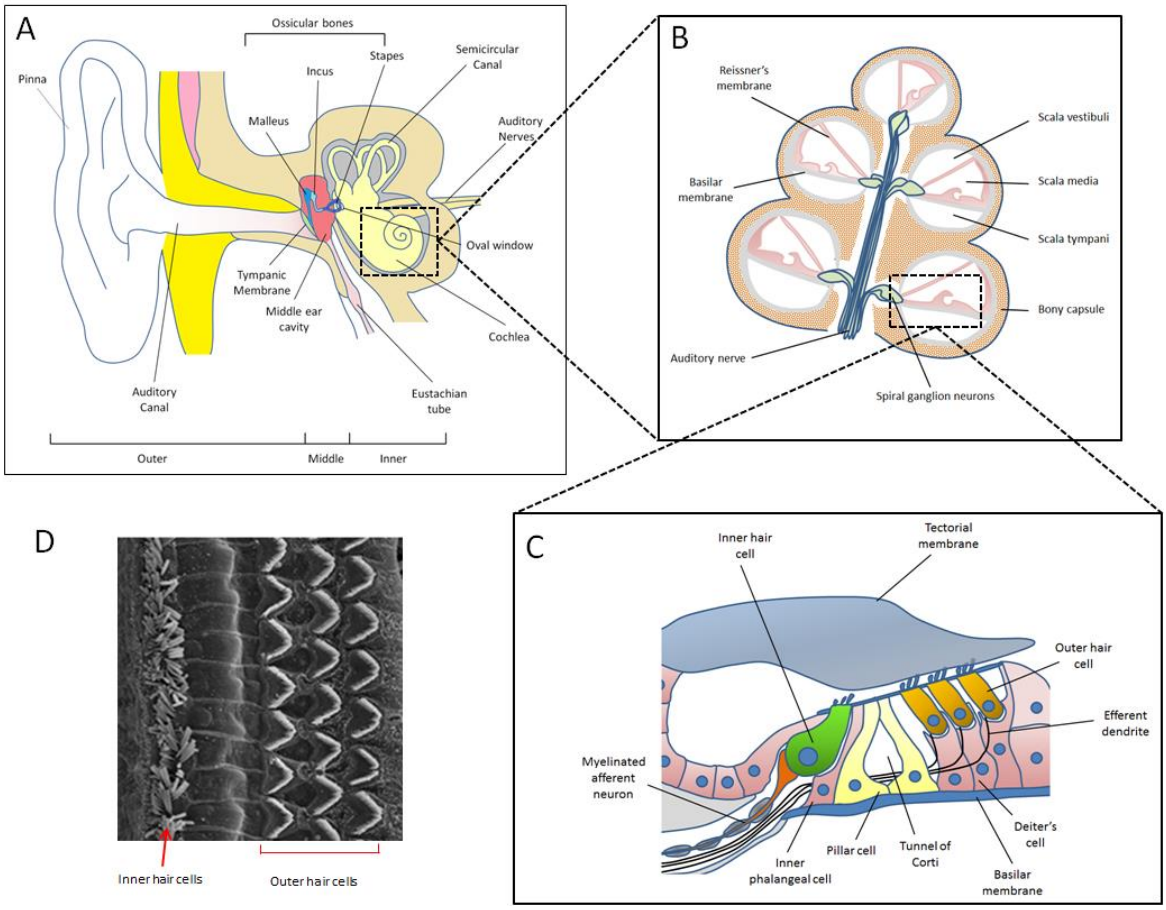

Figure 2. Auditory transduction occurs in the organ of Corti.

A) Sound waves travel from the pinna, down the auditory canal and cause the tympanic membrane to vibrate. The tympanic membrane articulates the ossicular bones within the middle ear cavity, causing the stapes to depress the opening of the oval window and change the fluid pressure within the cochlea. **B)** A cross-section through the cochlea shows the spiral structure. Each turn has three separate compartments: the scala tympani, scala media and the scala vestibuli. The sensory epithelium of the cochlea, the organ of Corti, is located within the scala media. When fluid pressure changes in the scala tympani the basilar membrane oscillates, stimulating the organ of Corti. **C)** A cross-section of the organ of Corti shows its location atop the basilar membrane. The sensory hair cells are organised into a single row of inner hair cells and three rows of outer hair cells, which are supported by the inner phalangeal cells and the Deiter's cells respectively. Both classes of hair cells have microvilli at their apex, known as stereocilia. A gelatinous extracellular matrix, known as the tectorial membrane, rests across the top of the organ of Corti and has the stereocilia bundles of the outer hair cells embedded within it. **D)** A scanning electron micrograph of a P16 C3H/HeH mouse cochlea shows a top down view of the sensory hair cells. A single row of stereocilia from the inner hair cells and 3 rows of V or W shaped stereocilia bundles characteristic of the outer hair cells are observed (LeMasurier and Gillespie, 2005).

1.1.3.1. The cochlea

The human cochlea duct is a highly organised structure comprising 2 and 3/4 turns around the central modiolus bone. The cochlea duct is divided into three chambers known as scala tympani, scala media and scala vestibuli (Figure 2B, Figure 3). The scala media is the central chamber and contains the organ of Corti, the sensory epithelium of the cochlea (Figure 2C). The organ of Corti is located above the basilar membrane, the membrane which separates the scala media from the scala tympani, and is composed of sensory hair cells and supporting cells. Two classes of sensory hair cell are present in the cochlea: the inner hair cells (IHCs) which form a single row proximal to the modiolus bone and the outer hair cells (OHCs), which are organised into 3 rows and reside on the opposite side of the tunnel of Corti from the IHCs (Figure 2D). The two types of sensory cell originate from common progenitor cells, but differentiate early in human development establishing differential morphology and electrophysiology, which allows the IHCs and OHCs to perform separate and distinct functions. In mice this differentiation occurs at early postnatal stages (Kuhn et al., 2011).

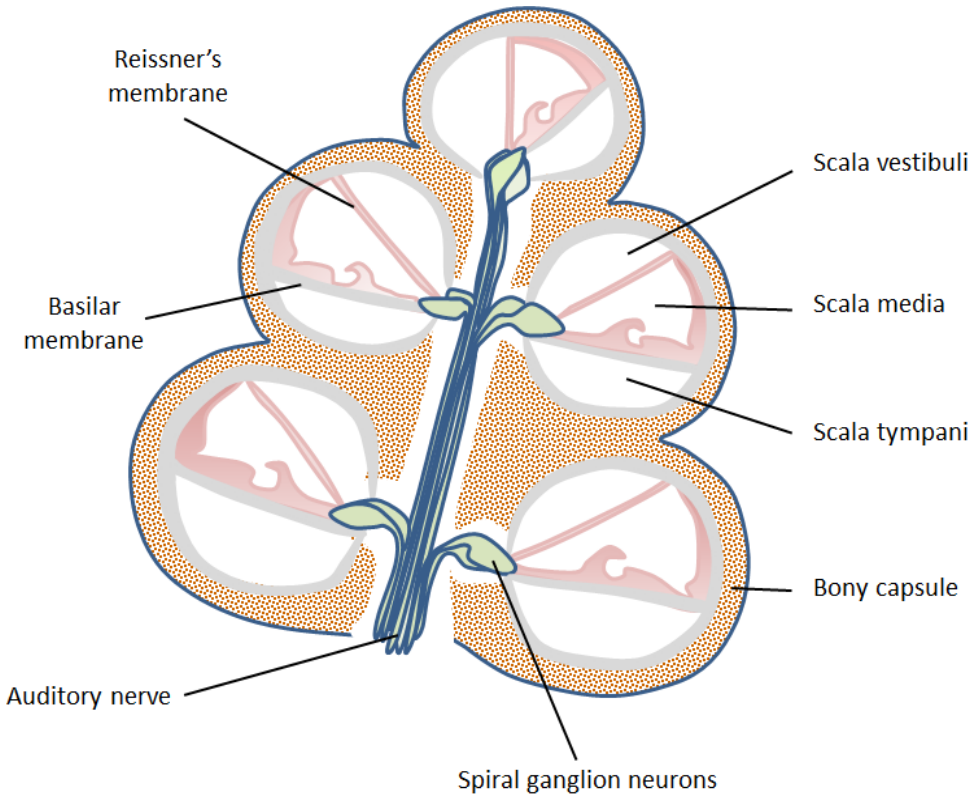

Figure 3. Cross-section of the mammalian cochlea.

Cross-section through the centre of the modiolus bone reveals the $2^{3/4}$ spiral internal structure of the membranous labyrinth of the human cochlea. The cochlea duct is divided into 3 fluid filled chambers: the scala vestibuli, the scala media and the scala tympani. The sensory apparatus is located within the central scala media chamber, separated from the scala tympani below by the basilar membrane and from the scala vestibuli above by the Reissner's membrane. The spiral ganglion neurons extend from the auditory nerve (8^{th} cranial nerve) to the base of the sensory apparatus, where synapses are formed.

The sensory hair cells

The IHCs are responsible for the transduction of sensory signals received in the cochlea. They are supported by the inner phalangeal cells, the border cells to their medial aspect and the inner pillar cell on their lateral side (Figure 4). The inner phalangeal cells have large microvilli separating the IHC from its neighbouring IHC (Lim, 1986). The majority of afferent dendrites in the cochlea form synapses with IHCs and signal in an excitatory manner (Hudspeth, 1989). These synapses are formed with a specialised structure known as the ribbon, which is located at the basal aspect of the cell (Safieddine et al., 2012).

The OHCs are responsible for detecting the finer discriminative properties of sound in the cochlea and are primarily innervated by efferent neurites (Pujol et al., 1980). The OHCs are supported by the Deiter's cells (Figure 4).

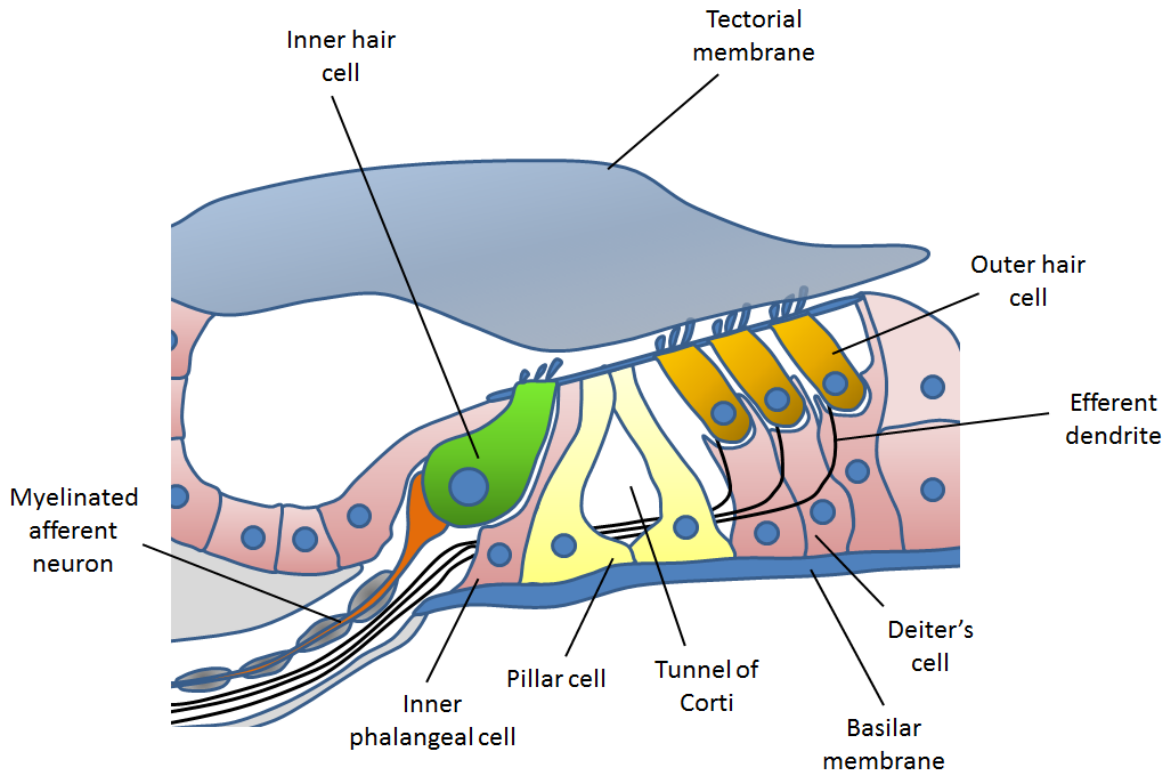

Figure 4. The organ of Corti.

The organ of Corti is contained within the scala media and contains the mechanosensory machinery required for sound transduction in the inner ear. There are two distinct types of sensory cell: the inner hair cells and the outer hair cells. The inner hair cells are organised into a single distinct row supported by the inner phalangeal cells and the pillar cells, which form the tunnel of Corti. The inner hair cells are contacted primarily by the type I myelinated neurons, whilst the type II unmyelinated efferents extend across the tunnel of Corti and form synapses with the outer hair cells. The outer hair cells are arranged in 3 distinct rows, supported by the Deiter's cells. Both sensory cells have stereocilia extending from the cytoplasmic cuticular plate at their apical aspect. The stereocilia of the outer hair cells are embedded in the tectorial membrane and upward movement of the basilar membrane causes a shearing force between the tectorial membrane and the basilar membrane, causing deflection of the stereocilia. Conversely, the stereocilia atop the inner hair cells are not attached to this membrane and are instead deflected by changes in fluid pressure.

Despite their different functions, IHCs and OHCs are considered to be mechanically similar and signalling to the neurons associated with them occurs via the same method. The apical surface of the hair cell (known as the cuticular plate) faces into the fluid filled scala media and is topped with elongated microvilli, known as stereocilia (Raphael and Altschuler, 2003). The stereocilia are not true cilium containing an inner pair of microtubules and 9 outer doublets; they are small actin-rich projections that are more similar to microvilli (Flock and Cheung, 1977). They narrow towards the cuticular plate, forming a flexible hinge that allows for around 10^{O} deflection in both directions (Figure 5). The stereocilia are graded by height and organised into 3 rows, giving the effect of a staircase, with the shorter stereocilia attached to those behind them by fine filaments called tip links, as reviewed by (Fettiplace and Hackney, 2006). This organised structure is often termed the stereocilia bundle or hair bundle. The hair bundles vary in size, with shorter stereocilia more commonly observed at the base of the cochlea and longer stereocilia towards the apex.

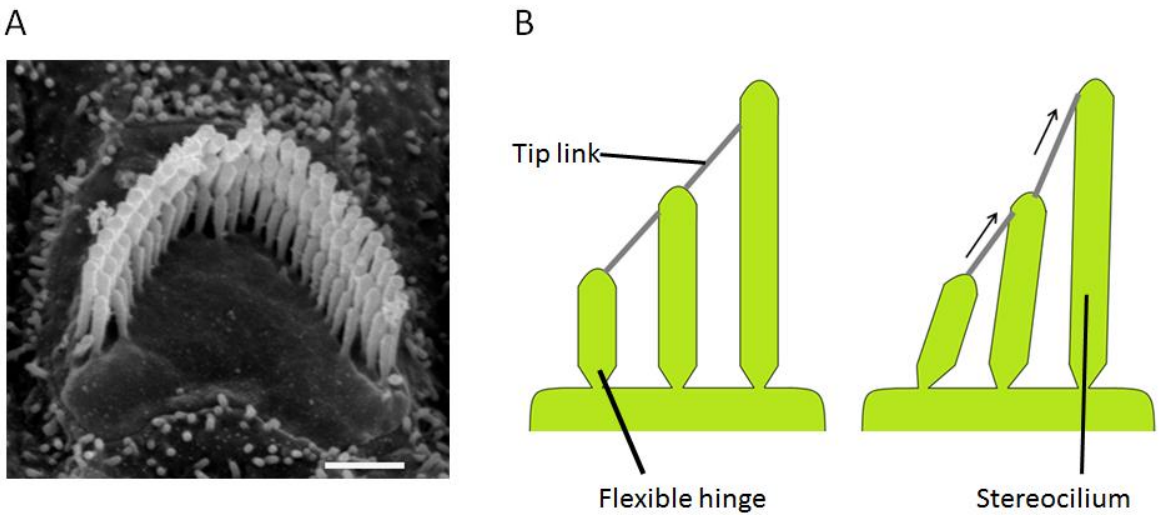

Figure 5. Stereocilia form a staircase arrangement.

A) A scanning electron micrograph of an outer hair cell bundle from a P16 C3H/HeH mouse shows the graded height of the stereocilia, with the shortest at the front and two longer rows behind. **B)** A cross-section of the stereocilia bundle. The stereocilia narrow towards their base, forming a flexible hinge. Fine filament tip links join each stereocilium to a stereocilium in the row behind. The hinges allow for stereocilia bundle movement, stretching the tip links between the rows of stereocilia when deflected towards the longest row.

Curling over the apical surface of the organ of Corti is a gelatinous structure known as the tectorial membrane. The stereocilia bundles of the OHCs are embedded in the tectorial membrane, which moves with fluid pressure changes in the cochlea duct (Lim, 1986). Conversely, the stereocilia bundles of the IHCs are not attached to this membrane and are instead surrounded by the fluid of the scala media (Lim, 1986, Fettiplace and Hackney, 2006).

1.1.3.2. The vestibular organs

The vestibular labyrinth comprises the semicircular canals, utricle and saccule. As a whole the vestibular system is responsible for the detection of movement and acts with the body's proprioceptive centres to control balance and spatial orientation. The semicircular canals are responsible for perceiving rotational movement, whilst the utricle and saccule determine movement in the linear plane.

The semicircular canals

There are three fluid filled semicircular canals which extend and return to ampullae at the base of each canal. Known as the superior, horizontal and posterior canals, they are positioned at approximate right angles relative to each other and determine movement in the coronal, transverse and sagittal planes respectively by detecting fluid movement (Gernandt, 1960) (Brown, 1874). The ampulla contains the crista ampullaris, the sensory epithelium of the semicircular canals. The crista ampullaris is composed of vestibular hair cells (similar to the IHCs in the cochlea - with stereocilia at their apical surface) and supporting cells (Figure 6).The sensory epithelium is surrounded by a large gelatinous mass, known as the cupula which extends across the full diameter of the ampulla (Gernandt, 1960). The hair cells are innervated by vestibular afferent neurons.

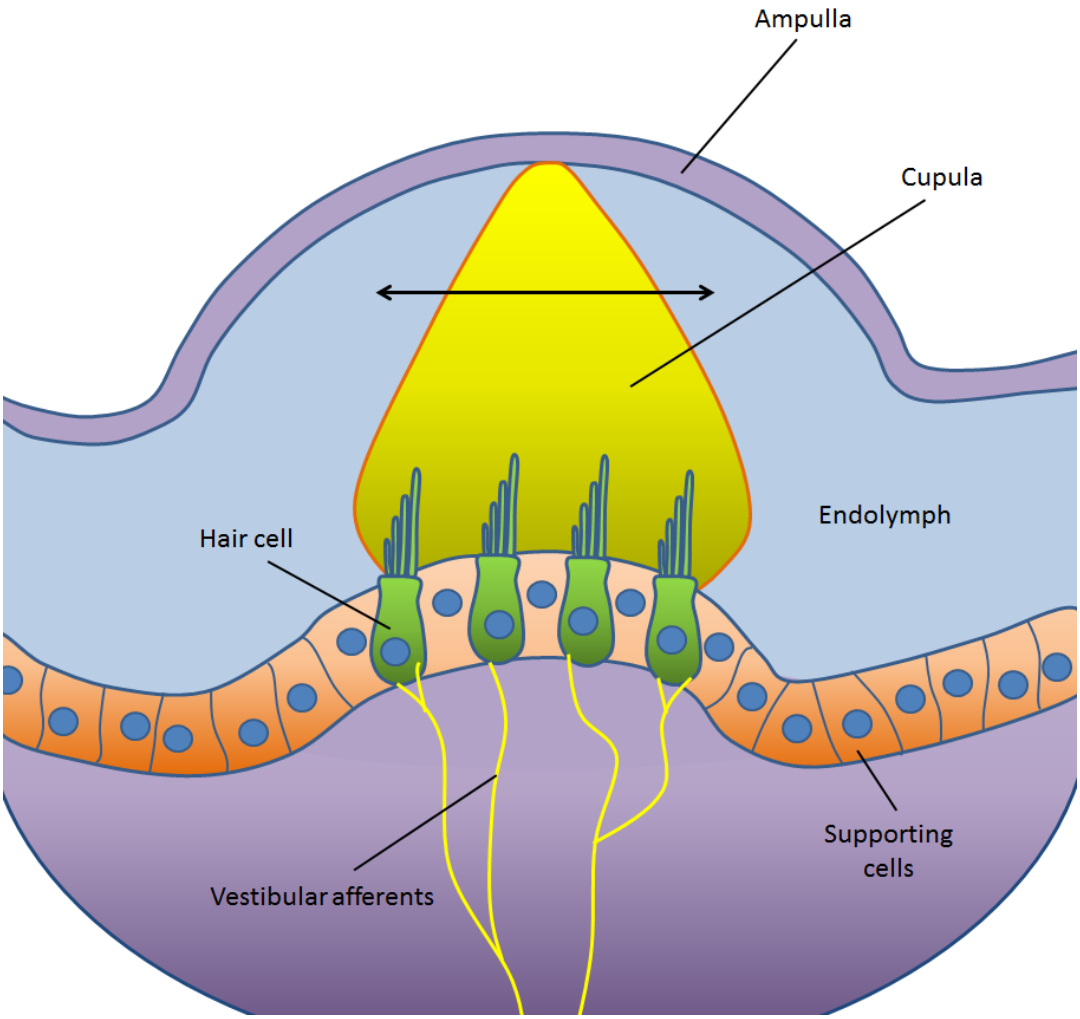

Figure 6. Movement of the cupula causes stereocilia bundle deflection and signalling of rotational movement in the ampulla.

The ampullae are located at the basal region of the endolymph-filled semicircular canals. The crista ampullaris is a structure within the ampullae, covered in supporting cells and stereocilia-topped hair cells. A gelatinous mass, known as the cupula extends across the diameter of the ampulla, engulfing the stereocilia within the crista. Rotational movement of the head causes the endolymph to accelerate in the direction of movement. The accelerating endolymph exerts force on the cupula in the direction of rotation, causing the cupula to deflect the stereocilia. Stereocilia deflection leads to cell depolarisation and neuronal transmission via the vestibular afferents.

The utricle and saccule

The utricle and saccule are fluid filled sacs with a thickened region at the anterior surface known as the macula. The macula is comprised of vestibular hair cells with stereocilia at the apical surface and supporting cells (Figure 7). The macula is embedded in a dense gelatinous glycoprotein matrix, known as the otolithic membrane. Attached at the apical surface of the otolithic membrane are

small calcium carbonate stones, commonly referred to as otoconia or otoliths, which move in response to acceleration (Carola et al., 1992). The vestibular hair cells of the utricle and saccule are innervated by vestibular afferent neurons.

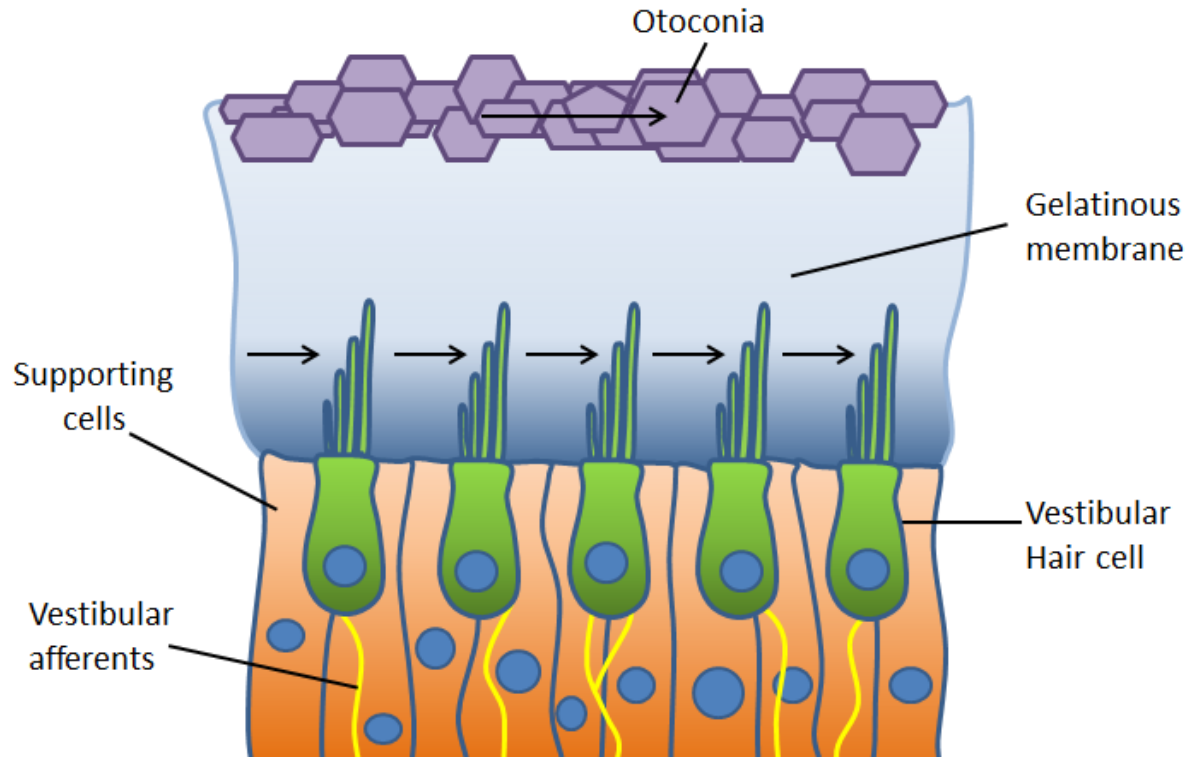

Figure 7. Otoconia movement leads to stereocilia deflection and detection of linear movement in the utricle and saccule.

The macula in the utricle and saccule are topped with hair cells. The stereocilia of these hair cells are embedded in the gelatinous otolithic membrane, which is topped with calcium carbonate otoliths, known as the otoconia. When linear movement occurs, the otoconia travel in the same direction, stimulating movement of the otolithic membrane and deflection of the stereocilia hair bundles. Stereocilia deflection leads to cell depolarisation and neurotransmission.

1.2. Function of the mammalian ear

The sensory apparatus for transduction of sound and spatial orientation/movement detection are both located within the inner ear, in the cochlea and the vestibular apparatus respectively. Despite their physical proximity the two structures maintain separate functions and require different

external stimuli. In order to transduce sound the cochlea relies on the outer and middle ear apparatus to transfer sound wave information to the inner ear. Conversely, the vestibular organs do not require input from the outer or middle ear, but instead rely on movement of the head to evoke signalling via the sensory epithelium.

1.2.1. The outer ear

The pinna captures sound waves in the air around us. These sound waves are conducted down the external auditory canal and reach the lateral wall of the tympanic membrane. The tympanic membrane links the outer and middle ear, stretched tight across the auditory canal with its medial wall facing into the middle ear cavity. Sound waves cause the tympanic membrane to vibrate and articulate the ossicular bones in the middle ear.

1.2.2. The middle ear

The malleus is connected to the tympanic membrane and moves in accordance to the vibrations of the membrane. The malleus attaches to the incus, which bridges the malleus and the stapes, consequently passing movement from the malleus to the stapes when the tympanic membrane is stimulated (Figure 1). The stapes is the smallest named bone in the body and has a shape reminiscent of a stirrup, with the footplate resting on the oval window of the cochlea (Emslie-Smith and Bell, 1988, Carola et al., 1992). Movement leads to depression of the oval window causing changes in pressure of the fluid within the scala vestibuli. The scala vestibuli and scala tympani are joined at the apex, and when the oval window is depressed fluid is pushed through the scala vestibuli to the round window at the end of the scala tympani (Figure 8). The change in pressure at the oval window also occurs at the round window, but the pressure varies slightly and in the opposite phase (Stenfelt and Goode, 2005, Merchant et al., 1997). The mechanism of sound conductance described is known as ossicular coupling (Merchant et al., 1997). There are two known types of ossicle stimulation: air conductance stimulation (AC) and bone conductance stimulation (BC). AC is attributed to a sound pressure entering the ear canal, causing the ossicles to vibrate and

move and leading to sound pressure being transmitted to the cochlea. BC stimulation can be due to a multitude of factors: inertia of the ossicles, inertia of the cochlea fluid, sound radiation in the ear canal or the expansion and retraction of the bone encapsulating the cochlea (Stenfelt, 2006). The mechanism of hearing in the cochlea does not differ whether the stimulation is AC or BC (Stenfelt et al., 2003). In addition to ossicular coupling there is a second mechanism underlying middle ear conductance known as acoustic coupling. Acoustic coupling is when sound pressure in the ear canal directly causes a change of pressure at the oval window or the round window of the cochlea. In normal hearing acoustic coupling is expected to play an almost negligible role. However, when the middle ear is damaged or impaired it is thought that this mechanism of stimulation becomes more dominant (Merchant et al., 1997).

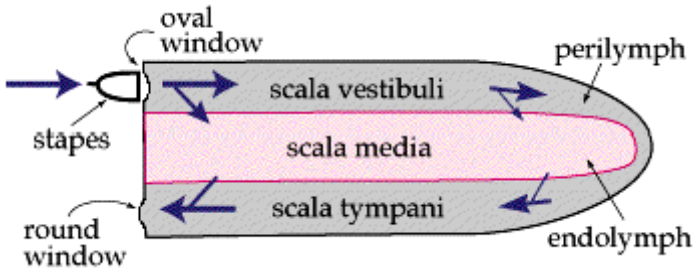

Figure 8. Fluid movement in a cross-section of an un-coiled cochlea.

Stapes depression of the oval window causes a fluid pressure wave to travel through the perilymph in the scala vestibuli. The wave travels through the apex of the cochlea and continues to travel in the same direction through the scala tympani, causing a pressure change in the opposite phase at the round window. Figure adapted from http://www.bioon.com/bioline/neurosci/course/audvest.html

1.2.3. The role of the cochlea in auditory transduction

Cross-section through the centre of the modiolus bone (mid-modiolus) show that the chambers of the cochlear duct are separated by two membranes. The basilar membrane separates the posterior scala media from the scala tympani, whilst the Reisnner's membrane separates the anterior scala media from the scala vestibuli (Carola et al., 1992, Tortora and Grabowski, 1993). Each of these

chambers are fluid-filled, the fluid pressure within the chamber changing when the oval window is depressed (Tortora, 1992). The change in fluid pressure is essential for auditory transduction in the organ of Corti.

1.2.3.1. The basilar membrane

The properties of the basilar membrane varies along the length of the cochlea duct (Lim, 1986). At the base of the cochlea the basilar membrane is thickest and widest. The size of the membrane is reduced in a steady gradient to the apex, where the basilar membrane is thinnest. Fluid pressure changes within the cochlear duct cause the basilar membrane to oscillate (Carola et al., 1992, Tortora and Grabowski, 1993).

The change in width and thickness throughout the basilar membrane alters the oscillation properties throughout the cochlea duct. Different sound frequencies cause characteristic resonance in specific parts of the cochlea, and this allows for the encoding of frequency information (Liberman and Beil, 1979, Davis et al., 1989). The highest frequencies are encoded at the base of the cochlea and the lowest frequencies encoded at the apex. The recognition of specific frequencies in specific parts of the cochlea is referred to as tonotopic organisation (Liberman, 1982). The oscillation of the basilar membrane, leads to oscillation of the organ of Corti and changes in fluid pressure within the scala media.

1.2.3.2. The scala media

The fluid within the scala media is known as endolymph. Endolymph is rich in potassium and has a high positive potential of approximately +80mV (Takeuchi et al., 2000, Hellier et al., 2002). When the basilar membrane oscillates, endolymph movement causes the stereocilia bundles of the IHCs to deflect. The basilar membrane oscillation also causes a shearing movement between the tectorial membrane and the basilar membrane, resulting in OHC hair bundle deflection (Lim, 1986, Fettiplace and Hackney, 2006).

1.2.3.3. Stereocilia bundle deflection

When the stereocilia bundle is deflected in the planar direction towards the longest stereocilia, the tip links between the individual microvilli are stretched (Figure 9). This mechanically opens selective cation channels, known as mechano-electrical transduction (MET) channels (Assad et al., 1991). Conversely, when the hair bundle is deflected away from the longest stereocilia the tip links relax and the MET channels close. In the hair cells resting state a small number of MET channels remain open at the apical surface (Purves and Williams, 2001).

The hair cells have an internal resting potential of around -60mV (Hudspeth, 1989). This potential is extremely negative in comparison to the potassium rich endolymph, so when MET channels open passive influx of K^+ and Ca^{2+} from the endolymph occurs, despite high internal K^+ levels in the hair cell (Jentsch, 2000). Ca^{2+} entry at this point is believed to aid a process known as fast adaptation; the Ca^{2+} binds either the transduction channel or an element close to it, causing rapid closure of the MET channel and maintaining hair cell sensitivity (Schwander et al., 2010). The influx of K^+ leads to cell depolarisation (Shotwell et al., 1981), activating voltage-gated Ca^{2+} channels in the cell membrane. This drives neurotransmitter release from the presynaptic area at the base of the hair cell, known as the active zone.

Neurotransmission leads to action potential generation in post-synaptic terminals and afferent signalling to the auditory cortex via the spiral ganglion neurons (SGNs) of the auditory nerve (Purves and Williams, 2001).

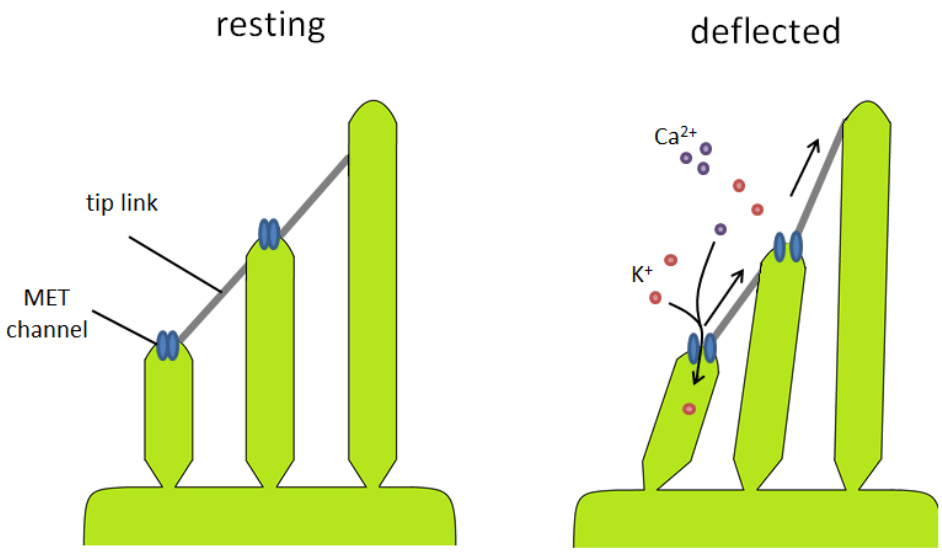

Figure 9. Stereocilia bundle deflection induces mechanotransduction.

The stereocilia in the shorter two rows are connected to the stereocilia behind them by small filamentous links throughout the trunk of the stereocilium and by a singular tip link extending from the very apex of the shorter cilium. When the bundle is deflected towards the longest stereocilia, either by endolymph pressure changes in the IHCs or shearing force in the OHCs, the tip links stretch forcing the MET channels to open and influx of cations into the hair cells. Cation influx leads to hair cell depolarisation and neurotransmitter release.

1.2.3.4. Synaptic organisation and transmission

Mice are initially born deaf, however when the hair cells have fully matured by post-natal week 2 hearing is established (Burda and Branis, 1988, Glowatzki and Fuchs, 2000). Synaptic organisation is dynamic during cochlear maturation with both afferent and efferent dendrites extending to make contacts with the IHCs and the OHCs (Walsh and Lichtman, 2003, Glowatzki and Fuchs, 2000). Neurite retraction and refinement at the end of post-natal week 1 ensures that the correct pathways are in place for hair cell innervation (Echteler, 1992). Full maturation of synapses at the IHCs relies on spontaneous action potentials modulated by transient efferent cholinergic signalling between the first and second week of development (Johnson et al., 2013).

The type II unmyelinated SGNs serve as the main efferent connection at the OHCs and primarily function through cholinergic signalling, acting in an inhibitory capacity on the inner hair cells (Fuchs,

2002). The type I myelinated SGNs are established as the primary afferent connection with the presynaptic active zone of the IHC (Barclay et al., 2011), transducing acoustic signals from the cochlea to the auditory cortex. There are normally between 10 and 30 presynaptic active zones on a single IHC, which form synapses with the postsynaptic density (PSD) of afferent glutamatergic neurons (Lenzi and von Gersdorff, 2001). The neurotransmitter (glutamate) is encapsulated within vesicles stored in large quantities around the active zones at the basolateral aspect of the IHC and released rapidly after membrane depolarisation. These vesicles are tethered by ~20nm fibres into a large, electron dense structure known as the ribbon (Usukura and Yamada, 1987, Lenzi and von Gersdorff, 2001).

1.2.3.5. The ribbon synapse

The ribbon synapse is a structure that facilitates fast neuronal signalling where a graded response to stimuli is required, such as at the ear or the eye. Whilst the active zone is no larger than that found at a conventional presynaptic terminal, the electron dense fibres that extend from the cytomatrix of the active zone to tether vesicles are ellipsoid in shape and have a larger surface area than conventional fibres (Figure 10). This allows the ribbon synapse to have a much larger readily releasable pool (RRP) of vesicles and sustain neurotransmission when continuously stimulated (see Figure 9) (Zhai and Bellen, 2004).

Conventional neuronal signalling relies on detecting the rate at which action potentials are fired, however sound stimuli is perceived almost constantly leading to sustained signalling, and therefore requires a more complex signalling system to elucidate the differences. In order to encode differences in the sound we hear, changes in tonic neurotransmitter release are detected and used to identify interaural time differences in the auditory brainstem (Khimich et al., 2005). This process requires fast and precise release of vesicles in large quantities, sometimes in the thousands (Moser et al., 2006). Through tethering vesicles into its structure by ~20nm fibres, the synaptic ribbon is able to organise the vesicles into pools that are readily available to be docked at the active zone and

released into the synaptic cleft (von Gersdorff et al., 1996). This enables the ribbon to coordinate exocytosis of hundreds of vesicles per second with high precision, and activate fast responding α-Amino-3-hydroxy-5-methyl-4-isoxazolepropionic acid (AMPA) receptors at the PSD of the afferent, as reviewed (Moser et al., 2006).

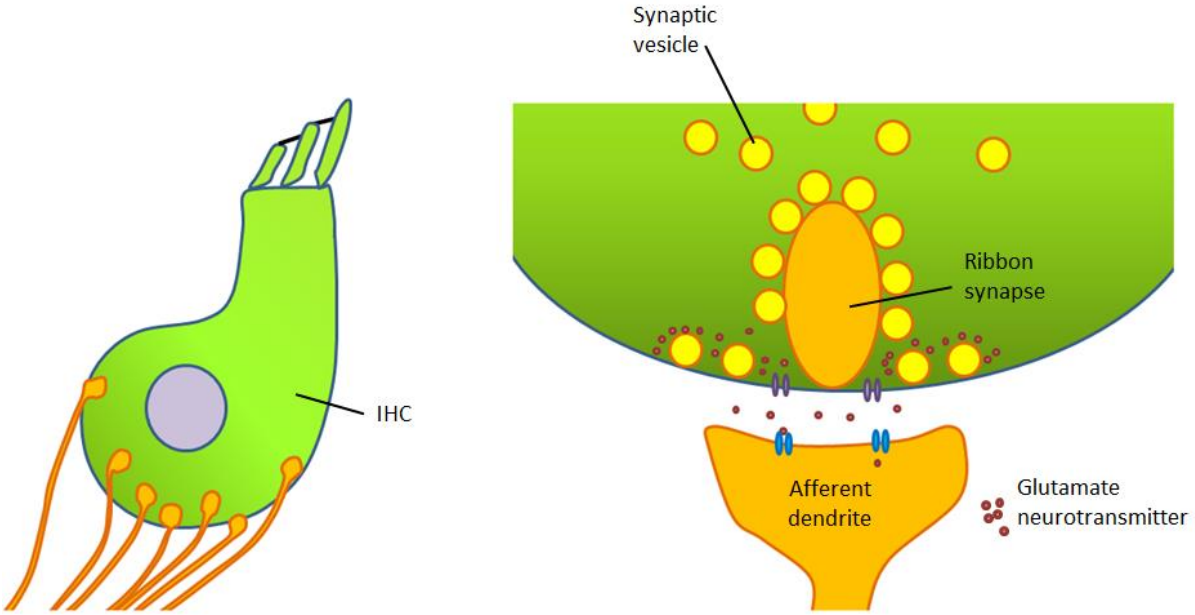

Figure 10. The ribbon synapse coordinates rapid vesicle release in the inner hair cell.

The ribbon synapse is responsible for coordinating excitatory neurotransmission in the ear. Glutamate neurotransmitter is packaged into synaptic vesicles, which are coordinated around the ellipsoid ribbon. The ribbon tethers the vesicles using small fibres and vesicles diffuse along the ribbon to the active zone at the cell surface where they are docked. Neurotransmission occurs simultaneously from docked vesicles. After glutamate is released into the synaptic cleft the vesicles are recycled and replenished with glutamate to be used again.

In the eye the ribbon coordinates synaptic signalling between the bipolar cells and the photoreceptors of the retina. Whilst these structures are thought to have the same role in vesicular release, subtle differences have been reported between the two structures. For example whilst the auditory ribbon synapse relies on Cav1.3 mediated Ca^{2+} influx to induce vesicle release, the retinal ribbon synapse couples vesicular release with the influx of Ca^{2+} through Cav1.4, as reviewed in (Nouvian et al., 2006). Studies of the retinal ribbon synapse suggest that the RRP is smaller in the

eye, reported as 70+/-7 vesicles (Singer and Diamond, 2006), whereas estimates in the IHC are between approximately 150 and 200 (Nouvian et al., 2006) vesicles at each active zone. However, this may be attributable to the different levels of receptor cells in their respective organs (millions of photoreceptors in the retina vs thousands of IHCs in the ear). Conversely, there are multiple similarities reported, such as expression of Ribeye, Bassoon and Piccolo proteins at the ribbon of the eye and ear, as well as vesicle depletion leading to adaptation at the afferent synapses, allowing for responses to changes in pre-synaptic neurotransmitter release rather than absolute firing values (Singer and Diamond, 2006).

1.2.4.6. Potassium recycling after neurotransmission

At their basal aspect the hair cells are bathed in perilymph, the fluid that fills the scala tympani and the scala vestibuli, which is sodium rich, but poor in potassium and calcium. Perilymph is thought to be similar to other extracellular fluids, such as cerebrospinal fluid (CSF), and is believed to originate from the blood plasma. However, evidence suggests that this is not the only mechanism for perilymph production (Scheibe and Haupt, 1985).

Once signalling has occurred K^+ efflux becomes favourable due to the negative equilibrium potential of K^+ and the relative low K^+ concentration in the perilymph. Voltage gated K+ channels (KCNQ4) as well as Ca^{2+} dependent K^+ channels (BKCa) are activated in the basolateral membrane allowing transport of K^+ out of the hair cells into the basal cleft and repolarisation of the hair cell (Hibino and Kurachi, 2006).

K^+ entry from the basal cleft into the surrounding supporting cells is mediated by K^+, Cl^- co-transporters (Kcc3 and Kcc4) in the Deiter's cells. In the inner phalangeal cells Kcc3 performs this function alone. K^+ passage into the supporting cells is thought to preferential due to a low Cl^- concentration in these cells and also a high K^+ concentration in the cleft between the supporting cells and the basal aspect of the hair cells (Zdebik, 2009). K^+ is then transported through the epithelial gap

junction network to the outer sulcus cells located in the spiral ligament and released into the extracellular space (Figure 11). Up until this point, K^+ recycling is almost entirely passive, requiring no energy input. The K^+ is then uptaken into the type II and IV fibrocytes using Na^+K^+ATPases and the Na^+K^+2Cl co-transporter NKCC1, from where it is able to move through the fibrocytes, into the basal cells of the stria vascularis and eventually reach the stria intermediate cells via the connective tissue gap junction network (Hibino and Kurachi, 2006).

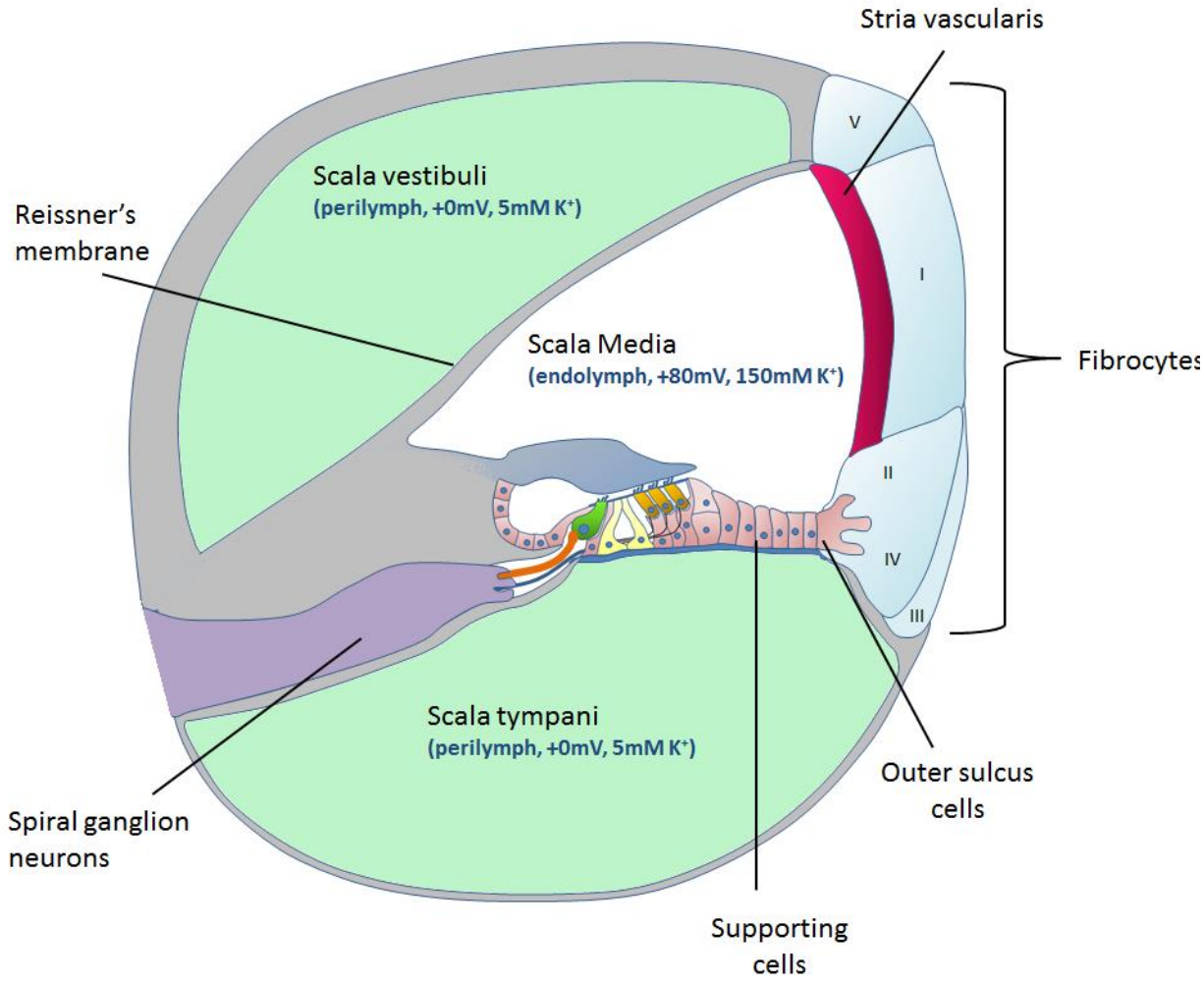

Figure 11. K^+ is transported to the stria vascularis after sensory cell depolarisation through the supporting cell and fibrocyte network.

After depolarisation K^+ exits the sensory cells with the aid of the KCNQ4 and BKCa channels, allowing repolarisation of the hair cell. K^+ is removed from the cleft around the basal aspect of the hair cell and transported into the supporting cells by K^+Cl^- co-transporters. K^+ is then transported through the epithelial gap junction network to the outer sulcus cells, where it exits into the extracellular space. K^+ is up-taken by the type II and IV fibrocytes, via the NKCC1 co-transporter and Na^+K^+ATPases, and transported through the fibrocyte network via gap junctions to the stria vascularis.

The stria vascularis has three cell layers: basal, intermediate and marginal (Figure 12). Gap junctions link the basal and intermediate cells, ensuring K^+ transport into the intermediate cells and exit via K^+ Kir4.1 channels into the interstrial space (Ando and Takeuchi, 1999, Nin et al., 2008), which has a low K^+ concentration due to a reliance on K^+ being pumped into the stria marginal cells, as reviewed by (Zdebik, 2009). NKCC1 (also known as Slc12a2) co-transports $Na^+/K^+/2Cl^-$ into the marginal cells, in conjunction with a $3Na^+/2K^+$-ATPase (Flagella et al., 1999) which actively moves K^+ into the cells, whilst removing Na^+ to the interstrial space (Adachi et al., 2013). Na^+ and Cl^-, which exit the marginal cells at the basolateral membrane via the ClC/-K channel, are then used to re-energise NKCC1 and co- transport K^+ into the marginal cells, perpetuating this cycle of ion movement between the interstrial space and the marginal cells. The abundant K^+ pumped into the marginal cells exits at the apical aspect via a K^+ channel, re-entering the scala media and maintaining the high positive potential of the EP (Nin et al., 2008).

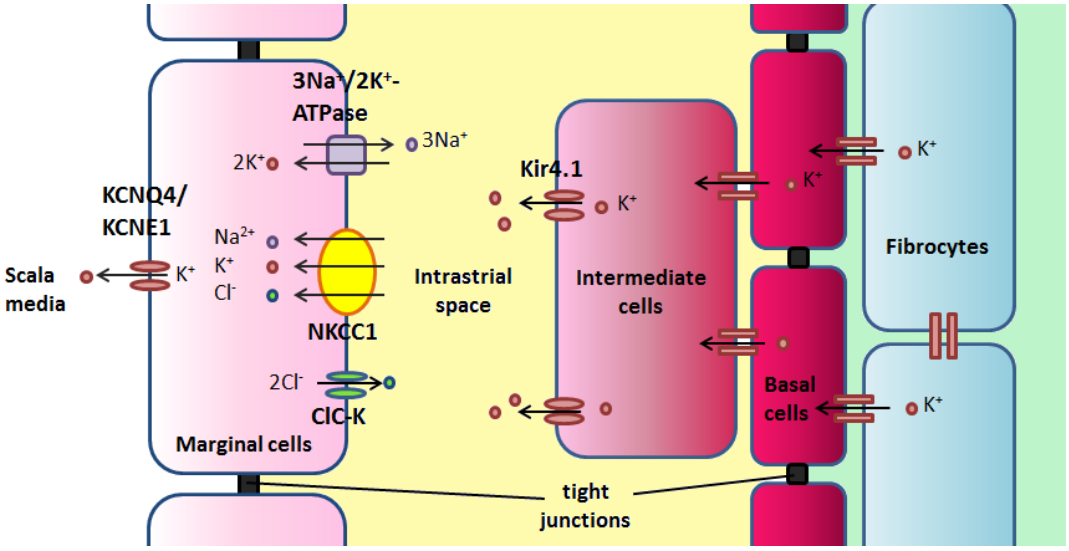

Figure 12. The stria vascularis is required for K^+ re-entry into the endolymph and maintenance of the endocochlear potential.

The stria vascularis is composed of 3 layers: the basal, intermediate and marginal cells. K^+ moves from the fibrocytes into the basal cells via the gap junction network, and also moves from the basal cells into the intermediate cells via gap junctions. Once in the intermediate cells, K^+ is transported into the intrastrial space by Kir4.1 channels due to the relative low K^+ concentration in this space. K^+ from the intrastrial space is transported into the marginal cells via NKCC1 and an ATP dependent mechanism, and the high internal K^+ concentration of the marginal cells drives K^+ movement into the endolymph of the scala media via KCNQ4 and KCNE1 channels.

1.2.4. The role of the vestibular apparatus in balance and orientation

The labyrinth of the semicircular canals as well as the utricular and saccular sacs, are endolymph filled structures. Whilst the vestibular apparatus detects sensory information related to balance rather than sound, the process of sensory transduction is fairly similar to that in the organ of Corti.

1.2.4.1. The semicircular canals

Perception of rotational movement is determined by movement of the endolymph within the canals (Brown, 1874). When movement of the head occurs endolymph accelerates in the direction of the movement, deflecting the cupula and therefore the stereocilia on the crista ampullaris (Tortora, 1992). When these stereocilia are deflected, MET channels open causing vestibular hair cell

depolarisation and neurotransmitter release. Action potentials are transmitted via the auditory nerve to areas in the brain coordinating responses in the eye, spine and muscles that are responsible for the reflexes of balance and stability (Tortora, 1992).

Gradually as the speed of the endolymph movement slows and matches the speed of rotation the cupula returns to normal and the stereocilia return to a resting position, closing the MET channels. When movement of the semicircular canal ceases, inertia of the endolymph causes the cupula to once again deflect, signalling the cessation of movement (Carola et al., 1992, Gernandt, 1960).

1.2.4.2. The utricle and the saccule

When the head moves, endolymph within the utricle and saccule accelerate towards the direction of the movement. Similar to the semicircular canals, endolymph movement displaces the otoconia, causing movement of the otolithic membrane and stereocilia deflection. MET channels open leading to hair cell depolarisation and neurotransmission via the auditory nerve, also known as the 8th nerve (Tortora, 1992). It is believed that signals from the utricle primarily influence postural reflexes, whilst signals from the saccule are not perfectly understood (Gernandt, 1960).

1.3. Types of hearing loss

Auditory impairment broadly falls into three “pure” categories: conductive, sensorineural and central hearing loss. There is an additional category known as mixed, which has components of both conductive and sensorineural deficit. In both conductive and sensorineural loss there is the potential for hearing loss to be caused by a genetic mutation or environmental exposure (Table 1).

Table 1. The different classifiers used to describe auditory impairment.

Classification	Description
Onset	Congenital, pre-lingual or post-lingual
Aetiology	Genetic or acquired (e.g. environmental)
Severity	Mild (25 - 40 dB), moderate (41 - 70 dB), severe (71-90 dB) and profound (+90dB)
Presentation	Syndromic (associated with additional clinical features) or non-syndromic (the only clinical feature)
Site affected	Conductive (outer and/or middle ear) or sensorineural (inner ear, auditory nerve, auditory cortex)
Sidedness	Bilateral (both ears) or unilateral (one ear)

Hearing impairment can be classified using a number of descriptive factors including age of onset, aetiology, severity of presentation and whether the pathology is standalone or seen in conjunction with other disease. Other describers include where the pathology is caused and whether pathology affects both ears. (Rehm and Morton, 1999, http://www.healthyhearing.com/content/faqs/Hearing-loss/Test/41775-Degrees-of-hearing-loss, Healthy-Hearing, 2014)

Environmental hearing loss tends to be a standalone pathology, exhibiting no known associated symptoms. Within genetic hearing loss further classification is used to specify whether the gene causing auditory impairment is associated with a wider pattern of pathology (syndromic) or thought to cause deafness alone (non-syndromic). There are currently 45 identified syndromic deafness genes associated with multiple syndromes such as Treacher Collins or Usher Syndrome (Van Camp and Smith, 2014). Treacher Collins is a ribosomopathy and mutations in TCOF1 (*Treacle)*, POLR1C or POLR1D lead to craniofacial deformities, including malformed or absent ears and a conductive hearing loss (The-TCS-Collaboration, 1996, Dauwerse et al., 2011). Usher syndrome is a deaf-blind sensorineural syndrome linked to mutations in 11 known genes, with the condition itself subdivided into 3 distinct classes associated with the onset and severity of symptoms (Riazuddin et al., 2012, Jaworek et al., 2012, Millan et al., 2011). Type I Usher syndrome patients' exhibit severe to profound congenital deafness and vestibular dysfunction with onset of retinitis pigmentosa (RP) in the first decade of life. Type II sufferers have a moderate congenital hearing impairment with no vestibular dysfunction and RP usually onsets at puberty or post-puberty. Type III Usher syndrome has a more

variable progressive deafness phenotype, variable vestibular dysfunction and RP onset and severity. Usher syndrome accounts for 50% of deaf-blind sufferers and 5% of congenital hearing loss cases (Millan et al., 2011, Bonnet and El-Amraoui, 2012).

1.3.1 Conductive Hearing Loss

Conductive hearing loss is the decreased ability to conduct sound waves to the cochlea and may be caused at any point between the outer ear canal and the middle ear ossicles. Conductive hearing loss is characterised by moderately increased auditory thresholds (+30dB) usually commencing at lower frequencies (Petit, 2006). Symptoms of conductive hearing loss can be experienced in one ear (unilateral) or both ears (bilateral) and is generally receptive to therapeutic intervention with the exception of cases where part of the auditory apparatus is missing. Causes of conductive hearing loss include OM, craniofacial defects, otosclerosis and tumours in the middle ear or on the tympanic membrane (Klein, 1994, Goudy et al., 2006, Yoon et al., 2014).

The leading cause of outer ear conductive hearing loss is a build-up of cerumen (ear wax). Use of cotton buds to remove the wax often leads to further impacting and worsened hearing. Most commonly, conductive hearing loss in children is reported as a symptom of OM, with around 75% of children having experienced at least one episode of acute OM by the age of 3 (Klein, 1994). OM is often coupled to bacterial upper respiratory tract infections, causing the Eustachian tube to become blocked and the middle ear to fill with fluid which thickens over time. This pressure change slows the movement of the tympanic membrane or the ossicles, preventing correct conductance (Isaacson and Vora, 2003). There is also a type of OM known as adherence OM, where a weakened retracted tympanic membrane adheres to the ossicles preventing correct movement and conductance. Usually the bacterial infection will clear naturally or can be easily treated with antibiotics within a matter of days (although prescriptions for OM is believed to be accelerating antibiotic resistance, (Grevers, 2010, Schraff, 2008). In some cases infection may be recurrent, referred to as recurrent acute OM

(RAOM) or continue to display symptoms for much longer than the infection period should last, referred to as chronic OM with effusion (COME). Grommet insertion is used to treat RAOM and COME and involves the insertion of a small tympanostomy tube (grommet) through the ear drum in order to drain the fluid from the middle ear (Figure 13) (Schraff, 2008, Klein, 1994). Grommets are usually effective, but other techniques such as adenoidectomy and adenotonsillectomy may be used as a further intervention (Paradise et al., 1999). Adenoidectomy and adenotonsillectomy may be effective as air from the nasopharynx is used to ventilate the middle ear cavity, via the Eustachian tube. The tonsils and adenoids have bacterial biofilms covering their surface and have been shown to contain OM causing bacteria in children with recurrent OM, as reviewed by (Post et al., 2007). As bacteria in biofilms have enhanced resistance to antibiotic treatment (up to 1000 times versus bacteria not in a biofilm) these bacteria survive antibiotic treatment for the initial occurrence of OM and cause recurrence when ventilated into the middle ear cavity. Removal of these organs may prevent recurrence.

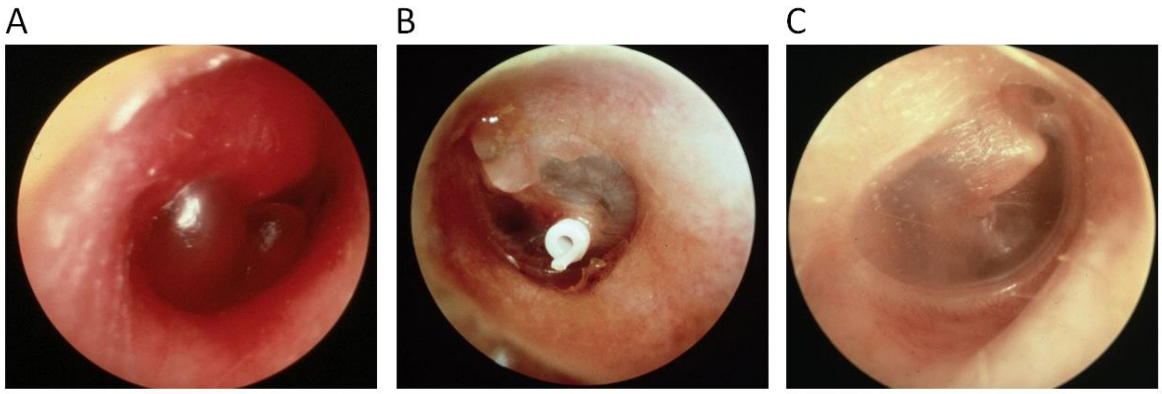

Figure 13. Otoscopy images of the tympanic membrane.

An OM infected ear drum in a paediatric patient. The tympanic membrane has reddened and inflamed, appearing to bulge. The ear canal also appears to be irritated. **B)** A tympanic membrane with a tympanostomy tube (grommet) inserted. **C)** A tympanic membrane that has been treated for OM and is now clear of infection. The tympanic membrane is translucent and thin in comparison to the OM infected ear drum and has no visibly fluid, reddening or inflammation.
Figure adapted - http://www.onmedica.com/newsarticle.aspx?id=d9d59537-ce18-428a-81d4-c02860868981

Whilst OM infection is undeniably related to environmental factors, for example children attending nursery are more likely to get OM, cases of RAOM and COME often run in families and meta-analysis of twenty two studies performed by Uhari et al. (1996) observed a 1.63 fold increase in relative risk of OM infection when there was a positive family history of acute OM. These findings illustrate that there is a genetic component to OM susceptibility. Indeed, studies performed in the monogenic mouse mutants *Jeff* and *Junbo* have identified *Fbox11* and *Evi1*, respectively, as genes that are essential for middle ear health, with mutations in these genes leading to OM and conductive hearing loss (Hardisty et al., 2003, Hardisty-Hughes et al., 2006, Parkinson et al., 2006). Further downstream studies in both of these models have identified the importance of the HIF-VEGF pathway in OM (Cheeseman et al., 2011). In human GWA studies recruited from families with children undergoing grommet surgery, associations have been identified between genes in the TGF-β pathway (a pathway that influences the HIF-VEGF pathway) and OM. However, these were not replicated in a cohort of 645 affected families and require further exploration in mice to confirm a role in OM (Rye et al., 2012).

1.3.2. Sensorineural hearing loss

Sensorineural hearing loss occurs when dysfunction of the cochlea or the eighth nerve leads to reduced or absent auditory transduction (Smith et al., 2005). As the name suggests sensorineural deficits most commonly arise when there is a defect at the sensory cells (both IHCs and OHCs), or at the synapses that junction these cells, and/or the neurones that carry the auditory-evoked signal to the brain (e.g. type II Neurofibromatosis where tumours grow on the eighth nerve) (Evans et al., 2000). Due to the complexity of cochlea transduction there are many factors that may lead to sensorineural deafness including: developmental failure of the cochlea hair cells, disruption of synapses or the SGNs leading to the eighth cranial nerve and ionic dysregulation in the scala media.

The most common form of sensorineural deafness is age-related hearing loss (AHL) due to damage of the cochlea apparatus. Damage will be accumulated over the patient's lifespan and is commonly associated with accelerating environmental factors (e.g. noise exposure). Damage to cells becomes more prevalent with age, and because the sensory cells are terminally differentiated it is not possible to replace damaged cells leading to a permanent auditory deficit. Human twin studies suggest that genetics accounts for around 40-50% of presbycusis cases (Christensen et al., 2001), with SNPs in genes such as *GRM7* (Friedman et al., 2009) and *GRHL2* (Van Laer et al., 2008) identified in human GWA studies as potentially conveying risk for AHL.

Patient presentation varies and whilst some sufferers experience a mild impairment or loss of hearing at specific frequencies, others are profoundly deaf (Petit, 2006) and may be taught to communicate by signing or require therapeutic interventions such as a cochlea implant in order to perceive speech .The level of hearing impairment may also worsen with time, progressive hearing loss being a key feature of AHL (Millan et al., 2011).

As with severity, there's a wide age range for the onset of sensorineural hearing loss. In the cases of hearing loss caused by genetic mutation, a defined onset window is often described. Mutation of *Connexin 26* (*GJB2*, DFNB1 locus) is a common cause of congenital deafness, reported to be responsible for around 50% of all congenital hearing loss cases worldwide (Denoyelle et al., 1997). Conversely, those who have mutations in *Clarin1* (Usher 3A) initially have a mild sensorineural hearing loss that progresses with age, often eventually leading to profound deafness (Joensuu et al., 2001, Adato et al., 2002), reviewed by (Bonnet and El-Amraoui, 2012). In cases where the hearing loss is due to environmental damage (e.g. ototoxia, noise damage), damage through multiple pathways to any part of the cochlea (e.g. stria vascularis, organ of Corti, hair cells, dendritic afferents, etc) can cause hearing impairment which may be permanent or recovers (Campo et al., 1997), as reviewed in (Henderson et al., 2006). However, due to the variable nature of how these insults occur there is no real way to predict the onset of hearing loss in these cases (Figure 14).

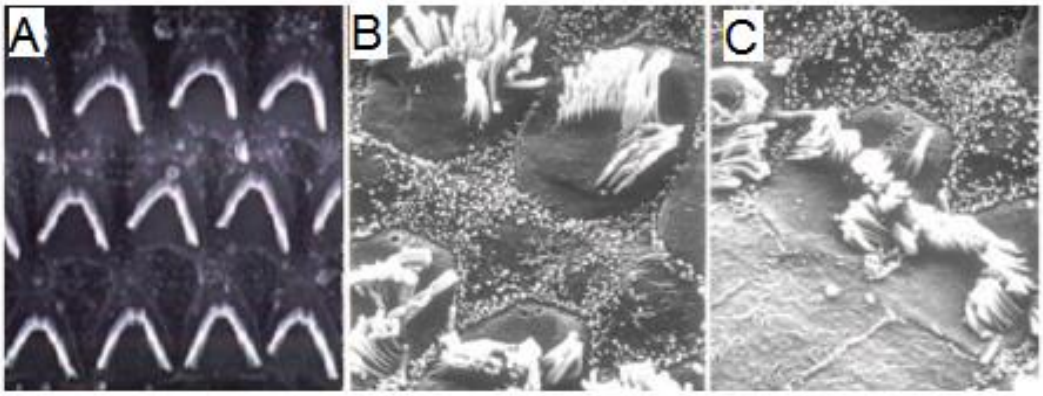

Figure 14. Noise-induced hearing loss.

A) A scanning electron micrograph of OHCs from a healthy cochlea. **B** and **C)** scanning electron micrographs of OHCs after noise exposure. B) The stereocilia appear to have splayed and are not maintaining the rigid staircase formation. C) Stereocilia appear shortened and damaged, on the left hand side of the image some stereocilia also appear to have been broken away from the cuticular plate. Figure adapted from (Henderson et al., 2006)

1.3.3 Central hearing loss

Central hearing loss is the inability to perceive speech or certain types of sound due to pathology within the brainstem or the auditory cortex. Unlike conductive or sensorineural hearing loss, the ear and cranial nerve are functional in central hearing loss (Jerger et al., 1988). However, due to the presence of lesions in specific brain areas certain noises cannot be distinguished or understood (Hain, 2003).

1.4. The mouse as a model for human disease

Mouse models are commonly used for the investigation of human disease. Comparison of the human and mouse genome suggest there is around 97% similarity of coding DNA (Mural et al., 2002), with approximately 76% of genes residing within syntenic regions in the mouse genome. Advantageously, mice are small in size, have an accelerated lifespan and can be kept in controlled environmental conditions relatively inexpensively (The-Jackson-Laboratory, 2014a). They are capable of reproduction from around 2 months of age, have fairly large litters and a relatively short gestation period (18 – 22 days depending on the strain) (Murray et al., 2010). These factors allow experiments

to be completed in a reproducible and timely manner, making the mouse an excellent research model.

Through the use of inbreeding across many generations, mice within a specific laboratory strain are considered to be genetically identical (isogenic), and differences between inbred strains are well characterised. For example C3H derived strains display adult retinal degeneration due to the *rd1* (*Pde6b*) allele (Chang et al., 2002), and multiple inbred strains (including C57BL/6N) display age-related hearing loss due to the *ahl* (*Cdh23*) allele (Johnson et al., 2000). By comparing the genome sequences available for a number of inbred strains, strain-specific single nucleotide polymorphisms (SNPs) have been identified between strains, as reviewed in (Wade and Daly, 2005). These SNPs can be used to identify the origin of DNA in outcrossed mice. Although inbred strains are considered genetically identical, it is important to note that repeated in-house breeding may lead to spontaneous mutations entering the general population of this stock and therefore differences may be detectable between strains supplied by different centres, such as the Jackson Laboratory or Charles River. For this reason inbred stocks must be systematically checked for changes in the genetic background.

There are two main approaches for generating mouse models, referred to as 'reverse genetic' and 'forward genetic'. Reverse genetic models are commonly used when a specific gene is of interest to a research question. In order to test the hypothesis, a lesion would be introduced to the gene in mice followed by testing to identify associated changes in the mouse. Conversely, forward genetics uses a random mutagenesis approach to generate mouse models of disease. Mice are induced to contain genetic lesions throughout their genome and mutants displaying phenotypes of interest are identified for further investigation. The gene containing the causative lesion can then be mapped and cloned, and the mutation further interrogated. There are benefits and limitations to both types of mouse model. Reverse genetic models have the advantage of prior knowledge of the gene, allowing for relatively fast answers to the research hypothesis proposed prior to the study. However,

traditional knock out models used for reverse genetics tend to render the protein encoded by the gene completely non-functional and this may have implications on the survival of the animals. Forward genetic models have no prior assumptions regarding the genes involved and are therefore phenotype-driven and hypothesis generating. Unlike reverse genetic models, the gene is unknown and only after identifying the phenotype is the underlying causative gene identified. (Balling, 2001) As such, the phenotype-driven approach paves the way for discovery of novel disease causing genes. N-ethyl-n-nitrosourea (ENU) is a potent chemical mutagen commonly used to induce random mutations enabling mouse mutagenesis screens. It induces many different types of mutation, for example hypomorphic, hypermorphic and neomorphic alleles (Justice et al., 1999). Compared to the targeted knock out lesions used for reverse genetics, the ENU-induced mutations may cause more subtle phenotypes and are more representative of the disease-causing mutations found in the human population. There are several disadvantages to the forward genetics approach: large numbers of animals may need to be mutagenized in order to find a model with a phenotype of interest, which is both expensive and requires significant time investment from a husbandry and phenotyping perspective. In addition to this, the models found may have lesions in genes that are already known and well characterised. At MRC Harwell, forward and reverse genetic approaches are used to complement each other for disease gene discovery, the models allowing identification and characterisation of underlying molecular pathways and associated pathologies to be studied.

1.4.1. Using the mouse to inform the human hearing pathways

The mouse is the predominant model organism for auditory research. Although the timeframe associated with development and maturation of the hearing organ is different between human and mouse, the mechanistic pathways are thought to be very similar. In addition, the adult ear shows a high degree of similarity in structure and function between the two species. The close evolutionary relationship between the mouse and human genome has allowed the study of hearing loss genes in

the mouse to inform our knowledge of the molecular pathways underlying the human auditory system (Hardisty-Hughes et al., 2010).

Since the discovery of the first known human auditory gene, the mouse has played an integral role in the identification of human deafness genes. Initially, *Myo7a* was identified as the causative gene in the mouse model, *Shaker 1*. Subsequent screening of USH1B patients found several mutations in *MYO7A*, as reviewed in (Bedell et al., 1997) and confirmed it as the causative gene. Since then mouse models of deafness have successfully identified many genes responsible for human hearing loss. *Pou4f3* (*Brn3.1)* was identified as deaf by a group who created a knock out after identifying a neural development phenotype in a close homologue *Brn3.2* (Erkman et al., 1996). Subsequently, a novel deafness locus in a syntenic region (*DFNA15*) was identified in an Israeli family, and the mutation was mapped to *POU4F3* (Vahava et al., 1998). Indeed, many human deafness genes including *MYO15* (*shaker 2* mouse model), *PAX3 (splotch* mouse model) and *MITF (microphthalmia* mouse model) were first identified in the mouse and then associated with known human deafness loci, as reviewed in (Probst and Camper, 1999). Many human orthologues of known mouse deafness genes have been shown to cause human hearing loss, making the mouse a compelling and logical model for auditory research (Petit, 2006).

1.4.2. Phenotype-driven approaches to genetic disease

There are several approaches to creating forward genetic models of disease. However, they are all saturation techniques that insert mutations throughout any part of the genome. These techniques include X-ray mutagenesis, chemical mutagenesis and insertional mutagenesis. In this section I will focus primarily on ENU mutagenesis, the form of chemical mutagenesis preferentially used at MRC Harwell to generate forward genetic models.

1.4.2.2. ENU mutagenesis

ENU mutagenesis is the predominant way of generating models of disease at MRC Harwell. ENU is a potent chemical mutagen which inserts mutations throughout the DNA of its primary target, the spermatogonial stem cells (Acevedo-Arozena et al., 2010). The chemical is an alkylating agent that transfers ethyl groups on to nucleotides, preferentially thymine, resulting in single base changes (Brown et al., 2008). The frequency of mutation insertion is predicted to be one every 1.2Mb (Quwailid et al., 2004) with the highest mutation rate detected in the pre-meiotic spermatagonial stem cells. ENU generally induces point mutations, allowing the generation of multiple allele types including, loss-of-function and gain-of-function mutations, as reviewed by Justice et al. (1999). As a point mutagen, ENU exerts an advantage over radiation induced mutagenesis, which commonly causes inversions or deletions of multiple genes making it unlikely a phenotype is due to a single gene effect, as reviewed by Balling (2001).

At MRC Harwell ENU mutagenesis is used to enable phenotype-driven screens (Acevedo-Arozena et al., 2008). The following paragraph details how mutagenized animals are generated and screened at Harwell, remembering the genetic background can vary depending on the screen being undertaken. Male C57BL/6J mice (known as Generation (G)0 or founder males) are injected with ENU which causes induction of point mutations in the DNA of their spermatogonial stem cells, making them temporarily sterile. Upon repopulation of the sperm carrying the ENU-induced mutations, G0 males are mated with wild type (WT) C3H/HeH females to produce G1 offspring. These G1 mice have a mixed genetic background (B6J/C3H) and carry ENU-induced lesions within the DNA inherited from their C57BL/6J father (Figure 15). If a mutation is dominant a phenotype will be exhibited in G1 animals. Following initial dominant screens, G1 male mice are crossed to WT C3H/HeH females to produce G2 offspring. The genomes of these mice now comprise more C3H-derived genetic material than B6J-derived material, but importantly the ENU-induced mutations inherited by the mice can only be present within the B6J-derived DNA. The G2 females from these litters can then be crossed to their G1 fathers to homozygose ENU-induced lesions in the G3 offspring. G3 animals are

phenotyped using multiple phenotyping platforms and can display recessive, semi-dominant or dominant phenotypic traits. Typical phenotyping tests may include wheel running activity tests to identify circadian rhythm disturbances, grip strength or rotarod to identify motor neuron disease, or glucose tolerance testing to identify diabetes-associated phenotypes.

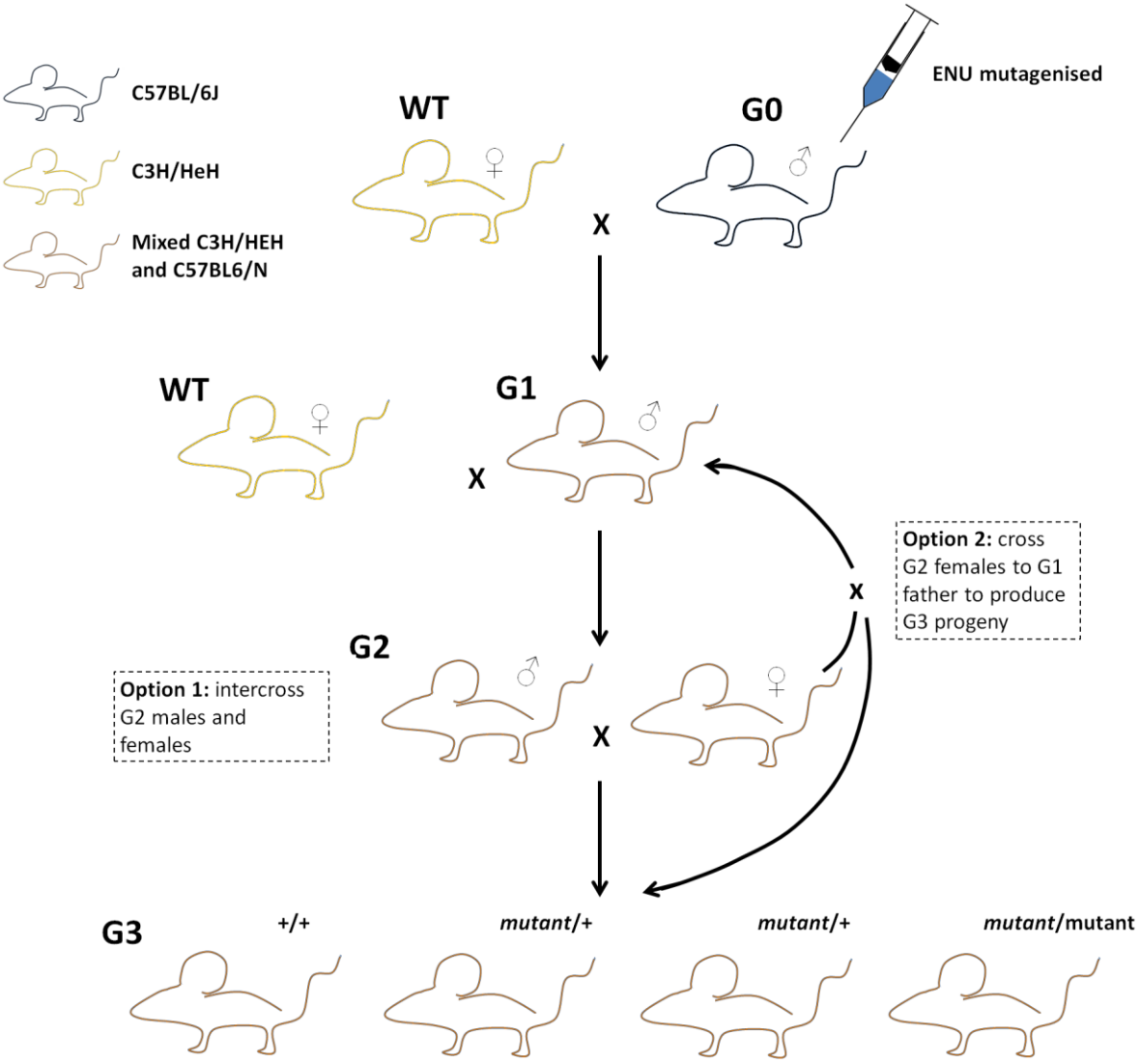

Figure 15. MRC Harwell breeding scheme to homozygose recessive ENU mutations for forward genetic screening.

Male C57BL/6J mice are injected with ENU, which induces genetic lesions in the spermatogonial stem cells after a short period of sterility. G0 males are bred to C3H/HeH WT females to produce a G1 litter. G1 mice can display dominantly inherited phenotypes. G1 males are crossed to WT C3H/HeH females to produce G2 pedigrees. G2 littermates are then intercrossed, or the G2 females are crossed to their G1 father, to produce G3 pedigrees. G3 pedigrees can display dominant, semi-dominant, and/or recessive phenotypic traits.

At MRC Harwell several platforms are used to identify auditory phenotypes, as described by Hardisty-Hughes et al. (2010). Initially animals will be assessed for their response to a sound stimuli produced by a click box – an electronic device that emits a loud (>90dB), high frequency (~20kHz) "click" tone. When administered 30cm above a hearing mouse a Preyer reflex (ear flick) and/or startle response is elicited. This response may be reduced or absent in a hearing impaired mouse. The mice are scored between 0 and 2 – '0' no response, '1' reduced response, and '2' normal response (Figure 16A).

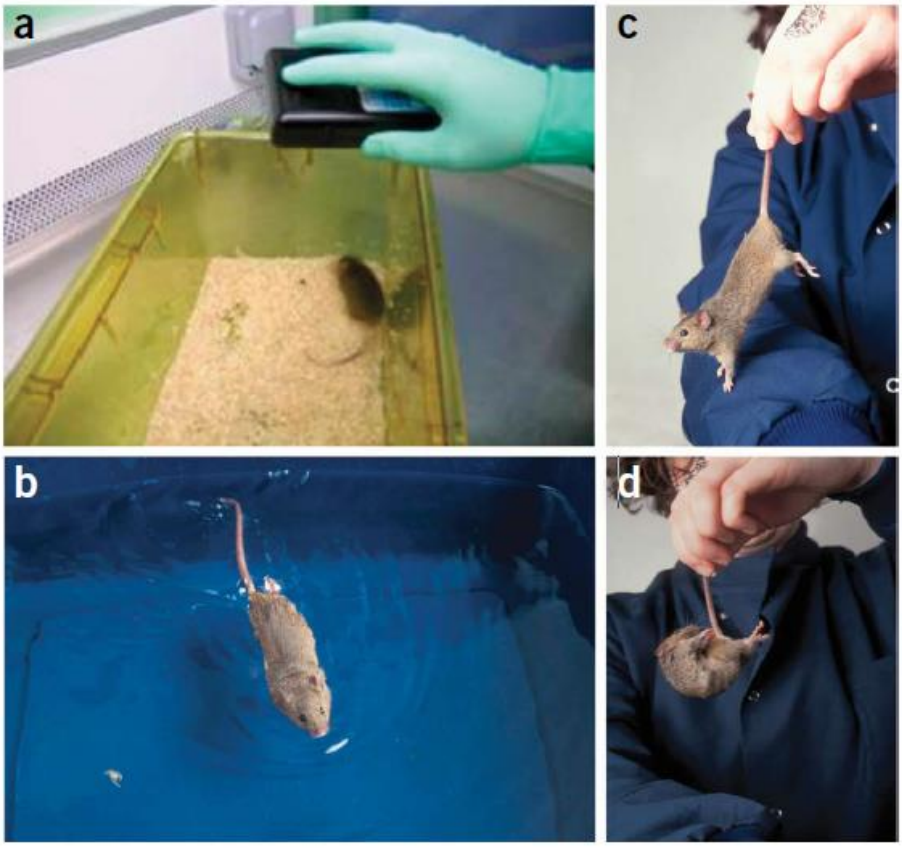

Figure 16. Non-invasive tests of hearing and vestibular function.

A) Click box test for auditory function: A mouse undergoing click box testing. The click box emits a high frequency tone which induces a Preyer reflex and/or startle response in normal hearing mice. Operators may also hold the mouse on the palm of their hand to perform this procedure in order to more easily detect a startle. **B)** Swim test for vestibular dysfunction: Mice with normal vestibular function swim in relatively straight lines, with a straight body and tail. Mice with vestibular deficits may fail to swim entirely, curl, or show abnormalities in the way they swim e.g. tumbling. **C)** Trunk curl test for vestibular dysfunction: A mouse without vestibular defects will reach towards a horizontal surface. **D)** A mouse with vestibular defects will curl, rather than reaching for the surface when suspended by their tail. Figure adapted from (Hardisty-Hughes et al., 2010).

To confirm a hearing loss phenotype identified by click box, auditory-evoked brainstem response (ABR) testing is performed (Figure 17). This test measures the electrical activity generated in the auditory nerve in response to a sound stimulus. By altering the frequency and intensity of the sound stimulus the operator can estimate the frequency-specific hearing thresholds of the mouse being tested. ABR is much more sensitive than the crude click box test, and can identify frequency-specific hearing loss and mild forms of hearing loss. During ABR testing, the animal is anaesthetised, placed in a sound proof booth, three needle electrodes are placed subdermally, sound stimuli presented to the mouse via a speaker, and electrical activity in the auditory nerve monitored and recorded. At each frequency an initial tone is presented at 95dB, which is then decreased in 5-10 dB steps until a readable trace is no longer observed. A second, independent, operator will also analyse the traces to confirm the frequency-specific hearing thresholds.

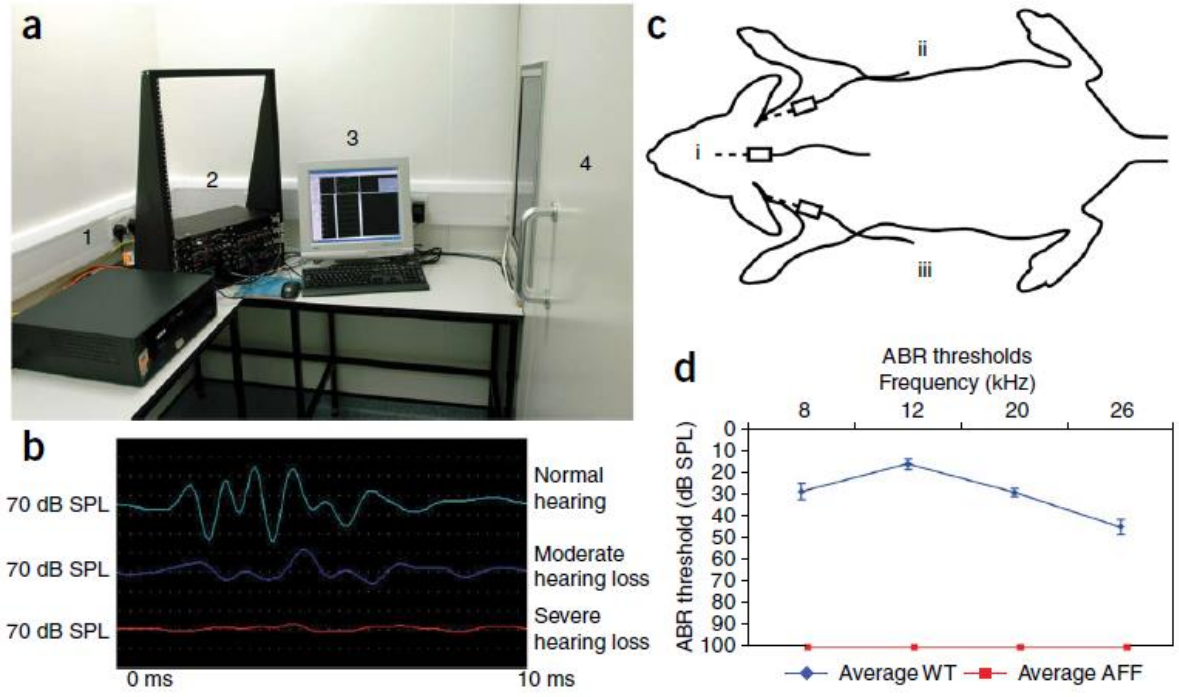

Figure 17. Auditory assessment of mice using ABR.

A) Apparatus used for ABR testing. The computer (1) is connected to the tone generating hardware (2) providing a sound stimulus to the speaker placed in the sound proof booth (4) the speaker is orientated parallel to the mouse's right ear. 3) The software depicts the trace generated. **B)** An example of a typical 12kHz trace in a normal hearing mouse, a mouse with moderate hearing loss and a mouse with severe hearing loss. In the mouse with severe hearing loss the peaks of the trace are not visible. **C)** Electrode placement for ABR assessment: i) the active electrode is placed down the mid-line of the skull, ii) the reference electrode iii) the ground electrode. **D)** An example of an audiogram showing average ABR threshold data for normal hearing (WT) and profoundly deaf (AFF) mice. Data from each frequency is mean with error bars depicting the standard error of the mean. Figure adapted from (Hardisty-Hughes et al., 2010).

To indicate vestibular defects the ability of a mouse to swim can be tested (Figure 16b). When vestibular defects are present, mice are often able to correct for balance problems using proprioceptive cues. By swimming the mouse, these proprioceptive cues are removed and vestibular phenotypes become manifest. In the swim-test mice are placed in a bath of water and the swimming is observed and reported. Mice with a vestibular deficit may exhibit abnormal behaviour including failure to swim, listing to one side and spinning/circling/tumbling. Other tests can also be used: trunk-curling - an assessment of whether a mouse will reach out for a flat surface when suspended by the tail (those with vestibular defects do not reach but instead curl their trunk, (Figure 16c and d)

and contact-righting – an assessment of whether proprioceptive pressure can convince a mouse they are upright when on their backs (normal animals ignore proprioceptive pressure and right themselves, mice with vestibular defects attempt to walk when upside down) (Hardisty-Hughes et al., 2010).

The benefit of these tests (with the exception of ABR) is that they are non-invasive and relatively quick to perform. The limitations of the click box and vestibular tests are that they are relatively crude and the results can be subject to operator bias and are therefore somewhat qualitative. However, whilst ABR testing may take up to 30 minutes per mouse, the threshold estimations are less subjective and hence are more quantitative. To maintain an unbiased assessment the ABR operator should be blinded to the animals genotype and the traces should be analysed by a second, independent, operator.

Once a phenotype is identified in a pedigree, the next step in the forward genetic screen is to identify the underlying gene that harbours the causative mutation. The mixed B6J/C3H background of the G3 animals in this screen allows mapping of the candidate interval containing the ENU-induced lesion. As previously mentioned, the ENU-induced lesion must reside within a region of DNA inherited from the original B6J G0 male. Therefore, for a recessive phenotype the affected mouse must be homozygous for B6J-derived DNA in the genomic region containing the causative mutation. In order to identify such regions genome-wide SNP genotyping is undertaken utilizing DNA from affected and unaffected littermate mice. The SNPs used are those showing strain-specific alleles between B6J and C3H. As such, we are able to narrow down candidate intervals by identifying regions where all affected animals are homozygous for B6J-derived SNPs (unaffected should not be homozygous B6J for the region containing the causative lesion). If large, or multiple candidate intervals are found, additional strain-specific SNPs can be employed to narrow the candidate interval, or DNA from additional affected and unaffected animals can be analysed. Once candidate intervals are appropriately reduced, Sanger sequencing of “prioritized” candidate genes can be

undertaken in order to identify the gene harbouring the causative mutation. This approach is relatively inexpensive, but may take a considerable amount of time to undertake.

Alternatively, with the availability of more affordable next generation sequencing (NGS) methods it is now possible to sequence the genome, or exome, of the G1 or an affected G3 mouse to identify the lesion and validate the presence of the mutation in the other affected mice (and absence in unaffected mice) in the pedigree. This sequencing technology has now made it possible to perform ENU-mutagenesis screens on inbred backgrounds as SNP mapping to identify critical regions is no longer essential.

1.4.2. Gene-driven approaches to genetic disease

Gene-driven approaches are most commonly used when a specific gene is of particular interest in a structured research question, for example they may be used to validate genes identified from phenotype-driven mouse models or human GWA studies, or to expand general knowledge of the role of individual genes in the genome. Commonly the gene in question is removed (partially, or completely) from the genome to observe the effects/phenotypes associated with loss of the gene and its encoded protein product. An animal in which a gene has been targeted for disruption/removal is called a knock out (KO). Conventional KO mice develop in the absence of the targeted gene being investigated. However, a proportion of conventional KO's (thought to be around 15%) are embryonic lethal, preventing their use in postnatal experiments. To combat neonatal lethality use of conditional and tissue-specific knockouts is often implemented, thus circumventing any embryonic lethality issues (Rajewsky et al., 1996). Another gene-driven approach for the generation of mutant mouse models is to screen DNA from ENU-mutagenized male mice to identify mutations in a gene of interest. In this section I will focus on conventional KOs, and the use of KO animals in an international phenotyping pipeline, and gene-driven screens of MRC Harwell's ENU archive.

1.4.2.1. Conventional KO

Conventional KO animals are bred to have two mutated copies of the gene of interest, preventing functional protein from being produced, known as a "knock out" or a *null*. Creating these animals is a relatively simple but lengthy process, often taking 18 months from conception of the idea to production of the KO mice.

A mutation is introduced into a DNA construct for part, or the whole, of the gene of interest. The mutation is specifically designed to be deleterious to the targeted gene. Flanking the mutation are long regions of wild type sequence. The construct also contains a selectable marker, such as a *Neo* cassette, which conveys resistance to an antibiotic. A plasmid containing the construct is electroporated into embryonic stem (ES) cells cultured *in vitro*. The construct is incorporated into the genome by homologous recombination, due to the similarity of the sequence flanking the mutation being inserted (Figure 18). The ES cells that have incorporated the mutant sequence are then selected using the selectable marker. The ES cells are then injected into blastocysts derived from a mouse line with a different coat colour to those the ES cells were derived from. This allows the use of coat colour to track the incorporation of ES cells containing the mutation, and blastocysts are implanted into a pseudo-pregnant female. When offspring are born, a chimeric coat colour indicates that the mutated ES cells have contributed to the developing blastocyst. Chimeras are crossed to WT animals and when offspring display the coat colour expected for the mouse line from which the ES cells were derived, it suggests that germline transmission of the induced mutation has occurred. To confirm germline transmission, animals are genotyped for the mutation and bred to determine that the mutation is heritable. If inheritance is confirmed the animals are bred to homozygosity to produce the KO (Silver, 1995).

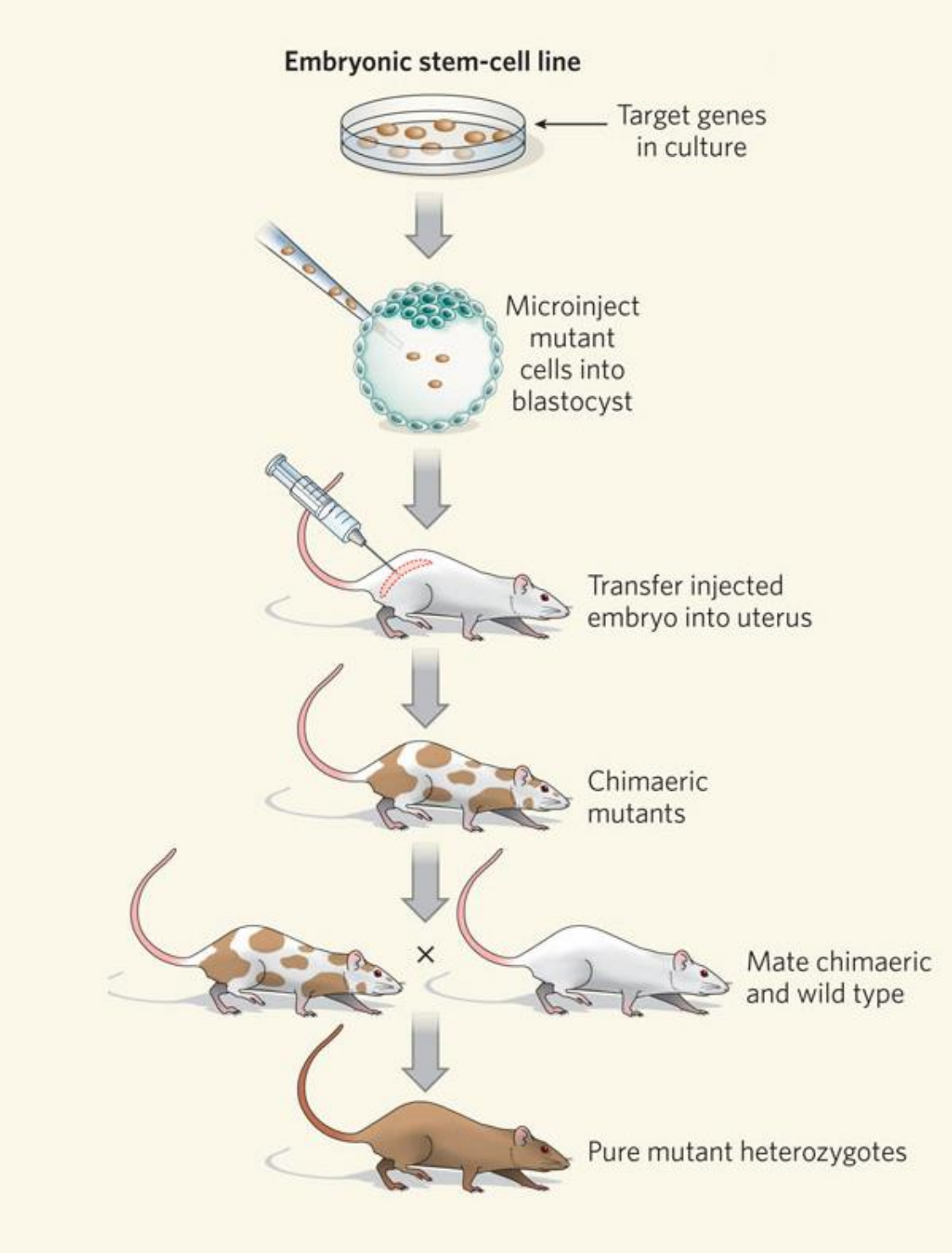

Figure 18. Generation of conventional KO mice using an embryonic stem cell line.

The mutated gene construct is packaged into a plasmid, which is electroporated into ES cells. Incorporation of the mutant construct into the genome occurs via homologous recombination, and this can be selected for using the appropriate selection marker. The selected ES cells are microinjected into a blastocyst derived from a mouse of a different coat colour and implanted into the uterus of a pseudo-pregnant female. Chimaeric pups are born and outcrossed until the coat colour of the mouse from which ES cells were derived appears, indicating these animals harbour the desired mutation. Figure adapted from (Hamra, 2010).

1.4.2.2. International Mouse Phenotyping Consortium (IMPC) – an example of a large scale gene-driven screen

IMPC is a large international project involving a multitude of murine genetics and bioinformatics laboratories across the world including centres such as the Jackson Laboratory, the Sanger and the Charles River laboratory. The long term goal of the project is to generate knock out models for 20,000 known and predicted genes in the mouse genome and characterise these knock out animals using a broad spectrum phenotyping pipeline. KO's are generated in ES cells and transplanted into pseudo pregnant C57BL/6NTac females, with subsequent offspring being used to establish colonies. As well as producing and phenotyping KO mice, MRC Harwell is a centre for data coordination, data management and reporting. All results produced by this process can be accessed at the IMPC portal (www.mousephenotype.org) and interest can be registered for specific genes or phenotypes.

In the IMPC process four alleles are possible, known as Tm1a, Tm1b, Tm1c and Tm1d (Figure 19). The Tm1a allele is in fact the starting point for all other alleles listed and is designed with a reporter gene coupled to a polyA termination sequence upstream of the critical region to prevent gene expression. From here Tm1b animals are generated by crossing Tm1a to a cre-recombinase expressing mouse, removing the *loxP* flanked *neo*-cassette and critical region creating a full conventional KO. Tm1c animals are produced by crossing Tm1a to a FLP-recombinase expressing mouse line, removing the gene trap and the promoter-driven *neo*- cassette, but leaving the critical region intact, creating a conditional potential animal. Tm1c animals can then crossed to a cre-recombinase expressing mouse line to remove the critical region, generating the Tm1d allele which is a KO lacking the gene trap and *neo*-cassette. Homozygous Tm1b animals that are viable (or heterozygous animals if homozygous lethal) are bred and enter the IMPC phenotyping pipeline with wild type littermates used as controls.

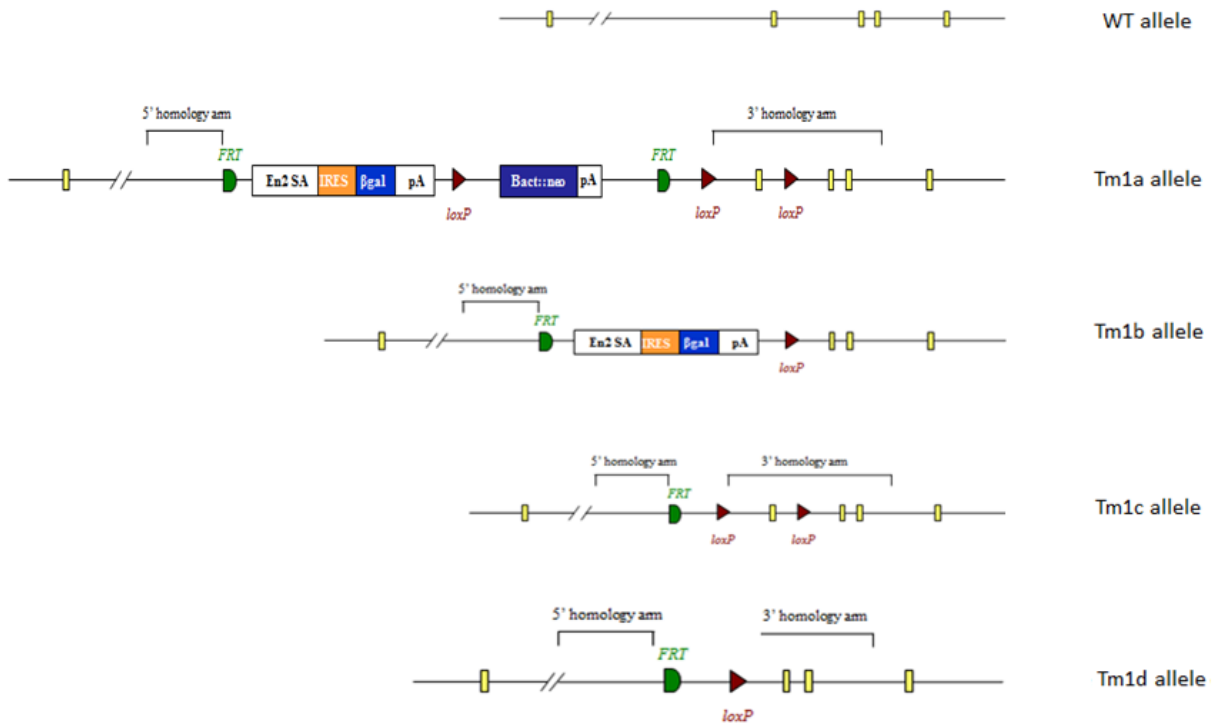

Figure 19. The IMPC alleles used for generating targeted KO animals for phenotypic screening.

IMPC plans to generate knock-out models for each of 20,000 known and predicted genes in the mouse genome. The Tm1a allele should act as a genetrap, with an encoded reporter gene and a selectable marker gene, both coupled to polyA tails, hence preventing transcription of the targeted gene. The Tm1b allele is generated by breeding Tm1a animals to a cre-recombinase expressing line, causing *LoxP* recombination and excision of the selectable marker and a critical coding region of the gene. Tm1b should function as a classical KO. Tm1c animals are generated by breeding Tm1a to a *FLP* recombinase expressing line, removing the reporter gene and selectable markers. Tm1c is a conditional KO allele expressing WT protein. When crossed to a *cre* expressing line (e.g. tissue-specific *cre*) a *LoxP*-flanked critical exon is excised. The resulting Tm1d allele is equivalent to a classical KO allele. In the IMPC pipeline, Tm1b animals undergo phenotypic screening.

The pipeline is a mixture of mandatory and non-mandatory tests conducted to standardised protocols across all centres. For each model seven males and seven females plus controls enter the pipeline. Whilst body mass is measured weekly from 4 weeks of age to 16 weeks, most other procedures (such as startle reflex, calorimetry, eye morphology) are organised in order to ensure that more severe/invasive procedures are performed at the end of the pipeline. After all in-life 16 week metrics are taken, the animals are sacrificed and a battery of post-mortem testing is

performed looking at parameters such as clinical blood chemistry, haematology and gross morphology.

The purpose of this project is to assemble a database detailing the observable effects, associated with each gene knock out, upon mouse physiology. It is hoped that the project will generate a large number of mouse models of disease, which can be used to further research in those fields. Also, novel observations may be instrumental in elaborating upon new molecular pathways in diseases processes.

1.4.2.3. The MRC Harwell ENU archive

The MRC Harwell ENU archive consists of parallel DNA and frozen sperm samples from G1 ENU-mutagenized mice, and allows for the systematic, gene-driven based screen for ENU-induced mutations (Coghill et al., 2002). Currently, the archive consists of samples from more than 10,000 mice, meaning the identification of an allelic series of mutations in a given gene is highly likely.

Upon sacrifice of the G1 animal, sperm is harvested and stored in the frozen embryo and sperm archive (FESA) at MRC Harwell, and tissues are collected (whole tail, kidney, spleen and heart) (Quwailid et al., 2004). DNA is prepared from the tissues and stored at -80^{O}C. Stocks of working DNA are stored in 96-well archive plates, with DNA from 4 animals pooled in each well.

The archive plates can be screened for mutations in specific genes using a standard Lightscanner polymerase chain reaction (PCR) (Idaho Technology Inc.) and analysed to detect variations in melting point of the amplicon caused by heterozygous mutations. Upon identifying a potential mutation, the four single DNAs from that particular pool are retrieved, and Sanger sequencing is used to determine the sequence variant and the individual G1 with the heterozygous mutation. Once identified, frozen sperm from the mouse found to harbour the mutation can be used for re-deriving the line.

The Harwell ENU archive is an important resource for gene-driven studies, not only will it identify multiple alleles of a gene, but in cases were a KO is lethal, a less 'harmful' allele may be viable and allow study of gene function *in vivo.* Alternatively, when a gene mutation has been identified following a phenotype-driven approach, the ENU archive can be screened to identify additional alleles of that gene as a means to validate it as the causative lesion. Once a second allele has been re-derived the mice can be used to compare phenotypic traits, and for generation of compound heterozygous mutants, with the original allele. If the phenotype replicates and the alleles do not complement, it is highly probable that the correct causative gene has been identified.

1.5. The *pitch* mouse model

1.5.1. Identification of the *pitch* mouse model

The *pitch* mouse model was identified at MRC Harwell during a G3 recessive pedigree screen. The initial screen used a forward genetics approach to identify mice with visual defects. However, when the PEDV/66 pedigree was observed as having an abnormal click box response the model was passed to the Deafness Models and Mechanisms team for further exploration. The model was later renamed *pitch* in reference to an observed balance phenotype.

In the G3 *pitch* pedigree 14 out of 91 animals tested had a click box response of '0.5' which is considered deaf, and a further 4 animals were scored as '1', having a reduced response. In total 18/91 (19.8%) displayed a potential hearing impairment (see supplemental information S1). When the G3 animals were outcrossed to C3H/HeH, the G4 mice did not display a hearing phenotype. However, upon intercrossing G4 mice the G5 offspring once again displayed a hearing phenotype, with 41 out of 175 (23.6%) G5 animals showing a reduced or absent click box response (see supplemental information S2). These results suggested the *pitch* mutation is a recessive allele.

To confirm the auditory phenotype, ABR testing was performed on 8-week old mice (Figure 20). Using haplotype analysis, WT, heterozygous and homozygous animals were identified within a litter of 18 animals. ABR testing showed thresholds of ≥90 decibels (dB) at all tested frequencies in *pitch* homozygotes, implying that *pitch* animals are affected by profound sensorineural deafness. In contrast, heterozygous and WT animals showed normal hearing thresholds at all tested frequencies, between 20 and 30dB.

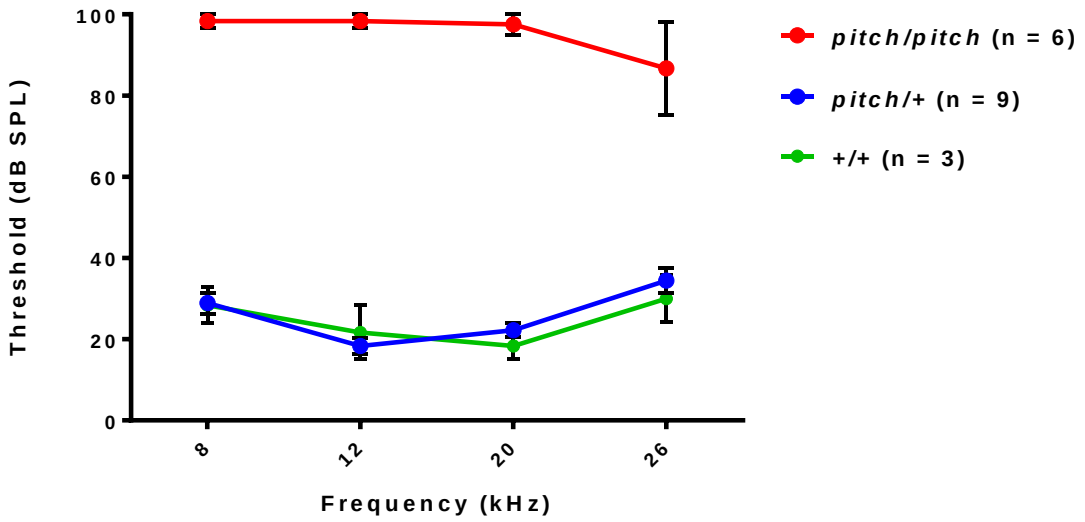

Figure 20. Auditory-evoked brainstem response thresholds of 8-week old *pitch* mice identifies a profound hearing deficit in *pitch* homozygous haplotyped animals.

Auditory evoked brainstem response thresholds were measured in *pitch* haplotyped animals at 8, 12, 20 and 26kHz. Homozygous (*pitch/pitch*) animals were found to have profound hearing loss (+90 dB) at all frequencies tested, whereas wild type (+/+) and heterozygous (*pitch/+*) haplotyped littermates were shown to have normal hearing thresholds (between 20 and 30dB). Data shown is mean, with standard error of the mean. ABR performed and analysed by A. Parker, MRC Harwell.

Affected *pitch* animals were also identified as having a late-onset head tilt phenotype, a trait often associated with vestibular defects (see supplemental information S3). In order to assess this further, *pitch* affected and unaffected littermates were swim-tested to observe their righting reflexes in the absence of proprioceptive cues. Whilst unaffected mice were able to swim normally, affected *pitch* animals were unable to right themselves and failed to swim, suggesting a vestibular defect (see supplemental information S4).

1.5.2. Mapping the causative gene

Initial mapping was undertaken using DNA from 12 G3 animals. SNP panel mapping performed by pyrosequencing revealed linkage to a candidate region of 5.13Mb on chromosome 9 between reference SNP (rs)4227685 and rs4227704. From the 75 genes in this region, several candidate genes were identified based upon known protein function and expression, such as *Radixin, Hexa* and *BBS4.* These genes were Sanger sequenced across coding exons in an attempt to find the causative mutation, however no mutations were found at this stage.

Further SNPS were designed to expand the SNP panel for this region and fine mapping was completed using an additional 21 G5 animals, reducing the candidate region down to a 1.59Mbp interval containing 25 genes (Figure 21). Within this refined region there were several candidate genes including *LoxL1, Hcn4* and *Neuroplastin*. A total of 10 genes within this region were prioritised for Sanger sequencing (Figure 21a) and from this effort a single mutation was identified in the gene *Neuroplastin.*

The *pitch* mutation was identified as a T-to-A transversion at nucleotide 943 of *Neuroplastin* (*Nptn*) (ENSMUST00000177292), causing a non-synonymous cysteine-to-serine substitution at residue 315 (Figure 21b). The Cysteine residue is highly conserved across evolution and is common to both Neuroplastin isoforms - Np65 is encoded by a longer 8 exon transcript (Cys315) and Np55 is encoded by a shorter 7 exon transcript (Cys199), skipping exon 2 that encodes Ig-like module 1 (Ig1) (Figure 21 c and d).

Genotyping confirmed that all hearing impaired animals were homozygous for this mutation, whereas all normal hearing animals were heterozygous or WT suggesting this is a recessive mutation.

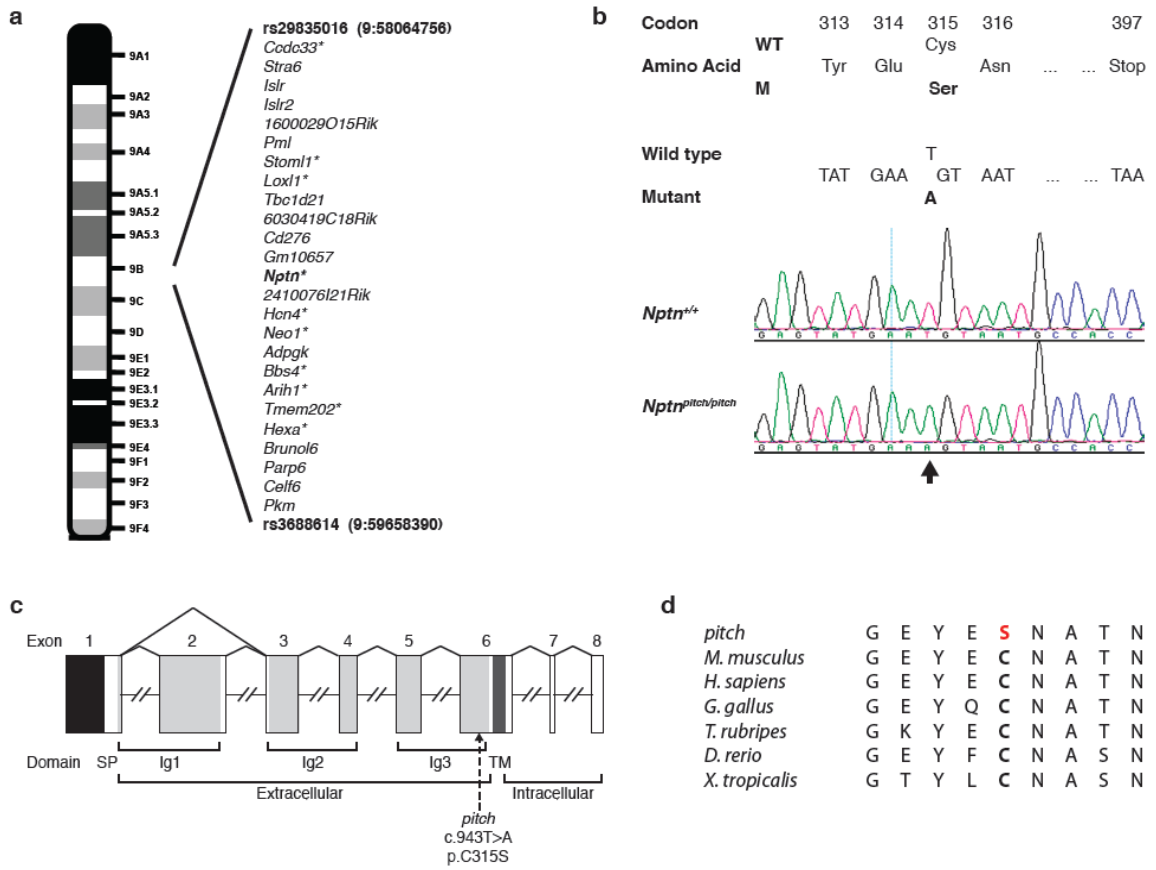

Figure 21. Mapping, identification and consequence of the *pitch* mutation.

(**a**) Ideogram showing the SNP mapped critical interval for the *pitch* mutation on chromosome 9. Prioritized sequencing of 10 (marked with an asterisk) of the 25 candidate genes in the interval was undertaken. (**b**) Detection of a *Nptn* non-synonymous mutation in exon 6 in *pitch*. DNA sequence analysis of wild type and *pitch* mice revealed an ENU-induced nucleotide transversion (c.943T>A) at codon 315, thus altering the wild-type (WT) sequence TGT, encoding a cysteine (Cys, C), to the mutant (m) sequence **A**GT**,** encoding a serine (Ser, S). Electropherograms derived from a *pitch* mutant mouse (*Nptn*$^{pitch/pitch}$) and a wild type littermate (*Nptn*$^{+/+}$) control showing the sequence surrounding *Nptn* nucleotide 943 (indicated by an arrow). (**c**) Schematic representation of the genomic structure of the *Nptn* gene illustrating the location of the mutation identified in *pitch*. The murine *Nptn* gene consists of 8 exons, spanning ~69 Kb of genomic DNA on chromosome 9. Due to alternative splicing of the gene transcript two protein isoforms are produced, Np55 and Np65. Np65 is a 397 amino acid cell adhesion molecule that contains a signal peptide sequence, three extracellular immunoglobulin-like domains (*Ig1-3*) (light grey bars), a transmembrane domain (*TM*) (dark grey bar), and a short intracellular domain. Whereas, Np55 is a 281 amino acid cell adhesion molecule that contains only two immunoglobulin-like domains (Ig2 and Ig3), lacking Ig1 due to in-frame skipping of exon 2. The location of the homozygous *Nptn* mutation identified in *pitch* is shown. (**d**) Evolutionary conservation of the structural cysteine (**C**) residue of *Nptn* altered to serine (**S**) in the *pitch* mutant. *H. Sapiens*, ENSG00000156642; *M. musculus*, ENSMUSG00000032336, *G. gallus*, ENSGALG00000001741; *T. rubripes*, ENSTRUG00000010655; *D. rerio*, ENSDARG00000043864, *X. tropicalis*, ENSXETG00000005188. Mapping performed by R. Hardisty-Hughes, G. Ball and M. Bowl, MRC Harwell. Candidate gene sequencing and subsequent verification of the mutation undertaken by M Bowl, MRC Harwell.

1.6. Neuroplastin

Neuroplastin is expressed as two splice isoforms, Np55 and Np65 (previously referred to as gp55 and gp65 respectively). Neuroplastin, Basigin and Embigin form a small family of synapse-enriched neural cell adhesion molecules (CAMs), which belong to the much larger immunoglobulin (Ig) superfamily (SF). Np55 and Np65 share two common Ig domains (Ig 2 and 3), a single membrane spanning sequence and a short hydrophobic intracellular domain (Marzban et al., 2003). Np65 has an additional Ig domain (Ig 1), which is not present in Np55 (Figure 22). The Ig1 domain is thought be required for homophilic adhesion, Np65 being able to bind homophilically in trans whereas Np55 cannot. Np65 also has a fucose α (1-2) linkage to a galactose molecule in its carbohydrate moiety, which is not present in Np55 (Smalla et al., 2000).

Neuroplastin was discovered and characterised using the monoclonal antibody Smgp65 (Kreutz et al., 2001). The splice variants were initially named due to their apparent molecular masses, 65 kDa for Np65 and 55 kDa for Np55, however de-glycosylation studies using Endo H/ PNGase F, have shown the actual molecular masses to be lower, 40 and 28 kDa respectively (Langnaese et al., 1998).

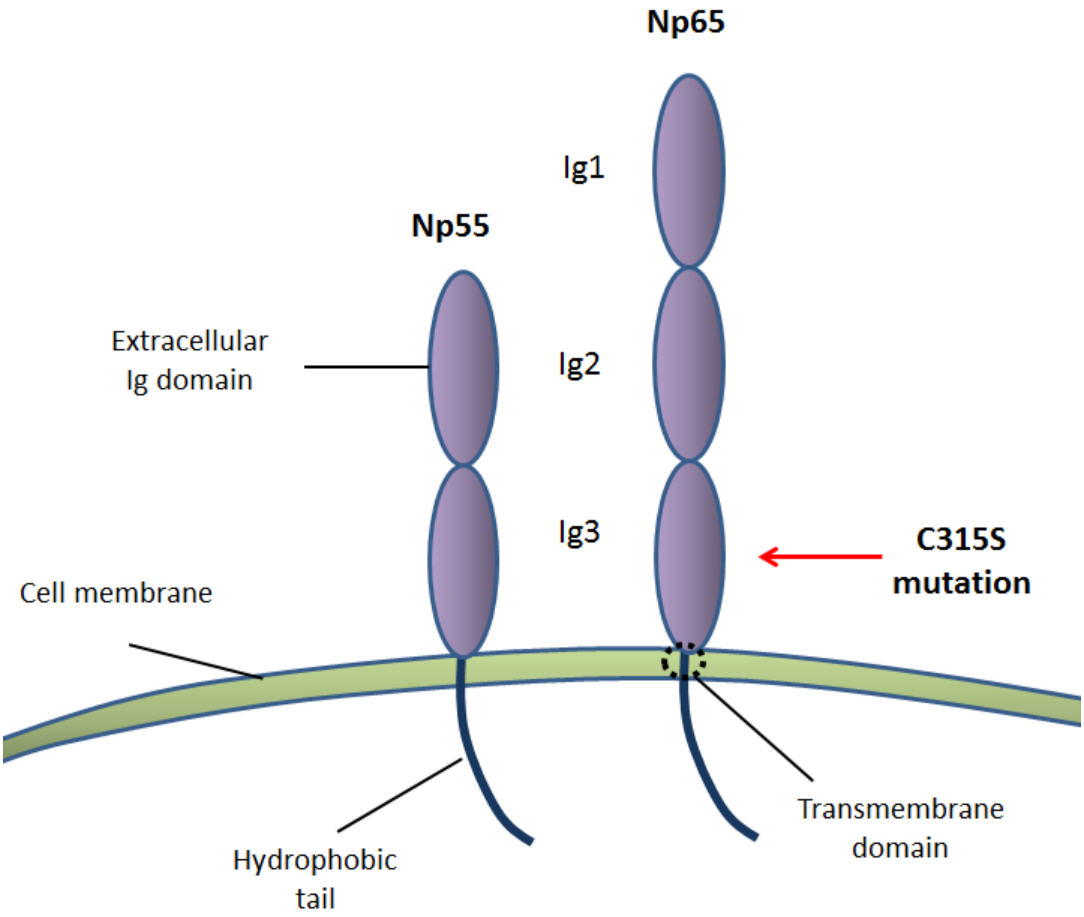

Figure 22. Neuroplastin is an alternatively spliced neural CAM, encoding extracellular Ig domains, a single membrane spanning sequence and a short hydrophobic intracellular domain.

Both isoforms contain extracellular Ig domains 2 and 3 (Ig2 and Ig3), a short membrane spanning sequence and intracellular domain. Np65 also contains an extra Ig domain (Ig1). The *pitch* mutation causes a Cysteine to Serine substitution in the common Ig3 domain (Np55 Cys199Ser, Np65 Cys315Ser).

Both protein isoforms are highly glycosylated and due to the availability of 6 glycosylation sites there are believed to be multiple glycoforms of each. Despite the similarity of the domains present and the number of glycosylation sites, the two splice variants of Neuroplastin localise differently. Np55 is expressed in a range of tissues throughout the body, including the brain, kidneys, thymus and lungs. In rat, Np55 has been shown to be present in the brain from embryonic day 14 (E14) increasing to maximal level by post-natal day (P) 12 (Owczarek and Berezin, 2012). Np65 was until recently believed to be expressed only postnatally (Langnaese et al., 1998). However, recent studies by Owczarek et al. (2011) have shown expression in the hippocampus at E19 and confirmed this by

western blot. Np65 was initially reported as being a brain specific isoform, found predominantly in post synaptic density in forebrain neurones, but also in the midbrain. More recent studies have shown both Np55 and Np65 to be present at the ribbon synapse in the plexiform layers of the retina, as well as the optic nerve, but at considerably lower levels (Kreutz et al., 2001).

1.6.1. Known functions of Neuroplastin

Neuroplastin has not previously been associated with auditory function, however previous studies have implicated roles for Neuroplastin in the brain and retina.

The neural CAMs are reported to be integral for the development and maintenance of synapses, and are reported to be involved in synaptogenesis and synaptic restructuring in the hippocampus (Kreutz et al., 2001, Buckby et al., 2004). In addition, both Neuroplastin isoforms have been implicated as mediating long-term potentiation, neurite outgrowth and synaptic plasticity (Owczarek and Berezin, 2012, Owczarek et al., 2010, Owczarek et al., 2011, Smalla et al., 2000).

Both isoforms have been implicated as activators of p38MAPK to promote long-term depression (LTD) and therefore synaptic stability; however the mechanism of action appears to differ. Np55 has significant structural similarity (77%) with fibroblast growth factor receptor 1 (FGFR1) and the two proteins were shown to bind with high affinity (K_d = 11 ± 0.11 μM). Further investigation in HEK293 cells indicated that Np55 neurite outgrowth was mediated by FGFR1 activation of p38MAPK and in the presence of a p38MAPK inhibitor neuritogenesis was abolished (Owczarek et al., 2010). Multiple studies have shown Np65 to promote LTD (Marzban et al., 2003, Smalla et al., 2000). Empson et al. (2006) reported that Np65 binding causes increased levels of p38MAPK phosphorylation at the synapse in slices of CA3 hippocampal tissue. Previous data had shown that p38MAPK inhibitors block metabotropic glutamate receptor (mGluR) mediated LTD (Bolshakov et al., 2000) and Empson et al. (2006) confirmed that the mechanism by which Np65 reduces long term potentiation (LTP) is p38MAPK-dependent accelerated loss of cell surface mGluR, specifically GluR1. Treatment with a

p38MAPK inhibitor reversed the loss of these receptors and identified a correlation between decreased LTP and increased phosphorylation of p38MAPK when Np65 had formed homophilic bonds. Empson et al. asserted that Np65 may be able to interpret homophilic binding to create a response within the cell, acting as signal trafficker and causing intracellular activation of p38MAPK.

Both Neuroplastin isoforms have been identified in the inner plexiform layer (IPL) and the outer plexiform layer (OPL) of the rat retina (Kreutz et al., 2001). Kreutz et al. observed increased Np65 expression to coincide with the formation of the synaptic ribbon at the photoreceptors. The ribbon is essential for maintaining high levels of neurotransmission to the post-synaptic bipolar cells. Np65 immunoreactivity coincided with the presynaptic marker synaptophysin in the OPL. However, in the IPL immunoreactivity was determined to be more diffuse, suggesting Np65 is involved in both conventional and ribbon synapses (Kreutz et al., 2001).

1.6.2. Implication of Neuroplastin in pathology and disease

To date, no human mutations of Neuroplastin have been identified, and mutations of Neuroplastin have yet to be shown to directly cause disease in any species. However, Neuroplastin has been associated with several pathologies including schizophrenic behaviour, depression and reduced intelligence. These associations have been made using a variety of experimental methods, such as GWA, gene expression analyses and immunohistochemistry. In this section I give a brief description of these studies and the associations made.

Neuroplastin was identified as a tumour associated antigen (TAA) for breast cancer (Rodriguez-Pinto et al., 2009). In brief, an Ig heavy chain variable domain gene cDNA library was used to assess areas of the lymph nodes from human breast cancer patients that showed B cell activation and cell proliferation. This analysis identified Ig heavy chain domain sequences which could be used as recombinant single domain antibodies in an antibody-trap assay. The antibody-trap assay was used to select proteins from tumour extracts, and identified peptides were analysed by liquid

chromatography coupled to mass spectroscopy (LC-MS). Only one protein was identified to bind specifically, and a protein database search identified this protein as Np65. Further investigation of Neuroplastin over-expressing tumours showed enhanced blood vessel formation and a highly integrated vascular network by anti-CD31 vascular staining. Also, tumours derived from cell lines transfected with Neuroplastin show a five-fold increase in vascular epithelial growth factor (VEGF) *in vivo*, evidence suggesting that Neuroplastin enhances tumour growth through an angiogenic mechanism. Subsequent investigation identified that in tumours with a higher level of Np65 isoform expression have significantly higher levels of angiogenesis and microvascular density than those expressing lower levels, reinforcing the likelihood that Np65 has a significant impact upon the ability of a tumour to metastasize.

Methamphetamine (METH) and phencyclidine (PCP) are both psychotomimetic agents that have been linked with inducing schizophrenia; causing paranoid symptoms in METH users and both the negative and positive symptoms in subjects that abuse PCP (Javitt, 2001). Serial analysis of gene expressions (SAGE) in human populations have been used to identify METH- and PCP- reactive tags that are associated with up-regulation of mRNA after acute administration of METH or PCP; amongst this group were *NEUROPLASTIN* and *BASIGIN* (Ouchi et al., 2005). Saito et al. hypothesised that if substrates underlying METH/PCP-induced psychosis are associated with a tendency towards schizophrenic behaviours, there is a likelihood that genes that have been upregulated, in the rodent expression studies, after treatment with METH and PCP, may be candidate genes for schizophrenia or modifiers of schizophrenia (Saito et al., 2006).

The minor A allele of the rs1171755 SNP, which resides 2kb downstream of Neuroplastin, has been associated with reduced cortical thickness in the left hemisphere (Desrivieres et al., 2014). Cognitive testing identified a significant association between this allele and reduced intelligence quotient (IQ) (1.81 points, 1.41 per allele for verbal and non-verbal IQ). The reduction in cortical thickness was attributed to reduced Neuroplastin expression in the brain from adolescence to early adulthood.

In their recent review of the Neuroplastins role as key regulators of neuronal plasticity and synaptic function, Beesley et al (2014) eluded to unpublished data from Wyneken et al suggesting that Np65 may play a role in depression. A preliminary study showed reduced Np65 expression at the synaptic membrane of rats after chronic stress, which could be ameliorated with treatment using Fluoxetine, a selective serotonin reuptake inhibitor (SSRI).

1.6.3. Differential expression of Neuroplastin in the brain of rats and humans

In the rat brain, Np65 is shown to be enriched in the post-synaptic density (PSD) of the forebrain, whilst Np55 is widely expressed throughout many organs. Immunoreactive studies have identified distinct differences between localisation of Neuroplastin splice isoforms between human and rat brains, suggesting a substantially different brain organisation in these regions (Bernstein et al., 2006). In rat, Np65 is highly expressed at the synaptic terminals in the hippocampus; in neuropils in the CA1 region and in the proximal molecular layer of the dentate gyrus, likely functioning as a cell adhesion molecule (Buckby et al., 2004). In human brains the highest levels of immunoreactivity was observed in the purkinje and granule cells of the cerebellum, as well as the cortical grey matter. Immunoreactivity was also observed in the hippocampus; however the high level of segregation in staining observed in rat is not present in human brain. Np55, which is the predominant splice isoform detected in rat cerebellum, could not be detected in the human cerebellum. Although localisation appears to be markedly different in human, Np65 staining was observed in pyramidal and non-pyramidal neurons with localisation at the ectomembranes of nerve cell dendrites and somata in the hippocampus, whilst in the cerebellum Np65 reactivity was present in the cell membranes of the dendrites and somata.

Significantly, in both human and rat localisation of Np65 is found at the cell membrane of the synapse. This expression pattern suggests that despite differences in brain organisation, Np65 is likely to serve a similar function between species (Bernstein et al., 2006).

1.6.4. Research aims

Based on the preliminary data gathered, I hypothesise that Neuroplastin is essential for hearing function. In order to confirm this and to elaborate upon the requirement of Neuroplastin within the mammalian auditory system I plan to undertake the following studies:

1) Establish if *Neuroplastin* is a new deafness-related gene (Chapter 3)
2) Elucidate the functional requirement of Neuroplastin in the auditory system (Chapter 4)
3) Explore additional phenotypes in Neuroplastin mutant models (Chapter 5)

Chapter 2. Materials and Methods

This chapter outlines the methodologies used for the experiments reported in chapters 3, 4 and 5. Methods performed by collaborators have been omitted from this chapter and are instead briefly described when the collaborative data is reported.

2.1. General Methods

Standard solutions were made up in accordance with Molecular cloning: A Laboratory Manual (Sambrook and Russell, 2001) or as specified by the supplier when obtained from an external source. Ultrapure double deionised (dd) RNase-free water (Milli-Q Plus) was used as standard.

2.2. Mouse Lines

All experiments on mutant animal models were performed under the designation of the following Home Office Project Licences: 30/2540 (years 2008 – 2012), 30/3015 (2013 onwards). Care and welfare of all laboratory animals was monitored in accordance with the Animals (Scientific Procedures) Act 1986. Mice were culled by a Home Office approved Schedule 1 method, namely cervical dislocation (Scudamore, 2014). Death was confirmed by cessation of heart beat and ensuring that the spine was broken.

Experiments performed on WT tissue, where littermate controls were not relevant, used tissues from a C3H.Pde6b (sighted-C3) background maintained as breeding stock by the Mary Lyon Centre (MLC), MRC Harwell (The-Jackson-Laboratory, 2014b).

2.2.1. Maintenance

Experimental animals were maintained as a heterozygous stock of a mixed C57BL/6J and C3H.Pde6b strain background, unless otherwise stipulated. The mixed background was generated to allow SNP-based genome wide mapping of ENU induced lesions, as only C57BL/6J regions of the genome may contain the causative mutation. All *Nptn*^{pitch} animals in this study were greater than 5 generations

backcrossed to C3H.Pde6b. All *Nptn*^{Y219X} animals in this study were greater than 3 generations backcrossed to C3H.Pde6b.

2.2.2. Genotyping

Genotyping was performed using several platforms, with custom assays designed as appropriate. PCR amplification followed by restriction digestion and gel electrophoresis was the preferred method of genotyping; however as neither *Nptn*^{pitch} nor *Nptn*^{Y219X} mutations lead to the creation or loss of a restriction site high resolution melting curve analysis was used to genotype these lines.

2.2.2.1. DNA extraction

Mouse ear biopsies were lysed in microcentrifuge tubes using 500µl of lysis buffer: 10ml of 1M Tris–HCl pH8, 1ml 0.5M Ethylenediaminetetraacetic acid (EDTA), 2ml 10% Sodium dodecyl sulphate (Sigma-Aldrich), 20ml 1M NaCl made up to 200ml in ddH_2O + 20mg/ml Proteinase K. Biopsies were incubated in a water bath at 55^{o}C for a minimum of two hours. Once fully digested, tubes were centrifuged for 1 minute at 14,000 rpm and the supernatant removed to fresh tubes. To precipitate the DNA 2-propanol (isopropanol) was added to the supernatant in equal parts, mixed thoroughly and centrifuged for 10 minutes at 14,000 rpm. The supernatant was removed and discarded, and the remaining pellet resuspended in 50µl of Tris-EDTA (TE) at 4^{o}C overnight. DNA was stored at -20^{o}C long term.

2.2.2.2. Retinal degeneration genotyping

Nptn^{pitch} were initially backcrossed to the C3H/HeH strain. The C3H/HeH strain carries the *Pde6b*^{rd1} allele, which causes a severe early onset retinal degeneration. To allow for retinal phenotyping of *Nptn*^{pitch} the line was crossed to the sighted-C3 strain, which does carry the *rd1* allele. To determine the *rd1* genotype of the animals a gel based assay was used, allowing for selective breeding to remove the allele from the *Nptn*^{pitch} colony.

A standard PCR was performed at 60°C for 35 cycles using the following primers, Forward – 5'-TGC AAG CAT TCA TTC CTT CGA CCT C- 3', Reverse – 5'-AGG AGG TAG CAG GCT AGC ACA TAT-3'. C3H and F1 DNA were used as positive controls, in addition to B6 DNA as a negative control and a non-template (water) control. The PCR product was digested with the restriction enzyme Dde I (New England Bioscience, NEB) for 3 hours at 37.5°C. The reaction volumes are detailed in Table 2.

Table 2. Restriction Digest Mix for *rd1* genotyping

Restriction digest mixture	Volume (µl)
Buffer 3 (NEB)	2
BSA (NEB)	2
dde I (NEB)	0.5
ddH_2O	5.5
PCR product	10

Agarose was dissolved in Tris-acetate EDTA (TAE) buffer to make a 2% solution. 10µl of ethidium bromide (10mg/ml) was added to the agarose solution whilst still warm and the gel was poured into a mould to set. Once set the digested DNA was analysed by gel electrophoresis using a Hyperladder IV running ladder (Bioline) and band size was determined by exposure to Ultra-violet (UV) light using the Gel Doc XR system (Biorad). If *rd1* positive two bands (approx. 100bp and 200bp) were visible on the gel, if *rd1* negative only the larger band was visible.

2.2.2.3. High resolution melting curve analysis genotyping

DNA from *Nptn*^{pitch} and *Nptn*^{Y219X} was quantified using a Take3 plate on the Epoch microplate spectrophotometer (Biotek). To determine the genotype, DNA was diluted to 5ng/µl and amplified in a Lightscanner (Idaho Technology Inc.) PCR then analysed using High Resolution Melt (HRM) technology.

An exhaustive asymmetric PCR assay was designed. The assay contained forward and reverse primers that bind to the genomic DNA flanking the potential mutation site. The assay also contained

a 3'blocked forward probe. The probe was designed to bind across the SNP in the mutant DNA sequence, resulting in a higher binding affinity to the mutant sequence than the WT sequence. Finally the PCR reaction contained a fluorescent dye, LC Green (Idaho Technology Inc.) that binds double stranded DNA (dsDNA). When LC green was bound to dsDNA it fluoresced strongly, however when DNA was denatured LC Green dissociated and fluorescence was only detectable at much lower levels, for a review of Lightscanner PCR see Vossen et al. (2009). Thermocycling reactions were performed using a Biorad DNA Engine Tetrad 2 peltier thermal cycler or the G-Storm GS-4 thermocycler, in both instances using the heated lid function. PCR was performed for 53 cycles at 60^{O}C, in a Framestar 96 well plate (4titude). DNA from known WT, heterozygous and homozygous mice were used as positive controls, in addition to a non-template (water) control. The composition of each reaction is detailed in Table 3. Table 4 details the oligonucleotides used to genotype *Nptn*^{pitch} and *Nptn*^{Y219X}.

Table 3. **Composition of a single PCR reaction for HRM melt curve analysis genotyping using the Lightscanner platform.**

PCR Mixture	Volume (µl)
Hotshot Master Mix (Idaho Technology inc.)	5
LC Green	1
Forward primer (20ng/µl)	0.1
Reverse primer (20ng/µl)	0.5
Forward probe (20ng/µl)	0.5
ddH_2O	0.9
DNA (5ng/µl)	2

Table 4. Oligonucleotides used for HRM melt curve analysis genotyping.

Allele	Oligonucleotide	Oligonucleotide sequence
Nptn^{pitch}	*Nptn*^{pitch} Forward primer	5'-GCT CTG GTC GCT TCT TCA TC-3'
	Nptn^{pitch} Reverse primer	5'-TGA GGA CGG TGG AAA CGG A-3
	Nptn^{pitch} Forward probe	5'-GGA GAG TAT GAA AGT AAT GCC ACC AAC TC-3'
Nptn^{Y219X}	*Nptn*^{Y219X} Forward primer	5'-TAA GCC AAG AGG TGA GGA TT-3'
	Nptn^{Y219X} Reverse primer	5'-GGC TGT ACC TTT CAC TTC AA-3'
	Nptn^{Y219X} Forward probe	5'-CGA ATA CCA GTG TGT ATA ACA TTT TGT CAG-3'

The PCR products were heated slowly from 53^{O}C to 95^{o}C using the Lightscanner and monitored to observe the point when dsDNA denatures and separates into single stranded (ss)DNA. When the DNA denatured, LC Green dissociated and a drop in the fluorescence level was observed. The fluorescence was detected by the Lightscanner and used to determine the melting curve of each PCR reaction. Software provided by the manufacturer was used to record the melting curves and identify the genotype of each sample. Homozygous samples had a higher melting temperature due to complete match of sequence and probe, WT samples had the lowest melting point due to mismatch of the mutant base pair on each strand with the probe and heterozygous samples had an intermediate melting point. When data was plotted to show normalised melting peaks the peaks for the WT sample were seen at the lowest temperature, homozygous at the highest temperature and heterozygous samples displayed two smaller peaks, one at the low temperature and one at the high temperature, representative of having one WT strand and one mutant strand (Figure 23).

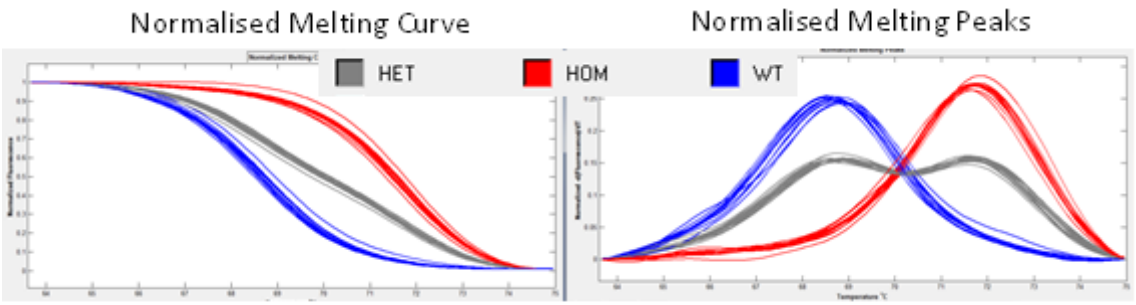

Figure 23. Genotype is determined by differences in melting point.

The probe for the PCR to genotype *Nptn*^{pitch} is designed against the mutant allele. The probe is bound to the mutant sequence more strongly, resulting in a higher melting point (illustrated in red). The curves of the heterozygous and WT (grey and blue respectively) have reduced melting points related to the number of mismatches between the probe and the alleles (1 in het, 2 in WT). Figure adapted from the Idaho Technology Lightscanner user guide.

2.3. Auditory phenotyping platforms

There are multiple phenotyping platforms available for identifying auditory phenotypes. At MRC Harwell, click box and ABR testing have been successfully implemented for phenotype-driven screening of mutant pedigrees.

2.3.1. Click box

Click box was performed as previously described by Hardisty-Hughes et al. (2010). In brief, mice were assessed on or after the onset of hearing, typically P21. Animals were removed from their home cage and placed on the operator's palm. Hearing was assessed using a purpose built frequency calibrated click box (obtained from the MRC Institute of Hearing Research, Nottingham, UK), which emits a 90dB SPL tone at 20kHz. The "click" tone elicits the Preyer reflex, a visible flick of the pinna, or a startle response in hearing mice. The absence of a response to the "click" tone is indicative of hearing impairment. The response was scored by the operator as follows: "2" – normal startle, "1" – reduced startle, "0" – no startle. To avoid operator bias testing is performed without prior knowledge of the genotype. To prevent mice in the home cage (that are yet to be tested) from becoming attenuated to the "click" tone, testing is performed away from the home cage.

2.3.2. Auditory-evoked brainstem response

ABR testing of mice was performed as previously described by Hardisty-Hughes et al. (2010). In brief, mice were injected intraperitoneally (IP) with anaesthetic containing 1 ml Ketamine, 0.5ml Xylasine, 8.5 ml sterile water, administered at the rate of 0.1ml/10 grams body mass. The mouse is placed in a heated cage until movement ceases and then placed on a heated mat in a sound proof booth. Electrodes were inserted sub-dermally as follows: the ground electrode was inserted below the right pinna, the reference electrode into the muscle mass below the left ear; and, the active electrode on the midline of the skull. The mice were placed with the auditory canal 1.5cm from the speaker and exposed to a battery of test tones before being exposed to the following experimental frequencies:

click, 8, 12, 20 and 26kHz. Brainstem response to the auditory cues were recorded using the electrodes and the Tucker Davies Technology (TDT) System III was used to calibrate, generate and process the data recorded: SigCal software was used to calibrate the system using a test file, SigGen software was used to produce the stimuli, and BioSig software presented, processed and averaged the data produced. The following equipment was used to generate the tones and record the response elicited: ED1 speaker driver, MA3 microphone amplifier, RA4PA pre-amp and RA4L1 low impedance headstage, ¼" measuring microphone 7016 kit (all ACO Pacific) and RP2.1 processor (X2), RA16 base station (Medusa). After testing the electrodes are removed and the mice were IP injected with anaesthetic reversal agent Antipamezole 0.1ml in 9.9ml sterile water, administered at rate of 0.1 ml <50g or 0.2ml > 50g. Animals were placed in a recovery cage and monitored until full recovery was made. ABR recordings were made from *Nptn*^{pitch} and *Nptn*^{Y219X} at P16, P27 and 8 weeks of age. ABR at P16 was required to be performed as a terminal procedure to comply with humane endpoints specified by the Home Office. When ABR was performed terminally, animals were culled by a Home Office approved Schedule 1 method, specifically cervical dislocation, and tissues were taken for further use.

2.4. Dissection, Tissue Collection and Storage

To investigate the role of Neuroplastin in the auditory system, it was essential to perform *ex vivo* experiments using mouse cochleae. The sensory epithelia can rapidly show signs of damage or degeneration if removal of inner ear and subsequent processing is not performed efficiently.

2.4.1. Removal of the inner ear

After death had been confirmed (described in section 2.2), mice were decapitated. The head was skinned and then scissors were used to bisect the skull.

For drop-fixed samples, the following additional steps were taken: Strong forceps were used to pull back the parietal bone and expose the brain. The brain was removed allowing access to the inner

ears. Ligaments around each inner ear were carefully pulled aside and the inner ear extracted from the skull. The bulla was removed to expose the round and oval window, which were cleared using fine dissection forceps and then ears were placed in the appropriate fixative solution.

2.4.2. Wholemount immunolabelling

Wholemount immunolabelling was performed on *Nptn*^{pitch} and sighted C3 cochlea at ages P12 - P27. Forceps were used to remove small section of bone and expose the apical cochlea sensory epithelia. The cochleae were perfused using a Plastipak 1ml syringe (BD) and a Microlance 3 25G $^{5/8}$ needle (BD) and drop-fixed in 4% paraformaldehyde (PFA) in 0.1M phosphate-buffered saline (PBS) solution, pH 7.4, on a roller for 1 hour at room temperature.

A different fixation was required for cochleae that were to be immunolabelled with a primary antibody against GluR2 (Millipore): ears were perfused and fixed in 100% methanol (Fisher Scientific) at -20^{O}C for 25 minutes, then 50% methanol in ddH_2O for 10 minutes at -20^{o}C, followed by 25% methanol in ddH_2O for 10 minutes at -20^{o}C.

Once fixed, ears were washed 3 times in fresh PBS, for 10 minutes per wash and stored at 4^{o}C until fine dissection.

2.4.3. Thick-cut vibratome sections

Thick-cut vibratome sections were cut from *Nptn*^{pitch} inner ears at P16. Forceps were used to remove bone exposing the apex. The cochleae were perfused through the round window using a 1ml syringe with a 25G $^{5/8}$ needle and drop-fixed in 4% PFA in PBS solution, on a roller for 1 hour at room temperature. The ears were washed 3 times in fresh PBS, for 15 minutes per wash and decalcified in 4% EDTA in PBS, pH 7.4, at 4^{O}C until no bone could be detected. Once decalcified, the ears were washed 3 times in fresh PBS, for 15 minutes per wash and stored at 4^{o}C until mounting.

2.4.4. Paraffin wax sections

Bisected heads were drop-fixed in 10% neutral buffered formalin supplied in ready filled pots (Leica) for 3 - 4 hours before decalcification, wax processing (Bancroft and Stevens, 1990) and sectioning by the Histology core group at MRC Harwell.

2.4.4.1. Cryosectioning of Inner ears

Cryosections were cut from inner ears of *Nptn*^{pitch} at P16, P21 and P27. Cochleae were perfused through the round window using a 1ml syringe and a 25G $^{5/8}$ needle, then drop-fixed in 4% formaldehyde (FA, Sigma Aldrich) on ice for 10 minutes. Samples were washed 3 times in fresh PBS, for 15 minutes per wash and then decalcified in 4% EDTA in PB, at 4^{O}C. Once decalcified, the samples were washed 3 times in fresh PBS, for 15 minutes per wash and incubated in 25% sucrose in ddH_2O overnight, at 4^{O}C. Samples were stored at 4^{O}C until mounting. Whole inner ears were mounted in an 8mmx20mm better electron microscopy (BEEM) capsule (TAAB Laboratories Ltd), containing TissueTek OCT compound (Sakura), and snap-frozen in isopentane (Fisher Scientific) on dry ice.

2.4.5. Inner ears for ultrastructural analyses

Ultrastructural analysis was performed using ears from *Nptn*^{pitch} and C3-sighted strain at P16, P27, P60-69, P178, and P256. The apex of cochleae were opened with forceps. Cochleae were perfused through the round window with 2.5% Glutaraldehyde in 0.1M sodium cacodylate buffer, pH7.2, using a 1ml syringe and a 25G $^{5/8}$ needle. Fixation continued in glass coc vials (Samco) for 3-4 hours at 4^{o}C. Ears were washed in 0.1M Sodium phosphate buffer 3 times, for 15 minutes per wash at room temperature and then incubated in 4% EDTA in PBS until fully decalcified. Once decalcified, the ears were washed 3 times in 0.1M Sodium phosphate buffer and stored at 4^{o}C until fine dissection.

2.4.6. Inner ears for semi-thin sectioning

Semi-thin sections were cut from *Nptn*^{pitch} ears at P16, P27 and P60. The apex of the cochleae was opened using forceps. The cochleae were perfused through the round window, using a 1ml syringe

and a 25G $^{5/8}$ needle. Whole inner ears were drop-fixed in 2.5% Glutaraldehyde (Sigma-Aldrich, G5882) in 0.05M Sodium cacodylate buffer, for 2 -3 hours at 4°C. Cochleae were perfused with 1% Osmium tetroxide (Agar) in 0.05M Sodium cacodylate, until dark colouring was observed throughout the cochlear turns. The ears were then washed 3 times, for 15 minutes per wash in 0.05M Sodium cacodylate buffer, before incubating in 4% EDTA in 0.1M Sodium phosphate buffer with 1% Glutaraldehyde until fully decalcified (approximately 7 – 10 days). Samples were then processed for resin sectioning.

2.4.7. Inner ears for RNA and qRT-PCR

RNA was extracted from *Nptn*^{pitch} and C3-sighted strain whole inner ears at P4, P8, P12, P16, P21 and P27. The round and oval windows of the cochleae were cleared and then ears were dropped into RNAlater RNA stabilisation reagent (Qiagen). Ears were stored at -70°C until use.

2.4.8. Cryosectioning of eyes

Cryosections were cut from the eyes of *Nptn*^{pitch} and C3-sighted strain at P8, P10, P12, P14, P16, P18 and P21. Death was confirmed by cessation of heart beat and ensuring that the spine was broken. The mice were then decapitated and skinned and scissors were used to bisect the head. Eyes were removed by using curved forceps to apply pressure to either side of the eye socket.

Eyes were snap-frozen in BEEM capsules containing Tissuetek OCT compound, using isopentane at -40°C. Once in the OCT compound, the optic nerve was pulled gently upwards to ensure the correct orientation for cryosectioning. The embedded eyes were stored at -20°C until sectioning by the Histology core group at MRC Harwell. In brief, the samples were mounted on the cutting chuck of the cryostat using OCT; 5µM sections were cut and laid on slides to adhere at room temperature, before refreezing to maintain structural integrity.

2.5. Cell lines, maintenance and plating

All cell culture experiments were completed using Cos-7 (Gluzman, 1981) and HEK293 cell lines (Harrison et al., 1977). Cells were incubated at 37^{o}C, 5% CO_2, in T75 tissue culture flasks (Greiner). The following growth media (referred to as complete media) was used to maintain the cells for optimal growth:

- Gibco Dulbecco's Modified Eagle Medium with L Glutamine (DMEM, Life Technologies) – 500ml
- Foetal Calf Serum (FCS, Life Technologies) – 50ml
- Penicillin/Streptavidin solution (Pen/Strep, Life Technologies) – 5ml

2.5.1. Splitting cells

At 70 – 85% confluence cells were split. The growth media was removed, and the flask carefully washed with 5ml of Gibco Dulbecco's PBS (Life Technologies). The PBS was removed and the cells were trypsinised using 2mls 0.05% Trypsin EDTA (Life Technologies) for 3 – 5 minutes at 37^{o}C, 5% CO_2. The T75 flask was tapped (in the case of the Cos 7's quite aggressively) to release the cells from the adherent surface and the trypsin EDTA was neutralised using 8ml growth media. After thorough mixing 3ml of the cell suspension was removed to a fresh T75 flash containing 12ml growth medium.

2.5.2. Cell counting for plating

Cells were washed, trypsinised and neutralised as described in section 2.5.1. 20µl of cell suspension was counted using an improved Neubauer single cell counting chamber (Hawksley), whilst the remaining cell suspension was centrifuged at 3000 rpm for 2 minutes to pellet the cells.

2.5.3. Plating cells for *in vitro* protein studies

The supernatant was removed from the pelleted cell suspension, and the cells were resuspended in 10ml of complete media using a Pasteur pipette. The cell suspension was diluted in fresh complete media to obtain 1.5 x 10^5 cells/ml and then seeded in 6 well plates (2ml/well).

2.5.4. Plating cells for cellular expression studies

The supernatant was removed from the pelleted cell suspension, and the cells were resuspended in 10ml of complete media using a Pasteur pipette. The cell suspension was diluted in fresh complete media to obtain 1.5 x 10^5 cells/ml. High performance #1,5 coverslips (0.17mm ± 0.0005mm, Zeiss) were dipped in ethanol and flamed to sterilise. Once completely dry, single coverslips were placed in each well of a 6-well plate, using anti-capillary T588 cross-over tweezers (Agar). The cell suspension was seeded on top of the coverslips, 2ml per well, ensuring that the coverslips remained at the bottom of the well.

2.6. Generation of WT and *Nptn^{pitch}* constructs

WT and *Nptn^{pitch}* Myc- and EGFP-tagged constructs were generated for *in vitro* expression studies. Constructs corresponding to both the short, Np55, and the long, Np65, isoforms of Nptn were generated. The sub-cloning strategy had 4 main steps, illustrated in Figure 24.

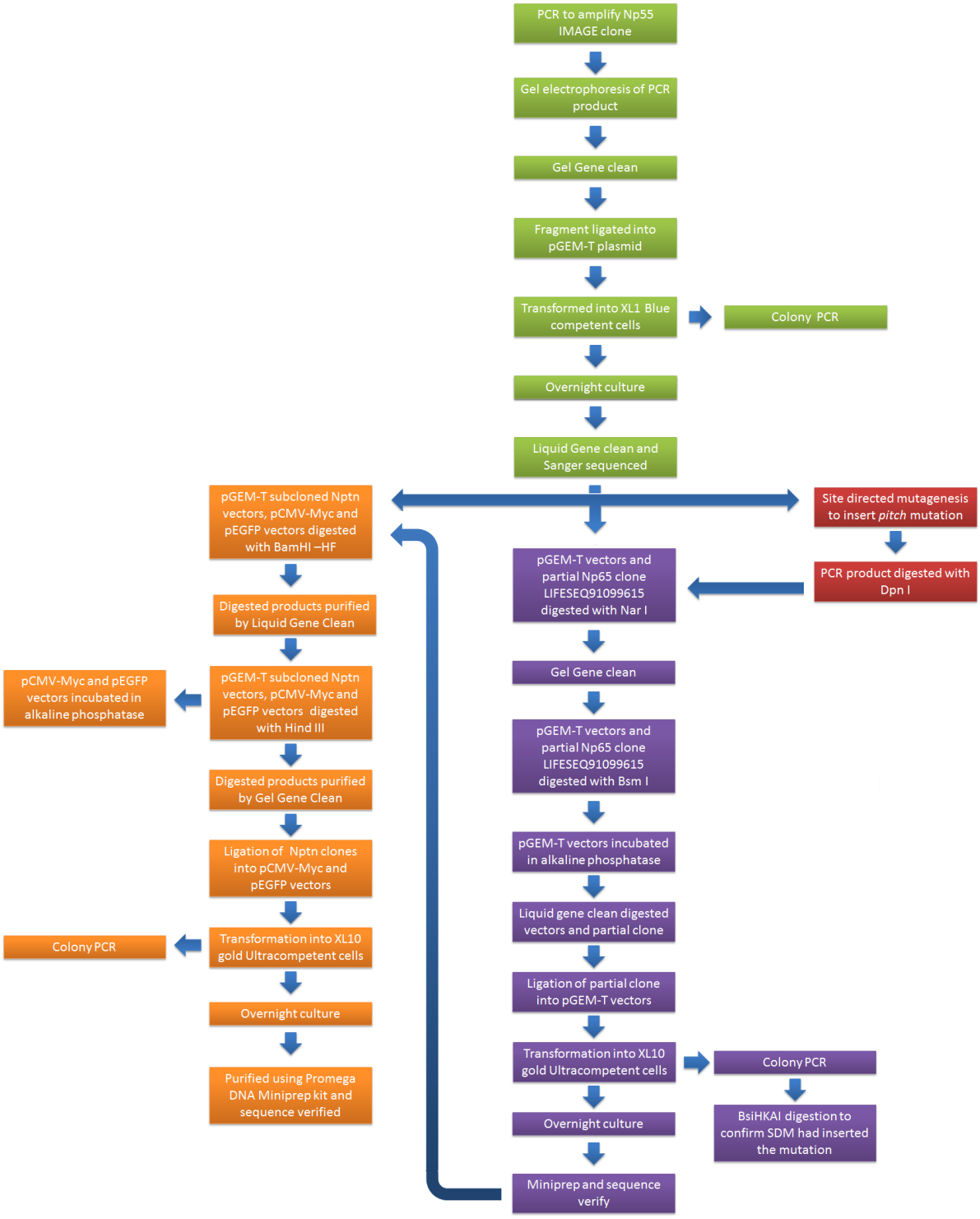

Figure 24. Sub-cloning strategy for generation of WT and *pitch* Myc- and EGFP-tagged constructs.

The protocol illustrated in green details the initial amplification and insertion of an Np55 IMAGE clone into a pGEM-T vector. The protocol detailed in red describes the process of site directed mutagenesis to introduce the *pitch* mutation to pGEM-T vector containing WT Np55. The protocol illustrated in purple details the conversion of Np55 WT and *pitch* constructs into Np65 WT and *pitch*. The protocol illustrated in orange details the insertion of WT and *pitch* Np55 and Np65 clones into Myc- and EGFP-tagged vectors.

2.6.1. Cloning and insertion of Np55 into a pGEM-T vector

The steps to insert Np55 into a pGEM-T vector are illustrated by the green panels in Figure 24. As a full length commercial clone was not available for Np65, both the Np55 and Np65 WT and *pitch* constructs were generated using an Np55 image clone as a template.

2.6.1.1. Amplification of Np55 from a commercial clone

Np55 IMAGE clone, hs6163693, was purchased from Life Technologies and used as a template to generate copies of Np55 by PCR. PCR primers were designed to amplify full length Np55, excluding the stop codon. The primers were also designed to contain a restriction site which overlapped the end of the target sequence in order to easily excise the full length DNA insert later using a restriction digest. PCR was performed for 30 cycles at 65^{o}C, using the oligonucleotides in Table 5.

Table 5. Oligonucleotides used for amplification of Np55 from a commercial IMAGE clone.

Oligonucleotide	Oligonucleotide sequence
Forward-HindIII	5'-ACA AGC TTG ATG TCG GGT TCG CTG CCC AGC-3'
Reverse – BamHI	5'-GTG GAT AAT TTG TTT TCT CTG GCG CAA G-3'

2.6.1.2. Gel electrophoresis and purification of the PCR product

The amplified fragment was excised from a 1% Agarose gel following electrophoresis. The DNA fragment was purified using the gel based protocol for the GeneClean kit (MP Bio) following the manufacturer's instructions.

2.6.1.3. Ligation of the Np55 fragment into pGEM-T vector

The purified fragment was ligated into a pGEM-T vector using the reaction mixture described in Table 6. The ligation reaction was incubated for 2 hours at 16^{O}C.

Table 6. Ligation mixture for insertion of cloned DNA into digested plasmid vector.

	Volume (µl)		
Reagent	**Clone**	**Positive control**	**Negative control**
Cloned DNA	1	0	0
T4 DNA ligase (NEB)	1	1	1
10 x Ligase buffer (NEB)	1	1	1
Gene cleaned pGEM-T vector	0.5	0.5	0.5
ddH_2O	6.5	6.5	7.5
pUC18	0	1	0

2.6.1.4. Transformation into XL1 blue cells

2µl of ligation reaction was incubated for 30 minutes with 100µl XL1 Blue competent cells (Agilent) in 14ml BD Falcon polypropylene tubes. The tubes were heat shocked for 45 seconds at 42^{O}C before chilling on ice for 2 minutes. 200µl of 37^{O}C super optimal broth with catabolite repression (SOC) media was added to each tube, which were incubated (shaking) at 37^{O}C for 1.5 hours, 225 rpm. 100µl of cells were plated on Ampicillin 50 Luria-Bertani (LB) agar plates and incubated at 37^{O}C overnight. XL1 Blue competent cells were used in order to identify whether the plasmid had recombined with itself (blue colonies) or incorporated the DNA insert (white colonies).

2.6.1.5. Colony PCR

White colonies were picked and resuspended in 100µl LB broth (small culture). PCR was performed to ensure that the DNA insert was still present and of the expected mass (1.2kb), as described in Table 7. T7 and Sp6 sequences flank the insert in pGEM-T. PCR was performed for 30 cycles at 50.9^{o}C and the products were analysed by electrophoresis on a 2% agarose gel.

Table 7. Colony PCR mixture for identification of insert size in a pGEM-T plasmid vector.

Colony PCR mixture	Volume (µl)
1.1x Reddymix (Thermoscientific)	20
T7 primer	0.75
Sp6 primer	0.75
Small culture	2.5

2.6.1.6. Overnight cultures

20µl of the small culture (described in 2.6.1.5) was transferred into 20ml of LB broth containing 40µl of Ampicillin 50 to create a large culture. The large culture was shaken overnight, at 37^{O}C.

2.6.1.7. Purification and creation of glycerol stocks

Glycerol stocks were made as a precaution and in the event that experiments failed downstream this stock could be returned to. 750µl of the large culture was added to 250 µl of 80% Glycerol and stored at -70^{O}C.

The remaining large culture was purified using the Promega DNA miniprep kit, following the manufacturer's instructions.

2.6.2. Site directed mutagenesis

Site directed mutagenesis (SDM) was used to generate *Nptn*^{pitch} from the WT Np55 clone. The SDM protocol is illustrated by the red panels in Figure 24. The Quikchange Lightning kit was used as according to the manufacturer's instructions (Agilent). Briefly, the WT Np55-pGEM-T plasmid was used as a template and amplified using complementary oligonucleotides that contain a mismatch corresponding to the *pitch* mutation. PCR was performed at 60^{O}C for 18 cycles, with the primers detailed in Table 8.

Table 8. The oligonucleotides used to insert the *pitch* mutation into WT Np55 using SDM.

Oligonucleotide	Oligonucleotide sequence
Forward	5'-GTG GGA CCG TGC TCG GAA GCG CCG-3'
Reverse	5'-CGG CGC TTC GGA CCG TCC CAC-3'

The plasmids were incubated with Dpn I for 5 minutes at 37^{O}C. Dpn I digests the methylated and hemi-methylated parental DNA, leaving only the PCR amplified DNA which contains the *pitch* mutation remaining (Figure 25).

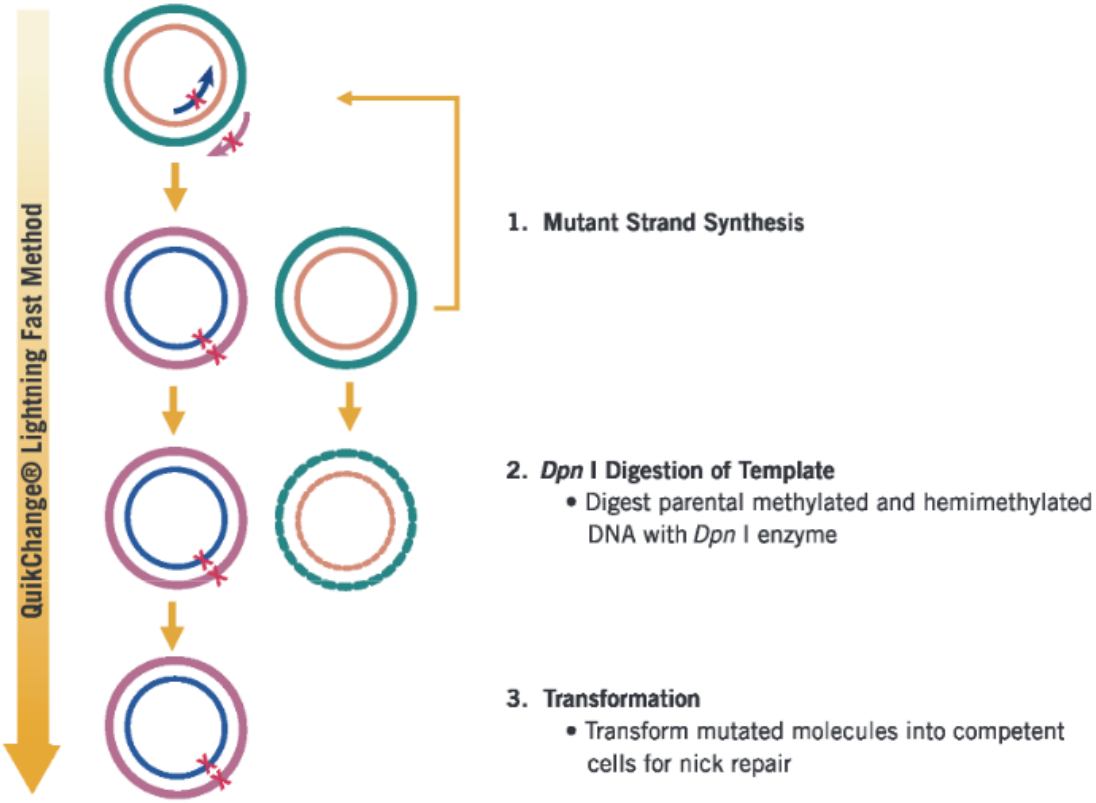

Figure 25. Overview of the Quikchange Lightning SDM method.

Figure was adapted from http://www.chem.agilent.com/library/usermanuals/Public/210518.pdf.

2.6.3. Generation of an Np65 clone

As no full length Np65 commercial clones were available, Np65 clones were created using a partial template for Np65 (containing the correct sequence for exon 2) and the WT and *pitch* Np55-pGEM-T plasmids (generated in sections 2.6.1 and 2.6.2 respectively). The protocol for creating the Np65 clone is illustrated by the purple panels in Figure 24.

A partial clone of Np65 LIFESEQ91099615 was purchased (Open Biosystems). As exon boundaries for exon 1-2 and exon 2-3 do not form restriction digest sites, restriction sites were instead identified within exon 1 and exon 3 that were close to the exon boundaries, Nar I and Bsm I (NEB). The partial clone and the WT and *pitch* Np55-pGEM-T plasmids were sequentially digested and purified as follows:

1. Digested with Nar I in Buffer 2 (NEB), at 37^{O}C for 1 hour
2. Gel electrophoresis and gel Gene Clean, as described in section 2.6.1.2
3. Digested with Bsm I in Buffer 2, at 37^{O}C for 3 hours
4. WT and *pitch* Np55-pGEM-T digested plasmids incubated with alkaline phosphatase (NEB) in Buffer 2, for 1 hour at 37^{O}C to prevent self-ligation
5. Purification of digested fragments using the liquid protocol of the Gene Clean kit, as according to the manufacturer's instructions

2.6.3.1. Ligation of the partial clone fragment into WT and *pitch* Np55-pGEM-T plasmids

The fragment from the partial clone was ligated into the sequentially digested WT and *pitch* Np55-pGEM-T plasmids to create vector containing Np65 WT and *pitch.* Ligations were performed for 2 hours at 16^{O}C, using the ligation mixture detailed in Table 9.

Table 9. Ligation reaction mixture for inclusion of the Np65 partial fragment into the Np55-pGEM-T plasmids.

	Volume (µl)	
Ligation reaction mixture	**Clone**	**Control**
Np65 partial clone fragment	1	0
WT or *pitch* Np55-pGEM-T plasmid	0.5	0.5
T4 DNA ligase	1	1
10x Ligase buffer	1	0.5
ddH_2O	6.5	7.5

2.6.3.2. Transformation into XL10 gold Ultracompetent cells

2µl of ligation reaction was transformed into 100µl of XL10 gold Ultracompetent cells, using the protocol described in section 2.6.1.4.

2.6.3.3. Colony PCR

Self-ligation cannot be conferred from the colours of XL10 gold colonies, therefore colony PCR was essential to identify if the partial clone fragment had inserted into the Np55-pGEM-T vectors. Colony PCR was performed as described in section 2.6.1.5 with the following modification: The PCR products were digested with BsiHKAI for 1 hour at $65^{O}C$. If SDM had worked correctly a BsiHKAI restriction site would have been introduced. If two bands were observed by gel electrophoresis it confirmed SDM had worked, however one band indicated failure of SDM.

2.6.3.4. Overnight cultures

Overnight cultures were performed as described in section 2.6.1.6.

2.6.3.5. Purification and generation of glycerol stocks

The plasmids were purified and glycerol stocks were made as described in section 2.6.1.7.

2.6.4. Insertion of WT and *pitch* Np55 clones into pCMV-Myc and pEGFP vectors

To express WT and *pitch* Np55 and Np65 in mammalian cell lines, the DNA was digested from the pGEM-T vector and inserted into pCMV-cMyc and pEGFP-N1 (gifts from Chris Esapa and Mike Bowl

respectively). These plasmids were chosen as they contained reporter tags, which could be used to detect protein expression *in vitro.* The steps associated with this protocol are depicted by the orange panels in Figure 24.

2.6.4.1. Sequential digestion of Np55 and Np65-pGEM-T, pCMV-Myc and pEGFP plasmids

A sequential restriction digest with HindIII and BamHI (both supplied by NEB) was performed to remove the full length Np55 and Np65 inserts from the pGEM-T plasmids. pCMV-cMyc and pEGFP were also sequentially digested in order for the DNA sequences to be inserted. Sequential restriction digests were performed as follows:

1. Digested with BamHI-HF in buffer 4, at 37^{o}C for 1 hour
2. Digested products purified using the Liquid Gene Clean protocol
3. Digested with HindIII in buffer 2, at 37^{O}C for 1 hour
4. pCMV-cMyc and pEGFP incubated with alkaline phosphatase in buffer 2, for 60 minutes at 37^{o}C
5. Gel electrophoresis and purification using the Gel protocol for the Gene Clean kit, as described in section 2.6.1.2.

2.6.4.2. Ligation of *pitch* and WT Np55 and Np65 into the reporter tagged plasmids

The purified Np55 and Np65 (WT and *pitch*) DNA was ligated into the pCMV-cMyc and pEGFP for 2 hours at 16^{O}C, using the ligation mixture detailed in Table 10.

Table 10. Ligation Mixture for the insertion of WT and *pitch* Np55 or Np65 into a tagged reporter plasmid.

	Volume (µl)	
Ligation Mixture	**Clone**	**Control**
cloned DNA	1	0
pre-digested reporter plasmid	0.5	0.5
T4 DNA ligase	1	1
10x Ligase buffer	1	0.5
ddH_2O	6.5	7.5

2.6.4.3. Transformations, Colony PCR and Overnight cultures

Transformations into XL10 gold cells were performed as described in section 2.6.1.4. Colony PCR was performed as described in sections 2.6.1.5 and 2.6.3.3 with additional modifications: PCR was performed for 30 cycles at $59^{O}C$. T7 and Sp6 primers were used for the pCMV-cMyc plasmid, whilst the primers used for pEGFP are detailed in Table 11.

Table 11. Oligonucleotides used to confirm the correct insert size in pEGFP.

Plasmid	**Oligonucleotide**	**Oligonucleotide sequence**
pEGFP-N1	Forward- EGFP-N1	5'-GTC GTA ACA ACT CCG CCC-3'
	Reverse - EGFP-N1	5'-GTC CAG CTC GAC CAG GAT G-3'

Overnight cultures were performed as described in section 2.6.1.6.

2.6.4.4. Purification, sequence verification and storage

The plasmids were purified using the Promega DNA miniprep kit and Sanger sequenced. The plasmids were stored at $4^{O}C$.

2.7. Protein expression studies

To assess the implications of *pitch* on Neuroplastin protein, *in vitro* analyses of protein expression were completed using the plasmids generated in section2.1.

2.7.1. Transient transfections

Transfections were undertaken using a polyethylenimine (PEI) approach. Cells were seeded as described in section 2.5.3. 1µg of construct per well in 100µl 150mM NaCl solution (Polyplus transfection) was added to 6µl of JetPEI® (Polyplus transfection) in 100µl 150mM NaCl solution for 15 minutes at room temperature. A total volume of 200µl of solution was carefully pipetted in individual drops, into each well. Plates were agitated gently to distribute the solution and incubated at 37^{O}C, 5% CO_2.

2.7.2. Cell lysis

Forty eight hours post-transfection, cells were washed 3 times in Dulbecco's PBS and lysed in 150µl of 1x Glycoprotein denaturing buffer in ddH_2O (Life Technologies). A cell scraper was used to ensure full lysis of the protein from the cells, and the protein lysates were collected into 1.5ml PCR tubes on ice.

2.7.3. Lysate denaturation and PNGase F treatment

Lysates were incubated at 94^{O}C for 10 minutes to denature. Lysates were split into two aliquots; the first aliquot was treated with PNGase F (Life Technologies), an amidase that removes N-linked glycans, in order to assess the status of protein processing in WT and *pitch* Nptn. The second aliquot was treated as a control and received a sham detail. The reactions were setup as described in Table 12 and all reagents were supplied by Life Technologies. Reactions were incubated at 37^{O}C for 2 hours and if not being used immediately the treated samples were stored at -70^{O}C. Untreated lysates were stored at -70^{O}C for future use.

Table 12. PNGaseF enzyme digest used to remove n-linked glycans from whole cell lysates. Whole cell protein lysates (generated from cells transfected with WT and *pitch* mutant constructs and untransfected cells) were divided into two aliquots. One sample was treated with PNGase F (tube 2, 4, 6) whilst the other sample (tube 1, 3, 5) was sham-treated under the same conditions. Comparison of the lysates by Western blotting allowed direct comparison of glycosylation levels

		Tube 1	Tube 2	Tube 3	Tube 4	Tube 5	Tube 6
37µl	Denatured protein lysate	Nptn-EGFP WT	Nptn-EGFP WT	Nptn-EGFP Mut	Nptn-EGFP Mut	Untransfected	Untransfected
5µl	10x NP-40	✔	✔	✔	✔	✔	✔
5µl	10x G7 buffer	✔	✔	✔	✔	✔	✔
2µl	PNGase F enzyme	-	✔	-	✔	-	✔
4µl	ddH_2O	✔	-	✔	-	✔	-

2.7.4. Western blotting using PNGaseF and sham treated whole cell lysates

To prepare the samples for Western blotting the following were added: 20µl NuPage LDS sample buffer (Life Technologies), 8µl NuPage antioxidant (Life Technologies) and 2µl ddH_2O. The samples were incubated at $70^{O}C$ for 10 minutes and cooled on ice. Lysates were loaded into NuPage Bis-Tris 8 – 12% precast gel (Life Technologies) and run at 200V constant for 60 minutes in 1 x MES buffer (Life Technologies) as per manufacturer's instructions. The gel was transferred onto a Novex pre-cut nitrocellulose membrane (Life Technologies) for 1 hour at 30V, then blocked for an hour at room temperature in 5% milk powder in 0.1% tris buffered saline-Tween (TBS-T).

2.7.5. Probing and development of Western blots

Blots were incubated with primary antibodies against the vector tag that was attached to Nptn; Rabbit anti-cMyc (1:1000, Santa Cruz), Rabbit anti-EGFP (1:1000, Santa Cruz) diluted in 5% Marvel in TBS-T and incubated for 1 hour at room temperature. Blots were washed for 2 x 5 minutes in TBS-T

and then re-blocked in 5% Marvel in TBS-T for 2 x 5 minutes. Blots were incubated in goat anti-rabbit horse radish peroxidase (HRP) conjugated antibody (1:6000, Biorad) for 1 hour at room temperature then washed thoroughly for 5 x 5 minutes in TBS-T to remove any trace unbound secondary antibody. Blots were developed by enhanced chemiluminescence (ECL) using the Pierce ECL plus kit (Thermo Scientific) for 1 minute at room temperature, wrapped in cling film to prevent the blot from drying. The blot was visualised by exposure of the membrane to Amersham Hyperfilm, using a light tight Amersham Hypercassette (GE Healthcare). Blots were exposed to the film for varying lengths of time and developed using an X-ray developer. Films were aligned with the original Western blot and the ladder marked on to the film in order to determine size.

Separate blots were also probed with antibodies against Nptn and Np65, however these antibodies were found to not be suitable for Western blotting. Controls were performed in the absence of primary antibody to assess non-specific binding of the secondary antibody.

2.7.6. Stripping and re-probing Western blots

Antibody was stripped from the blots using the following buffer for 30 minutes at room temperature: 15g glycine, 1g SDS, 10ml Tween 20 made up to 1L with ddH_2O and adjusted to pH 2.2. Blots were then washed for 2 x 5 minutes in PBS, then 3 x 5 minutes washes in TBS-T. The blots were re-probed using Rabbit anti-beta actin (1:1000, Santa Cruz) as per the original primary antibody step in 2.9.5 and subsequent wash steps, secondary antibody and development were repeated.

2.8. Protein localisation studies

In order to determine the *in vitro* subcellular localisation of WT and mutant Neuroplastin protein the EGFP- and Myc- tagged Np55 and Np65 WT and mutant constructs were transfected into Cos7 and HEK293 cells.

2.8.1. Transient transfections

Transfections were undertaken using a linear PEI derivative. Briefly, 1µg of construct per well in 100µl of 150mM NaCl solution was added to 6µl of JetPEI in 100µl of 150mM NaCl solution for 15 minutes at room temperature. Post incubation the solution was carefully pipetted on to the surface of a seeded coverslip, as described in section 2.5.4. Plates were agitated gently to distribute the solution and incubated at 37^{O}C, 5% CO_2 for 48 hours post-transfection.

2.8.2. Fixation and immunolabelling

Forty-eight hours post-transfection media was removed from the wells and the cell-coated coverslips were washed gently with ice cold PBS for 3 x 5 minutes in the wells. The final PBS wash was removed and the cells were fixed with ice cold 4% PFA for 10 minutes. Cells were washed for 3 x 5 minutes in PBS and then permeabilised using 0.5% Tween-20 in PBS for 10 minutes at room temperature. Cells were blocked in blocking solution (10% goat serum in PBS) for 30 minutes at room temperature. The cells were incubated for 1 hour at room temperature with antibodies diluted in blocking serum, anti-GM130 (golgi marker, 1:500, BD Biosciences), anti-PDI (endoplasmic reticulum (ER) marker, 1:500, Assay Designs) or Texas-Red Phalloidin (an actin marker, 1:200, Molecular Probes). The coverslips were washed 3 x 5 minutes in PBS and those labelled with anti-PDI or anti-GM130 were counter labelled with Alexafluor goat anti mouse 594 (1:200, Life Technologies) for 1 hour at room temperature. The cells were washed 3 x 5 minutes in PBS and mounted using Vectashield with 4',6-diamidino-2-phenylindole (DAPI) (Vector Laboratories). Controls were performed in the absence of primary antibody to assess secondary antibody specificity. **Additional step:** for the pCMV-cMyc tagged construct and additional primary antibody rabbit anti cMyc (1:1000, Santa Cruz) was used to detect the construct and counter-labelled with Alexafluor goat anti rabbit 488 (Life Technologies) in order to visualise.

2.8.3. Imaging of immunolabelled coverslips

Images were taken using a Zeiss LSM 710 NLO multiphoton microscope operating in single-photon confocal mode, equipped with standard 405nm, 488nm, 561nm and 633nm diode and gas lasers. A series of objectives were fitted to the upright Axio-Examiner Z1 stand; the 5x EC plan-Neofluar NA 0.16 was used as a spotting objective to locate sections and wholemount preparations. The 10x plan-Apochromat NA 0.45 was used to take overview images; the 63x plan-Apochromat NA 1.4 oil-immersion objective was used to take high resolution images for recording fine detail. To observe the tissues prior to imaging, a 150 watt metal-halide lamp was used in conjunction with standard red (DsRed: 49), green (GFP: 38) and blue (DAPI: 43) filtersets.

The lasers were operated at 2% strength, the pinhole setting was set at 1.29 Airy Units (for the mid-spectrum green wavelength), which gave an optical slice of 0.9 μm for the 63x objective. Each image was scanned 16 times to improve the signal-to-noise ratio (SNR). The images were collected at 1024x1024 pixels across each dimension. For the 63x objective, the image length and height, at zoom = 1x, was 134.8 μm x 134.8 μm with a pixel pitch of 0.26 μm to satisfy Nyquist sampling. The Hamamatsu photomultiplier tubes (PMTs) fitted as standard were used to collect the images. Where required, single maximum intensity projections (MIPs) were collected from a z-stack of sections through the tissue. The images were collected using proprietary Zeiss ZEN 2010 software version 6.0.0.485 running on a HPZ800 workstation (Hewlett-Packard) with 6GB RAM under 64-bit Windows 7 Ultimate (Microsoft).

Co-localisation of WT and *pitch* Np65-EGFP and the ER marker, PDI, was assessed using the Mander's coefficient plugin to generate the Pearson's correlation co-efficient in Image J (both available at http://imagej.nih.gov/ij/). Correlation coefficients were analysed between groups using an unpaired Student's *t*-test (two-tailed) with Welch's correlation, as described by (2013).

2.9. Histology of the cochlea and vestibular apparatus

In order to identify any gross morphological differences caused by mutant Neuroplastin, histological sections were cut from *Nptn*^{pitch} at P16, P27, P90 and P180. Whole heads were fixed and decalcified as described in section 2.4.4 . Heads were mounted in paraffin wax and 10µM sections were cut before and after the cochlear mid-modiolus and before and after the saccule and vestibule by MRC Harwell's histology core. Alternate slides were haematoxylin and eosin (H&E) stained, whilst the remaining slides were silanized (charged). H&E slides were visualised on a Zeiss Axiostar plus microscope.

2.10. Semi-thin histology

To identify morphological differences in the organ of Corti, semi-thin histology was used to complement the existing H&E stained paraffin wax slides. Ears were removed, fixed and osmicated as described in section 2.4.6. Ears were decalcified in 4% EDTA in 0.1M Sodium phosphate buffer with 25% Glutaraldehyde for 3 – 10 days at 4^{O}C. Samples were dehydrated through an increasing gradient of ethanol (25%, 50%, 75%, 95%, 100%) and stored at 4^{O}C until embedding.

2.10.1. Araldite resin embedding of inner ears

Following dehydration ears were incubated in Epoxypropane for 30 minutes. Araldite resin was made up to the following recipe: 50ml Araldite 502, 42.5ml DDSA, 13ml DBP, 1.75ml DMP-30 (all supplied by TAAB Laboratories Equipment Ltd.). Ears were moved through an increasing gradient of resin: 2 hours at room temperature in 50% resin in PO, overnight at room temperature in 65% resin in PO, 2 hours in 100% resin. The ears were mounted in coffin moulds and orientated as shown in Figure 26, where the round window is orientated upwards and the vestibular portion is higher than the cochlea portion of the inner ear. The moulds were placed in an oven at 65^{o}C and hardened for 2 – 3 days.

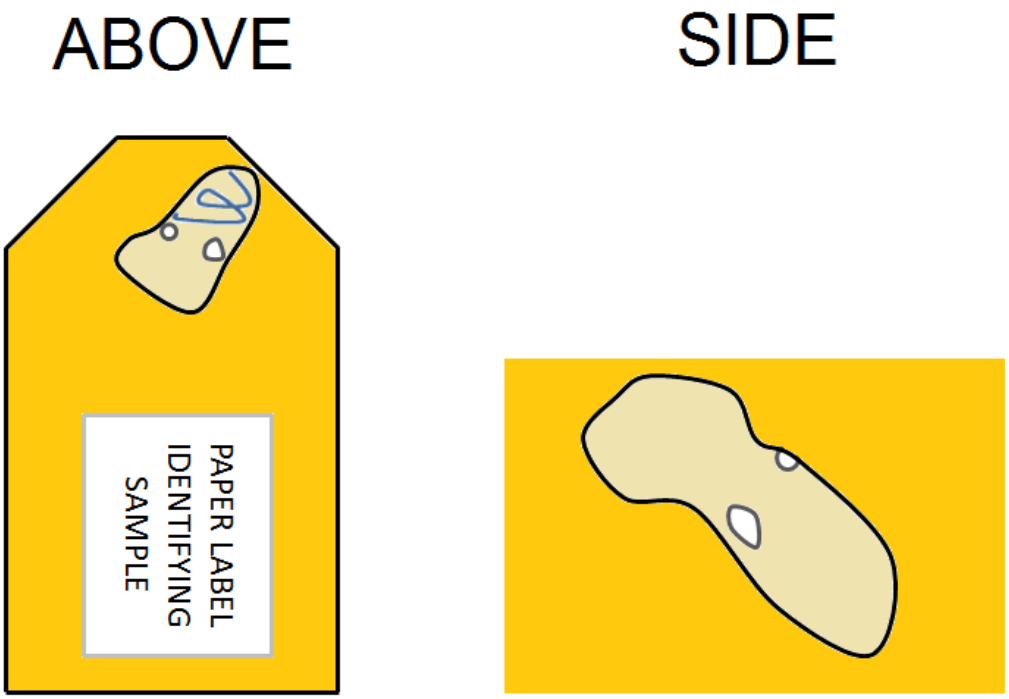

Figure 26. Inner ear orientation for Araldite embedding.

Inner ears were positioned in the coffins as indicated with the cochlea pointed toward the outside edge and the vestibular orientated to be higher than the cochlea. Once set, the parallel edge to the cochlea is cut down and polished in order to cut sections mid-modiolar, whilst a substantial amount of the block was left to position in the chuck of the ultramicrotome. Ears were positioned using size 5 forceps in the unset resin and a paper label inserted (with pencil lead writing). Once positioned coffin moulds were cured in an oven.

2.10.2. Ultramicrotome sectioning of resin embedded inner ears

Ears were sectioned by Jeremy Sanderson, manager of the microscopy facility at MRC Harwell. The resin blocks were inspected and marked to identify the mid-modiolus and trimmed using a single edge razor blade. The face of the block was mounted in the Ultracut E ultramicrotome (Reichert-Jung) and gradually cut down with a dry 6.4mm glass knife to create a “polished” surface just short of the mid-modiolus of the cochlea. Glass knifes were created from standard glass strips using the Leica EM-KMR3 knifebreaker. Each glass knife had a blue plastic preformed ‘truf’ attached with melted dental wax (held in an LKB 2208 Multiplate hot-plate) to form a boat around the knife. 5 – 10

µm sections were taken off and checked to see if the mid-modiolus had been reached. Upon reaching the mid-modiolus 0.5 - 1µm sections were cut and floated in ddH_2O in the boat. The sections were stretched using chloroform vapour and then picked up using an eyelash probe and transferred onto a drop of water on a Superfrost Plus 25x75mm slide (Thermo Scientific) in groups of 2 – 3 sections per slide. Slides were dried and then stained with a 50% aqueous solution of pre-filtered Richardson's stain for 30 seconds, washed in ddH_2O to remove any excess stain and allowed to dry. Slides were mounted in DPX using a 22x22mm No. 1.5 thickness coverslip (Thermo Scientific).

2.10.3. Imaging of semi-thin sections

Images were taken using a Zeiss Axio-Observer Z1 microscope adjusted for Köhler illumination using a series of objectives: Plan-Apo 10x/NA 0.3; EC-Plan Neofluar 20x/NA 0.5; EC-Plan Neofluar 40x/NA 0.75 and EC-Plan Neofluar 100x/NA 1.30 oil-immersion. The images were captured using a Zeiss 1.4 megapixel AxioCam HRc CCD colour camera coupled to the microscope. The camera was run using Zeiss AxioVision40 version 4.8.2.0 image-capture software.

2.11. Wholemount cochlear immunolabelling

In order to identify expression of Neuroplastin and other auditory markers in the ear, cochlear wholemount immunolabelling was performed in the C3-sighted strain and *Nptn*^{pitch} at P8, P10, P12, P14, P16, P18, P21, P24 and P27.

2.11.1. Sub-dissection/fine-dissection of cochlear

In order to label the sensory epithelia, the cochleae required sub-dissection. Ears were fixed as detailed in section 2.4.2 and placed in PBS in a 5cm sterile dish (Sterilin). Using a Zeiss discovery V.20 stereo dissection microscope with a Zeiss PlanApo S 0.63x FWD 81mm objective, the vestibular portion of the ear was held with forceps and the bone covering the cochlea removed. Forceps were used to detach the cochlea from the vestibular apparatus and the sensory epithelium was dissected away from the modiolus and spiral ganglion (see Figure 27). Fine forceps were used to tease the stria

vascularis, lateral wall and Reissner's membrane away from the cochlea, exposing the inner and outer hair cells.

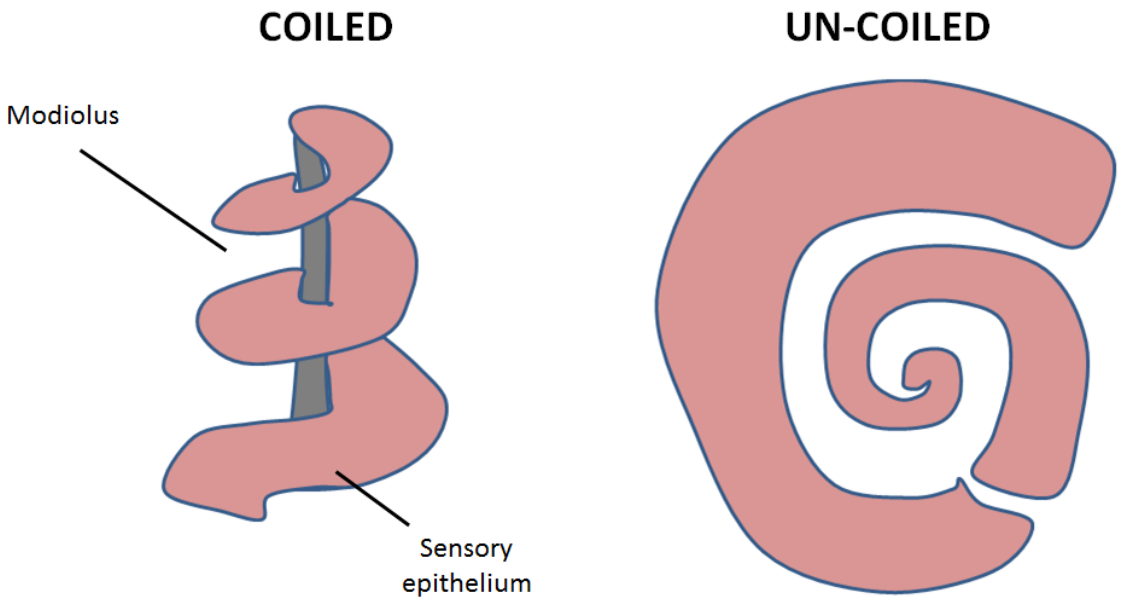

Figure 27. Removal of the sensory epithelium from the modiolus bone for wholemount immunolabelling.

To expose the IHCs and OHCs for immunolabelling, the sensory epithelium was carefully removed from the coiled position around the modiolus bone, dissecting the cochlear turns away from the spiral ganglion. The stria vascularis, lateral wall and Reissner's membrane were then removed to expose the sensory hair cells

2.11.2. Immunolabelling – all antibodies excepting anti-GluR2

The sensory epithelia were permeabilised using 0.25% Tween 20 (Sigma-Aldrich) in PBS and washed with 0.1% PBS-Tween (PBST) for 5 minutes, followed by 3 x 5 minute washes in PBS. Cochleae were blocked in 10% Donkey Serum (Sigma-Aldrich) in PBS for 1 hour at room temperature. The primary antibodies (see below) were diluted in 10% Donkey Serum and applied to samples overnight at 4^{o}C. The following morning samples were washed for 5 minutes in PBST, followed by 3 x 5 minute washes in PBS and samples were re-blocked in 10% Donkey serum in PBS for 30 minutes. Secondary fluorescence labelled antibodies were applied for 1 hour at room temperature (see list below). The samples were washed for 5 minutes in PBST, followed by 3 x 5 minute washes in PBS and then

mounted onto Menzel Gläser (Thermoscientific) slides using SlowFade Gold mounting agent (Life Technologies) and compressed under a 20 x 22mm #1 Menzel Gläser coverslip (Thermoscientific). Controls were performed in the absence of primary antibody to assess secondary antibody specificity. In addition, alternate control samples were treated with primary antibody which had been pre- blocked with the immunizing peptide used to raise the Np65 antibody in the host species, and were utilised to assess the specificity of the primary antibody.

Primary antibodies: Various combinations of the following antibodies were used - goat anti-Np65 IgG (1:40, R&D systems), mouse anti-Otoferlin IgG (1:100, Abcam), rabbit anti-NF-200 IgG (1:500, Sigma-Aldrich), mouse anti-NF-200 IgG (1:150, Sigma-Aldrich), mouse anti-CtBP2 (1:100, BD Biosciences), rabbit anti-Parvalbumin (1:500, Swant), sheep anti-Np (1:40, R&D systems), chicken anti-MCT1 (1:100, Millipore), chicken anti-MCT2 (1:100, Millipore).

Secondary antibodies: Various combinations of the following antibodies were used – Alexafluor donkey anti-mouse IgG 488 (1:200, Life Technologies), Alexafluor donkey anti-mouse IgG 568 (1:200, Life Technologies), Alexafluor donkey anti-rabbit IgG 488 (1:200, Life Technologies), Alexafluor donkey anti-rabbit IgG 568 (1:200, Life Technologies), Alexafluor donkey anti-rabbit IgG 647 (1:200, Life Technologies), Alexafluor donkey anti-goat IgG 488 (1:200, Life Technologies), Alexafluor donkey anti-goat IgG 568 (1:200, Life Technologies), Alexafluor donkey anti-chicken IgG 488 (1:200, Life Technologies), Alexafluor donkey anti-chicken IgG 568 (1:200, Life Technologies), Phalloidin-405 conjugate (1:200, Biotium), Phalloidin-488 conjugate (1:200, Life Technologies), Texas Red Phalloidin conjugate (1:200).

2.11.3. Immunolabelling – anti-GluR2 (with anti-ribeye)

Initial immunolabelling attempts with anti-GluR2 failed using a 4% PFA or 4% FA fixation and the protocol specified in section 2.11.3. Instead, the following protocol was optimised for methanol fixed tissues (see section 2.4.2) and produced reliable immunolabelling. The sensory epithelia were permeabilised in 0.1% Tween 20 in PBS for 10 minutes and blocked in 10% donkey serum for 1 hour

at room temperature. Primary antibodies were diluted in blocking solution: mouse anti-GluR2 (1:100, Millipore), rabbit anti-Ribeye (1:200, Synaptic Systems). Tissues were incubated in primary antibody for 3-4 hours at room temperature, washed for 3 x 10 minutes in wash buffer, which was made up in 100ml volumes and stored at room temperature: 8.3ml 240mM Sodium phosphate buffer, 3ml 10% Triton-X 100 in PBS, 11.25 ml 4M NaCl and GIBCO ddH_2O up to 100ml. Secondary antibodies were diluted in blocking solution as follows: Alexafluor donkey anti-rabbit IgG 488 (1:200), Alexafluor donkey anti-mouse 568 (1:130). Tissues were incubated in secondary antibody solution at 4^{o}C overnight. Samples were washed for 3 x 10 minutes in wash buffer and then incubated in 1µg/ml DAPI (Life Technologies) in PBS for 5 minutes at room temperature. Tissues were washed for 5 x 10 minutes in wash buffer and mounted onto Menzel Gläser microscopy slides using SlowFade Gold mounting agent and compressed under a 20 x 22mm #1 Menzel Glázer coverslip. Controls were performed either in the absence of primary antibody to assess secondary antibody specificity, or in the presence of the anti-GluR2 primary antibody pre-blocked with the GluR2 immunizing peptide to ensure primary antibody specificity.

2.11.4. Imaging of wholemount immunolabelled cochlea

The samples were imaged as per section 2.8.3.

2.11.5. Analysis of GluR2 and RIBEYE synaptic labelling

GluR2 and RIBEYE synaptic puncta were counted to identify the number of synapses. Punctum was also assessed for co-expression, indicating synaptic coupling between the presynaptic active zone and the postsynaptic density. ImageJ software (NIH) was used to process images in order to count GluR2 and RIBEYE labelled puncta. Unprocessed z-stacks were rotated to align hair cells horizontally with the Y axis. Stacks were then cropped to 80µM in the Y axis (no X axis, or Z axis cropping was undertaken) and a 3D projection was generated with the following settings: Axis of Rotation – X axis, Total Rotation: 45^{o}, Depth cueing: 0, Interpolated: Yes. Total RIBEYE and GluR2 puncta were counted on separate fluorescence channels using the Image J cell counter plugin. A composite coloured

image was used to count the number of co-expressed RIBEYE and GluR2 punctum. Counts were scored blind to the genotype and verified by a separate operator. Counts were analysed for the percentage of uncoupled GluR2 and RIBEYE puncta, and also the total puncta numbers between C3-sighted strain and *Nptn*$^{pitch/pitch}$. Graphpad prism software was used to perform unpaired student's *t*-test with Welch's correlation for both analyses.

2.12. Thick-cut vibratome section immunolabelling

Thick cut vibratome sections were used to identify Np65 expression throughout the cochlear. Ears were removed and fixed as described in section 2.4.3. Whole inner ears were then mounted in 4% low melting point agarose in PBS, with the circular window orientated upwards as shown in Figure 28.

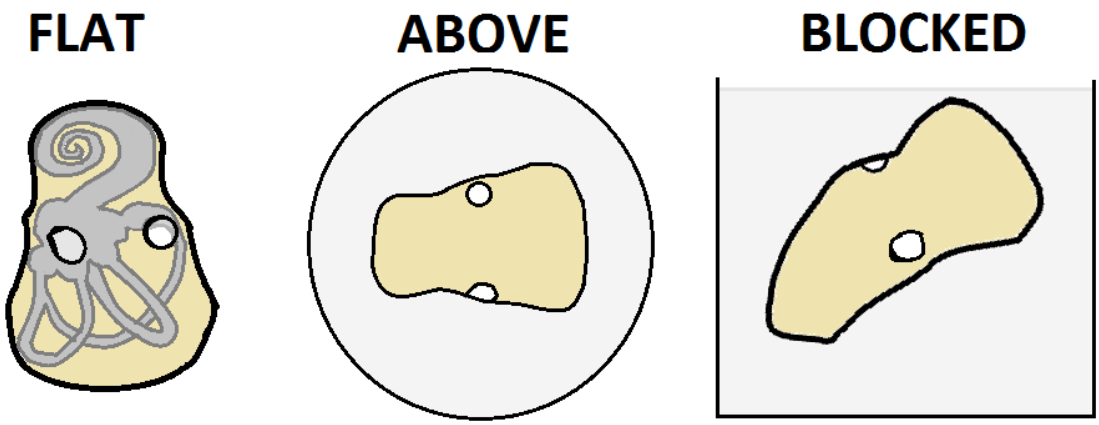

Figure 28. Inner ear orientation for agarose embedding and subsequent vibratome sectioning.

Inner ears were placed into cooling low melting temperature agarose in BEEM capsules and positioned quickly using size 5 forceps. Once positioned with the vestibular towards the top of the capsule and the round window facing upwards the ears were continually monitored, repositioning as necessary until the agarose was fully set.

2.12.1. Vibratome sectioning

The blocked ear was adhered with super glue to the cutting chuck of the vibratome and set in a well of PBS, with the vestibular portion orientated towards the cutting edge and the cochlear portion

located furthest from the cutting edge. Sections were cut at low speed and low frequency using a Leica VT 1000s vibratome. Sections were cut at 200 µM thickness through the entire inner ear and a fine paint brush was used to transfer the sections into PBS in a 24-well plate.

2.12.2. Immunolabelling

Sections were sorted by eye to identify areas of interest (mid-modiolus, saccule, utricle) and removed to a new 24-well plate for labelling. Sections were blocked and permeabilised in blocking solution (0.3% Triton-X in PBS containing 10% Donkey serum) at room temperature for 30 minutes. Primary antibodies were applied at specified dilutions (below) for 2-3 hours at room temperature. Sections were washed 3 times for 15 minutes in PBS before incubating in blocking solution containing diluted secondary antibodies (see below) for 1 hour at room temperature, then overnight at $4^{O}C$. Samples were washed 3 times for 15 minutes in PBS before undergoing a 5 minute room temperature incubation, if required, in DAPI (1:1000 in blocking solution, Life Technologies). After thorough washes in PBS the samples were stored in a light-tight environment at $4^{O}C$ in PBS (with 0.02% Sodium azide for long term storage) until examination by microscopy. Controls were performed in the absence of primary antibody to assess secondary antibody specificity.

Primary antibodies: Various combinations of those stated in section 2.11.2 were used for labelling. In addition the following antibodies were used: mouse anti-β-tubilin IgG (1:1000, Life Technologies).

Secondary antibodies: Various combinations of those stated in section 2.11.2 were used for labelling.

2.12.3. Imaging of immunolabelled vibratome sections

Sections were placed in PBS and imaged free-floating in a 0.17mm #1.5 22mm diameter Willco-dish glass bottom dish (Intracel). Imaging was undertaken using a Zeiss Observer Z1 inverted confocal microscope with a Zeiss Fluar 20x/0.75 coverslip corrected objective. The images were captured using a Zeiss 1.4 megapixel AxioCam HRc CCD colour camera coupled to the microscope. The camera

was run using AxioVision40 version 4.8.2.0 image-capture software. An extended focus module in the software was used to create z-stack images through the focal plane, with sampling distribution dictated by the Nyquist-Shannon theory.

2.13. Cryo-section immunolabelling

Cyrosections from inner ears and eyes were used to assess morphology (in the case of retinal sections) and for immunolabelling expression studies in *Nptn*^{pitch} and C3-sighted strain.

Inner ears and eyes were collected as described in sections 2.4.4.1 and 2.4.8 respectively. Sections were cut 2-3 per slide at 12µM thickness by the MRC Harwell Histology core team. Sections were stored a -20^{O}C avoiding freeze thaw cycles until required for labelling.

2.13.1. Immunolabelling

Slides were inspected visually to identify structures of interest (the cochlear mid-modiolus, outer plexiform layer (OPL) and the inner plexiform layer (IPL) of retina) and allowed to air dry. Sections were outlined with a wax pen. Retinal sections were fixed in 4% FA on ice (ears were fixed prior to embedding in OCT) for 10 minutes. Slides were washed 3 times for 15 minutes in PBS and then permeabilised in 0.25% Tween-20 in PBS for 10 minutes at room temperature. Samples were then washed 3 times for 15 minutes in PBS and blocked in 10% Donkey serum (blocking serum) for 30 minutes at room temperature. Primary antibodies (described in section 2.11.2 and 2.11.3) were diluted in blocking serum and applied for 1 hour at room temperature. Slides were washed 3 times for 15 minutes in PBS and secondary antibodies (described in section 2.11.2) were diluted in blocking solution and applied overnight at 4^{O}C in a light tight chamber. Slides were washed 3 times for 15 minutes in PBS, incubated in DAPI (1:1000) for 5 minutes in blocking solution (if required) and mounted with Slowfade Gold mounting agent using 50 x 24mm Menzel Gläser coverslips.

2.13.2. Imaging of immunolabelled cryosections

The samples were imaged as per section 2.8.3.

2.14. Quantitative reverse transcriptase-PCR of whole inner ears

Quantitative reverse transcriptase-PCR (qRT-PCR) was used to analyse the levels of Np55 and Np65 transcript in C3-sighted and *Nptn*^{pitch} ears. Analysis of Nptn expression at the transcript level was performed using complimentary (c) DNA synthesised from RNA obtained using whole inner ear preparations. Tissues were stored as detailed in section 2.4.7 and blotted with tissue paper before use to remove any excess RNAlater reagent.

2.14.1. RNA isolation

Total RNA was isolated from single inner ears using the Direct-Zol™ RNA MiniPrep kit (Zymo Research). Ears were homogenised in 350µl Trizol reagent (Zymo research) using Precellys CK14 lysing tubes, at 12,000 rpm for 20 seconds. Lysates were cooled on ice to reduce degradation. Lysates were then mixed with equal parts 100% ethanol and RNA was isolated as per the manufacturer's instructions. RNA was extracted in a 30µl volume of DNase and RNase free water. RNA concentration and the absorption ratios 260/230 and 260/230, were assessed using a Nanodrop 8000 spectrophotometer (Thermo-Scientific),

2.14.2. RNA integrity analysis

To analyse the integrity of the RNA produced using the Direct-zol kit, 1.5µl of 200ng/µl RNA from each sample was heat denatured for 2 minutes at 70^{O}C and then analysed using an Agilent RNA 6000 Nano-Chip. RNA Integrity Number (RIN) and RNA peaks at 260nM and 280nM were analysed and only samples with clear RNA peaks, low degradation and RIN >5 were used for cDNA synthesis and q-RT PCR.

2.14.3. cDNA synthesis

cDNA was synthesised from the inner ear RNA. Total RNA was diluted to 200ng/µl. The High Capacity cDNA Reverse Transcription kit (Applied Biosystems) was used as per manufacturer's instructions to synthesise single strand cDNA at a ratio of 1:1 total RNA to cDNA. In brief the following reaction was setup for each sample: 2µl 10x RT buffer, 0.8µl dNTPs, 2µl Random primers, 1µl Reverse

transcriptase, 4.2µl ddH_2O and 10µl 200ng/µl RNA. The reaction was thermocycled as follows: 25^{O}C for 10 minutes, 37^{O}C for 120 minutes, 85^{O}C for 5 minutes, store at 4^{O}C indefinitely. A total yield of 2µg (100ng/µl) of cDNA was obtained in this reaction. cDNA was stored at -70^{O}C if not being used immediately.

2.14.4. qRT-PCR

Custom Taqman assays were designed to span the exonic boundaries in order to specifically identify transcripts for each isoform (Figure 29):

Np55 (exon 1 – 3 junction) Forward primer: GCTCAGAACGAACCAAGAATTGT, Np55 reverse primer: CAGGAAGGAGGCTTTCTCGAA, Np55 probe: ACCAGTGAAGAGGTCA.

Np65 (exon 1 -2 junction) Forward probe: GCTCAGAACGCTGGGTTTGT, Np65 reverse primer: CGTCCCCCGTGAGCTTAGT, Np65 probe: AAGTCGCCCATGTCAG.

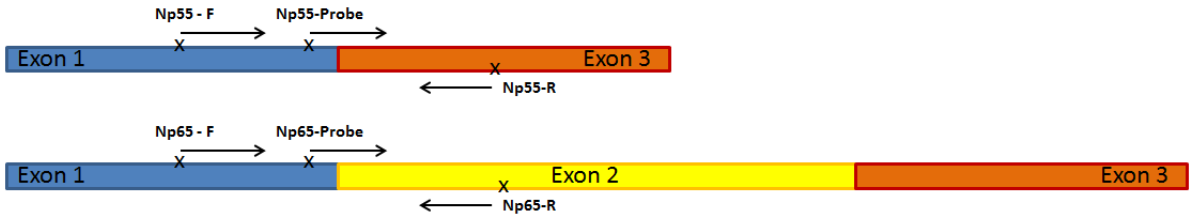

Figure 29. Custom Taqman assays were designed to identify the specific transcript for each isoform.

X identifies the sequence recognised by the oligonucleotide. The assay for Np55 was designed to recognise exon 1 with the forward primer, exon 3 with the reverse primer and the probe designed to bind across the boundary between exon 1 and 3. The primers for the Np65 assay recognised exon 1 with the forward primer, exon 2 with the reverse primer and the probe bound across the exon 1-2 boundary. The custom assay was designed in the same manner, recognising exon 5 with forward primer, exon 6 with the reverse primer and the probe binding across the exon 5-6 boundary.

The probes contained a 5' fluorophore (FAM), which is usually inhibited by a TAMRA quencher at 3'. Taq polymerase activity when primer and probe are bound to the amplicon leads to 5' probe displacement and degradation. This degradation leads to separation of FAM and TAMRA, preventing

fluorophore quenching and therefore increased fluorescence. Assays were designed using primer 3 express software (Life Technologies) using the default settings for TaqMan assay design and supplied fully-formulated (pre-mixed primers and probe). Care was taken to ensure primers and probes selected were not able to self-recognise or form hairpins. Pre-designed β-actin-, GAPDH- and Hprt1-FAM TaqMan assays (Life Technologies) were also ordered and used to assess the variability across the technical and biological replicates. Upon confirmation in preliminary testing that the assays showed similar expression profiles, the assay with the least variability (β-actin) was selected to be used as an endogenous control throughout the experiment. Reactions were set up as technical triplicates, using 5 biological replicates to ensure accuracy across each time-point. Reactions were set up as follows in 96 well plates: Fast TaqMan Master Mix 10µl, TaqMan assay 1µl, ddH_2O 4µl, cDNA (5ng/µl) 5µl. The plates were prepared in low light to prevent break down of the FAM fluorescent dye. qRT-PCR was performed using the Applied Biosystems 7500 Fast-Real Time PCR machine under the following conditions: 20 second hold at $95^{O}C$ (polymerase activation), 40 cycles of PCR – 3 seconds (denaturing) $95^{O}C$, 30 seconds (anneal/extend) $60^{O}C$.

Efficiency of each assay was confirmed by serial log10 dilution of WT RNA from whole ears. Each assay was within the standard accepted boundaries of between 90 and 110% efficiency, as measured by plotting C_T (y axis) vs log10 RNA concentration (x-axis) (Pfaffl, 2001). The Np65 assay was determined to be 106.8% efficient, whilst the Np55 assay was determined to be 90.0% efficient.

2.14.5. qRT-PCR analyses

Amplification data was recorded by the 7500 Real-Time machine and saved in .sds format. Files were imported into 7500 v.2.0.6 software (Applied Biosystems), cleaned to remove outlying results (where results varied by more than 1 cycle threshold (Ct) within technical triplicates) if necessary and saved in the .eds format. The .eds format files were imported into a study allowing for analysis of data points across all time points and replicates. *Nptn* mRNA levels were first normalised to *Actin* ($\Delta Ct=Ct_{Nptn}-Ct_{Actin}$) for each *Nptn* isoform at each age, and changes in expression relative to P4 were

calculated for each *Nptn* isoform as $2^{-(\Delta Ct-\Delta CtP4)}$. Relative quantities (RQ) values were exported for the biological groups and individual technical replicates. Technical replicates were analysed using the Levene's test to assess parametricity, followed by Student's *t*-test and Welch's correlation to determine any significant difference in transcript expression levels associated with the age at which tissue was obtained.

2.15. Ultrastructural analyses

Scanning electron microscopy (SEM) was used to assess the ultrastructure of *Nptn*^{pitch}. In order to perform ultrastructural analyses ears were removed, fixed and decalcified as described in section 2.4.5. Ears were further sub-dissected and processed in order to observe the ultrastructure.

2.15.1. Sub-dissection of inner ears

Decalcified inner ears were pinned to a Sylgard matrix through the vestibular portion using ultrafine 30 gauge pins as illustrated in Figure 30, and bathed in 0.1M Sodium phosphate buffer, pH 7.4. The otic capsule was torn towards the apex of the cochlea and carefully peeled away using size 5 fine forceps to reveal the entire cochlear turn *in situ.* The stria vascularis/lateral wall was dissected away with care to cause minimal damage to the cochlea. Ears were then returned to the small glass pots and incubated in 0.1M Sodium phosphate buffer overnight.

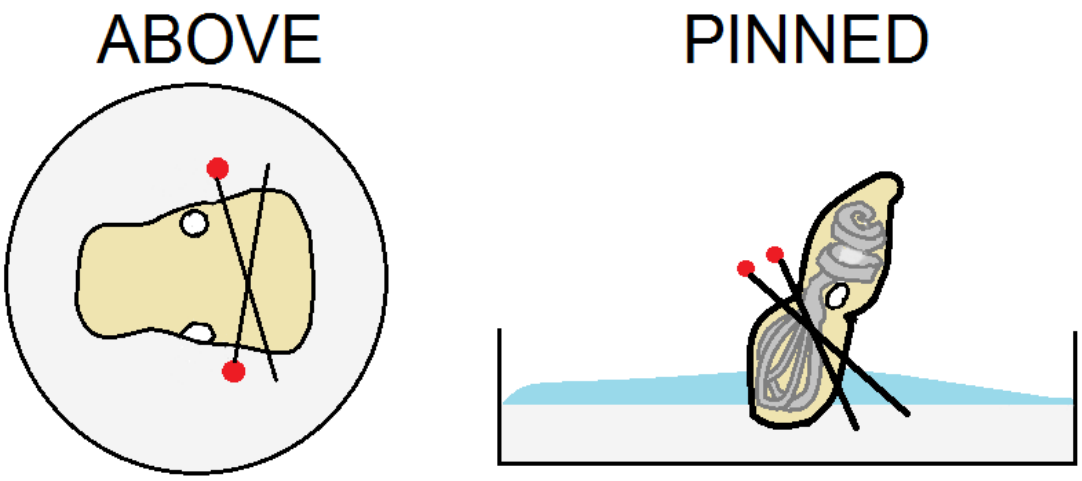

Figure 30. Attachment of the inner ear to a Sylgard matrix in order to fine dissect for ultrastructural analysis.

The inner ear was placed on the Sylgard matrix and positioned using size 5 forceps to manipulate the vestibular portion, ensuring that the cochlea points upwards. 30 gauge needles were inserted through the vestibular portion of the inner ear and pinned at angles into the Sylgard matrix to prevent the ear moving during fine dissection.

2.15.2. Osmium tetroxide and Thiocarbohydrazide (OTOTO) processing

Osmication was used to post-fixation to increase conductivity of the samples for SEM imaging. This increased morphological preservation and reduced charging of the sample. Thiocarbohydrazide treatment allows more osmium to be absorbed. Osmium (**O**) and Thiocarbohydrazide (**T**) steps were alternated (**OTOTO**) to provide optimum osmication. **Step O**: Ears were incubated in 1% Osmium tetroxide solution (Agar Scientific) in 0.1M Sodium cacodylate buffer, for 1 hour at room temperature. Ears were washed 6 times for 3 minutes in ddH_2O. **Step T**: Ears were incubated in fresh filtered 1% Thiocarbohydrazide (Sigma Aldrich) in ddH_2O for 30 minutes at room temperature. Ears were washed 6 times for 3 minutes in ddH_2O. After OTOTO processing was completed, ears were dehydrated in an increasing gradient of ethanol in ddH_2O for 45 minutes at $4^{O}C$: 25%, 40%, 60%, 80%, 95%, 100%, 100% (overnight), followed by 100% Acetone (overnight).

2.15.3. Critical Point Drying and mounting

Samples were Critical Point Dried (CPD) in accordance with the manufacturers instruction using the Emitech K850 critical point dryer and liquid CO_2. Ears were mounted on G301F 12.5mm specimen stubs (Agar Scientific) using Agar 12mm adhesive carbon tabs and silver paint (both Agar Scientific). Stubs were sputter-coated in an Argon atmosphere on a Quorum Q150RS, using a platinum target.

2.15.4. Imaging of stubs using SEM

Ears were imaged using a JEOL LSM 6010-LV Scanning Electron Microscope using a range of magnifications and voltages. Overview images were taken to assess gross morphology, higher magnification (x1500+) was used for more detailed images of the ultrastructure. Hair cell counts were made using the following method, detailed in Figure 31: 10 pillar cells were identified and highlighted, OHCs were counted in a diagonal from the first pillar cell to the diagonal of the final pillar cell and IHCs were counted for the 10 highlighted pillar cells. Hair cell counts were analysed using the Levene's test and One-way ANOVA to assess any difference.

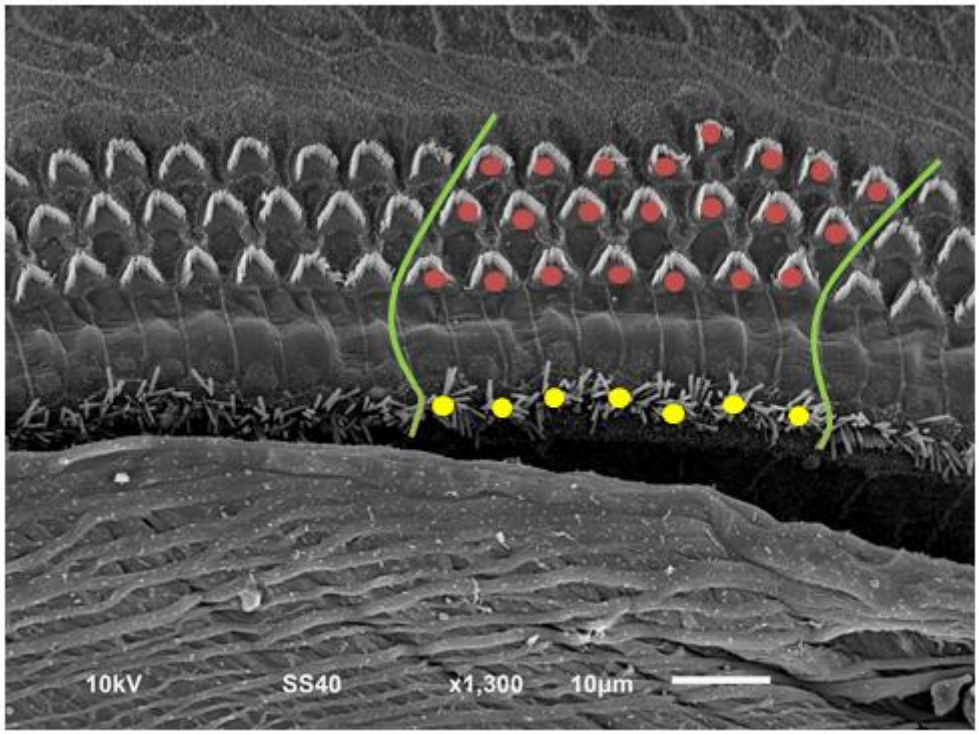

Figure 31. Hair cell counts were performed using images of the organ of Corti obtained by SEM.

Ten pillar cells with an unobstructed view of the inner and outer hair cells were selected. The pillar cells were highlighted (green) from the IHC row, following the edge of the pillar cell and following a 45^{O} angle from the first row of OHCs to the final row of OHCs. OHCs and IHCs are marked as they are counted (red and yellow respectively) and the counts were recorded and analysed in Graphpad Prism software.

2.16. 3-3'diaminobenzidine (DAB) staining

DAB immunostaining was intended to be used to detect expression of Neuroplastin on both wax sections and whole sensory epithelia in conjunction with transmission electron microscopy (TEM) to be performed by David Furness at Keele University. However in both instances the technique was unsuccessful and this is likely due to incompatibility of the primary antibody for Np65 with the labelling kit. Paraffin wax sections cut onto silane-coated slides were prepared as detailed in sections 2.4.4 and 2.9, whilst sensory epithelia tissue was prepared as described in sections 2.4.2 and 2.11.1.

2.16.1. De-waxing (paraffin sections only)

Slides were de-waxed using an automatic processor and the following protocol: 15 minutes in SubX followed by 2 x 5 minute SubX incubations, 2 x 3 minute washes in 100% ethanol, 1 x 3 minute wash in 70% ethanol. This was followed by a long wash with ddH_2O.

2.16.2. Hydrogen peroxidase treatment

To inhibit endogenous peroxidase activity slides and sensory epithelia tissue were incubated in 3% Hydrogen peroxide in Isopropyl alcohol for 30 minutes at room temperature. Following incubation samples were washed for 3 x 5 minutes in ddH_2O.

2.16.3. Antigen Retrieval (paraffin sections only)

Slides were placed in a ChemMate incubation container (DAKO), with blank slides filling all available gaps to ensure even heat distribution. The box was filled to the indicator line with 10mM Sodium citrate buffer, pH 6.0 and microwaved at 50% power for 7 minutes. The microwave box was refilled to the line using ddH_2O and heated for a further 7 minutes at 50% power. Slides were allowed to cool for 15 to 30 minutes and then rinsed in PBS. Sections were outlined with a wax pen.

2.16.4. DAB immunostaining

Tissues were DAB immunolabelled using the Vectastain ABC Rabbit anti Goat kit (Vector Labs) following the manufacturer's recommended protocol. Briefly, samples were blocked in diluted rabbit serum for 30 minutes then Goat anti-Np65 (1:40) antibody was applied in diluted rabbit serum and incubated for 1 hour at room temperature. Secondary antibody (Rabbit anti-Goat biotynalated-HRP) was applied at the dilution specified in the kit and incubated for 30 minutes at room temperature. Avidin-Biotin (AB) solution was made up following the manufacturer's instructions. Samples were washed for 3 x 5 minutes in PBS, then immediately incubated in AB solution for 30 minutes at room temperature. Liquid DAB Chromagen + substrate (DAKO) were made up as described in the manufacturer's protocol and applied to the samples, washing off with PBS when

brown staining was observed. Samples were washed for 3 x 5 minutes in PBS. Controls were performed in the absence of primary antibody to assess secondary antibody specificity.

2.16.5. Counterstaining (paraffin sections only)

Slides were counterstained in an automatic processor and placed in solutions as follows: dipped in haemotoxylin for 30 seconds, 5 minute wash in ddH_2O, 10 second dip in acid alcohol, 5 minute wash in ddH_2O, 30 second dip in lithium carbonate, rinsed in ddH_2O, 4 x 1 minute washes in 100% isopropanol. Slides were mounted with Clearium (Leica Biosystems) using 24 x 50mm Menzel Gläser coverslips.

2.16.6. Imaging of DAB stained sensory epithelia and

Sensory epithelia were placed in a Willco-dish #1,5 (Intracel) and submerged in PBS. Both wholemount sensory epithelia and paraffin wax sections were imaged using an inverted Zeiss Axio-Observer Z1 microscope adjusted for Köhler illumination with the following objectives: Plan-Apo 10x/NA 0.3; EC-Plan Neofluar 20x/NA 0.5. The images were captured using a Zeiss 1.4 megapixel AxioCam HRc CCD colour camera coupled to the microscope. The camera was run using AxioVision40 version 4.8.2.0 image-capture software.

2.16.7. Araldite resin embedding of sensory epithelia

If DAB labelling had worked for our antibody then the following protocol would have been followed in order to identify expression at a higher resolution: DAB stained whole sensory epithelia were resin-embedded as per section 2.10.1. Blocks were then sent to our collaborator David Furness to be ultrathin sectioned onto TEM grids and imaged using TEM, in order to view the electron dense deposits left by DAB and more clearly isolate the expression of Np65.

Chapter 3. Confirmation that *Neuroplastin* is the causative gene for auditory impairment in *pitch*

Given that the *pitch* model was generated using ENU-mutagenesis, which induces random point mutations through-out the genome, it is possible that there could be additional mutations within the mapped 1.6Mb candidate interval, and that the mutation identified in *Neuroplastin* is not the cause of deafness in this model. Therefore, I first needed to determine if the mutation identified in *Neuroplastin* would have an effect on protein function. In order to do this I undertook a series of *in silico*, *in vitro* and *in vivo* analyses.

3.1 *in silico* analysis

The high sequence identity between the human and mouse Neuroplastin orthologues (95%) suggests evolutionary pressure to conserve Neuroplastin. Thus, I used the human and mouse sequence to model the effects of the *pitch* mutation on Neuroplastin protein with *in silico* mutation prediction tools.

3.1.1. Analysis of pitch Np55 and Np65 using mutation prediction models

I employed three commonly cited mutation prediction programs (SIFT, PROVEAN and Polyphen-2), that are available online, to assess the likely impact of the mutation on protein function. A study performed by Choi et al. (2012) suggests that mutation prediction accuracy is very similar amongst these three tools.

The SIFT computational tool relies solely on conservation of amino acids (AA) through evolution. It uses a PSI-BLAST algorithm to search for functionally related sequences and builds an alignment to the search sequence. SIFT then analyses each AA in the search sequence and determines the

probability of an AA substitution being damaging or non-damaging (Kumar et al., 2009). Limitations of this computational model are that: structural data is not used; only missense mutations can be assessed; and, if a particular protein has been sequenced many times these sequences will most likely be used to create the alignment creating a false appearance of AA conservation, making it more likely to report a false damaging effect. SIFT classifies substitutions as "tolerated", or "not tolerated". SIFT online tool can be accessed at http://sift.jcvi.org/.

Polyphen-2, like SIFT, is a tool that predicts the effects of missense mutations on protein function. The algorithm builds sequence alignments based on AA homology, but also three structural predictive features that allows it to build multiple alignments for analysis of variants by a naïve Bayes classifier (Adzhubei et al., 2010). Polyphen-2 classifies substitutions as one of three categories: "benign", "possibly damaging" or "probably damaging". This tool can be accessed at http://genetics.bwh.harvard.edu/pph2/.

PROVEAN is able to predict the effect of insertion and deletion events, as well as missense mutations, on protein function. PROVEAN uses an algorithm to generate a Δ score for each functional homologue that the search sequence aligns to, based upon the frequency and conservation of a variant. The Δ for all of the homologues is averaged to generate the predictive PROVEAN score. The method used within the model to score Δ allows for sequence alignment of gapped areas in other homologues and the prediction of effects of small indels (1-6bp) on protein function. The PROVEAN score predicts the relative biological activity of the mutant protein compared to wild type, and may indicate the degree of functional impact on the protein (Choi et al., 2012). Accuracy of the prediction is not thought to be affected by processing of indels or substitutions with this algorithm. PROVEAN classifies substitutions as "neutral" or "deleterious" if more negative than the threshold of -2.5. PROVEAN can be accessed at http://provean.jcvi.org/protein_batch_submit.php?species=mouse.

Table 13. Online tools predict *pitch* is damaging to protein function in Np55 and Np65.

Isoform (mutation)	SIFT prediction	Polyphen-2 score	Polyphen-2 prediction	PROVEAN score	PROVEAN prediction
Np55 (C199S)	Not tolerated	1.000	Probably damaging	-10.000	Deleterious
Np65 (C315S)	Not tolerated	1.000	Probably damaging	-9.778	Deleterious

SIFT predicted that the cysteine to serine amino acid substitution in *pitch* would not be tolerated in either Np55 or Np65. The Polyphen-2 score for *pitch* in both Np55 and Np65 was 1.000 indicating that the substitution is rarely or never seen and is considered "probably damaging". The PROVEAN analysis identified the *pitch* mutation to be deleterious in both isoforms. The PROVEAN scores were very negative for *pitch*, exceeding the 'deleterious' threshold of -2.5 by 7.5 and 7.228 for Np55 and Np65, respectively. These scores suggest that the *pitch* mutant protein will have reduced biological activity compared to the wild type protein and thus affect protein function.

Table 13 illustrates the results obtained from computational modelling of the *pitch* mutation. The amino acid substitution was predicted as 'Not tolerated' by SIFT analysis. The only variant at this residue that was predicted to be tolerated was a valine substitution, a non-polar aliphatic amino acid. Analysis with the Polyphen-2 tool indicated the *pitch* mutation is 'Probably damaging', giving a high score of 1.000, indicating that this residue is highly conserved and variation is rarely or never seen at this residue position in homologues. PROVEAN analysis also identified the *pitch* mutation to be 'Deleterious'. The PROVEAN scores were very negative, predicting low biological activity of the *pitch* mutant protein.

3.1.2. Analysis of the 3D structure of Np55 and Np65

As the mutation prediction tools had indicated that the cysteine residue was important for the biological activity of Neuroplastin, I undertook three-dimensional (3D) modelling of the *pitch* mutant protein to assess for any structural requirements of this particular residue.

The crystal structure for the ectodomain of Np55 was solved by Owczarek et al. (2010) at a 1.95-Å resolution. The Ig2 domain was shown to have 8 β-strands, which form a classical β sandwich composed of 2 β sheets. Between Ig2 and Ig3 domains there is a short linker region (3 amino acids) and Ig3 is composed of 9 β-strands with the topology of an "intermediate type 1 (I1)-set Ig module". In both Ig2 and Ig3 a disulphide bridge is formed between the β-sheets, forming the tertiary protein

structure. In addition, there are 6 predicted N-glycosylation sites on the Np55 structure, with 4 sites showing electron density – indicating that these sites are glycosylated, under the conditions of crystal production used by Owczarek et al.

To model the *pitch* mutation I used the known Np55 structure, and a predicted structure for Np65 produced using Raptor X protein structure prediction server (Kallberg et al., 2012). The PyMol Molecular graphics system, version 1.3, Schrödinger, LLC, (Schrodinger, 2010) was used to generate three dimensional renderings of Np55 and Np65 from .pdb files obtained from the RSCB protein bank and using Raptor X protein structure prediction server, respectively (see Figure 32). Raptor X was further used to produce predicted protein structures for the *pitch* mutated Np55 and Np65 proteins and these were also 3-D rendered using PyMol (see Figure 32).

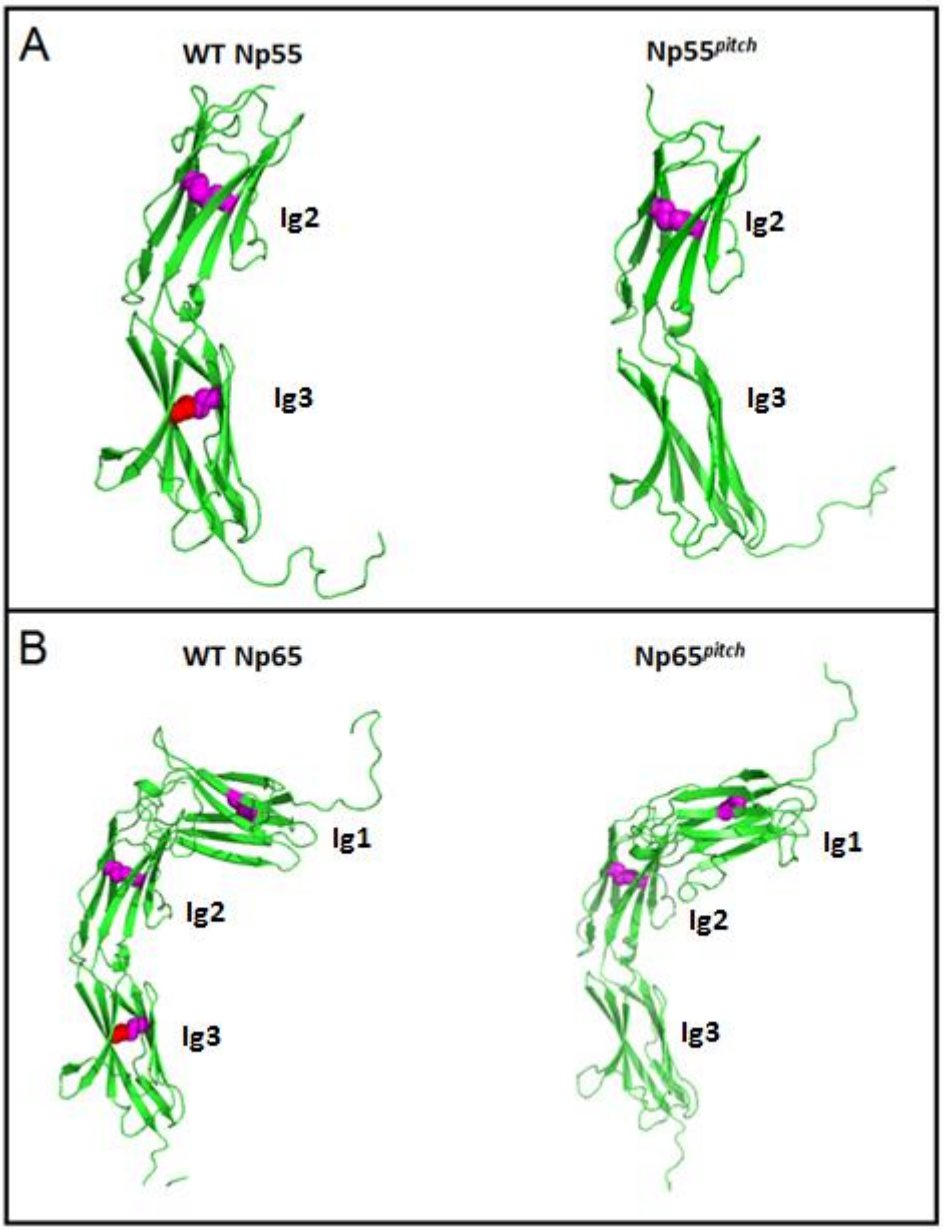

Figure 32. The *pitch* mutation causes substitution of a structural cysteine residue required for disulphide bridge formation in the Ig3 domain of Np55 and Np65.

A) Np55 ectodomain depicting WT and *pitch* mutant structure. B) Np65 ectodomain depicting WT and *pitch* mutant structure. A, B. Neuroplastin is expressed as two splice isoforms, Np55 and Np65. Although the Ig1 domain is unique to Np65, Ig2 and Ig3 are common to both isoforms. The Ig2 domain consists of 8 β-strands (illustrated by the green directional arrows), forming a classical β-sheet sandwich held in place by a cysteine (disulphide) bridge (cysteine residues are illustrated by purple spheres). Similarly, the Ig3 domain is composed of 9 β-strands in two sheets, which are supported in their structural conformation by a disulphide bridge. The *pitch* mutation causes substitution of one of these Ig3 structural cysteine residues (red spheres), C199 in Np55 and C315 in Np65. In the WT protein this cysteine residue forms a disulphide bridge to a second cysteine residue, C142 in Np55 or C258 in Np65. Therefore the *pitch* mutation will prevent the formation of this disulphide bridge in the common Ig3 domain and is likely to have an impact on protein folding and consequently protein function.

Three dimensional modelling of the Neuroplastin ectodomain indicates that the cysteine residue mutated in *pitch*, (shown as red spheres), is required for formation of a structural disulphide bridge in the common Ig3 domain. In the *pitch* mutant this cysteine is replaced by a serine residue. Cysteine and serine are chemically similar; both are polar amino acids with uncharged side chains, cysteine having a CH_2SH side chain, whilst serine has a CH_2OH side chain. However, serine lacks a sulphur ion and so is unable to form disulphide links. Therefore, it is likely that the absence of this structural disulphide bridge in *pitch* will lead to protein misfolding and hence protein dysfunction.

3.2. Protein processing in WT and *pitch* mutant Neuroplastin

In order to investigate the processing and sub-cellular localization of wild type (WT) and *pitch* mutant Neuroplastin protein I generated EGFP- and Myc-tagged, WT and *pitch,* Np55 and Np65 constructs. Experiments were performed in parallel using constructs with both tags in order to verify that the EGFP and Myc tags were not impacting upon protein expression or processing.

3.2.1. Protein production and post-translational modification studies

To assess protein production and post-translational modification, western blotting was performed using whole cell lysates obtained from cells transfected with WT and *pitch* EGFP- and Myc-tagged, Np55 and Np65 constructs.

The *pitch* allele causes a missense mutation in the encoded protein and is therefore still expected to produce a full-length protein. Additionally, Neuroplastin is reported to be highly glycosylated, with 6 known N-glycosylation sites (Owczarek et al., 2010). To assess the glycosylation status of WT and *pitch* mutant proteins, lysates were utilised from HEK293 cells that had been transfected with either WT or *pitch* mutant, Np55 and Np65 EGFP-tagged constructs. These lysates were assessed in their native state (-) or after treatment with PNGase F to remove N-linked glycans (+) (Figure 33).

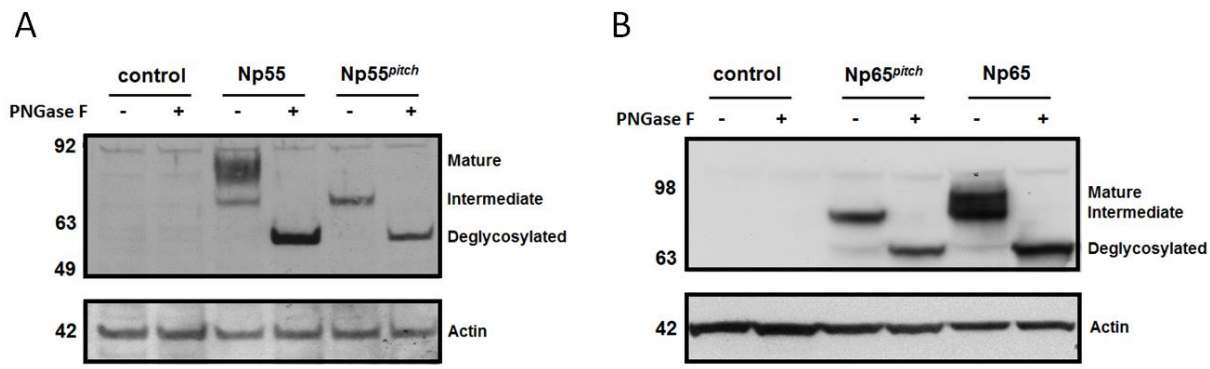

Figure 33. Post-translational modification of WT and *pitch* mutant Neuroplastin.

A) The *pitch* mutation affects Np55 protein glycosylation. Full-length Np55 protein is approximately 28kDa when fully deglycosylated (Langnaese et al., 1998), with the addition of the EGFP tag (27 kDa), gives a fusion protein of ~55 kDa. Both the WT (Np55) and *pitch* mutant ($Np55^{pitch}$) EGFP-tagged constructs produce proteins of the expected size when treated with PNGaseF (+). In untreated lysates (-), whilst both Np55 and $Np55^{pitch}$ show a common protein band at ~70kDa, only Np55 displays a larger molecular weight protein at ~85kDa. I suggest these correspond to 'intermediate' and a 'mature' glycosylated protein forms. These data suggest the *pitch* mutation prevents full glycosylation of Neuroplastin protein. The untransfected control shows no immunoreactivity to the anti-GFP antibody. Re-probing of the stripped blot using a primary antibody against beta-actin confirms protein levels are consistent across all samples. **B) The *pitch* mutation also affects Np65 protein glycosylation.** Full-length Np65 protein is ~40kDa when fully deglycosylated, with the addition of the EGFP- tag, gives a fusion protein of ~67kDa. As observed for Np55, both the WT (Np65) and *pitch* mutant ($Np65^{pitch}$) EGFP-tagged constructs produce proteins of the expected size when treated with PNGaseF (+). In untreated lysates (-), whilst both Np65 and $Np65^{pitch}$ show a common protein band, only Np65 displays a larger molecular weight protein at around 85kDa. . Re-probing of the stripped blot using a primary antibody against beta-actin confirms protein levels are consistent across all samples

Western blotting was used to assess the protein produced by the WT and *pitch* mutant Np55 and Np65 EGFP-tagged constructs, using lysates from transiently-transfected cells and an anti-EGFP antibody. Parallel experiments were also performed employing Myc-tagged constructs (see supplementary information S6).

PNGaseF-treated lysates gave immunoreactive bands for WT and *pitch* mutant Np55 and Np65 at ~55 and ~65 kDa, respectively (Figure 33). These are consistent with the molecular mass expected for full-length deglycosylated Np55 and Np65 fused to EGFP. Np55 alone has a deglycosylated mass

of ~28kDa, and Np65 alone of ~ 40kDa. EGFP is a relatively large tag at 27kDa, thus full-length Np55-EGFP is expected to have a mass of ~55kDa, and Np65-EGFP of ~67kDa. These results show that full-length proteins are produced from WT and *pitch* mutant constructs.

For both Np55 and Np65 untreated lysates, a difference in the glycosylation level was observed between WT and *pitch* mutant Neuroplastin (Figure 33). Lysates from cells transfected with WT constructs showed two separate glycosylated forms of Neuroplastin. The first is an intermediate band ~10kDa larger than that observed for fully deglycosylated Neuroplastin, with approximate molecular weights of 70kDa and 80kDa for Np55 and Np65, respectively. The second is ~15kDa larger than the intermediate band, with observed molecular weights ~85kDa and ~95kDa for WT Np55 and Np65, respectively. The intermediate band likely corresponds to a partially glycosylated form of Nptn, whereas the larger band is likely to correspond to fully glycosylated Neuroplastin protein. Analysis of lysates from cells transfected with *pitch* mutant constructs showed that only the intermediate glycosylation form of Np55 and Np65 was observed. The more highly-glycosylated form was not detected in the *pitch* mutant lysates. These results indicate the *pitch* mutation affects glycosylation of Neuroplastin, Np55 and Np65, and is likely to affect both isoforms equally.

In order to verify that the EGFP-tag was not interfering with the analysis, the same experiment was repeated with cMyc-tagged constructs. Equivalent results were obtained using the cMyc-tagged constructs (see supplementary information S6).

If as hypothesised, the *pitch* mutation causes protein misfolding it is conceivable that specific asparagine residues within the mutant protein are incorrectly orientated, such that their nitrogen containing side chains may not be available for N-linked glycosylation. N-linked glycans can play important roles in structural stability, mediation of cell signalling and glycoprotein trafficking, so a reduction in glycosylation is likely to have an effect on protein function (Schwarz and Aebi, 2011).

3.2.2. Subcellular localisation of Nptn

Neuroplastin is a cell adhesion molecule and as such is required to be expressed at the cell surface to fulfil its function. To assess subcellular localisation of WT and *pitch* mutant Neuroplastin I again used the EGFP- and Myc-tagged, WT and mutant, Np55 and Np65 expression constructs.

HEK293 cells were seeded on to coverslips and transfected with the tagged Neuroplastin constructs. Twenty four hours post-transfection cells were fixed and immunolabelled for two organelle markers: anti-GM130 to label the Golgi apparatus; anti-PDI to label the endoplasmic reticulum (ER). In addition, 4',6-diamidino-2-phenylindole (DAPI) was used as a nuclear label and phalloidin was used to label the actin cytoskeleton. The reason for selecting these cellular markers are: actin will demark the extent of the cytoplasm and the periphery of the cell; the ER is key in multiple functions including correct folding of newly made proteins (e.g. disulphide bridge formation by the enzyme protein disulphide isomerase, PDI) and initial N-linked glycosylation; the golgi is important for modifying, sorting and packaging proteins (e.g. it receives newly synthesised proteins from the ER and is the site of O-linked glycosylation)(Van den Steen et al., 1998, Tannous et al., 2014). The data from the transfections using WT and *pitch* mutant Np65-EGFP constructs are shown (Figure 34).

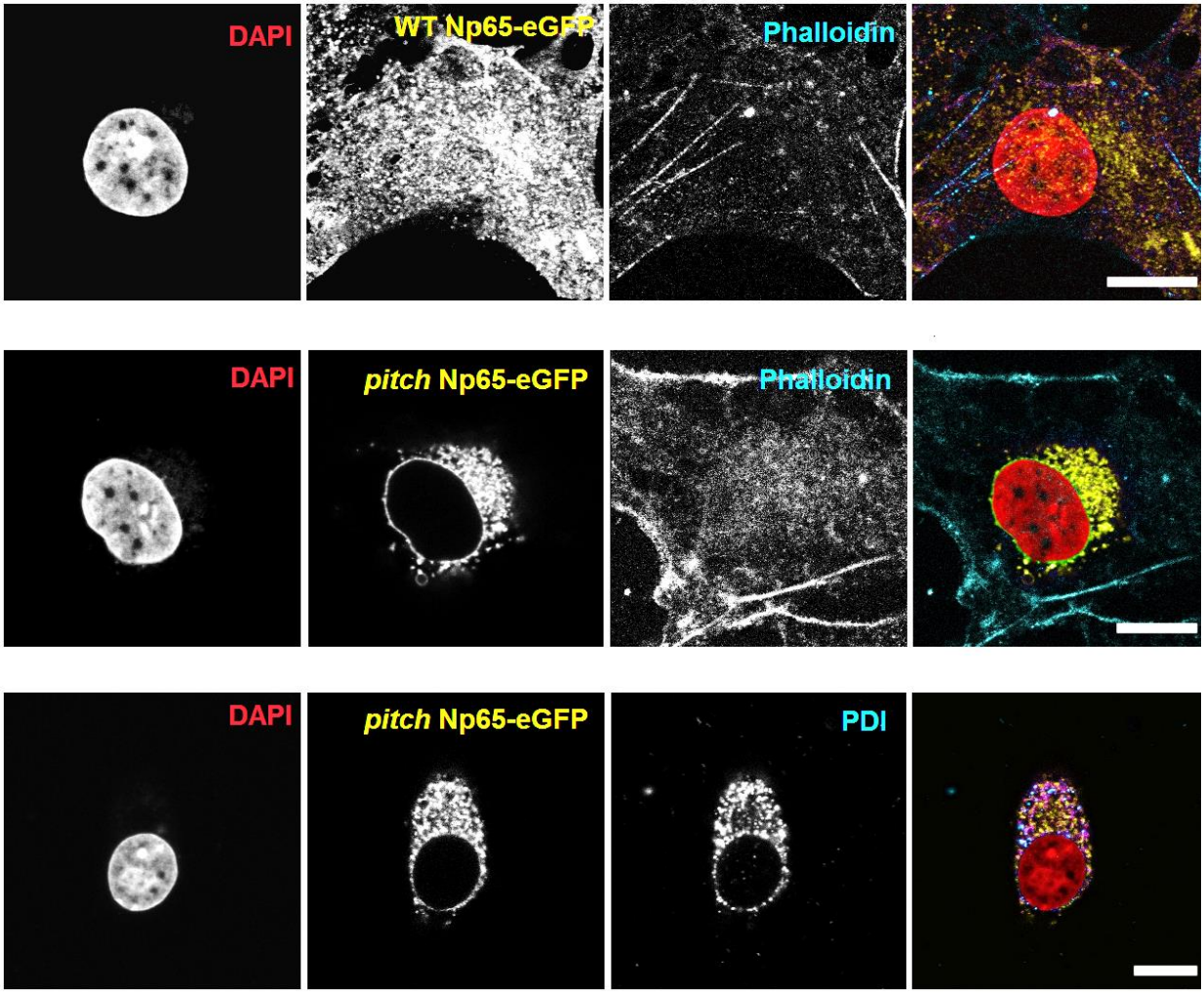

Figure 34. Mutant Neuroplastin is retained in the endoplasmic reticulum.

The top row of images shows the expression of WT Np65-eGFP in HEK293 cells, co-labelled with DAPI (a nuclear marker) and phalloidin (an actin marker). Np65 localizes throughout the cytoplasm and to the cell surface, as indicated by the overlap of Np65 (yellow) and the Phalloidin (cyan) signals. The second row shows the expression of *pitch* mutant Np65-EGFP. Mutant Np65-EGFP is retained close to the nucleus and does not extend throughout the cytoplasm or to the cell surface. The third row shows expression of *pitch* mutant Np65-EGFP, co-labelled with DAPI and the ER marker PDI. The *pitch* mutant Np65-EGFP (yellow) signal and the PDI (cyan) signal co-occur in the cell, as indicated by the overlap of their signals giving a pink/purple signal in the merged image. Pearson's correlation coefficient was generated to assess WT and *pitch* Np65-eGFP co-localisation with the ER marker PDI. WT Np65-eGFP (n = 8) has a mean correlation coefficient of 0.3857 (+/- 0.0504), whilst *pitch* Np65-eGFP (n = 7) shows a significantly higher mean correlation coefficient of 0.7746 (+/- 0.0108), p= 0.0013, indicating that *pitch* Np65-eGFP protein co-occurs with the fluorophore-conjugated secondary antibody, which is bound to the anti-PDI primary antibody, more frequently than observed for WT Np65-eGFP. Statistical analysis: two tailed Student's *t*-test with Welch's correlation. This data demonstrates that the *pitch* mutation causes retention of Neuroplastin within the ER. Scale bar = 10µM, Pearson's correlation coefficient reported as mean (+/- standard deviation).

Fluorescence microscopy revealed that WT Np65-EGFP protein was distributed throughout the cytoplasm and at the cell membrane. However, *pitch* mutant protein was shown to accumulate around the nucleus, and was not trafficked to the cell membrane. Co-labelling with anti-PDI demonstrated co-occurrence of the fluorescence signals for *pitch* mutant protein and PDI, demonstrating that *pitch* mutant Np65 protein is retained in the ER. Analysis using Pearson's correlation coefficient (Adler and Parmryd, 2010) confirmed significantly higher co-localisation between *pitch* Np65-eGFP protein and the ER marker, PDI (0.7746 +/- 0.0108), p=0.0013, than observed for WT Np65-eGFP protein (0.3857 +/-0.0504).

This experiment was repeated using the WT and *pitch* mutant Np55-EGFP constructs. In addition, to verify that the EGFP-tag was not interfering with subcellular localization, these experiments were repeated using the Myc-tagged WT and *pitch* mutant Np55 and Np65 constructs. Equivalent data to those shown for Np65-EGFP were obtained for Np55-EGFP, Np55-Myc and Np65-Myc constructs (supplemental information S6.2, not shown, supplemental information S6.3).

The rough ER (RER) is the site where correctly processed proteins are packaged into vesicles and sent to the Golgi apparatus for further refinement, such as mannose trimming (Lodish, 2003). In order for N-glycosylation to occur the protein must be correctly folded. However, if the protein is misfolded it is removed to the lumen of the ER where the unprocessed protein response (UPR) takes place in an attempt to repair the damage or refold the protein. If the damage cannot be repaired the defective protein is broken down by the ER-associated degradation (ERAD) pathway (Tannous et al., 2014).

Retention of *pitch* mutant Neuroplastin in the ER suggests my hypothesis regarding the mutation causing protein misfolding is correct. Indeed, these data complement those obtained from the Western blotting study, as incorrectly folded proteins will also fail to be correctly N-glycosylated, leading to the reduction of Neuroplastin glycosylation observed.

The data obtained from my *in silico* and *in vitro* studies support the supposition that *pitch* is a loss-of-function mutation.

3.3. Phenotyping of re-derived *Nptn*^{pitch}

Having confirmed that the mutation in Neuroplastin (Nptn) is likely to be damaging to protein function and as such is a likely cause of the auditory phenotype observed in the *pitch* model, the line was re-derived by the frozen embryo and sperm archive (FESA) team at MRC Harwell, using archived sperm. Re-derived mice were crossed to a sighted-C3H (C3H.Pde6b+) strain for 6 generations, genotyping and breeding for the *Nptn*^{pitch} allele. Once a colony was established, WT, heterozygous and homozygous littermate mice were phenotyped by click box and ABR.

3.3.1. 8-week ABR to confirm phenotype observed in *pitch* homozygous haplotyped animals

ABR of the newly established *pitch* mice was performed on mice at 8 weeks of age to give a direct comparison to the preliminary ABR data gathered during the initial ENU screen. Both male and female animals were used for this experiment and were click boxed prior to being anaesthetised.

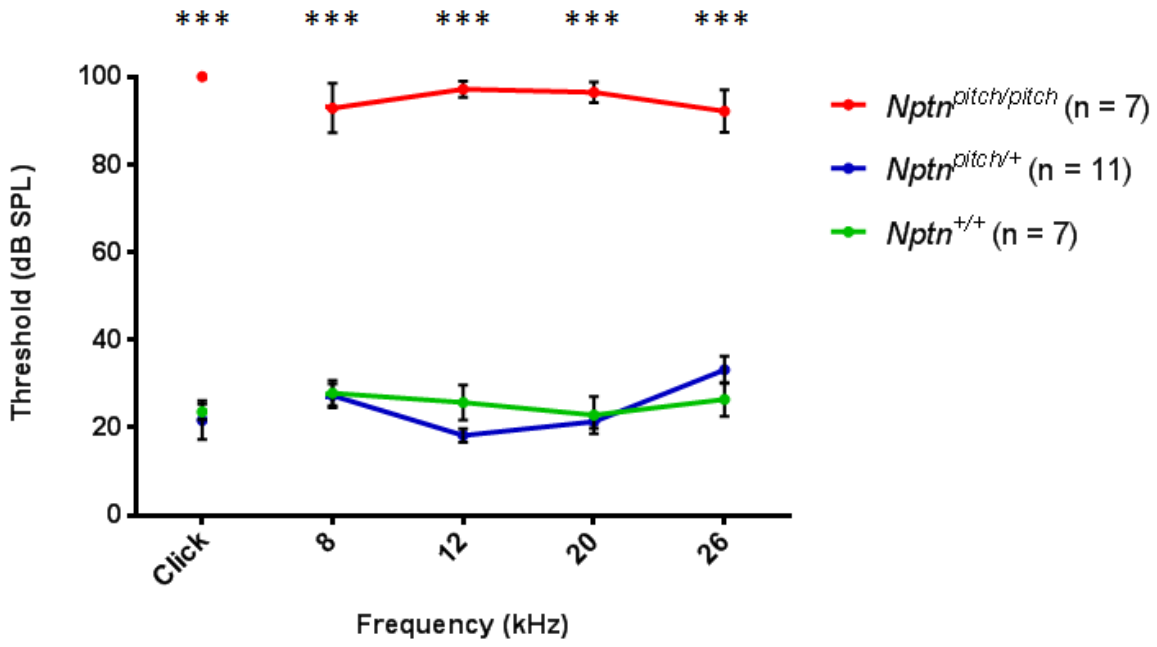

Figure 35. Re-derived *Nptn*$^{pitch/pitch}$ animals displayed profound sensorineural hearing loss at 8 weeks of age.

Animals were click boxed, anaesthetised and ABR testing undertaken. Traces were manually scored by two operators without knowledge of the genotype in order to remove bias. Wild type (*Nptn*$^{+/+}$) and heterozygous (*Nptn*$^{pitch/+}$) mice display normal hearing thresholds (20 – 30dB) at all frequencies tested. Homozygous (*Nptn*$^{pitch/pitch}$) animals display extremely elevated thresholds (≥90dB) at all frequencies tested. Statistical analysis: Levene's test followed by One-way ANOVA with post-hoc Tukey adjustment. No statistical differences were detected between *Nptn*$^{pitch/+}$ and *Nptn*$^{+/+}$ data. Significant statistical differences were observed between *Nptn*$^{pitch/pitch}$ and *Nptn*$^{+/+}$ data, ***p<0.00001 (Click – p= 1.94 x10^{-9}, 8kHz – p= 1.57 x 10^{-11}, 12kHz – p= 1.09 x 10^{-16}, 20kHz – p= 7.71 x 10^{-16}, 26kHz – p= 9.2 x 10^{-11}).

Click box testing of the *pitch* mice identified that all *Nptn*$^{pitch/pitch}$ animals were scored as '0' indicated by a complete lack of Preyer and startle reflex, whereas all WT and heterozygous littermates were scored as '2', showing a normal Preyer and/or startle response. ABR testing of the *pitch* mice identified that all *Nptn*$^{pitch/pitch}$ animals have extremely elevated thresholds of between 90 and 100dB (with 100 dB being the highest threshold measureable) at each frequency tested, whereas all WT and heterozygous littermates displayed thresholds expected of 8-week old hearing mice (15-35dB) (Figure 35). These thresholds for the *Nptn*$^{pitch/pitch}$ mice are comparable to those observed for the original ENU screen mice. In addition, no differences in hearing thresholds were observed between

female and male *Nptn*$^{pitch/pitch}$ mice, suggesting there are no gender effects. Therefore from this point cohorts were only selected based on genotype.

3.4. Identification and phenotypic analysis of a second Neuroplastin allele

Confirmation of an auditory phenotype in the re-derived *Nptn*$^{pitch/pitch}$ mice does not prove that *Nptn* is the causative gene, as there could be a second closely-linked ENU-induced mutation. To unequivocally confirm *Neuroplastin* as the gene underlying the *pitch* phenotype a second loss-of-function model is required to allow a complementation test. In the absence of an available knock-out model a second ENU-induced allele was sought from the Harwell ENU archive. The ENU archive was screened by C. Aguilar and J. Dorning using primers to amplify exons 1 – 6 of the *Neuroplastin* gene (see supplemental information S7) and this approach identified six alleles (Table 14).

Table 14. ENU induced lesions identified from the MRC Harwell ENU archive in *Neuroplastin*.

Nucleotide change	Amino acid change	Type	Prediction	
			Polyphen-2	PROVEAN
G>A	T59T	Synonymous change	N/A	Neutral
A>G	T172A	Missense	Benign	Deleterious
T>C	L190P	Missense	Probably damaging	Deleterious
T>A	Y219X	Premature stop codon, leading to truncated protein	N/A	Deleterious
T>C	P225P	Synonymous change	N/A	Neutral
G>T	Int+12	Intronic change	N/A	N/A

The ENU archive was screened for mutations in exons 1 – 6 of *Nptn*. From this screen six allelic variants were confirmed by Sanger sequencing. Of these, two variants contained synonymous changes and one variant led to an intronic change, and so these were discounted. The remaining 3 variants were assessed using online tools Polyphen-2 and PROVEAN tools to assess the likelihood that the predicted change would affect protein function. All three mutations were predicted to be damaging by at least one of these programs. I chose to have *Nptn*^{Y219X} re-derived, as the mutation generates a stop codon, which would lead to a severely truncated protein that is likely to be non-functional. *Nptn*^{Y219X} was re-derived by the FESA group at the Mary Lyon Centre (MLC) at MRC Harwell.

A nonsense allele (*Nptn*^{Y219X}) was chosen for re-derivation using frozen archived sperm. This allele causes the introduction of an early stop codon, which if translated would produce a non-functional protein lacking the Ig3 domain, transmembrane region, and intracellular C-terminal tail. If the mutation in Neuroplastin is the cause of hearing loss in *pitch*, and if the mutation is a complete loss-of-function allele, I would expect the *Nptn*$^{Y219X/Y219X}$ mice to display a very similar hearing phenotype to that of *Nptn*$^{pitch/pitch}$ mice.

3.4.1. 8-week ABR of *Nptn*$^{Y219X/Y219X}$ and littermate controls

The *Nptn*^{Y219X} model was established and cohorts of WT, Het and Hom mice produced. To allow a direct comparison with the *Nptn*^{pitch} data, *Nptn*^{Y219X} mice were tested by ABR at 8 weeks of age (Figure 36).

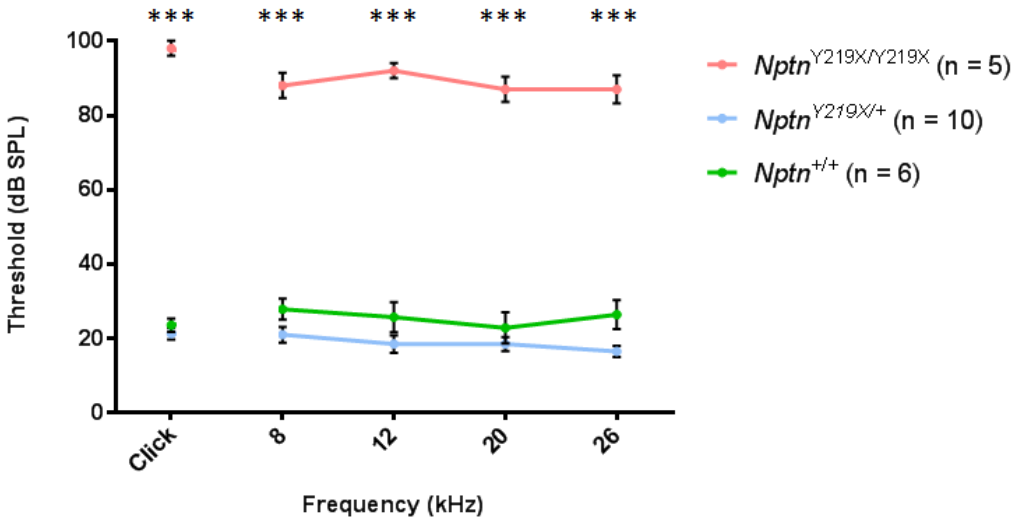

Figure 36. *Nptn*$^{Y219X/Y219X}$ mice are profoundly deaf at 8 weeks of age.

ABR traces were manually scored by two operators without knowledge of the genotype in order to remove bias. Wild type (*Nptn*$^{+/+}$) and heterozygous (*Nptn*$^{Y219X/+}$) mice display normal hearing thresholds (20 – 30dB) at all frequencies tested. Homozygous (*Nptn*$^{Y219X/Y219X}$) animals display extremely elevated thresholds (≥90dB) at all frequencies tested. Statistical analysis: Levene's test followed by One-way ANOVA with post-hoc Tukey adjustment. No statistical differences were detected between *Nptn*$^{Y219X/+}$ and *Nptn*$^{+/+}$ data. Significant statistical differences were observed between *Nptn*$^{Y219X/Y219X}$ and *Nptn*$^{+/+}$ data, ***p<0.00001 (click – 5.24 x 10^{-16}, 8kHz - 1.37 x 10^{-12}, 12kHz – 2.72 x 10^{-12}, 20kHz – 9.02 x 10^{-12}, 26kHz – 2.56 x 10^{-12}).

Eight-week ABR testing of *Nptn*$^{Y219X/Y219X}$ mice confirmed a profound auditory deficit (+90dB), whilst WT and *Nptn*$^{Y219X/+}$ mice had normal hearing thresholds. The replication of the profound deafness phenotype in mice with a second *Nptn* allele supports the theory that *Nptn* is the causative gene in *pitch*. However, to be completely certain that *pitch* is caused by mutation of *Nptn* and not by a mutation in another gene, a complementation test was undertaken using *Nptn*^{pitch} and *Nptn*^{Y219X} mice.

3.4.2. Complementation testing using the *Nptn*^{pitch} and *Nptn*^{Y219X} alleles

Complementation testing is a method used to identify whether similar recessive phenotypes observed in two models are caused by mutation of the same gene. In order to do this, mice are mated to produce compound heterozygotes, which can then be assessed for the phenotype. If the recessive phenotype is present in compound heterozygous offspring, complementation has not occurred, indicating the mouse has inherited two 'mutant' copies of the same causative gene, one from each parent, and as such the causative gene must be the same in each parental model.

In order to assess complementation of *Nptn*^{pitch} and *Nptn*^{Y219X}, *Nptn*$^{pitch/+}$ were crossed to *Nptn*$^{Y219X/+}$ mice to produce compound heterozygous offspring (*Nptn*$^{pitch/Y219X}$) as well as single allele heterozygotes (*Nptn*$^{pitch/+}$ or *Nptn*$^{Y219X/+}$) and WT littermates. Progeny were ABR tested at 8-weeks (Figure 37).

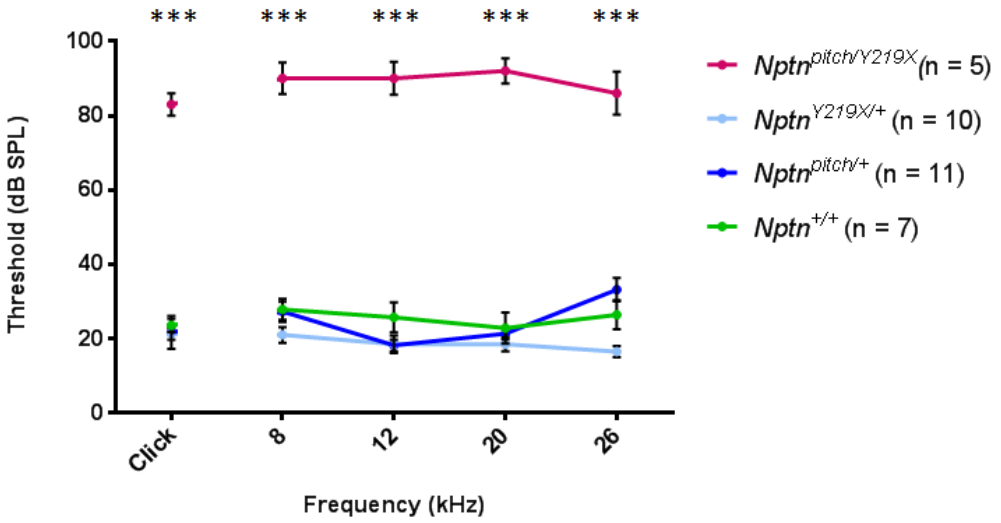

Figure 37. *Nptn*$^{pitch/Y219X}$ animals are severely to profoundly auditory impaired, indicating that *Nptn*^{pitch} and *Nptn*^{Y219X} alleles do not complement.

Wild type (*Nptn*$^{+/+}$) and heterozygous (*Nptn*$^{pitch/+}$ and *Nptn*$^{Y219X/+}$) mice display normal hearing thresholds (20 – 30dB) at all frequencies tested. Compound heterozygous (*Nptn*$^{pitch/Y219X}$) animals display extremely elevated thresholds (≥85dB) at all frequencies tested. Statistical analysis: Levene's test followed by One-way ANOVA with post-hoc Tukey adjustment. No statistical differences were detected between *Nptn*$^{pitch/+}$, *Nptn*$^{Y219X/+}$ and *Nptn*$^{+/+}$ data. Significant statistical differences were observed between *Nptn*$^{Y219X/Y219X}$ and *Nptn*$^{+/+}$ data, ***p<0.00001 (click – 1.11 x 10^{-13}, 8kHz - 6.37 x 10^{-15}, 12kHz – 5.85 x 10^{-16}, 20kHz – 3.28 x 10^{-17}, 6.97 x 10^{-13}). ABR traces were manually scored by two operators without knowledge of the genotype in order to remove bias.

Nptn$^{pitch/Y219X}$ animals have significantly raised auditory thresholds. The failure of the two mutants to complement indicates that neither parent is able to provide a WT copy of the causative gene, leading to inheritance of the recessive phenotype in the *Nptn*$^{pitch/Y219X}$ mice. Non-complementation in *Nptn*$^{pitch/Y219X}$ mice provides evidence to confidently assert that *Nptn* is the causative gene in *pitch*

3.5. Discussion

The results I have obtained through *in silico*, *in vitro* and *in vivo* studies of the *pitch* model confirm *Nptn* as a new deafness-related gene.

The three *in silico* prediction programs employed to assess the *pitch* missense mutation all suggested that substitution of the cysteine residue would be deleterious to protein function. Indeed, 3-D modelling of Np55 and Np65 show this residue (C199 and C315, respectively) to be an essential structural cysteine, required for disulphide bridge formation in Ig3 domain and the tertiary structure of this domain. Subsequent *in vitro* studies confirm the *pitch* mutation is not tolerated and that *pitch* is a loss-of-function allele with retention of mutant Neuroplastin in the ER of transfected cells. The ER is the site of the UPR pathway, which attempts to refold misfolded proteins and restore their function. However, as the *pitch* mutant Neuroplastin cannot form a disulphide bridge in Ig3, correct folding will not be possible, and thus will likely enter the ERAD pathway and protein degradation.

In the transfection studies, mutant Neuroplastin is present in cell lysates, but this is an over expression model with continuous production of transcript, giving much higher expression than would be seen in the normal state. It is interesting that although equivalent amounts of plasmid were transfected there appears to be less mutant Neuroplastin protein compared to WT when assessed by Western blot. It would be tempting to speculate that the mutant protein is being broken down. Importantly, the *in vitro* data showing reduced glycosylation and retention in the ER of mutant Neuroplastin will prevent it from being expressed at the cell surface, and thus from fulfilling its function as a CAM.

Auditory phenotyping identified profound deafness in *Nptn*^{pitch} mutant mice. Click box and ABR testing of a second Nptn mouse model, *Nptn*^{Y219X}, identified an identical phenotype in mutant mice to that observed in *Nptn*^{pitch} mutant mice. Complementation testing failed to recover auditory function in compound heterozygous (*Nptn*$^{pitch/Y219X}$) mice, confirming that Neuroplastin is the causative *pitch* gene and confirming the recessive nature of the mutation. The correlation of the auditory phenotype in both models supports the data obtained from the *in silico* and *in vitro* studies, showing that *pitch* is a loss-of-function allele.

Having established that the *pitch* mutation is the cause of the hearing loss phenotype and that Neuroplastin is essential for auditory function, I next wanted to ascertain the role of Neuroplastin protein within the auditory pathway. As discussed in chapter 1, sensorineural hearing loss can be caused by dysfunction of any part of the sensory transduction pathway. Very little has been published regarding *Nptn,* and neither Np55 nor Np65 have previously been reported to be expressed in the ear.

In order to elucidate the requirement of Nptn in the ear and to elaborate upon the molecular mechanism through which Nptn functions, several key questions remain to be explored:

- What is the onset of the hearing phenotype in *pitch* mice?
- What is the expression profile of *Nptn* in the inner ear?
- Which protein isoform of Neuroplastin (Np55/Np65/both) is essential for hearing?
- Where does Nptn protein localise within the ear?
- Does the temporospatial expression pattern implicate a potential mechanism?
- Are there developmental/physiological defects that may help explain the phenotype?

To answer these questions extensive *in vivo* and *ex vivo* studies were undertaken using WT and $Nptn^{pitch/pitch}$ mice.

Chapter 4. Characterisation of Neuroplastin in the auditory system

Auditory assessment at 8-weeks of age identified a profound hearing loss phenotype in *Nptn*$^{pitch/pitch}$. However, the onset of hearing in mice is around 6 weeks earlier, at approximately P12. Therefore I looked at earlier time points to assess when the hearing loss phenotype becomes evident in *Nptn*$^{pitch/pitch}$ mice.

4.1. Onset of auditory impairment in *Nptn*$^{pitch/pitch}$ mice

Most human recessive deafness genes result in a severe to profound, congenital hearing loss. In order to establish if the *pitch* mutation causes congenital auditory impairment, ABR was performed on P16 *pitch* mice, which is the earliest time point at which ABR testing can be completed in accordance with our Home Office Licence.

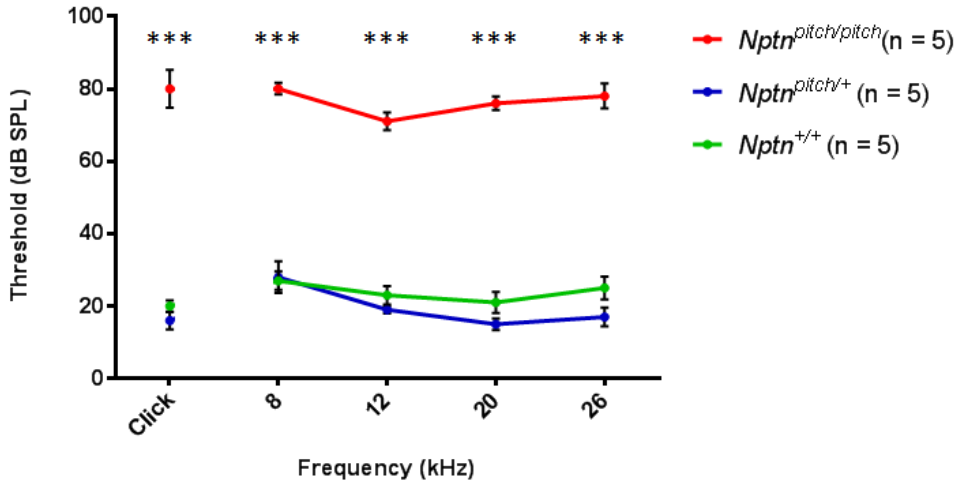

Figure 38. P16 *Nptn*$^{pitch/pitch}$ mice have severe auditory impairment.

At P16, wild type (*Nptn*$^{+/+}$) and heterozygous (*Nptn*$^{pitch/+}$) mice display normal hearing thresholds (20 – 30dB) at all frequencies tested. Homozygous (*Nptn*$^{pitch/pitch}$) animals display extremely elevated thresholds (≥70dB) at all frequencies tested, compared to *Nptn*$^{+/+}$ and *Nptn*$^{pitch/+}$ littermate mice. Statistical analysis: Levene's test followed by One-way ANOVA with post-hoc Tukey adjustment. No statistical differences were detected between *Nptn*$^{pitch/+}$ and *Nptn*$^{+/+}$ data. Significant statistical differences were observed between *Nptn*$^{pitch/pitch}$ and *Nptn*$^{+/+}$ data, ***p<0.00001 (click – 2.23 x10^{-8}, 8kHz – 3.59 x10^{-8}, 12kHz – 9.29 x 10^{-10}, 20kHz – 2.45 x 10^{-10}, 26kHz – 1.29 x 10^{-8}). ABR traces were manually scored by two operators without knowledge of the genotype in order to remove bias.

Similar to the 8-week ABR data, the hearing thresholds of *Nptn*$^{+/+}$ and *Nptn*$^{pitch/+}$ mice at P16 are within the normal range (between 20 and 35dB) at all frequencies tested. However, P16 *Nptn*$^{pitch/pitch}$ mice display very elevated average thresholds of 70 – 80dB at all frequencies tested (Figure 38).

The results obtained from P16 mice, suggest that *Nptn*$^{pitch/pitch}$ animals are likely to have a profound auditory impairment from P12, the onset of hearing in mice. However, it is interesting to note that the thresholds observed at P16 (70-80dB), are slightly less severe than those observed for 8-week animals (≥90dB), which suggests there may be some progression to the hearing loss. Therefore, in order to ascertain if the phenotype has a progressive nature, ABR was undertaken on P27 *pitch* mice, and a comparison made between P16, P27 and 8-week data for *Nptn*$^{pitch/pitch}$ mice (Figure 39).

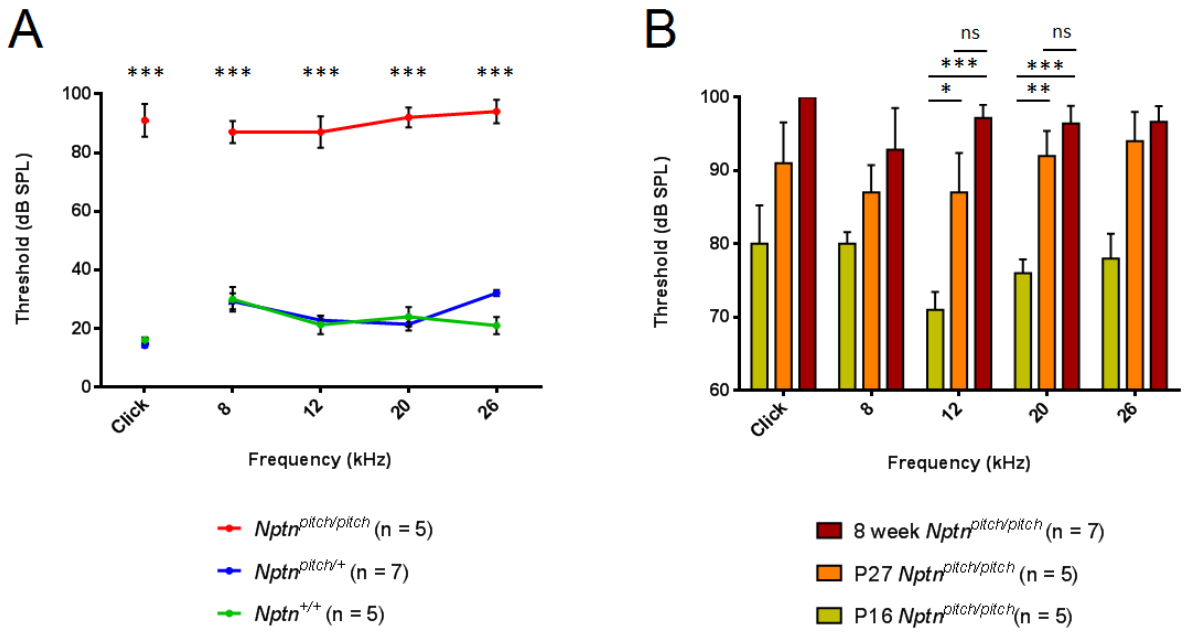

Figure 39. Progression of the hearing loss phenotype in *Nptn*$^{pitch/pitch}$ mice.

A) P27 *Nptn*$^{pitch/pitch}$ mice are severely hearing impaired. At P27, wild type (*Nptn*$^{+/+}$) and heterozygous (*Nptn*$^{pitch/+}$) mice display normal hearing thresholds (20 – 35dB) at all frequencies tested. Homozygous (*Nptn*$^{pitch/pitch}$) animals display very elevated thresholds (≥80dB) at all frequencies tested, compared to *Nptn*$^{+/+}$ and *Nptn*$^{pitch/+}$ littermate mice. Statistical analysis: Levene's test followed by One-way ANOVA with post-hoc Tukey adjustment. No statistical differences were detected between *Nptn*$^{pitch/+}$ and *Nptn*$^{+/+}$ data. Significant statistical differences were observed between *Nptn*$^{pitch/pitch}$ and *Nptn*$^{+/+}$ data, ***p<0.00001 (click – 3.02 x10^{-11}, 8kHz – 1.41 x10^{-8}, 12kHz – 4.55 x 10^{-9}, 20kHz – 7.70 x 10^{-11}, 26kHz – 3.66 x 10^{-11}). In order to remove bias ABR traces were manually scored by two operators without knowledge of the genotype. **B) Progression of hearing impairment in *Nptn*$^{pitch/pitch}$ mice.** Comparison of the P16, P27 and 8-week ABR data for homozygous (*Nptn*$^{pitch/pitch}$) mice shows there is a trend toward increasing ABR thresholds at all frequencies tested. However, the progression is only statistically significant between P16 and the later time points at 12 and 20kHz. (p values: 12kHz P16 vs P27 – 0.0147, 12kHz P16 vs 8 week - 0.0001, 20kHz P16 vs P27 – 0.003, 20kHz P16 vs 8 week – 0.0002, **p<0.01, ***p<0.001). Statistical analysis performed: Levene's test to assess parametricity, followed by One-way ANOVA with post-hoc Tukey test.

Similar to the P16 ABR data, the hearing thresholds of *Nptn*$^{+/+}$ and *Nptn*$^{pitch/+}$ mice at P27 are within the normal range (between 20 and 35dB) at all frequencies tested. However, P27 *Nptn*$^{pitch/pitch}$ mice display very elevated average thresholds of >80dB at all frequencies tested (Figure 39A). Comparison of the P16, P27 and 8-week ABR data obtained from *Nptn*$^{pitch/pitch}$ mice shows that between P16 and P27 there is an increase in hearing threshold at all frequencies tested, with a 5 to 15dB increase depending on the frequency examined (Figure 39B). However, the hearing threshold increases

observed between P16 and P27 are only statistically significant at two frequencies (12 and 20kHz). Between P27 and 8-week, there is a trend for an increase in hearing threshold at all frequencies tested, but none of these changes were found to be statistically significant. Comparison of P16 and 8-week data show there is an increase in hearing thresholds at all frequencies tested, with a 15 to 25dB increase depending on the frequency examined (Figure 39B). However, the threshold increases between P16 and 8-week are again only statistically significant at two frequencies (12 and 20kHz) (Figure 39B). Whilst these data are not entirely conclusive, they do suggest there is a slight progressive nature to the hearing loss in *pitch* mutant mice. Although, given the P16 data it is unlikely these mutant mice ever develop normal hearing thresholds at the onset of hearing, but instead have impaired hearing that rapidly worsens.

4.2. Expression of Neuroplastin in the inner ear

Having established *Neuroplastin* is the causative gene in the *pitch* model, and having established the hearing loss phenotype is evident from P16 (and likely from the onset of hearing), I proceeded to undertake studies to identify the role of this novel deafness gene within the auditory system. At the time I began my studies the only published information regarding expression of this protein was derived from rat and mouse *ex vivo* studies, identifying expression in the eye and brain. However, no studies had been performed to assess Np65 expression in the ear. Therefore, my first priority was to establish if, and when, *Neuroplastin* is expressed within the ear.

4.2.1. Expression profile of *Neuroplastin* isoforms in the postnatal mouse ear

To establish the normal expression profile of *Neuroplastin* in the ear I undertook qRT-PCR analysis of RNA derived from whole cochleae taken from sighted-C3H mice at a series of ages (P4, P8, P12, P16, P21, P24, and P27). I extracted total RNA from these ears and synthesised complementary DNA (cDNA). Five biological replicates were collected for each age and these were each assessed using three technical replicates. The quantitative reverse transcriptase (qRT)-PCR assays were performed

using custom TaqMan® assays designed to specifically recognise the Np55 transcript or the Np65 transcript. A β-actin TaqMan® assay was employed as an endogenous control, and used to determine that levels of cDNA did not vary between samples and replicates.

The aim of this experiment was to establish not only the timeframe of expression, but also to identify if there is isoform-specific expression of *Neuroplastin* within the ear.

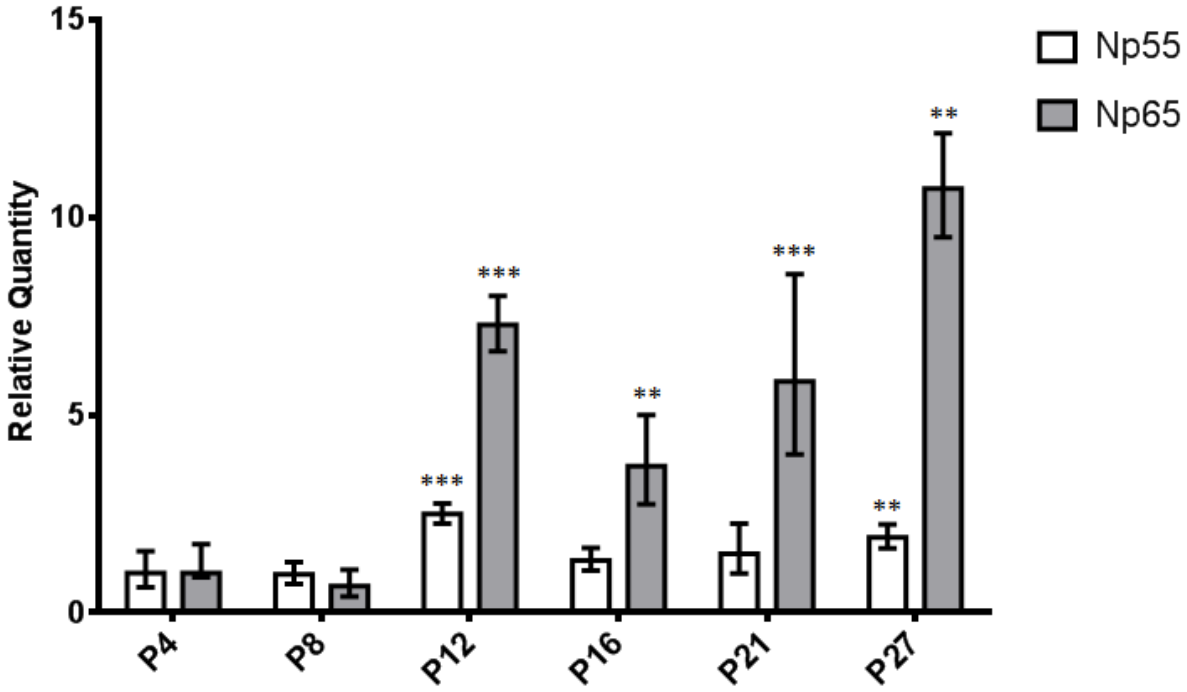

Figure 40. Neuroplastin transcripts are temporally regulated and isoform-specific in the postnatal mouse inner ear.

RNA was prepared from wild type inner ears at P4, P8, P12, P16, P21 and P27, and assessed using qRT-PCR assays to identify transcript levels of Np55 and Np65. B-actin was used an endogenous control and showed minimal variation across biological and technical replicates at all time points. Absolute transcript levels at each time point were compared to transcript levels at P4 and reported as relative quantities (RQ) for both the biological group as a whole and the technical replicates within each biological group. Transcript levels for Np55 were fairly consistent across all time points, displaying small increases at P12 (RQ = 2.49) and at P27 (RQ = 1.9). However, at P12 relative levels of the Np65 transcript were significantly elevated (RQ =7.28) and this trend was observed across all subsequent time points. Statistical analysis of technical replicates within biological groups: One-way ANOVA with post-hoc Tukey adjustment for multiple comparisons. Multiplicity p values reported. ** $p < 0.01$, *** $p < 1 \times 10^{-5}$. Error bars = RQ minimum and maximum.

The timecourse qRT-PCR is depicted in Figure 40. At P12 expression of Np65-specific transcripts were significantly increased approximately 7-fold compared to Np65-specific transcripts at P4. Increased Np65 transcript levels were sustained from P12 onwards. Np55-specific transcripts showed a small level of variaton across timepoints, however induction of Np55 transcripts was consistently several fold lower than observed for Np65.

The increased levels of Np65-specific transcripts within the cochlea, compared to the low levels of Np55-specific transcripts, indicates that the Nptn protein isoform Np65 is likely functionally important within the auditory system. The timing of the increase in expression of Np65-specific transcripts is coincident with the functional maturation of the inner ear sensory hair cells and the onset of hearing in mice. Therefore, this expression profile suggests Np65 could have an important role in the maturation of hearing.

To assess whether the *pitch* mutation affects transcription of Np65 in the ear, qRT-PCR of RNA extracted from P18 WT C3H (n = 5) and P18 $Nptn^{pitch/pitch}$ (n = 2) was undertaken.

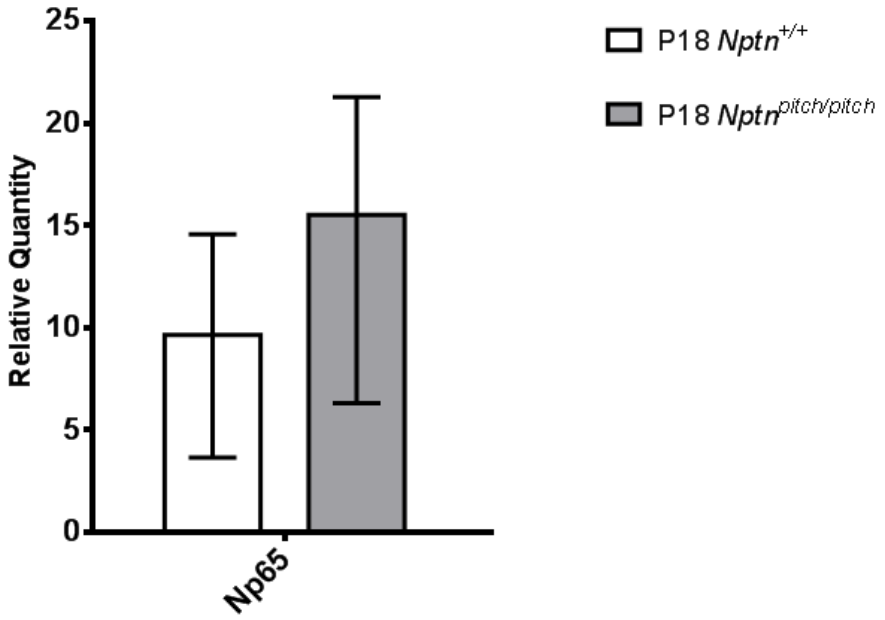

Figure 41. Np65 is expressed at the transcript level in P18 *Nptn*$^{pitch/pitch}$.
qRT-PCR of RNA prepared from *Nptn*$^{pitch/pitch}$ (n=2) whole ears identified an approximate 15 fold increase in relative Np65 transcript levels when compared to baseline levels established in P4 WT C3H mice (see figure). Np65 transcript levels in P18 WT (n = 5) C3H whole ear samples showed an approximate 10 fold relative increase to those identified at P4. Levene's test followed by One-way ANOVA and post-hoc Tukey test failed to identify any significant difference between WT and *Nptn*$^{pitch/pitch}$ mice, however this may be due to the low sample number for *Nptn*$^{pitch/pitch}$. These results indicate that transcription is not affected by the *pitch* mutation. Error bars = RQ min and max

Relative Np65 transcript levels at P18 were found to be elevated in both WT and *Nptn*$^{pitch/pitch}$ when compared to Np65 transcript levels at P4, however due to low sample number it was not possible to ascertain if there was any difference in transcript induction between WT and *Nptn*$^{pitch/pitch}$. These results indicate that the *pitch* mutation does not affect transcription, and thus it is likely that mutant Np65 protein is produced.

4.2.2. DAB staining of cochleae to identify Np65 expression

Having established that Np65 is the predominant Neuroplastin isoform expressed in the inner ear, I next wanted to identify where within the ear Np65 is expressed. In order to do this I used an indirect immunohistochemistry method to label cochlear mid-modiolar sections. Briefly, sections were immunolabelled with a primary antibody raised against Np65, followed by amplification with a

biotinylated secondary antibody that bound the primary antibody. Next an Avidin-Biotinylated enzyme complex was applied, which binds the secondary antibody. When DAB substrate is then added to the sections, the enzyme complex catalyses the reaction and produces a positive immunoreaction product, i.e. brown staining at the site where the initial primary antibody bound. Staining was assessed using light microscopy with a 40x objective (Figure 42).

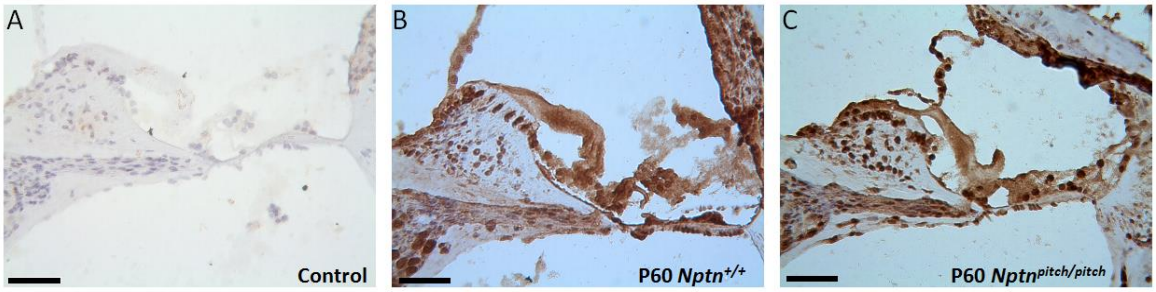

Figure 42. Np65 expression in the ear - DAB staining.

A) No non-specific DAB staining was observed in the 'no primary' control. **B)** DAB staining of a P60 *Nptn*$^{+/+}$ mid-modiolar cochlear section immunolabelled with a primary antibody against Np65 (1:40). Brown staining developed rapidly, within 5 – 10 seconds of DAB application, in the organ of Corti and surrounding tissues. Stained tissues displayed poor morphology. **C)** DAB staining of a P60 *Nptn*$^{pitch/pitch}$ mid-modiolar cochlear section immunolabelled with a primary antibody against Np65. Brown staining developed rapidly, as seen in *Nptn*$^{+/+}$, throughout the cochlea. Gross morphology of both samples appeared disrupted, likely as a result of poor fixation or sectioning. Scale bar = 10µM.

Unfortunately, this approach proved unsuccessful. The no primary antibody control showed very little non-specific brown staining (Figure 42a). However, when primary antibody was included (1:40), brown staining was observed almost ubiquitously throughout all cells within the section (Figure 42b and c). Serial dilutions of the primary antibody (1:100, 1:200, 1:500 and 1:1000) also produced rapid and widespread staining throughout the tissue (data not shown). Given these data I decided to stop employing this approach and moved on to use other techniques.

In addition to the failed staining, it was apparent from studying the slides that the tissue sections had very poor morphology. As this was observed for all of the charged slides generated from

sectioning of half heads, regardless of genotype, it is likely that the poor morphology is due to a defect of fixation, processing or sectioning of this tissue. As such further histological assessment of the cochlea was made using resin-embedded sections.

4.2.3. Immunofluorescence labelling of thick-cut vibratome sections

In order to improve section morphology and increase sensitivity of antibody detection, I next attempted immunolabelling of vibratome-cut cochlear sections. Cochlear sections were immunolabelled with anti-Np65 to identify Np65 expression, anti-Neurofilament NF-200 to demark the peripheral neuronal processes and the spiral ganglion neurones, and DAPI a nuclear marker.

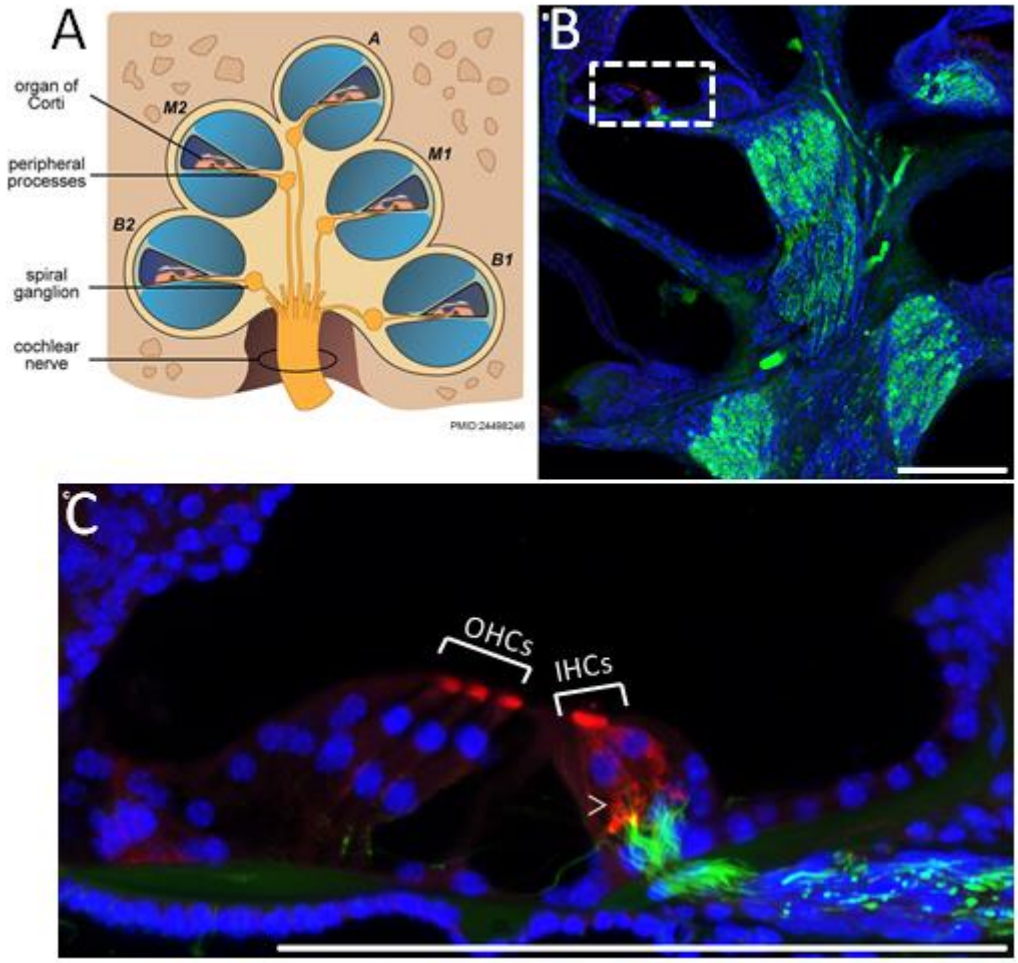

Figure 43. Immunolabelling identifies expression of Np65 at the basolateral aspect of the IHC and the cuticular plate of OHCs and IHCs.

A) Cartoon depicting a mid-modiolar section through the cochlea, adapted from (Locher et al., 2014) **B)** x10 image of a P16 *Nptn*$^{pitch/+}$ immunolabelled cochlea section. Sections were labelled with anti-Np65 (red), anti-NF200 (green) and co-stained with DAPI (blue). Np65 expression could be detected in the organ of Corti, boxed area. **C)** x40 confocal z-stack of a P16 *Nptn*$^{pitch/+}$ cochlear section. The organ of Corti (boxed area in B) was imaged using an x40 objective. Confocal z-stack images were taken through the section and maximum intensity projection generated. Images identified Np65 expression at the basolateral aspect of the inner hair cell (IHC) (>). However, at this resolution it is unclear whether Np65 is expressed in the IHC, dendritic projections, or both. Labelling was also observed at the cuticular plate of the IHCs and the outer hair cells (OHCs). There was no apparent difference in labelling observed between *Nptn*$^{+/+}$ and *Nptn*$^{pitch/+}$ cochleae. Scale bar = 100µM.

Confocal-microscopy imaging of the immunolabelled cochlear sections revealed that Np65 expression appears to be restricted to the organ of Corti, in particular the IHCs and OHCs (Figure 43).

In both sensory hair cell types, Np65 is apparent at the apical cuticular plate, the structure from which the stereocilia extend. Np65 is also expressed at the basolateral aspect of the IHCs. However, it is unclear whether this signal is coming from the IHCs, the afferent dendrites (labelled with anti-neurofilament NF-200 – green), or both.

Given that Neuroplastins are reported to be synapse-enriched proteins, identification of Np65 localization at the basolateral aspect of the IHCs is very interesting. It is reported that Np65 can homophilically bind across synaptic clefts and as such it would be tempting to speculate that within the ear Np65 homodimerizes across the IHC/afferent neuron synapse. Unfortunately, given the resolution it was not possible to ascertain the exact expression of Np65 from the confocal z-stack. Expression of Np65 at the cuticular plate of the sensory hair cells was less expected and it is more difficult to postulate a role for Neuroplastin within this structure.

This initial study had been performed using P16 mice, to further explore the expression of Np65, and to determine expression changes within the cochlea, mice at additional ages were assessed.

4.2.4. Wholemount immunolabelling time course for Np65 expression

Immunolabelling of vibratome-cut sections revealed that Np65 expression in the cochlear was localised in the IHCs and OHCs of the sensory epithelium. To study the expression of Np65 further, immunolabelling was performed on wholemount cochlear sensory epithelia derived from WT sighted-C3H animals at P8, P10, P12, P14, P16, P18, P21, P22, P23, P24 and P27. The use of cochlear wholemounts was preferable as they are: less labour intensive than thick-cut vibratome sections; can be completed in 1-2 days rather than 1 -2 weeks; and, are much easier to orientate for microscopy.

Cochlear sensory epithelia were immunolabelled with anti-Np65 and co-labelled with Phalloidin to identify the actin-rich hair cell stereocilia and Pillar cells.

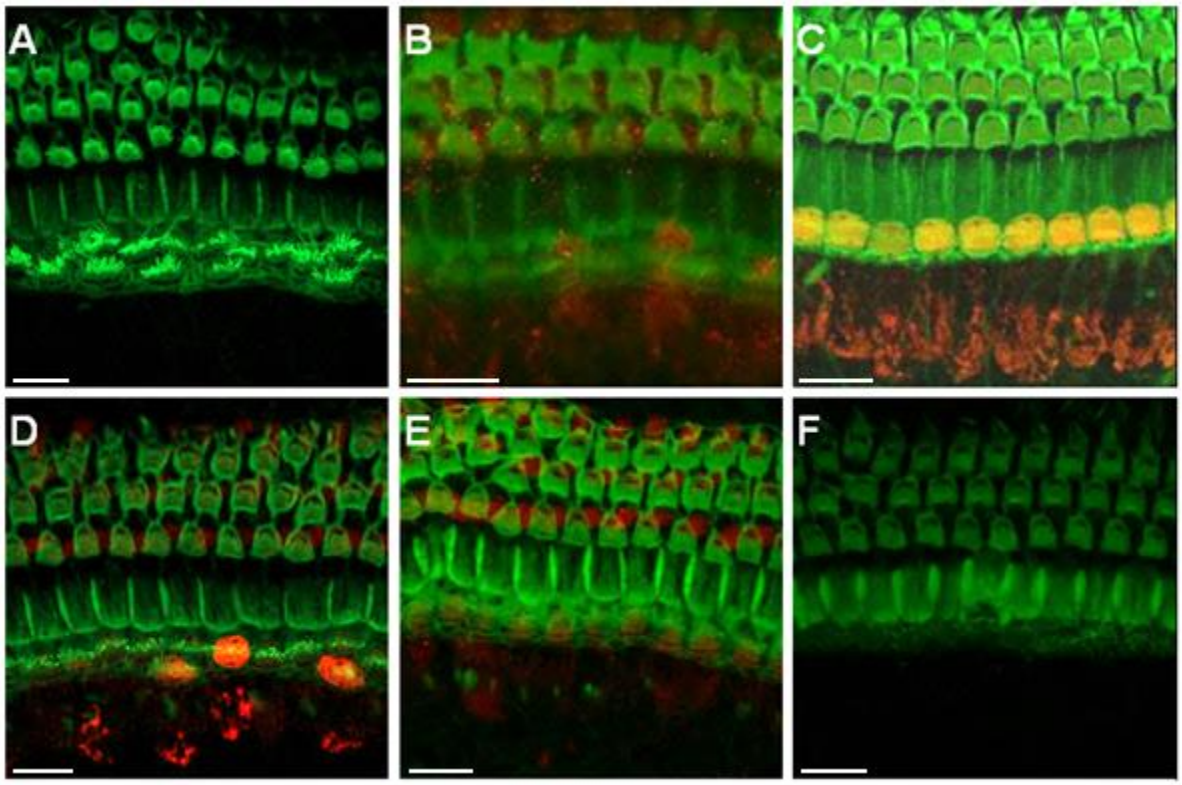

Figure 44. Time course of Np65 expression in cochlear whole mount sensory epithelia.

Whole mount cochlear sensory epithelia were immunolabelled with anti-Np65 (red) and co-labelled using Phalloidin to demark the actin-rich hair cell stereocilia and Pillar cells (green). **A)** At P12 no Np65 expression was detected in the cochlear sensory epithelium. **B)** At P14 a low level of Np65 expression was observed in the IHCs and OHCs. **C)** At P21 strong expression of Np65 was identified at the basolateral aspect of the IHC, and at the IHC cuticular plate. **D)** At P22 Np65 expression is detected at the basolateral aspect of some IHCs and the cuticular plate of some IHCs and most OHCs. **E)** At P23 Np65 expression is still detected in the OHC and at a very low level in some IHCs. **F)** At P24 no Np65 expression could be detected in either the IHCs or OHCs. Scale bar = 10µM.

This analysis revealed that Np65 is detectable in the sensory epithelium from P14 to P23 (see Figure 44). These data are only partially consistent with the data from the qRT-PCR study, which indicated that Np65 transcript levels increased in the ear between P12 and P27. The difference in onset of expression could be due to the sensitivity of the antibody, perhaps Np65 protein is present at P12 but is at a level below the detection threshold of the antibody. However, an explanation as to why no protein is detectable at P24, when transcript levels are still very abundant, is more difficult. It could be that Neuroplastin begins to be expressed elsewhere in the inner ear (qRT-PCR was

undertaken using RNA from whole inner ear), or the localization of the protein becomes very restricted such that it is not discernible as a broad labelling as seen at P14 to P23.

4.2.5. Absence of Np65 in the sensory hair cells of *Nptn*$^{pitch/pitch}$

Having established that Np65 is expressed in the sensory hair cells of WT sighted-C3H mice, I next performed wholemount immunolabelling of P16 *Nptn*$^{pitch/pitch}$ cochlear sensory epithelia to assess the effect of the *pitch* mutation on protein expression within the ear. In addition to the antibodies against Np65 and Phalloidin (see section 4.2.4), an antibody against Otoferlin was used to demark the inner hair cells.

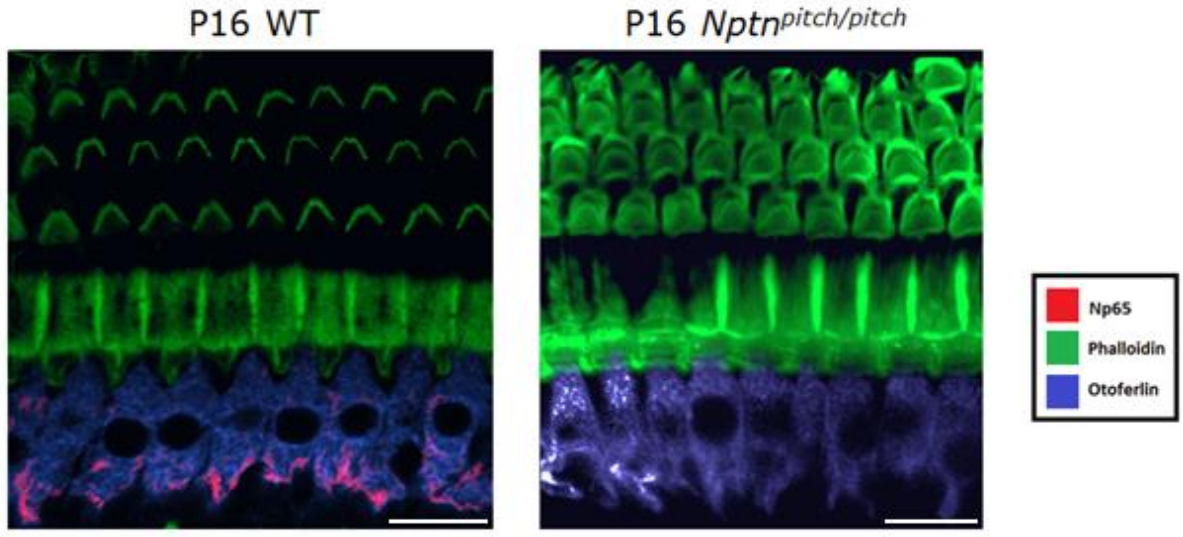

Figure 45. Np65 is not expressed in *Nptn*$^{pitch/pitch}$ mice.

Whole mount immunolabelling of P16 cochlea from *Nptn*$^{pitch/pitch}$ and WT (*Nptn*$^{+/+}$) littermates was undertaken using antibodies against Np65 (red) and Otoferlin (blue). Sensory epithelia were co-labelled with Phalloidin (green) to identify the hair cell stereocilia and Pillar cells. Confocal z-stack images were taken and used to generate maximum intensity projections. Np65 expression was observed at the basolateral aspect of the IHCs in *Nptn*$^{+/+}$ mice, with a cerise signal observed due to co-occurrence of red and blue signals from Np65 and Otoferlin, respectively. In *Nptn*$^{pitch/pitch}$ mice, no Np65 (red) signal could be detected in the sensory epithelia. Scale bar = 10µM.

Analysis of confocal z-stack images and maximum intensity projections identified localization of Np65 to the basolateral aspect of *Nptn*$^{+/+}$ IHCs. However, no expression of Np65 was seen within the

sensory epithelium of *Nptn*$^{pitch/pitch}$ mice (Figure 45). This finding supports the results obtained for the *in vitro* studies, which suggest that the *pitch* mutation causes loss-of-function due to retention of the misfolded protein in the ER.

Confirmation that Np65 transcript is produced was obtained using qRT-PCR analysis of RNA isolated from P18 *Nptn*$^{pitch/pitch}$ whole inner ears (see figure 41). This indicated that the Np65-specific transcript is expressed in *Nptn*$^{pitch/pitch}$ inner ears, and at a level similar to that observed in P18 WT sighted-C3H animals. These data suggest that if transcript is present, mutant Np65 protein is likely translated, but is not stable due to the presence of the *pitch* mutation.

4.2.6. Np65 immunogold labelling

To try and identify the specific subcellular localization of Np65 in cochlear hair cells, we established collaboration with David Furness (Keele University), who attempted to use the anti-Np65 antibody for immunogold labelling of P16 WT cochleae, coupled to transmission electron microscopy (TEM). This technique would provide a much higher optical resolution than I could achieve using confocal microscopy. Unfortunately, the anti-Np65 antibody was found to be unsuitable for immunogold labelling and this experiment had to be abandoned.

4.2.7. DAB staining of immunolabelled wholemount cochleae

At the suggestion of our collaborator (David Furness) I attempted DAB staining of Np65-immunolabelled sensory epithelia. The reaction produces an electron-dense chromogen at the site of DAB staining, which can be detected by TEM. Protein detection by this method is less sensitive that immunogold labelling, but has much higher sensitivity than conventional fluorescence confocal microscopy. To visualize the DAB-stained cochleae, tissue is resin embedded, ultra-thin sections produced, and assessed by TEM.

DAB staining was attempted using several dilutions of the anti-Np65 primary antibody (1:50, 1:500, 1:1000, 1:5000, and 1:10000).

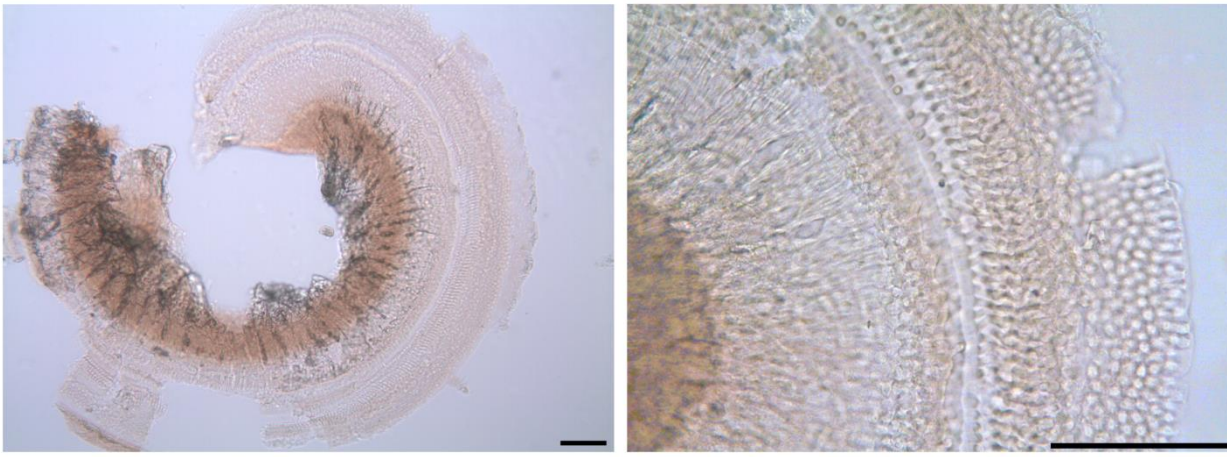

Figure 46. DAB staining of P16 C3-sighted WT cochlear sensory epithelia.

A) Light microscopy image of 1:10,000 dilution anti-Np65 DAB stained cochlear sensory epithelia using an x5 objective. Diffuse brown staining developed rapidly (<30 seconds) and was observed throughout the cochlea **B)** Light microscopy image of 1:10,000 dilution Np65 DAB stained cochlea using x20 objective. Further magnification revealed almost ubiquitous brown staining throughout the cochlea. Scale bar = 50µM.

Unfortunately, as was found for the DAB staining of wax sections, this technique proved unsuccessful. Brown staining developed rapidly (<30 seconds) and in almost every cell of the sensory epithelium (see Figure 46). Attempts to optimise the primary antibody dilution and tissue fixation did not improve the results obtained. Shortening the length of DAB chromogen incubation did not change the expression pattern observed and increasing the length of the incubation led to dark brown staining throughout the cochleae.

The data obtained suggests that the antibody used for this technique is not suitable for DAB staining.

4.3. Analysis of cochlear morphology

Having established that Np65 is absent in the sensory hair cells of *Nptn*$^{pitch/pitch}$, I next assessed gross cochlear morphology of *Nptn*$^{pitch/pitch}$ mice. Visible pathology may help to elucidate the role of Np65 and provide insight into a mechanism for the auditory deficit detected in *Nptn*$^{pitch/pitch}$ mice. Two

approaches were taken to assess morphology: histological examination of sectioned cochleae and ultrastructural analyses of whole cochleae.

4.3.1. Histological examination of semi-thin resin embedded cochlear sections

Since the DAB staining experiment had highlighted the poor morphology of my wax embedded cochlear sections (see section 4.2.2), I instead used resin-embedded cochlear sections to assess morphology. Mid-modiolar cochlear sections were stained using Richardson's stain and assessed by light microscopy.

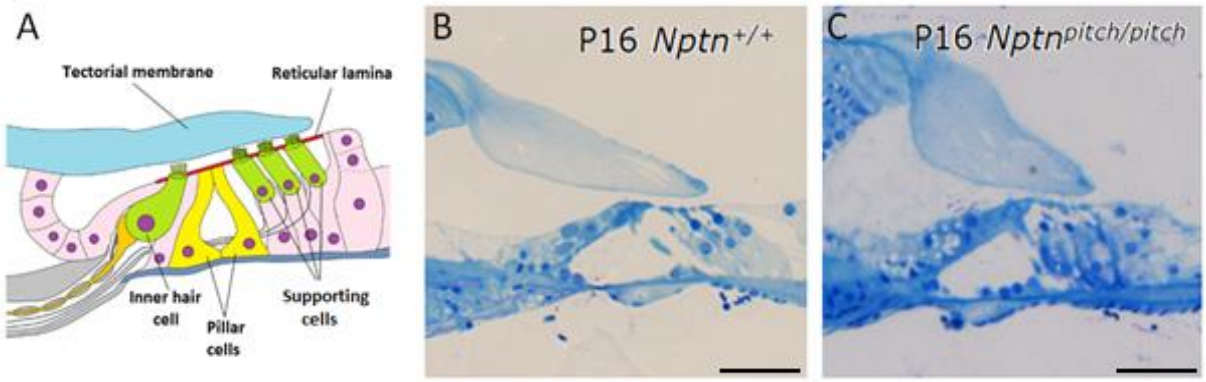

Figure 47. P16 *Nptn*$^{pitch/pitch}$ organ of Corti have grossly normal morphology.

A) Cartoon to depict the structures within the organ of Corti. **B)** A P16 *Nptn*$^{+/+}$ mid-modiolar cochlea section. A single IHC and three OHCs are apparent, with their respective supporting cells below. The tectorial membrane and tunnel of Corti appear to have normal structure. **C)** A P16 *Nptn*$^{pitch/pitch}$ mid-modiolar cochlea section. Again, a single IHC and three OHCs are distinguishable, along with their supporting cells. There did not appear to be any gross morphological disruption in *Nptn*$^{pitch/pitch}$. Scale bar = 10µM.

Cutting inner ears in an identical plane, especially at the early stage P16, is particularly difficult with this technique. The combination of low sample weight as well as the cochlea's multiple chambers lead to slight shifts of the sample as the resin diffuses and cures, resulting in minor differences in orientation. The sections shown have slightly different orientations, giving the impression that the *Nptn*$^{pitch/pitch}$ section has thickened sensory epithelia. However, closer inspection identifies that this section is not completely parallel through the tunnel of Corti, making the outer structures appear denser.

Analysis of the semi-thin resin sections did not identify any morphological differences between the *Nptn*$^{+/+}$ and *Nptn*$^{pitch/pitch}$ cochleae (Figure 47). In both sections, the nuclei of the OHCs are identifiable and are above their respective supporting cells. The tectorial membrane is appropriately positioned to exert the shearing force required for OHC signalling, and the basilar membrane appears unperturbed. The IHC nuclei are harder to identify in both sections, but there does not appear to be any gross differences. These data imply that the auditory phenotype detected in *Nptn*$^{pitch/pitch}$ mice is not attributable to a gross structural defect in the organ of Corti.

4.3.2. Ultrastructural analysis

To further assess the morphology of the hair cells in *Nptn*$^{pitch/pitch}$ mice, particularly at the apical aspect of the hair cells where Np65 expression was observed in the cuticular plate, ultrastructural analyses were performed using SEM at P16, P27 and P60. Whole cochleae were dissected and treated to Osmium tetroxide to maintain stereocilia rigidity, images taken along the length of the cochlea, and compared with images taken of equivalent *Nptn*$^{+/+}$ cochleae. A visual appraisal of the hair cells and quantification of hair cell number were used to assess the ultrastructure.

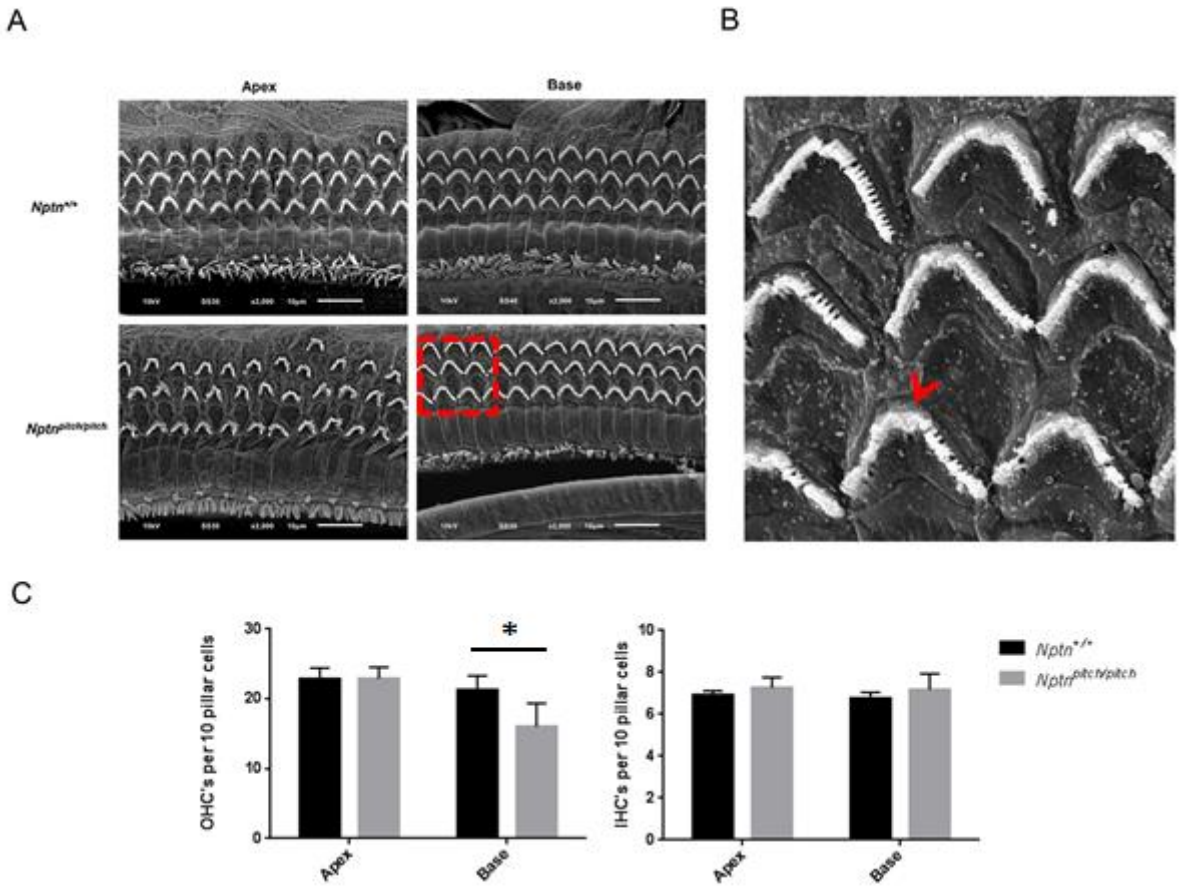

Figure 48. *Nptn*$^{pitch/pitch}$ mice have normal ultrastructure at P16.

A) SEM micrographs of P16 *Nptn*$^{+/+}$ and *Nptn*$^{pitch/pitch}$ apical and basal sensory epithelia. At the apex no obvious differences in the IHCs or OHCs were observed between *Nptn*$^{+/+}$ and *Nptn*$^{pitch/pitch}$ mice. For both genotypes, OHCs formed into 3 distinct rows. Apical IHCs were organised into a single row and appear to be of comparable length. Toward the base of the cochlea, normal IHC and OHC organisation is seen in *Nptn*$^{pitch/pitch}$ mice. However, some mild fusion of the stereocilia bundles in the OHCs was observed. **B)** A magnified image of the OHCs contained within the red box in panel A reveals that whilst the stereocilia are intact in *Nptn*$^{pitch/pitch}$ mice, the staircase arrangement of the three rows is not present in all OHCs. Fusion of stereocilia is observed (red arrowhead) in the majority of hair cells shown. This phenotype is not observed in the apical stereocilia. **C)** Hair cell counts from the apex and base of the cochlear spiral for P16 *Nptn*$^{+/+}$ and *Nptn*$^{pitch/pitch}$ mice. Hair cells were counted from images obtained from the cochlear apex and base (n≥4 for each genotype). There was no statistical variation in the numbers of IHCs or OHCs at the apex between genotypes. However, a decrease in basal OHC number is apparent in *Nptn*$^{pitch/pitch}$ mice. No difference in basal IHC counts between *Nptn*$^{+/+}$ and *Nptn*$^{pitch/pitch}$ was observed. Statistical analysis: Levene's test followed by Student's *t*-test one tailed. * = $p<0.05$. Scale bar = 10μM.

Analyses of P16 cochleae show the ultrastructure is grossly normal in *Nptn*$^{pitch/pitch}$ (Figure 48A and B). Hair cell counts identified a slight decrease in basal OHC number for *Nptn*$^{pitch/pitch}$ cochleae, but the organisation of the hair cells was mostly normal (Figure 48C). The slight reduction in OHC number in

the basal cochlea of *Nptn*$^{pitch/pitch}$ mice is unlikely to be the cause of the severe hearing loss phenotype observed at this age.

Some mild dysmorphology was visible at the very base of the cochlea in *Nptn*$^{pitch/pitch}$ mice. In some OHCs, stereocilium had started to fuse to neighbouring stereocilium, causing loss of the typical "staircase" organisation (Figure 48B). However, this fusion does not affect all basal OHCs at this age, and is not observed in the mid- or apical OHCs. No fusion is observed in IHCs. The presence of a grossly normal cochlear ultrastructure in *Nptn*$^{pitch/pitch}$ mice at P16 is surprising given that a broad-frequency, severe hearing loss is already present.

Stereocilia fusion can be an early sign of hair cell degeneration. In order to ascertain if the stereocilia fusion observed at P16 in *Nptn*$^{pitch/pitch}$ mice is a prelude to hair cell degeneration, the cochlear ultrastructure of P27 and P60 mice was assessed.

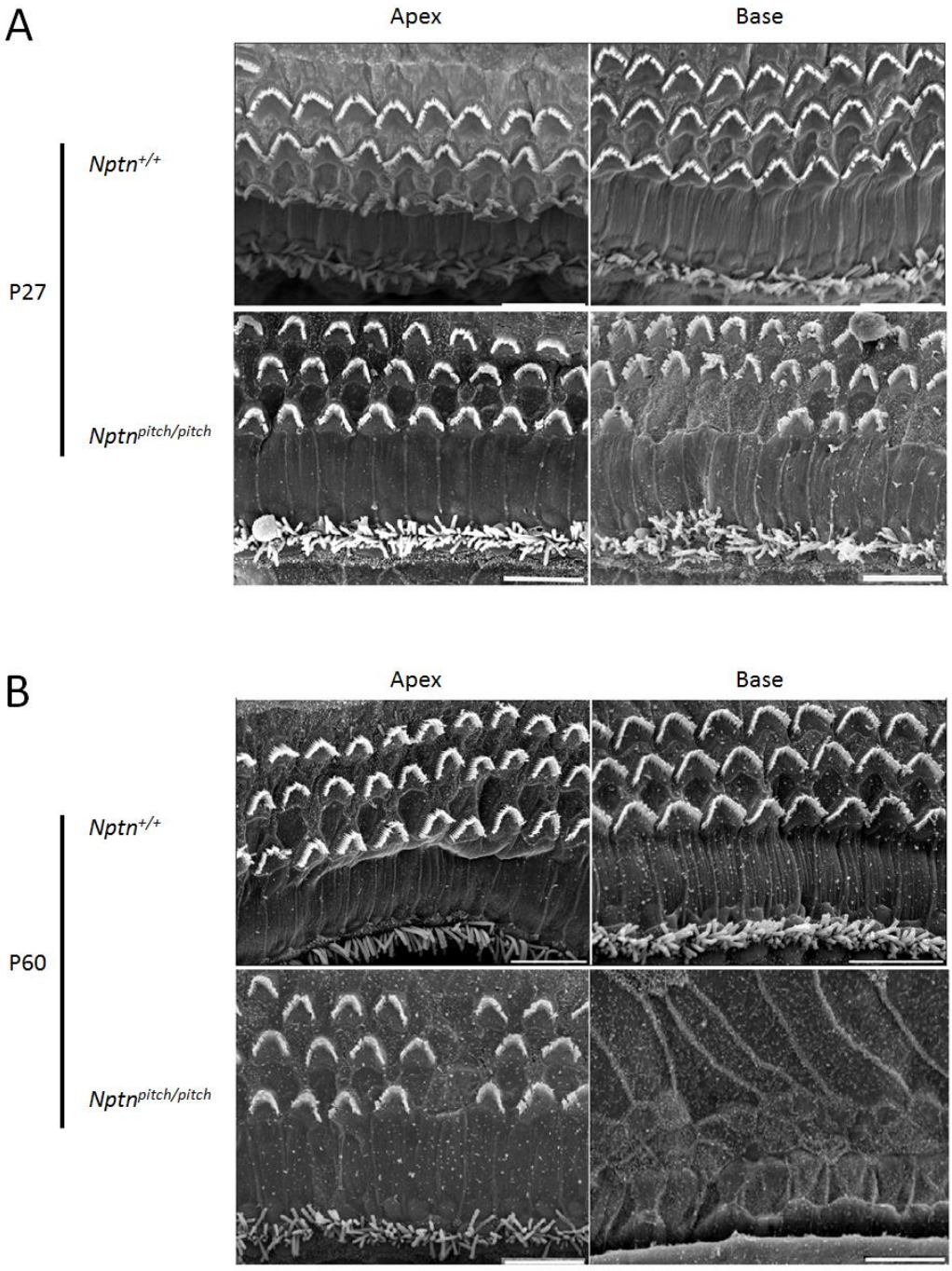

Figure 49. P27 and P60 ultrastructural assessment of *Nptn*$^{pitch/pitch}$ cochleae.

A) SEM images from the cochlear apex and base of P27 *Nptn*$^{+/+}$ and *Nptn*$^{pitch/pitch}$ mice. Hair cell dysmorphology is detected at both the apex and the base of *Nptn*$^{pitch/pitch}$ cochleae. Some stereocilia fusion is detected in OHCs at the apex of *Nptn*$^{pitch/pitch}$ and OHC degeneration is observed at the base of the cochlea. IHCs at the apex and base appear normal. **B)** SEM images from the cochlear apex and base of P60 *Nptn*$^{+/+}$ and *Nptn*$^{pitch/pitch}$ mice. OHC degeneration is observed at both the apex and base of *Nptn*$^{pitch/pitch}$ cochleae. Whereas, IHC degeneration is only detected in the cochlear base. As such, there appears to be a gradient of severity in the cochleae, with the base being more affected than the apex, and the level of degeneration increases with age. Scale bar = 10µM.

At P27 some mild OHC loss is observed at the basal turn of the cochlea, and in the apex some fusion of the stereocilia is visible (Figure 49A). By P60 OHC degeneration has also started to occur in the apex (Figure 49B). However, IHCs appear intact with no obvious dysmorphology. In the basal portion of P60 *Nptn*$^{pitch/pitch}$ cochleae there are no OHCs or IHCs present, suggesting these hair cells have all degenerated. The relatively late loss of the sensory hair cells, when compared to the early hearing loss phenotype, supports the hypothesis that the stereocilia fusion/hair cell degeneration is not the primary cause of the auditory phenotype observed in *Nptn*$^{pitch/pitch}$ mice.

As the cochlear ultrastructure is grossly normal at P16 in *Nptn*$^{pitch/pitch}$ mice, it suggests that stereocilia are likely functional. It would also suggest that the hearing loss is due to a pathology downstream of stereocilia function e.g. mechano-electrical transduction. The previously identified expression of Np65 at the basolateral aspect of the IHC (see section 4.2.3), coupled with the previously reported role of Np65 in synaptic maintenance and plasticity, and that synaptic innervation is required for the maturation of the auditory hair cells, suggests the pathology may be at the auditory synapse. Therefore cochlear electrophysiological studies were performed to assess hair cell maturity and synaptic function in *Nptn*$^{pitch/pitch}$ mice.

4.4. Electrophysiological analysis (collaborative work)

Electrophysiological analyses of *Nptn*$^{pitch/+}$ and *Nptn*$^{pitch/pitch}$ were performed at P6, P16 and P27 by our collaborators Stuart L. Johnson and Walter Marcotti at the University of Sheffield. The figures and legends presented in this section were prepared by Walter Marcotti for a manuscript we are currently preparing. The analysis in this section details my interpretation of the data obtained by our collaborators and their contextual relationship to the previous results I have reported for the *pitch* mouse model.

Electrophysiology was used to assess several electrophysiological parameters associated with OHC and IHC function. OHC cholinergic signalling was assessed to identify if the IHCs received normal

signals throughout postnatal development. Maturity of the IHC was assessed through the measurement of K^+ currents, which alter substantially throughout postnatal development. Vesicle replenishment and release was assessed to identify if neurotransmitter release was elevated or reduced, which may have an impact of the ability of the synapse to generate action potentials. These measurements would provide a profile showing whether auditory signalling is altered in *Nptn*$^{pitch/pitch}$ and give an indication of where the pathology is occurring.

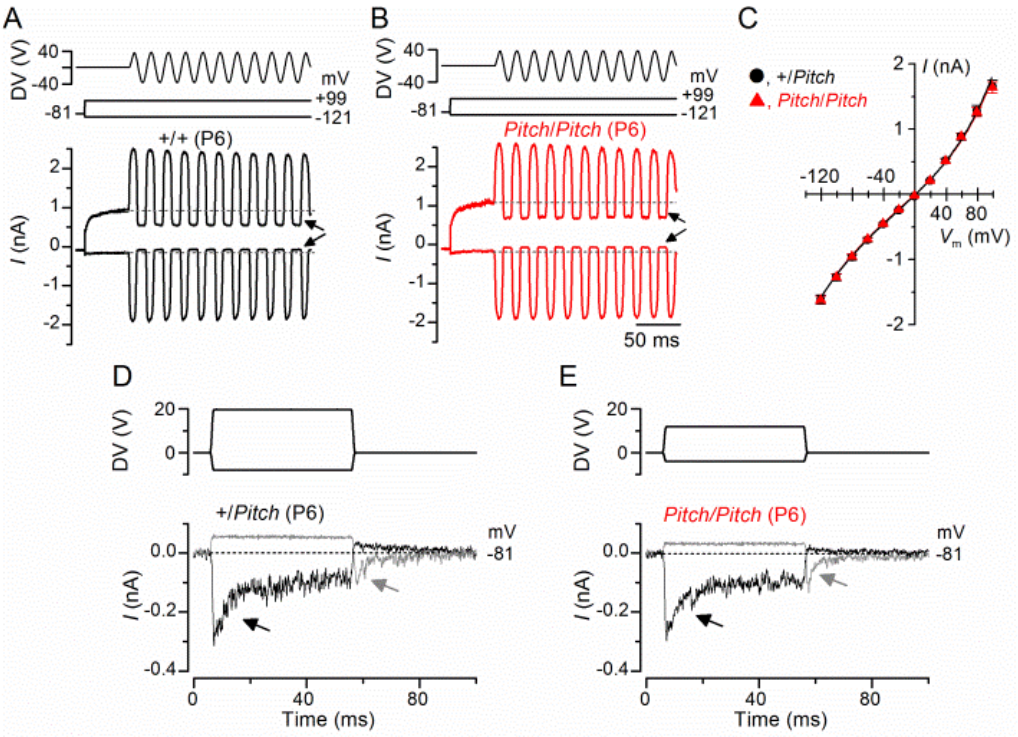

Figure 50. Mechanotransducer currents in outer hair cells from *pitch* mutant mice.

A and **B**, Saturating mechano-electrical transducer (MET) currents recorded from a P6 control (**A**) and *pitch* mutant (**B**) apical-coil OHC by applying voltage steps from −121 mV to +99 mV in 20 mV increments (holding potential −81 mV). For clarity, only two voltage steps are shown. During the voltage steps, hair bundles were displaced by applying a 50 Hz sinusoidal force stimuli (the driver voltage, DV, to the fluid jet is shown above the traces). Negative deflections of the DV are inhibitory. The arrows indicate the closure of the transducer channels, i.e. disappearance of the resting current, during inhibitory bundle displacements. Dashed lines indicate the holding current, which is the current at the holding potential of −81 mV. **C**, Peak-to-peak current-voltage curves obtained from ten controls and eight *pitch* mutant OHCs (P6). The fits through the data are according to a simple single-energy-barrier model (Geleoc et al., 1997): $I(V) = k\,[\exp((1-\gamma)(V-V_r)/V_s) - \exp(-\gamma(V-V_r)/V_s)]$ (eqn.1), where k is a proportionality constant, V_r is the reversal potential, V_s is a measure for the steepness of the rectification, and γ is the fractional distance within the membrane's electrical field of an energy barrier, as measured from the outside, with values: control $k = 445 \pm 37$, $V_r = 0.4 \pm 0.1$ mV, $V_s = 39 \pm 3$ mV, $\gamma = 0.42 \pm 0.01$; *pitch* mutant $k = 428 \pm 31$, $V_r = 0.1 \pm 0.2$ mV, $V_s = 38 \pm 2$ mV, $\gamma = 0.42 \pm 0.01$. **D** and **E**, Driver voltages to the fluid jet (top) and transducer currents recorded at –81 mV and +99 mV from a control and a *pitch* mutant OHC, respectively. Note that excitatory bundle deflection (positive DV) elicited inward transducer currents that declined or adapted over time (black arrows) in both genotypes. A small transducer current was present at rest (before t = 0) and inhibitory bundle displacements (negative DV) turned this off. Upon termination of the inhibitory stimulus, the transducer current in control and mutant OHCs showed evidence of rebound adaptation (grey arrows).

Mechano-electrical transducer (MET) currents were measured to assess OHC channel function (Figure 50). The results obtained indicate that there is no difference in MET channel function

between *Nptn*$^{pitch/+}$ and *Nptn*$^{pitch/pitch}$ at P6 (Figure 50A, B and C) Stereocilia bundle deflection was found to function correctly, with a small transduction current detectable in their resting state, and deflections causing excitation and inhibition of transduction as anticipated (Figure 50D and E).

This result indicates that OHCs are acting as expected in *Nptn*$^{pitch/pitch}$ and the cholinergic signalling required for postnatal maturation of K^+ currents in the IHC is occurring. This data implies that the common progenitor cell for the OHC and IHC is not defective and is capable of developing into hair cells that function in a physiological capacity.

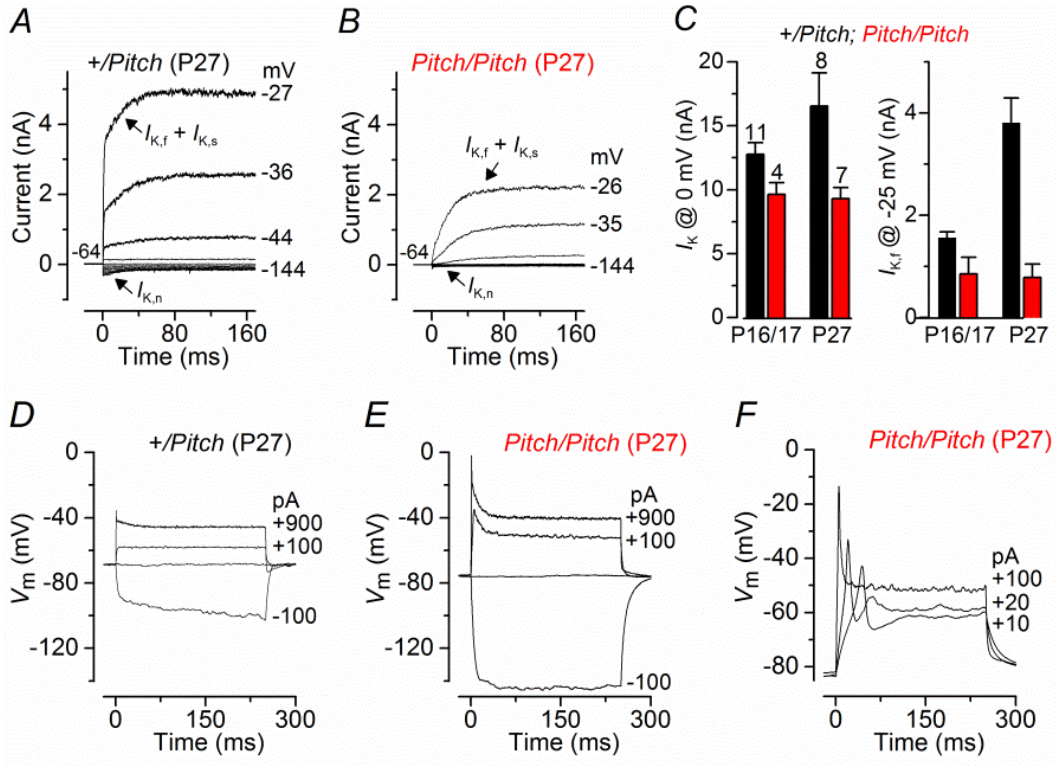

Figure 51. Current and voltage responses in adult IHCs from *pitch* mice.

A and **B**, Potassium currents recorded from mature control and mutant IHCs, respectively, elicited by depolarizing voltage steps (10 mV nominal increments) from –144 mV to more depolarized values from the holding potential of –64 mV. The K^+ currents characteristic of adult IHCs, $I_{K,n}$ and $I_{K,f}$, were smaller in mutant IHCs. **C**, Size of the total outward K^+ current and the isolated $I_{K,f}$ (measured at 2 ms from onset and at –25 mV: (Marcotti et al., 2003)) in adult (P16/17) and mature (P27) IHCs. **D**-**F**, Voltage responses from a control (**D**) and *pitch* mutant (**E** and **F**) P27 IHCs. Note that Ca^{2+}-dependent action potentials could be induced in mature IHCs (**F**).

The data shown in Figure 51 indicates that whilst hair cell maturation appeared to be normal at P6 and P16 in *Nptn*$^{pitch/pitch}$, development arrests at some point after the onset of hearing, and by P27

they have reduced K^+ currents with respect to those observed in *Nptn*$^{pitch/+}$ (Figure 51A, B and C). Voltage responses were altered in *Nptn*$^{pitch/pitch}$ (Figure 51D and E) and Ca^{2+}-dependent action potentials were inducible in P27 *Nptn*$^{pitch/pitch}$ (Figure 51F). The inability to produce mature membrane potentials rather than immature action potentials would explain the broad frequency hearing loss observed in *Nptn*$^{pitch/pitch}$; however it does not implicate a mechanism.

To test the hypothesis that synaptic dysfunction may be causing the auditory phenotype, rates of vesicular release and replenishment were assessed.

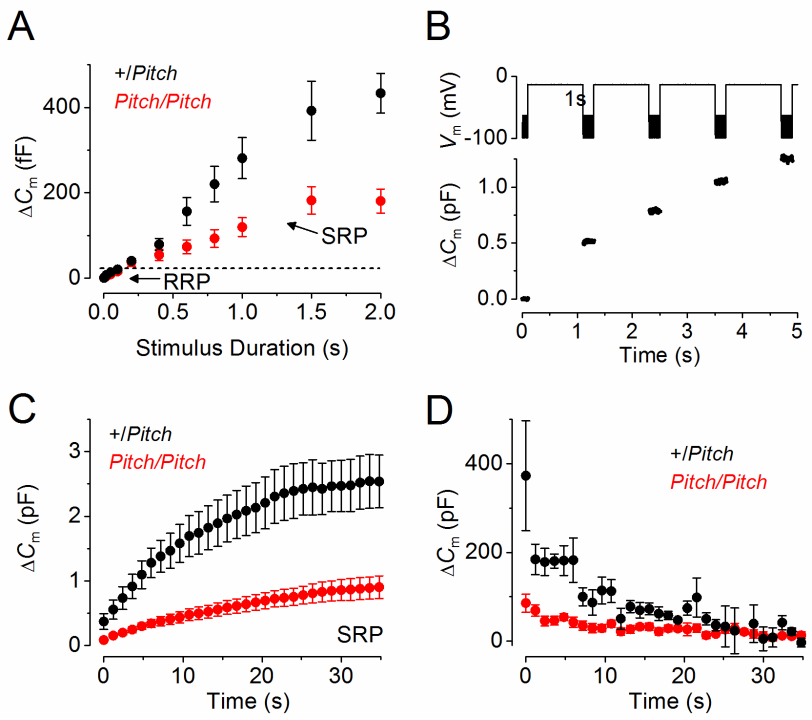

Figure 52. Kinetics of vesicle release and vesicle pool replenishment in adult IHCs of *pitch* mutant mice.

A, Average ΔC_m from seven control and nine mutant IHCs (P16-P22) in response to voltage steps from 2 ms to 2 s (to around −11 mV) showing the RRP and SRP. **B**, ΔC_m elicited using repetitive voltage steps to −11 mV of 1 s in duration in order to elicit the SRP. The inter-step-interval was 200 ms. For clarity, only the first few steps are shown. The voltage protocol used is shown above the traces. **C**, Average cumulative ΔC_m values obtained in response to the 1 s (35 steps) protocol, from four control and six mutant IHCs. **D**, Individual ΔC_m values from control and mutant IHCs measured following each voltage step from **C**.

Whilst the RRP is of normal size in *Nptn*$^{pitch/pitch}$ (see Figure 52A), when a train of 1s steps were applied to assess the secondarily releasable pool (SRP) (Figure 52B), the SRP was shown to be much smaller than that of littermate controls. Cumulative ΔC_m identified an earlier release saturation of the SRP in *Nptn*$^{pitch/pitch}$ (Figure 52C). The earlier depletion of the SRP was also evident when individual ΔC_m was assessed (Figure 52D). This data suggests a slower vesicle replenishment rate in *Nptn*$^{pitch/pitch}$ in comparison to littermate controls.

The results obtained indicate that initially IHCs develop normally in *Nptn*$^{pitch/pitch}$, however maturation arrests after the onset of hearing and mature K^+ currents cannot be observed in the adult IHC. The difference in vesicle release and replenishment rates at the SRP of *Nptn*$^{pitch/pitch}$ implies that there may be a lack of afferent innervation or a pathology at the auditory synapse, which is preventing vesicle recycling and maturation of the IHC. To assess this further investigation of the auditory ribbon synapse was undertaken.

4.5. Immunolabelling of the auditory ribbon synapse

In addition to my data, another manuscript published during my studies identified that Neuroplastin was required at synapses in the CA1 and dentate gyrus of the hippocampus. Herrera-Molina et al. (2014) identified that in the neurons of Neuroplastin KO (*Nptn*$^{-/-}$) mice there was a higher incidence of post-synaptic labelled terminals lacking a pre-synaptic signal than in WT neurons. This synaptic mismatching was found exclusively in glutamatergic neurons but not in γ-Aminobutyric acid (GABA)-ergic neurons, suggesting that Np65 is only essential for synaptic plasticity in excitatory neurons.

To assess the IHC auditory ribbon synapse immunolabelling studies were undertaken upon wholemount cochlear sensory epithelia from P16 *Nptn*$^{+/+}$ and *Nptn*$^{pitch/pitch}$ mice, using antibodies to identify the pre and post-synapse. For this purpose I used primary antibodies raised against RIBEYE, a scaffold protein expressed at the active zone of the IHC to demark the pre-synaptic terminal

(Magupalli et al., 2008), and mGluR2 the predominant AMPA receptor expressed in the auditory afferent synapses to label the post-synaptic terminal (Liberman et al., 2011).

RIBEYE and mGluR2 labelling are visible as puncta at the basolateral aspect of the IHC, and when the ribbon synapse is assembled these two puncta are juxtaposed, leading to co-occurrence of their immunofluorescence signals(Liberman et al., 2011).

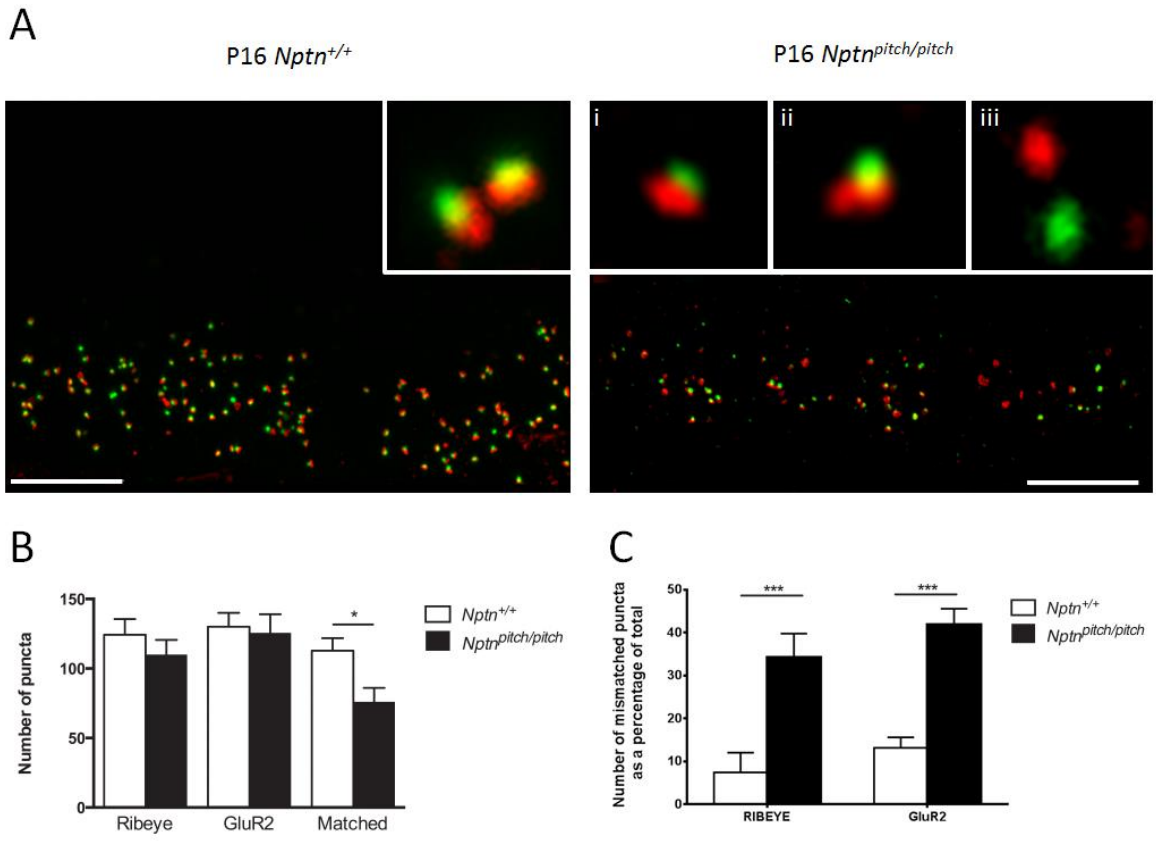

Figure 53. Immunolabelling of the auditory ribbon synapse.

A) Cochlear wholemounts prepared from P16 *Nptn*$^{+/+}$ and *Nptn*$^{pitch/pitch}$ mice labelled for the IHC presynaptic ribbon marker RIBEYE (green) and the afferent neurone postsynaptic density marker GluR2 (red). Maximum intensity projections of confocal z-stack images are shown. Closely apposed RIBEYE /GluR2-labelled puncta (matched) are present in both *Nptn*$^{+/+}$ and *Nptn*$^{pitch/pitch}$ cochleae (see inset panel in *Nptn*$^{+/+}$ and inset panels i and ii in *Nptn*$^{pitch/pitch}$). However an increase in the number of single-label punctum (mismatched) is observed in *Nptn*$^{pitch/pitch}$ cochleae (see inset panel iii in *Nptn*$^{pitch/pitch}$). **B)** Quantification of the total number of RIBEYE -positive and GluR2-positive puncta (matched + mismatched), and the total number of matched puncta in *Nptn*$^{+/+}$ and *Nptn*$^{pitch/pitch}$ cochleae. Whilst there is no difference in the total number of RIBEYE- or GluR2-labelled puncta between *Nptn*$^{+/+}$ and *Nptn*$^{pitch/pitch}$ cochleae, there is a reduction in the number of matched RIBEYE/GluR2-labelled puncta in *Nptn*$^{pitch/pitch}$ cochleae compared with *Nptn*$^{+/+}$ (p values: Number of RIBEYE- p = 0.118, Number of GluR2 – p= 0.266, Matched punctum – p = 0.002). Statistical analysis: Student's *t*-test, one tailed, assuming unequal variance. **C)** The percentage of mismatched RIBEYE and GluR2 puncta were determined in relation to the total number of RIBEYE and GluR2 puncta, respectively. This showed there is a low percentage of mismatched RIBEYE and GluR2 in *Nptn*$^{+/+}$ cochleae (<15%). However, in *Nptn*$^{pitch/pitch}$ cochleae the percentage of mismatched RIBEYE and GluR2 is greatly increased, ~35% and ~45%, respectively p values: RIBEYE – p= 1.66 x 10^{-5}, GluR2 – p= 9.57 x 10^{-9}). Data are mean ± s.e.m. of 5 cochleae, each from a separate animal. Statistical analysis: Student's *t*-test, one tailed, assuming unequal variance.* p=<0.05, ** p=<0.01, ***p=<0.001.

Upon first visual appraisal it appears that the number of synaptic puncta might be reduced in *Nptn*$^{pitch/pitch}$ cochleae compared to *Nptn*$^{+/+}$ cochleae (Figure 53A). To assess this, counts of RIBEYE- (green) and GluR2- (red) labelled punctum in *Nptn*$^{+/+}$ and *Nptn*$^{pitch/pitch}$ cochleae were made using 3D projections of confocal z-stack images. In addition, the number of juxtaposed pre- and post-synaptic signals were counted. These 'matched' signals were determined to be the co-occurrence of red and green signals to produce a yellow signal, and are deemed to represent a functional ribbon synapse.

Counts of the synaptic puncta do not identify a difference in the total number of RIBEYE- or GluR2-labelled puncta between *Nptn*$^{+/+}$ or *Nptn*$^{pitch/pitch}$ cochleae. However, the number of apposed (matched) RIBEYE- and GluR2-labelled puncta is significantly reduced in *Nptn*$^{pitch/pitch}$ mice compared to the number identified in *Nptn*$^{+/+}$ mice (Figure 53B). Correspondingly, the number of mismatched RIBEYE- and GluR2-labelled puncta is increased in *Nptn*$^{pitch/pitch}$ mice, showing a percentage mismatch of between ~35% and ~45%, respectively (Figure 53C).

In addition to the increase of synaptic mismatch observed in *Nptn*$^{pitch/pitch}$, matched synapses have a different appearance to those observed in *Nptn*$^{+/+}$. The matched synaptic terminals in *Nptn*$^{+/+}$ cochleae appear to have approximately equal-sized pre- and post-synaptic signals (see Figure 54A). Whereas, when matched signals do occur in *Nptn*$^{pitch/pitch}$ cochleae they often show a larger post-synaptic GluR2-label matched to a smaller pre-synaptic RIBEYE-label (Figure 54B). There also appears to be a smaller overlap of pre- and post-synaptic signals in *Nptn*$^{pitch/pitch}$ mice.

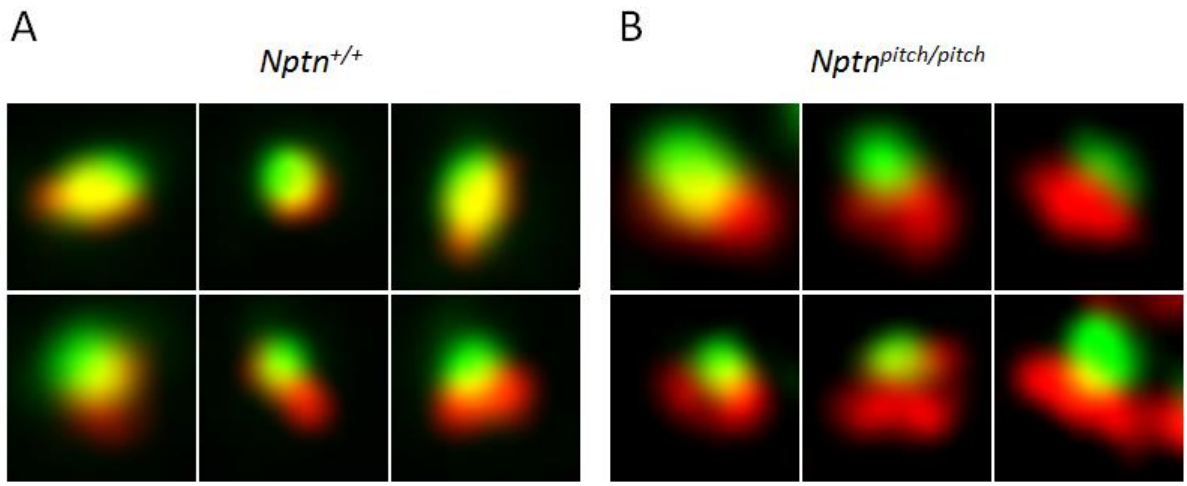

Figure 54. Typical matched synaptic puncta identified in *Nptn*$^{+/+}$ and *Nptn*$^{pitch/pitch}$.

P16 *Nptn*$^{+/+}$ and *Nptn*$^{pitch/pitch}$ cochleae were immunolabelled with anti-RIBEYE (green) to demark the pre-synaptic active zone and anti-GluR2 (red) to identify post-synaptic density. **A)** P16 *Nptn*$^{+/+}$ appear to have approximately equal sized pre- and post-synaptic punctum and co-occurrence leads to a strong yellow signal. **B)** P16 *Nptn*$^{pitch/pitch}$ appear to have larger post-synaptic puncta than pre-synaptic puncta, indicated by the strong presence of GluR2- (red). In some instances of co-occurrence an obvious yellow signal can be seen, but this is not as consistent as the overlap of signals observed in *Nptn*$^{pitch/pitch}$.

4.6. MCT2 Immunolabelling

Another manuscript published during my studies suggested that Np65 acts as an ancillary protein for monocarboylate transporter (MCT) 2, acting to chaperone MCT2 to the neuronal cell membrane (Wilson et al., 2013), implying a role in metabolic processing. The MCT proteins are responsible for transport of monocarboxylates into the neuronal cells to be used as respiratory substrates. Interestingly Embigin and Basigin have already been shown to be preferred ancillary partners to MCT2 and MCT1/4 respectively and these results suggest that Neuroplastin takes over this role as levels of Embigin decrease and Nptn increase postnatally (Humes et al., 2001). Moreover, Np65 has been shown to increase 3-fold at the PSD after ischemic insult (Smalla et al., 2000), and lactate deficiency has been shown to exacerbate neuronal damage after ischemia, suggesting increased Np65 at the PSD may be linked to MCT2 transport to facilitate neuroprotection and damage

response, as reviewed by (Beesley et al., 2014).

To investigate if Np65 is involved in metabolic processing of the auditory neurones, cochlear sensory epithelia derived from P16 WT C3-sighted mice were immunolabelled with an antibody raised against MCT2. Unfortunately I was not able to optimise this technique in order to label with anti-Np65 and anti-MCT2 at the same time, so I opted to co-label with anti-RIBEYE in order to visualise the ribbons at the base of the IHCs.

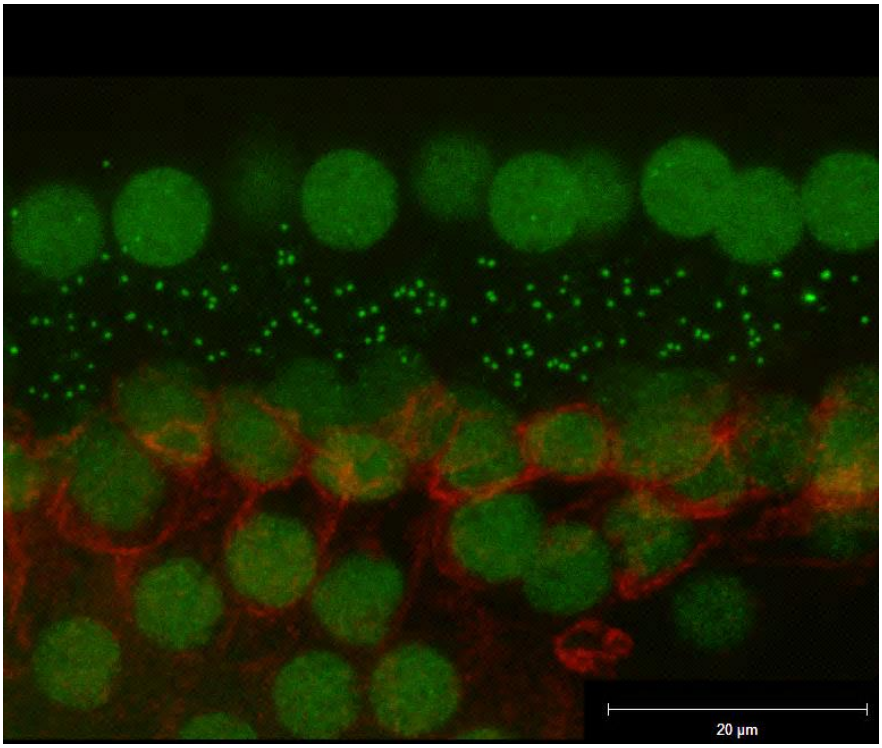

Figure 55. Wholemount immunolabelling of P16 WT cochlear sensory epithelia to show MCT2 expression.

Labelling with an antibody raised against MCT2 (red) showed expression in the inner ear, however this expression did not coincide with the RIBEYE puncta (green). This expression pattern is not consistent with the location of Np65 expression, identified in section 4.2.3.

MCT2 expression was identified in the auditory apparatus, however labelling was not observed at the auditory ribbon synapse or around the basal aspect of the IHC as observed for Np65 in section 4.2.3 (Figure 55). This result implies that Np65 does not chaperone MCT2 to the cell surface in the

ear.

MCT2's presence suggests that it is required for metabolic regulation in the neuronal population of the ear. However, the differential expression to Np65 suggests an alternative chaperone, possibly Embigin (the preferred partner in several other tissues), may fulfil this role in the auditory neurones.

4.7. Discussion

The data generated in this chapter form a strong picture regarding the expression and functional requirement of Neuroplastin, in particular Np65, in the auditory system. Np65 has only previously been reported to be expressed in the brain and retina. However, I have been able to show that Np65 is expressed in the ear and is an essential protein for the matching of synaptic terminals in the hair cell ribbon synapse.

ABR analyses identified that *pitch* mutant mice have severely impaired hearing from P16, and most likely never achieve normal hearing at the onset of hearing, ~P12. However, when compared to hearing thresholds of P27 and 8-week old mutant animals, it appears that there may be some residual hearing function at P16, albeit very slight, which deteriorates by 8-weeks of age.

Consistent with the early auditory phenotype, I have shown Neuroplastin begins to be expressed in the mouse inner ear at P12. Importantly, transcripts encoding the longer, Np65, protein isoform were found to be dynamically expressed in the ear, whereas Np55 transcripts displayed limited variation of expression. Interestingly, the onset of Np65 expression is concomitant with the postnatal functional maturation of the cochlear IHCs, which become adult-like at around P12. In addition, immunolabelling studies determined that Np65 is localised to the basolateral aspect of the IHC and is detectable from P14, which is consistent with previous reports of Np65 expression within synapses located in the brain and the retina (Smalla et al., 2000, Owczarek et al., 2011, Kreutz et al.,

2001). Immunolabelling also showed absence of Np65 protein at the base of the IHCs of *pitch* mutant mice, which is consistent with the *in silico* and *in vitro* study data showing that the *pitch* mutation is a loss-of-function allele. Together these data support the hypothesis that Np65 is required for IHC function.

Importantly, histological and ultrastructural studies show no gross morphological changes within the cochlea of P16 *pitch* mutant mice that could account for the severe hearing loss phenotype. Indeed, electrophysiological studies demonstrated normal MET function in P16 mutant mice, showing that bundle deflection leads to cell depolarisation and hyperpolarisation in *pitch* mutant mice. In addition to confirming that MET channel transduction is not deficient in *pitch* mutant mice, electrophysiology studies also show that IHCs are innervated as normal by OHCs and appear to initially mature. However, after the onset of hearing maturation is impaired, and by P27 IHCs fail to generate adult K^+ currents and vesicle replenishment is reduced. These results indicate that absence of Np65 prevents full maturation of IHCs, leading IHCs to continue to generate immature action potentials as opposed to mature membrane potentials. These results are consistent with hair cell dysfunction arising from a lack of afferent innervation or synaptic deficiencies.

Indeed, immunolabelling of the auditory IHC ribbon synapse identified a high level of mismatch between pre- and post-synaptic markers in the *pitch* mutant mice compared to wild type animals. Importantly the overall number of pre- and post-synaptic puncta is not different between *pitch* mutant and WT mice, but the occurrence of pre-synaptic puncta without an apposed post-synaptic puncta was significantly increased in *pitch* mutant animals.

In addition, when pre- and post-synaptic puncta are found 'matched' in *pitch* mutant mice, there appears to be less of an overlap between the two puncta in comparison to the matched puncta of WT animals. Also, in *pitch* mutant mice the pre-synaptic (RIBEYE) puncta appear smaller in size when

compared to the size of the post-synaptic (GluR2) puncta, whereas in wild type animals the sizes of the pre- and post-synaptic puncta appear similar. Smaller pre-synaptic ribbons could be the basis of the differences observed in the electrophysiology studies, showing an earlier vesicle release saturation of the SRP and a slower vesicle replenishment rate in mutant mice compared to littermate controls. Mismatched synapses, less tightly apposed matched synapses and reduced vesicle release will all lead to the failure of neurotransmission from the IHCs to the afferent nerves.

In addition to the basolateral localisation of Np65, immunolabelling studies also showed localisation at the apical cuticular plate of IHCs and OHCs. To investigate the requirement of Np65 at the cuticular plate ultrastructural analyses were performed. In wild type animals no IHC or OHC loss was observed up to P60. However, even at P16 some OHC degeneration was observed in the *pitch* mutant mice, and this increased with age. By P60 loss of the IHCs was also observed, however the stereocilia fusion phenotype was not observed at any time point tested. The loss of hair cells occurs after hearing loss is observed, suggesting that hair cell degeneration is a secondary phenotype. This is not too unexpected as a lack of innervation/function often leads to deterioration and eventual cell death in hair cells (Hequembourg and Liberman, 2001, Spiden et al., 2008).

Given Np65's reported functions, labelling in the cuticular plate was unexpected. There are several protein families localised to the cuticular plate which are known to cause hearing loss when the protein is mutated, for example the Myosins, as reviewed by Forge and Wright (2002), however only the Cadherin family members Pcdh15 and Cdh23 are reported to have a similar physiological function to Neuroplastin. The Usher type I proteins, Pcdh15 and Cdh23 localise to the stereocilia and cuticular plate within the cochlea and have a reported role in cell adhesion (Ahmed et al., 2003, Bolz et al., 2001, Di Palma et al., 2001). Expression patterns in the eye are reported to be similar (cadherin's are expressed at the photoreceptors, Np65 at the ribbon synapse that junctions the photoreceptors and the bipolar cells), however Pcdh15 and several other Usher proteins expressed

in the cuticular plate and the stereocilia have been shown to have a retinal disease mechanism that does not involve the photoreceptor synapses (Jacobson et al., 2008). The seemingly separate function of Np65 and the cadherin's in the eye leads me to believe that Np65 is probably not acting in a cell adhesion capacity and therefore I believe that this labelling is likely an artefact and not a true expression of Np65.

Immunolabelling studies identified MCT2 labelling in the auditory apparatus; however MCT2 protein does not localise to the basolateral aspect of the IHCs like Np65, implying that Np65 does not chaperone MCT2 in the ear. The data suggests roles for nCAM family members Embigin and Basigin within the auditory system; however it seems likely that these proteins support a different function within the ear to Np65. This is something I would like to investigate further, possibly by performing qRT-PCR to look at the transcript levels of the two genes in the ear, and if detected follow up immunofluorescence labelling and co-expression studies.

At the transcript level *Np65* was identified as being expressed at P12, with an increase in relative quantity up to P27. However, protein expression studies identified Np65 expression from P14 to P23 in the cochlea. There are several plausible explanations as to why protein expression does not correspond with data obtained by qRT-PCR. Transcript levels have been shown to correspond to only ~40% of protein levels, with the remaining 60% related to post-translational modification, degradation and processing, as reviewed by Vogel and Marcotte (2012). Another explanation is that Np65 is required somewhere else in the inner ear, for example in the vestibular apparatus, and this role persists and is perhaps enhanced beyond P23. This theory could be assessed by repeating qRT-PCR using RNA extracted from only the sensory epithelia as opposed to whole inner ears. A third possibility is that protein expression becomes less ubiquitous and more refined as the cochlea matures. The protein would be present but not detectable at the resolution at which we were able to image. This might be the case if the protein was highly localised and had a relatively high turn-over or replacement rate.

Analysis of the ribbon synapse suggested smaller pre-synaptic (RIBEYE) terminals and less tightly apposed pre- and post-synaptic terminals in 'matched' synapses of *pitch* mutant mice compared to WT littermates. In order to assess this, the following studies could be performed in *pitch* mutant mice and WT littermates: Quantification of the size of pre- and post-synaptic markers, immunogold labelling and TEM to assess pre- and post-synaptic marker clustering, and TEM to assess the distance between pre- and post-synaptic markers.

In summary, the data generated provides compelling evidence that Np65 is required for synaptic matching at the auditory ribbon synapse, a prerequisite for inner hair cell maturity and auditory transduction. I hypothesise that Np65 is expressed at both the pre- (IHC basolateral membrane) and post-synaptic terminals (afferent post-synaptic density) and homophilically binds *in trans* across the synaptic cleft to provide stability to the ribbon synapse. It could also act as a molecular cue for the 'incoming' afferent neurites during IHC innervation. However, it cannot be the only cue as the IHCs of *pitch* mutant mice do have afferent neurites extending to their base.

Chapter 5. Exploration of visual and additional phenotypes in the mutant *Nptn* models

The investigations performed in chapters 3 and 4 have identified the Neuroplastin isoform, Np65, as critical for hearing function in the mouse. In particular, the structure and function of the auditory ribbon synapse. Previously, Np65 has been reported to be expressed at hippocampal synapses and retinal ribbon synapses. Given the severity of the synaptic pathology observed in *pitch* mutant mice, it is plausible that these mice have other as-yet-unidentified phenotypes.

Initially two phenotypes were noted in *pitch* mice – a hearing loss and a head-tilt phenotype. Whilst I have characterised the auditory phenotype, the late-onset vestibular deficit requires additional investigation in order to identify the associated pathology and to determine if this phenotype may be due to a similar mechanism of action as the hearing loss.

In order to assess for additional phenotypes, I undertook a closer study of *Neuroplastin* mutant models.

5.1. Retinal immunolabelling

Previously, Np65 has been reported to be expressed in the inner plexiform layer (IPL) and the outer plexiform layer (OPL) of the rat retina. Therefore, I decided to assess whether the *pitch* mutation might disturb retinal function.

The vertebrate retina is a highly organised structure, comprised of multiple cell-types, which are organised into 3 specific layers (see Figure 56A):

1) Outer layer – comprised of the rods and cones, which detect light, the outer nuclear layer (ONL) and the OPL

2) Inner layer – comprised of the inner nuclear layer (INL) and the IPL

3) Ganglion cell layer

The synaptic organisation of the retina is complex, with ribbon synapses and conventional synapses both present in the OPL and IPL (Heidelberger et al., 2005). Light is initially received by the photoreceptors, leading to neurotransmission and perception of sight in the brain. There is a ribbon synapse at the base of the photoreceptor cells, and post-synaptic processes extend from this ribbon synapse to the horizontal and bipolar cells (see Figure 56B). Conventional synapses are formed between the horizontal and bipolar cells, allowing the horizontal cells to signal to the downstream bipolar cells. All synaptic signals from the photoreceptors are ultimately received in the bipolar cells.

A second ribbon is present in the bipolar cells, forming a ribbon synapse with post-synaptic processes extending from the amacrine and ganglion cells (see Figure 56B). The amacrine and ganglion cells also form conventional synapses, allowing for synaptic signalling from amacrine cells to the downstream ganglion cells. All synaptic signals from the bipolar cells are ultimately received in the ganglion cells. Axons from the ganglion cells exit the retina through the optic disk and form the optic nerve. The optic nerve exits at the back of eye.

Through this synaptic pathway, light information can be transmitted from the photoreceptors to the optic nerve, and then on to the brain.

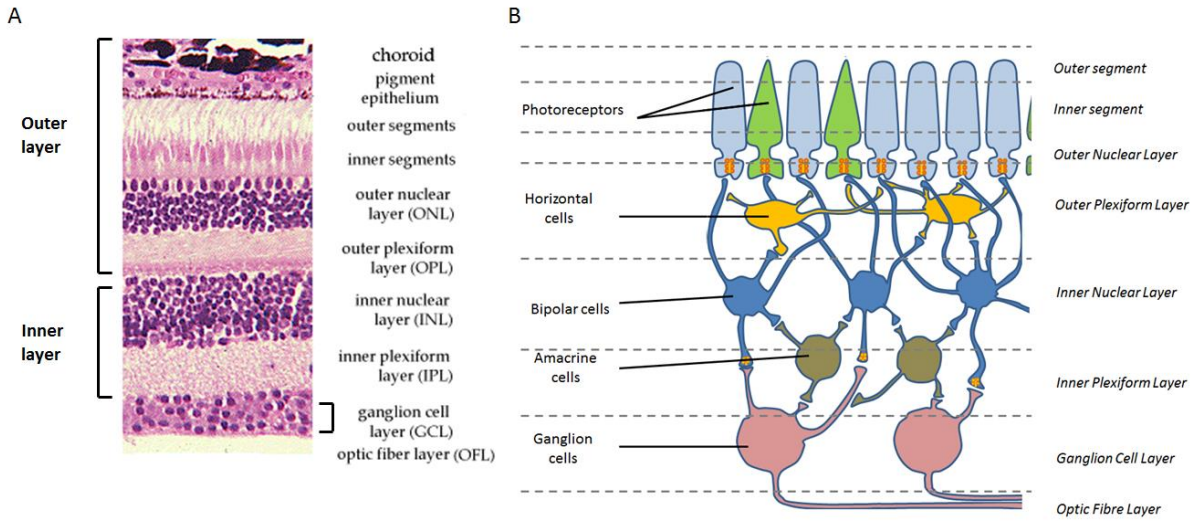

Figure 56. The vertebrate retina is organised into 3 distinct nuclear layers.

A) H&E stained retinal section, adapted from (Bioon, 2014). The retina is organised into 3 distinct layers, the outer layer (containing the pigmented epithelium, photoreceptors, ONL and OPL), the inner layer (containing the INL and IPL) and the ganglion cell layer (GCL and OFL). Synapses are found within the IPL and OPL. **B)** Both ribbon synapses and conventional synapses are present in the OPL and IPL of the retina. There are two ribbon synapses in the retina. One ribbon is present in the OPL at the active zones of the photoreceptors with post-synaptic terminals extending from the bipolar cells and horizontal cells. Conventional (normal) synapses form between the horizontal cells and bipolar cells in this region. The other ribbon synapse is present in the IPL at the terminals for the bipolar cells. The post-synaptic processes at this ribbon extend from the ganglion cells and the amacrine cells. In the IPL conventional synapses form between the amacrine and ganglion cell processes. The axons from the ganglion cells form the optic fibre layer, which exits through the optic disk and becomes the optic nerve.

Both retinal and auditory ribbon synapses are required for graded response to stimuli. However, whilst they maintain a similar function, the architecture is markedly different in order to support the function of the cells they serve (see Figure 57). The rod photoreceptor ribbons are long, thin plate shaped structures, which are tethered to the plasma membrane by an arciform density. The ribbons at the bipolar cells are much smaller in size, more abundant (between 30 and 100 ribbons per cell, tethering approximately 20 vesicles) and are believed to signal in a more transient manner (Matthews and Fuchs, 2010). The ribbons of the cochlear inner hair cells can vary in shape and size within hair cells, but are generally closer in size to the bipolar cell ribbons. Up to 200 vesicles may be tethered at the IHC ribbon (Matthews and Fuchs, 2010). Neither the hair cells, nor the bipolar cells have an arciform density.

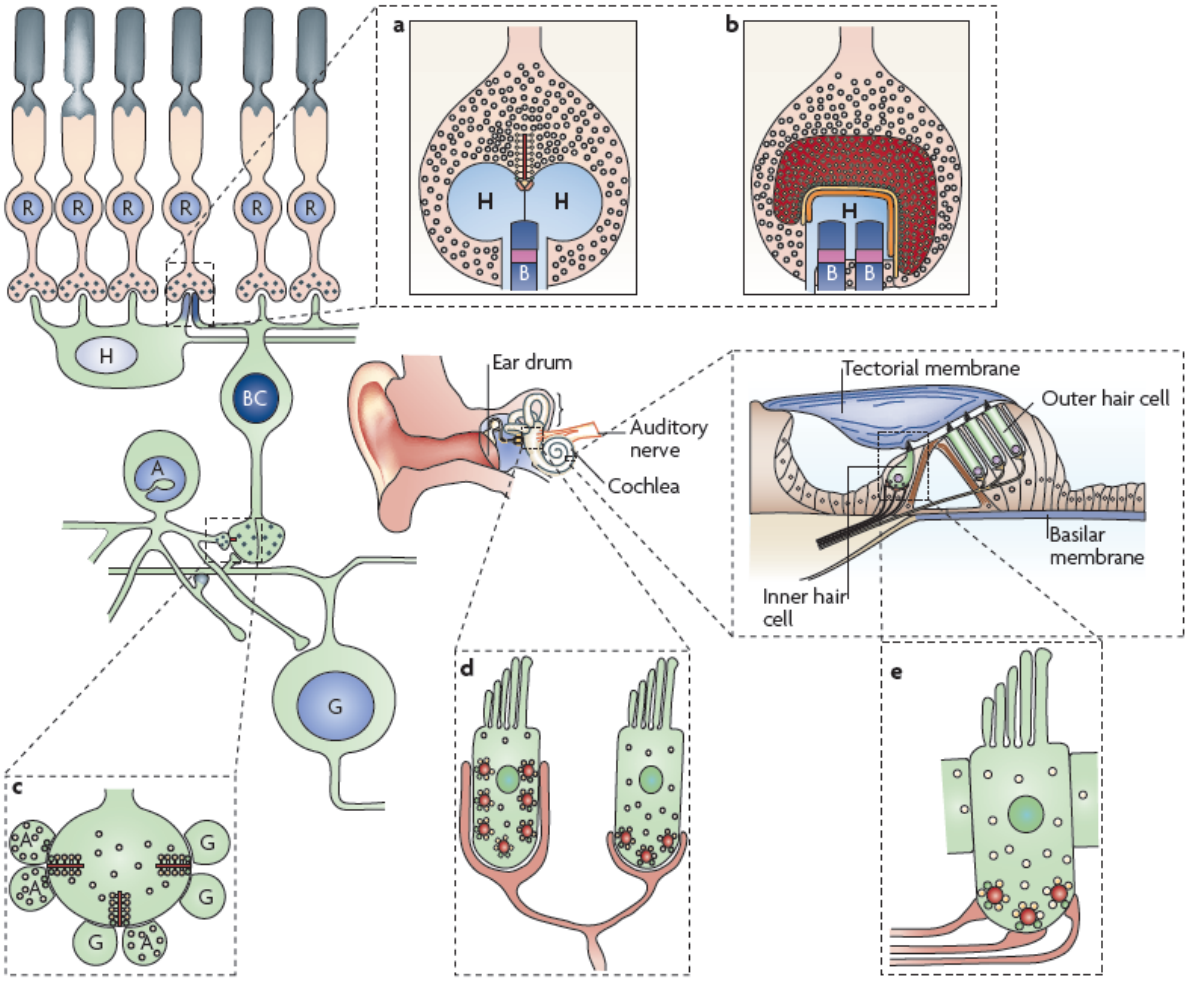

Figure 57. Diversity of ribbon morphology and postsynaptic architecture in different cell types.

A. Diagram of transverse photoreceptor ribbon synapse. **B.** en-face view of the mammalian photoreceptor ribbon synapse. **C.** Arrangement of synaptic terminals at bipolar cell ribbons. **D.** Vestibular afferents contact multiple ribbons in each cell. **E.** Synaptic arrangement at ribbons of cochlear inner hair cells. The locations of cochlear inner hair cells and the vestibular apparatus are shown schematically. Synaptic ribbons are shown in dark red, glutamate receptors in orange and the arciform density in yellow. Vesicles attached to ribbons are shown by yellow circles and docked vesicles by green circles. Horizontal cell dendrites (H) are shown in light blue. bipolar cell dendrites (B) are illustrated in dark blue and mGluR6 receptors in purple. A, amacrine cell process; BC, bipolar cell; G, ganglion cell dendrite; R, rod photoreceptor cell. Figure and associated text adapted from Matthews and Fuchs (2010).

Initially I performed immunofluorescence labelling with an antibody against Np65 in P16 retinal sections from *Nptn*$^{+/+}$ mice to confirm that like rats, mice also express Np65 in the OPL and IPL. I also labelled retinal sections from P16 *Nptn*$^{pitch/pitch}$ mice to determine if Np65 could be detected.

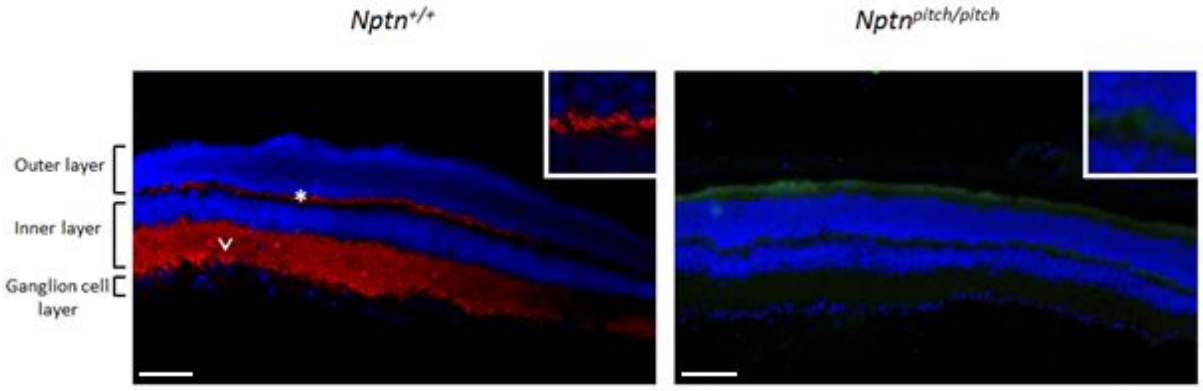

Figure 58. Np65 was detected in the IPL and OPL of P16 *Nptn*$^{+/+}$ but is absent in *Nptn*$^{pitch/pitch}$.

Retinal cryosections were immunolabelled with anti-Np65 (red) and co-stained with DAPI (blue) to identify nuclei. Np65 labelling was observed through the entirety of the IPL (arrowhead), whereas in the OPL labelling appeared restricted to outer boundary (see insert, *). In *Nptn*$^{pitch/pitch}$ there was no detectable Np65 in the retina, including the IPL or the OPL (see insert). Scale bar = 25µM.

The expression pattern of Np65 in P16 *Nptn*$^{+/+}$ mouse retina matches that reported for Np65 in rat retina (Figure 58) (Kreutz et al., 2001). The labelling in the OPL appears restricted to the upper boundary of the layer (close to the active zones of the photoreceptor layer), whereas expression in the IPL is less restricted and is observed widely throughout the layer. The widespread expression of Np65 in the IPL may support the hypothesis made by Kreutz et al. suggesting Np65 might be localised to both the ribbon synapses and conventional synapses of the retina. Further exploration of the ribbon was required to assess this.

Np65 protein could not be detected in *Nptn*$^{pitch/pitch}$ mouse retina, which is consistent with the results obtained in Chapters 3 and 4, and again confirm that *pitch* is a loss-of-function allele. There is no gross dysmorphology of the retinal cell layers (e.g. cell loss, disorganisation, etc.) when observed using immunofluorescence or H&E staining of cryosections (Figure 58 and Figure 59, and not shown).

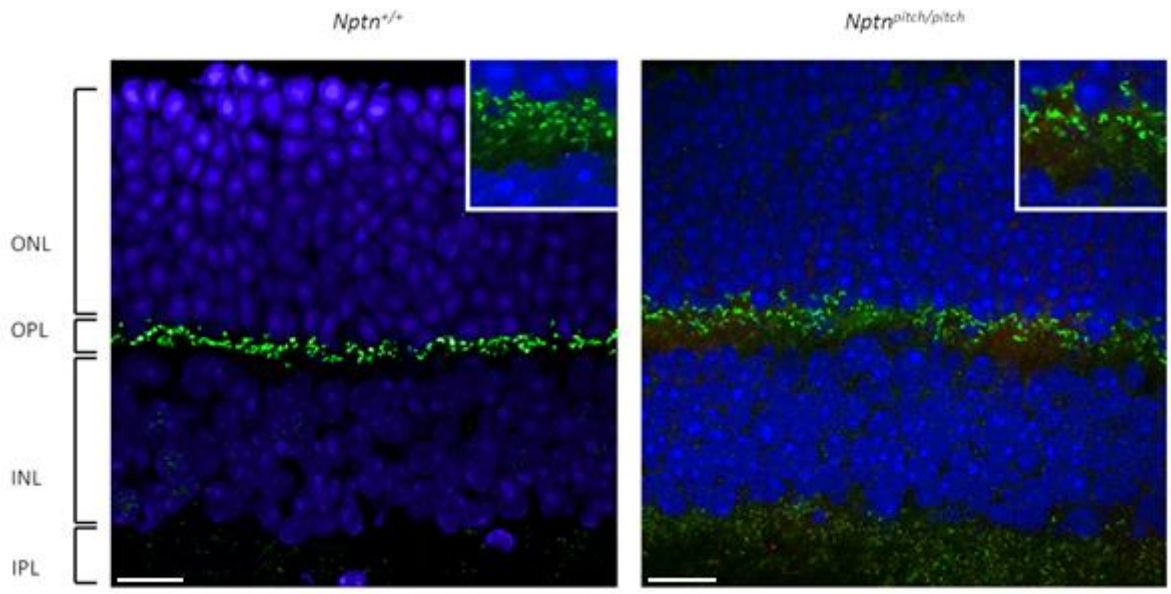

Figure 59. Retinal immunolabelling with anti-RIBEYE shows no gross differences between *Nptn*$^{+/+}$ and *Nptn*$^{pitch/pitch}$.

Cryosections from P16 retina were labelled with anti-RIBEYE (green) and co-stained with DAPI (blue). There was no detectable difference in the expression pattern of RIBEYE positive punctum (see inserts) and no obvious dysmorphology in the retina of *Nptn*$^{pitch/pitch}$. Scale bar = 10µM.

Immunofluorescence labelling of the ribbon using an antibody against the pre-synaptic active zone RIBEYE protein (see Figure 59) found no obvious difference in the expression pattern or number of puncta between genotypes. The pattern of RIBEYE expression in the OPL is similar to that observed for Np65 (Figure 58). Some diffuse RIBEYE puncta are observed in the IPL, which is consistent with observations made in other studies (Vaithianathan et al., 2013) .

In addition to labelling RIBEYE, I also attempted to co-label with antibodies against GluR2/3 and GluR2. Unfortunately, I was not able to optimise this method to observe the mGluR proteins in the cryosections. Therefore, I could not perform an analysis of ribbon synapse morphology, as I had done previously for the ear, to assess if a similar pathology was present.

Confirmation that Np65 is expressed in the synaptic layers of the WT retina, but is absent from *Nptn*$^{pitch/pitch}$ eyes, suggested *Neuroplastin* could be critical for visual function. Initially I considered

employing the optokinetic drum phenotyping platform to assess vision: in brief, mice are placed on a raised static platform inside a striped revolving drum and assessments are made of the animals' ability to pick a focus point and track it as the drum rotates. However, this technique is not suitable for animals with vestibular dysfunction, as the lack of non-rotating visual cues or proprioceptive cues (mice stand on their hind legs during the test to follow the stripe they've focused on) mean they repeatedly lose their balance and fall off of the platform, preventing an assessment being made. To get around this issue, mice were sent to a collaborator at the University of Oxford for electroretinography testing.

5.2. ERG testing of *Nptn*^{tm1b} mice (collaborative work)

The gold standard for vision phenotyping is electroretinography (ERG), a technique not available at MRC Harwell. Therefore I sent mice to a collaborator (Dr Alun Barnard) at the University of Oxford for these studies to be undertaken.

Unfortunately animals on a sighted-C3H genetic background cannot be used for ERG testing (Hoelter et al., 2008). Therefore, I requested a *Nptn*-KO through the IMPC project, for which MRC Harwell is a partner. The knock out, *Nptn*$^{tm1b(EUCOMM)Hmgu}$ (referred to as *Nptn*^{tm1b} from here on) was generated on a C57BL6/NTac background, which does not carry the *rd1* mutation and is therefore suitable for ERG testing.

In order to verify the *Nptn*^{tm1b} allele, ABR testing was undertaken (by IMPC staff at the Mary Lyon Centre, MRC Harwell) to assess hearing thresholds. ABR testing of *Nptn*^{tm1b} and WT littermate controls was performed at 14 weeks of age, at the following frequencies: click, 6kHz, 12kHz, 18kHz, 24kHz and 30kHz.

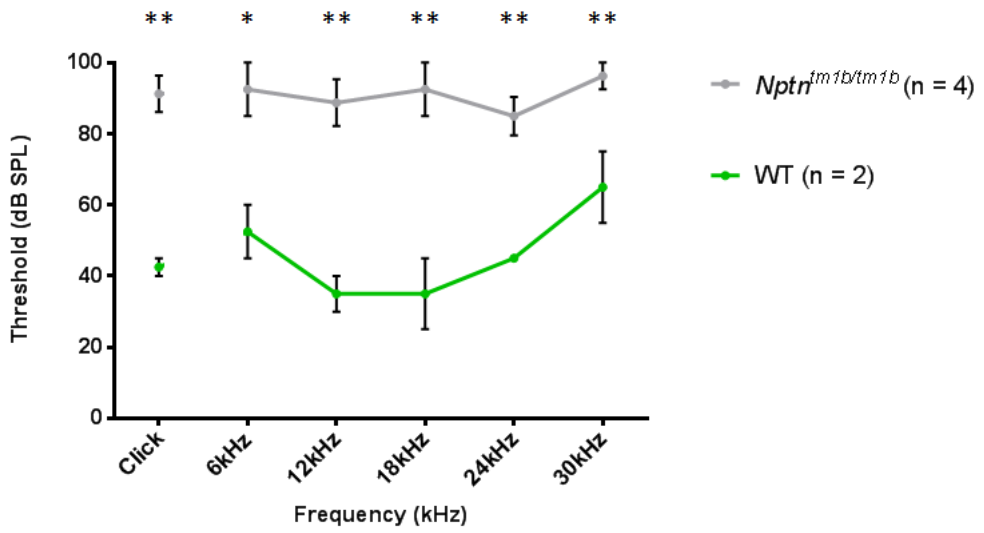

Figure 60. *Nptn*^{tm1b} knock out mice are severely to profoundly auditory impaired.

Nptn^{tm1b} animals (grey line) have significantly increased ABR thresholds at all frequencies tested (p values: click – 1.73 x 10^{-3},6kHz – 0.015, 12kHz – 3.25 x 10^{-3} , 18kHz – 5.46 x 10^{-3} , 24kHz – 3.92 x 10^{-3}, 30kHz – 9.90 x 10^{-3}). Statistical analysis: Student's *t*-test, single tailed. WT animals also have moderately elevated thresholds (40 – 60dB), which is due to the C57BL6/NTac genetic background. C57BL6 mice carry the *ahl* allele, which predisposes them to age-related hearing loss.

ABR assessment of *Nptn*^{tm1b} identified a severe to profound hearing loss at 14 weeks (see Figure 60). This result indicated that *Nptn*^{tm1b} model recapitulates the phenotype observed in the *Nptn*^{pitch} and *Nptn*^{Y219X} mutant models, and so would be a suitable model to assess the effects Nptn loss has on vision.

Cohorts of *Nptn*^{tm1b} mice were bred and exported to the University of Oxford. ERG testing was undertaken on age-matched *Nptn*^{tm1b} mutant and WT littermate controls.

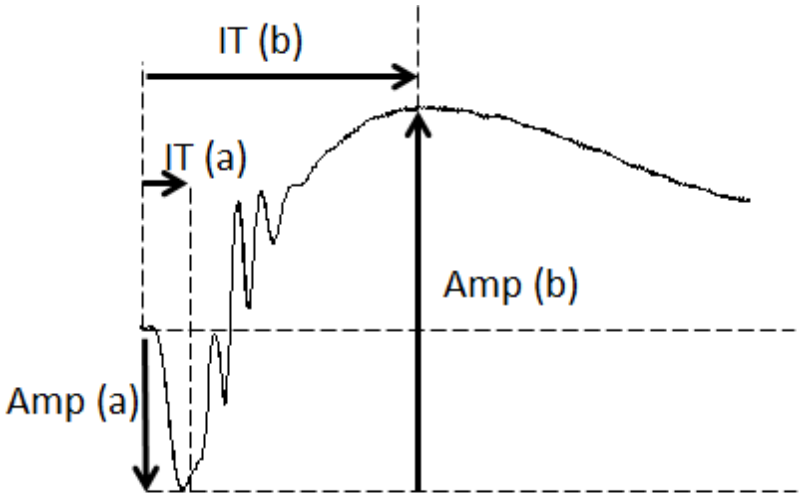

Figure 61. An example of a normal ERG trace.

The ERG trace is characterised by an a-wave (a) followed by a trough shortly after stimulation occurs. Following this trough, the b-wave (b) is initiated, and this peak is associated with bipolar cell activation. Amp = amplitude, IT = Implicit Time.

ERG testing is a recoverable procedure performed under anaesthetic, and produces traces that can be used to assess visual function (Figure 61). In brief, the mice are dark-adapted for a minimum of 12 hours (all setup performed under red light to prevent light response). Mice are anaesthetised, pupils are fully dilated using Phenylemide and Tropicamide and a silver coated nylon active electrode encapsulated in a custom made aclar film contact lens is placed over the animal's iris. Ground and reference electrodes are inserted subdermally, into the hind-leg and the forehead, respectively. Dark-adapted flash ERGs (4ms flashes of increasing light intensity) are performed before exposing the mouse to a rod-saturation level of background light for ten minutes and performing light-adapted ERGs.

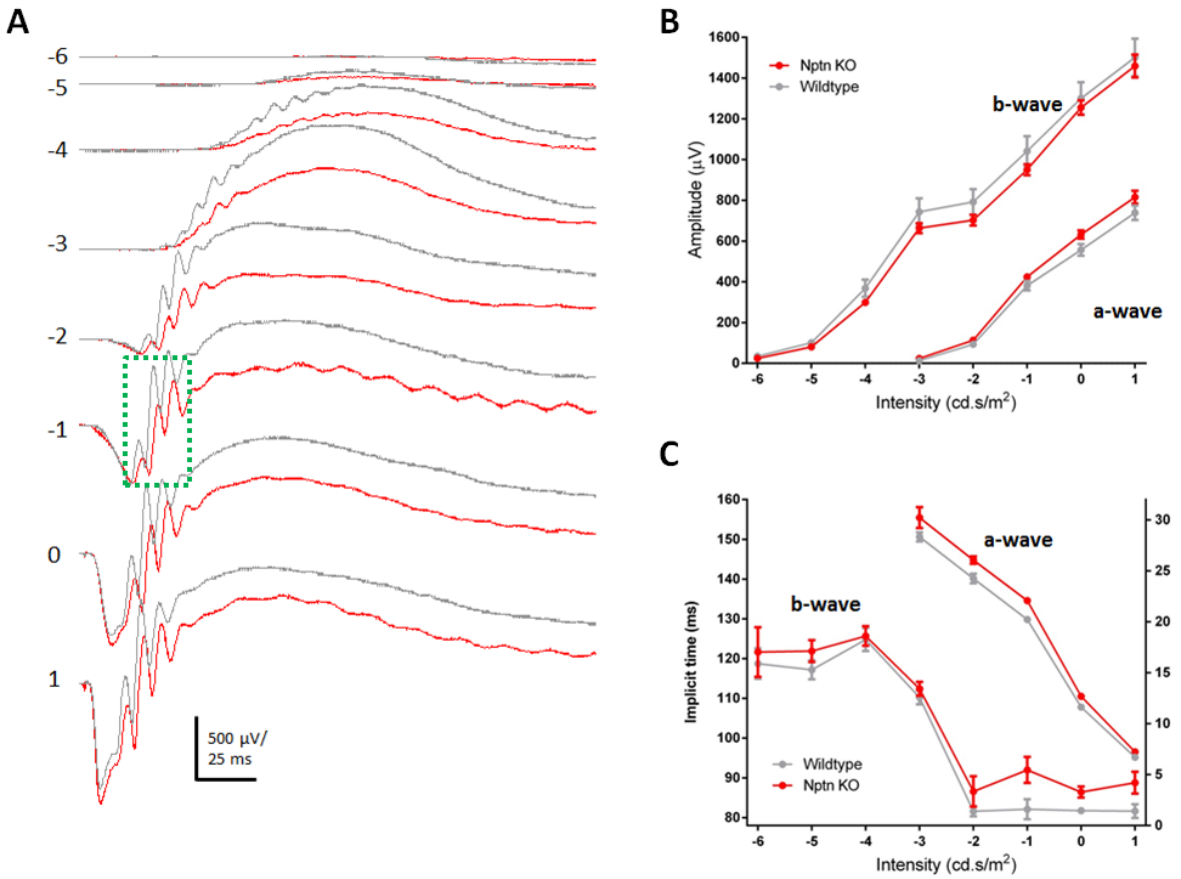

Figure 62. Dark-adapted ERGs appear to show a mild difference in the b-wave of P65 *Nptn*^{tm1b} knock out mice vs WT controls.

A) The b-wave of the ERG traces obtained from *Nptn*^{tm1b} KO animals (red line) appeared to be smaller in amplitude than that of WT littermate controls (grey line). The oscillatory potentials at -1cd.s/m^2 (peaks 3 – 5) are illustrated in the green dashed box. **B)** The mean amplitude of the waves were plotted against light intensity for each genotype in order to quantify the traces. Apparent lower amplitude of the b-wave in *Nptn*^{tm1b} animals was observed, and also a marginal increase in the amplitude of the a-wave could be seen. These differences were easiest to identify in the mid-range of the intensities tested, however at all intensities were shown not to be significant. **C)** A plot of the implicit time taken for the a-wave and b-wave to be detected indicates that *Nptn*^{tm1b} show a delayed response at all intensities in comparison to C57BL6/NTac.

The results obtained by dark-adapted ERG testing (Figure 62A) show a mild increase of the a-wave and mild decrease of the b-wave in *Nptn*^{tm1b}. However, due to the variation in individual data points this difference was not statistically significant (Figure 62B). The response time is shown to get faster in a similar manner for both genotypes as the intensity of the light bursts (visual stimulus) increased. However, the implicit time to generate the a-wave and b-wave in the *Nptn*$^{tm1b/tm1b}$ is elevated in

comparison to WT littermate control (*Nptn*$^{+/+}$) mice (Figure 62C). In particular, the a-wave is slower at lower intensities, whilst the b-wave appears slower at higher intensities.

In order to investigate this trend of slower wave formation in *Nptn*^{tm1b} a plot of the ratio between the amplitudes of the b- and a-waves for each genotype was generated. By examining this ratio an idea of the efficiency of synaptic transmission between the photoreceptors and the bipolar cells can be gained.

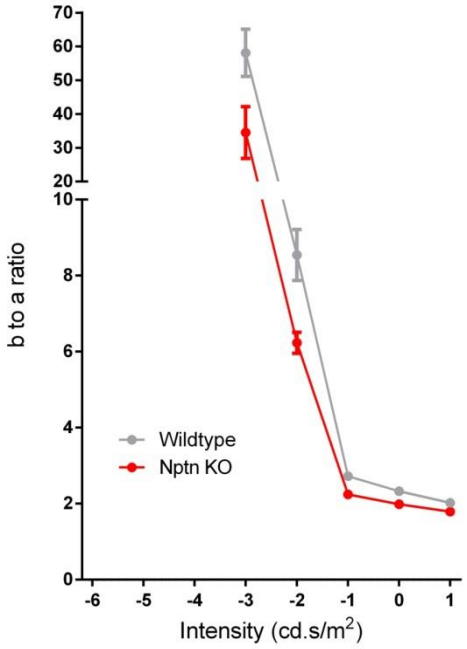

Figure 63. The b- to a-wave ratio is consistently lower in P65 *Nptn*^{tm1b} knockout mice.

The b-a ratio of *Nptn*^{tm1b} was shown to be reduced at all intensities measured in comparison to WT littermate controls. n = 7 for each genotype (5 male, 2 female)

The decreased b- to a-wave ratio in *Nptn*^{tm1b} knockout mice suggests there may be decreased efficiency of synaptic transmission between the photoreceptor cells and the bipolar cells (Figure 63). This result is consistent with my retinal immunolabelling study data showing Np65 expression within the OPL, the layer containing the photoreceptor: bipolar synapses. However, it is a very mild

phenotype in comparison to the striking auditory phenotype, and suggests that Np65 is non-essential for visual function.

It has been previously hypothesised that Np65 might also be present at conventional synapses within the retina (Kreutz et al., 2001). My data showing Np65 expression in the IPL is consistent with this hypothesis. In order to further investigate this theory the oscillatory potentials (see the green box in Figure 62A) at the beginning of the b-wave were analysed. The origins of the oscillatory potentials are somewhat controversial, but most agree that they are produced by the third order neurones; the amacrine, ganglion or horizontal cells, although exactly which cell type has yet to be established.

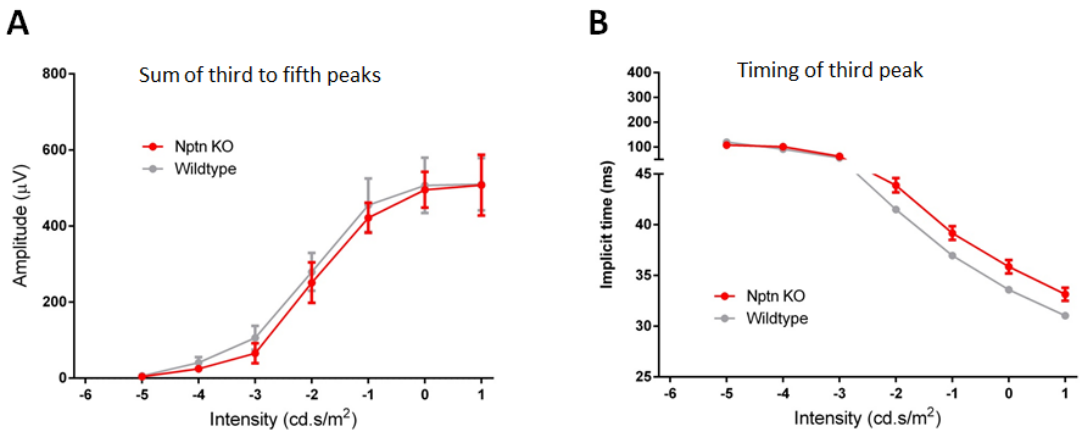

Figure 64. *Nptn*^{tm1b} animals have increased implicit time from wave initiation to detection of the oscillatory potentials.

A) Oscillatory potentials were isolated from the ERG traces using a specific bandpass filter (75-300 kHz). Analysis of the amplitudes between WT and *Nptn*^{tm1b} yielded no obvious differences. **B)** A plot of the implicit time between wave initiation and the detection of the third peak (the first peak in the oscillatory potentials) indicated that at higher intensities *Nptn*^{tm1b} had increased implicit time vs WT C57BL6/NTac controls. n = 7 for each genotype (5 males, 2 females). Age= 65±0.65 days.

Comparison of WT and *Nptn*^{tm1b} oscillatory potentials indicated that whilst the amplitude of potentials is similar in both genotypes, the implicit time for detection of the oscillatory potentials was higher in *Nptn*^{tm1b} knockout mice (Figure 64A and B). This result suggests there may be a delay in signals reaching the third order neurones.

5.3. Confirmation of additional phenotypes in *Nptn*$^{pitch/pitch}$

Initial phenotyping of the original *pitch* mice identified a vestibular defect, which was detectable as a head-bob and inability to balance without proprioceptive cues – demonstrated by swim testing. This phenotype was concomitant with hearing loss, and subsequent to identification of the causative gene, all of these animals have been genotyped as *Nptn*$^{pitch/pitch}$.

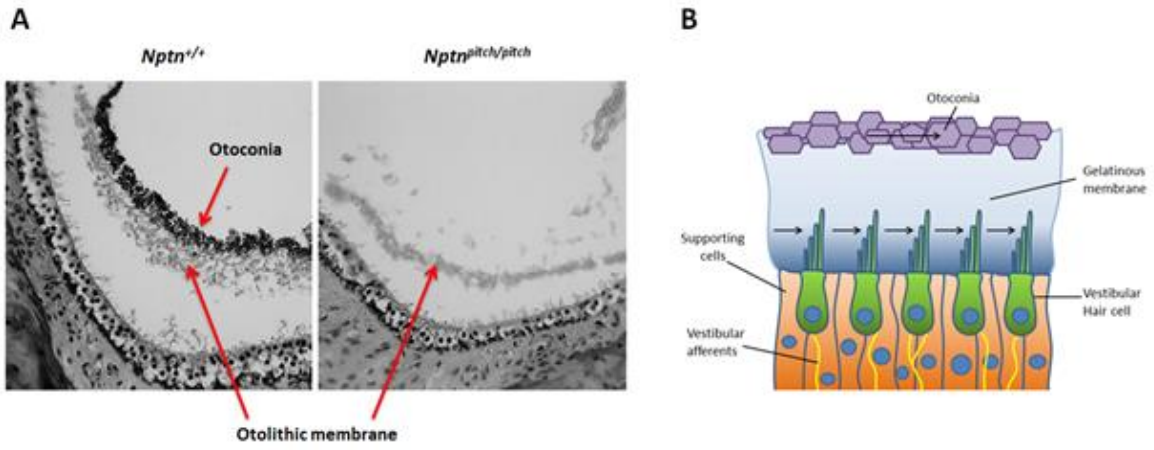

Figure 65. Otoconia are absent from the ears of P90 *Nptn*$^{pitch/pitch}$ that exhibit a head-bob.

A) Stained wax sections of P90 saccule identified presence of calcium carbonate otoconia in WT animals, but these were absent from *Nptn*$^{pitch/pitch}$ mice that displayed a head-bob. There also appeared to be a thinning or depletion of the otolithic membrane in *Nptn*$^{pitch/pitch}$ animals. **B)** The otoconia rest on the otolithic membrane, which surrounds the stereocilia of the vestibular hair cells. Movement of the otoconia cause deflection of the stereocilia and MET channel opening leading to signal transduction. See section 1.2.

In P90 *Nptn*$^{+/+}$ mice otoconia are apparent as darkly stained crystals juxtaposed to the sensory epithelium of the saccule. In *Nptn*$^{pitch/pitch}$ the otoconia is not apparent in the saccule or the utricle (Figure 65A and data not shown). The absence of these otoliths would prevent stereocilia deflection and therefore signal transduction (Figure 65B). This finding is consistent with the observed balance deficits identified in *Nptn*$^{pitch/pitch}$ mice. In addition, there also appears to be thinning of the otolithic membrane in *Nptn*$^{pitch/pitch}$ mice, compared to *Nptn*$^{+/+}$ mice (Figure 65B). However, given that the membrane is detached from the hair cells in both *Nptn*$^{+/+}$ and *Nptn*$^{pitch/pitch}$ inner ear sections, which

would not be expected in normal physiology, I assume this may be an artefact introduced from processing/sectioning of the tissue and perhaps not a true phenotype.

Interestingly, absence of otoconia was only observed in *Nptn*$^{pitch/pitch}$ animals that displayed a head-bob at the time they were sacrificed. All *Nptn*$^{pitch/pitch}$ exhibit a head-bob, however the onset of this phenotype is variable (2 – 4 months) and examination of inner ear sections in *Nptn*$^{pitch/pitch}$ mice that did not exhibit a head-bob at the time of sacrifice identified otoconia in the saccule and utricle (Figure 66).

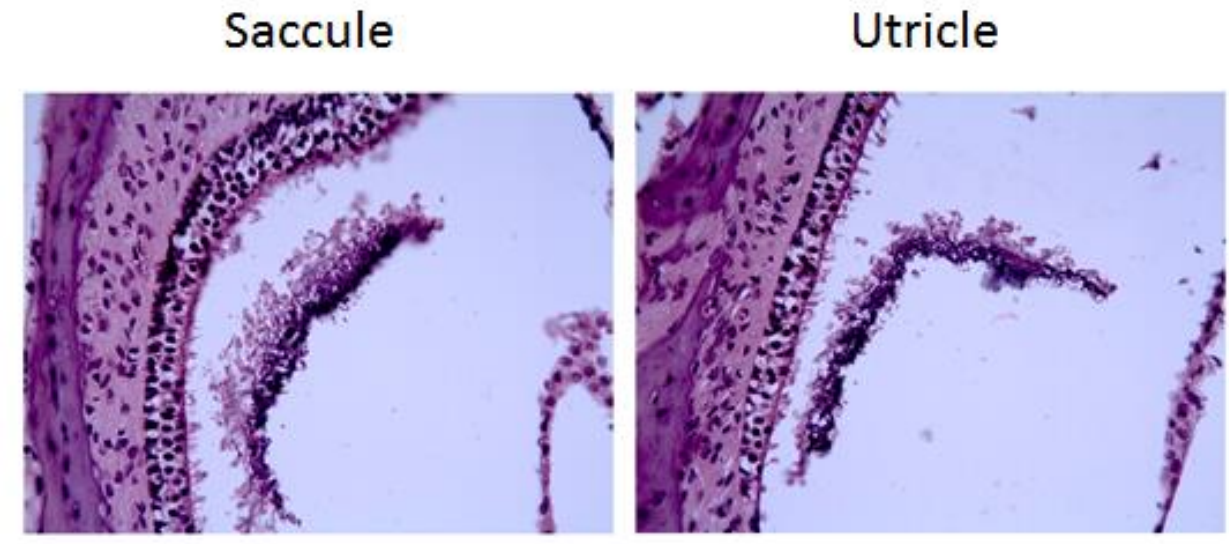

Figure 66. Otoconia is present in the vestibular organs of P90 *Nptn*$^{pitch/pitch}$ mice that do not exhibit a head-bob.

Otoconia were present on the otolithic membrane of the saccule and the utricle in the ears of a P90 *Nptn*$^{pitch/pitch}$ mouse that did not exhibit a head-bob phenotype.

The results presented imply that the head-bob phenotype observed in *Nptn*$^{pitch/pitch}$ mice is coincident with the absence of otoconia. Otoconia are present before the onset of the head-bob phenotype, but it is not clear whether the otoconia have detached from the otolithic membrane or are resorbed.

This phenotype requires further investigation to establish the fate of the otoconia and to determine how mutation of a cell adhesion molecule could lead to loss of otoconia.

5.4. Additional phenotypes characterised in *Nptn*^{tm1b}

As mentioned, I requested the *Nptn*^{tm1b} model to be generated at MRC Harwell so as to allow ERG phenotyping. These mice were generated as part of the IMPC programme (https://www.mousephenotype.org) and as such these animals were entered into the IMPC broad-based phenotyping pipeline (Figure 67).

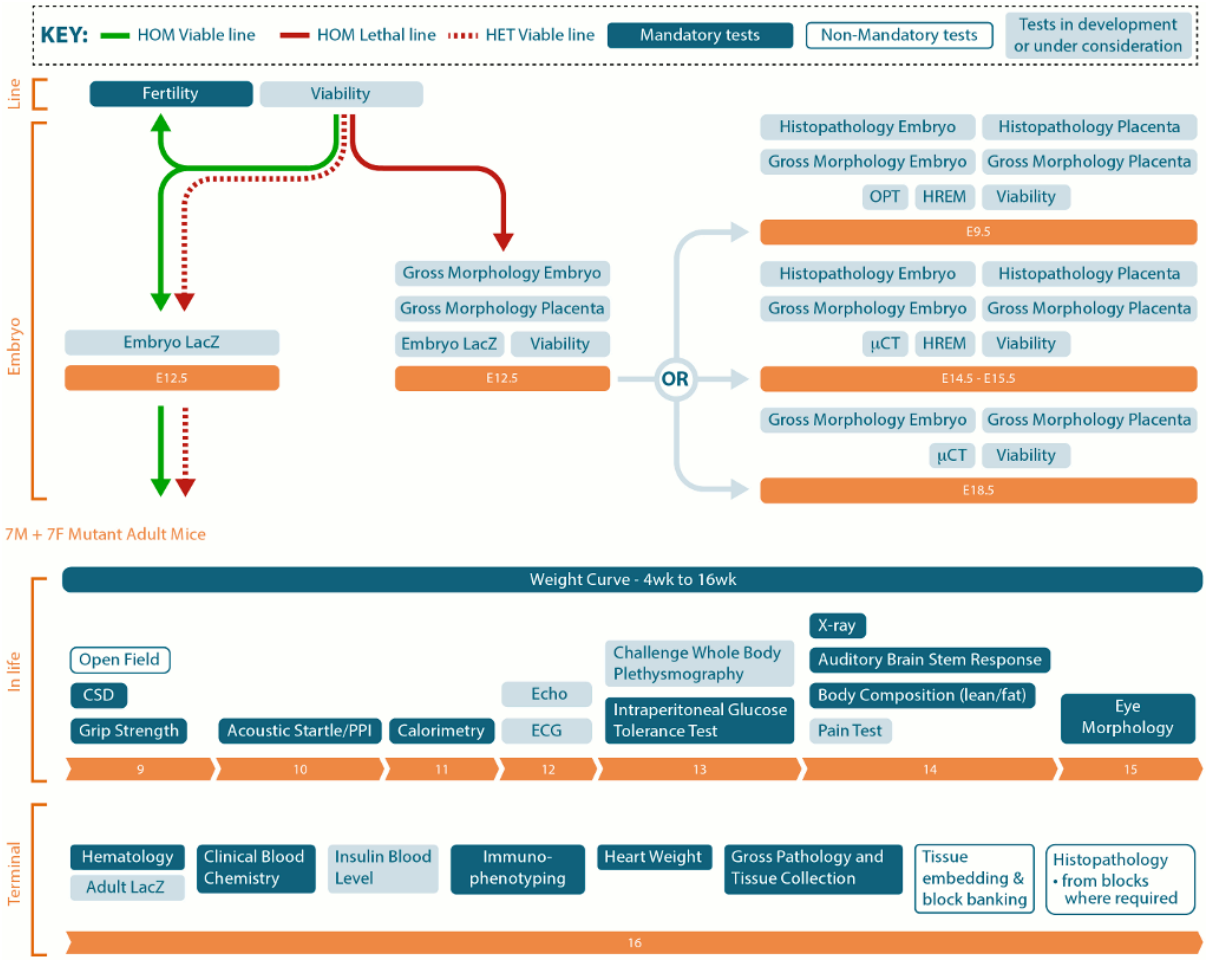

Figure 67. A schematic of the IMPC phenotyping pipeline.

Knockout mice are generated using targeted ES cells from the KOMP repository, and assessed for viability and fertility. Once viability of homozygous (HOM) or heterozygous (HET) mice is confirmed, pedigrees are bred and enter the post-natal phenotyping pipeline. Mandatory tests are performed on all pedigrees. Non-mandatory tests can be requested if an interest is registered in a specific phenotype. Figure adapted from https://www.mousephenotyping.org.

Phenotyping was completed by IMPC staff within the Mary Lyon Centre, MRC Harwell. I obtained the unprocessed data after quality checks had been undertaken, analysed the data and prepared it for reporting.

The IMPC phenotyping pipeline identified multiple phenotypes in *Nptn*^{tm1b} knockout mice (Table 15).

Table 15. Phenotypes identified in *Nptn*^{tm1b} knockout mice.

Parameter	Phenotype
ABR	Elevated auditory-evoked thresholds
Acoustic Startle	Decreased startle reflex
Acoustic Startle/pre-pulse inhibition (PPI)	Decreased PPI
Body composition	Increased lean mass
	Decreased fat mass
Bone mineral content	increased bone mineral content
Calorimetry	Decreased CO2 production
	Decreased energy expenditure
	Decreased oxygen consumption
Clinical chemistry	Abnormal circulating Iron
	Hyperphosphatemia
Dysmorphology	Ear appearance
Mean cell volume	Abnormal corpuscular volume
	Abnormal corpuscular haemoglobin
Open field	Decreased centre average speed
	Increased distance travelled
	Increased number of centre entries
	Hyperactive - reduced rest time
SHIRPA	Abnormal gait
	Limb grasp
	Tremor

The phenotypes previously identified in *Nptn*$^{pitch/pitch}$ were recapitulated in *Nptn*^{tm1b}. As described in section 5.2, auditory impairment was identified by ABR, and KO mice were also found to have an impaired acoustic startle response. SHIRPA (SmithKline Beecham, Harwell, Imperial College and Royal London Hospital phenotype assessment), a battery of tests designed to identify neurological and behavioural abnormalities, identified the gait and limb grasp phenotypes previously observed in *Nptn*$^{pitch/pitch}$ (see Supplemental Information S3).

Several phenotypes were identified in *Nptn*^{tm1b} that were not observed in *pitch* mice. For example, abnormal ear appearance (the pinna was reported to be bigger in *Nptn*^{tm1b} knock out mice) was not observed in *Nptn*$^{pitch/pitch}$. Tremors had been observed at approximately 4 months of age in *Nptn*$^{Y219X/Y219X}$; however *Nptn*$^{pitch/pitch}$ had not been aged beyond a few months to assess this. In addition, several phenotyping tests, which had not been employed for *Nptn*$^{pitch/pitch}$ mice, revealed significantly different results in *Nptn*^{tm1b} knockout mice, in comparison to WT littermate controls. Interestingly, open-field testing, a test to assess anxiety behaviour, identified several behavioural changes (increased speed, distance and number of centre entries) and also a hyperactivity phenotype. Body composition and adiposity testing revealed a lean phenotype in male *Nptn*^{tm1b} knockout mice. Some clinical chemistry markers were found to be unusual in *Nptn*$^{tm1b/tm1b}$ and assessment of bone mineral density indicated increased bone mineral content. Pre-pulse inhibition (PPI) testing, a measure of sensorimotor gating, identified that *Nptn*^{tm1b} knockout had decreased PPI, however the results from this test are considered unreliable as the test relies on a response to an auditory tone.

Due to the many phenotypes identified in *Nptn*^{tm1b} mice, I prioritised several interesting parameters for analysis. *Nptn* has previously been associated with schizophrenia, therefore I chose to analyse the behavioural differences observed in open-field testing. I also chose to analyse the mass phenotype observed in *Nptn*$^{tm1b/tm1b}$, as leanness has not previously been reported in association with sensorineural deafness.

5.4.1. Open field testing

Open-field testing of *Nptn*^{tm1b} mutant and WT littermate controls was performed at 9 weeks of age. Briefly, the open-field arena is divided into two zones: a peripheral zone measuring 8 cm from the arena walls and a central zone, which covers approximately 40% of surface area in the arena. Mice are placed into a mid-periphery zone and allowed to roam the arena for 20 minutes. ANY-maze (Stoelter) software is used to video record and track the movement of mice in the arena and can be

utilised to report the parameters of interest. Open-field testing is used to identify exploratory and anxiogenic behaviours. The centre of the arena is more anxiogenic, therefore it is expected that mice will remain within the periphery regions predominantly.

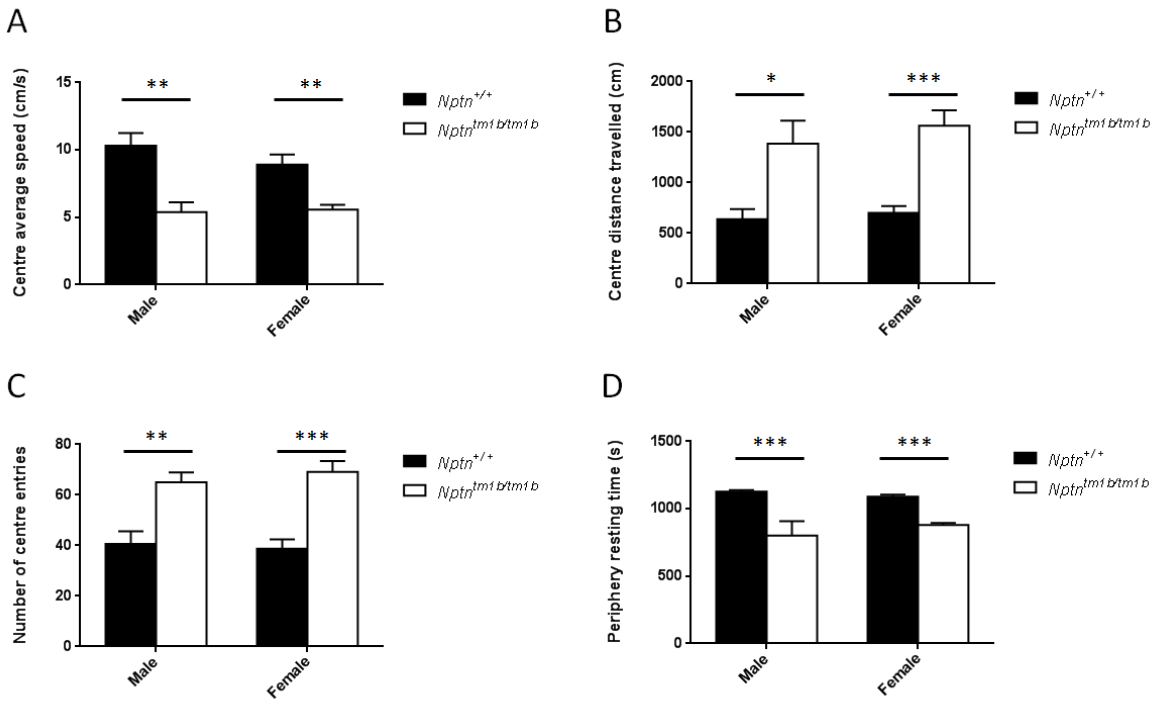

Figure 68. Open-field testing indicates reduced anxiety and hyperactivity in *Nptn*^{tm1b} knock out mice.

A) Both male and female *Nptn*^{tm1b} mutant mice showed decreased average speed when travelling through the centre of the open-field arena in comparison to WT littermate controls (p values: males – p= 0.0011, females – p=0.0024). Statistical analysis: Student's *t*-test, two tailed. **B)** Male and female *Nptn*^{tm1b} mutant mice travelled an increased distance through the centre of the arena in comparison to WT littermate controls (p values: males – p=0.0133, females – p=0.0003). Statistical analysis: Mann Whitney U-Test. **C)** Male and female *Nptn*^{tm1b} mutant mice had increased entries into the centre of the arena in comparison to WT littermate controls (p values: males – p=0.0075, females – p= 0.0006). Statistical analysis: Student's *t*-test, two tailed. **D)** Male and female *Nptn*^{tm1b} mutant mice rested for less time in the periphery of the arena before re-entering the centre zone (p values: males – p=0.0006, females- p=0.00062). Statistical analysis: Mann Whitney U-Test. Data shown = mean + S.E.M. For WT males, *Nptn*$^{tm1b/tm1b}$ males and WT females n = 8. For *Nptn*$^{tm1b/tm1b}$ females n = 9.

Nptn^{tm1b} mutant mice *s*howed decreased speed through the centre of the chamber, in comparison to WT littermates (Figure 68A). In addition, increased distance travelled and an increase in the number of entries into the centre of the arena is also observed in *Nptn*^{tm1b} mutant mice (Figure 68B and C).

All of these behaviours are suggestive of decreased anxiety in *Nptn*^{tm1b} mutant mice, as the animals more frequently enter the centre zone and travel through the centre zone at a slower pace indicating that this zone does not illicit the same fear that it did in WT littermate controls.

Assessment of peripheral resting latency identified that *Nptn*^{tm1b} mutant mice rest in the periphery of the arena for significantly less time than WT littermate controls, before moving into the centre zone (Figure 68D). This result indicates a hyperactivity phenotype, which may be a factor in *Nptn*^{tm1b} mutant mice travelling a higher distance and entering the centre of the arena more often, when compared to WT littermates. However, it seems unlikely that the hyperactivity phenotype would predicate slower movement through the centre of the arena; therefore it is likely that the reduced anxiety behaviour is a true phenotype in *Nptn*^{tm1b} mutant mice.

5.4.2. Body composition testing

Assessment of mass phenotypes is performed in male mice as hormonal fluctuations associated with the menstrual cycle in females may lead to weight fluctuation. *Nptn*^{tm1b} mutant mice and WT littermates were assessed at 14 weeks of age using the Dual Energy X-ray Absorptiometry (DEXA) analyser to identify fat and lean mass.

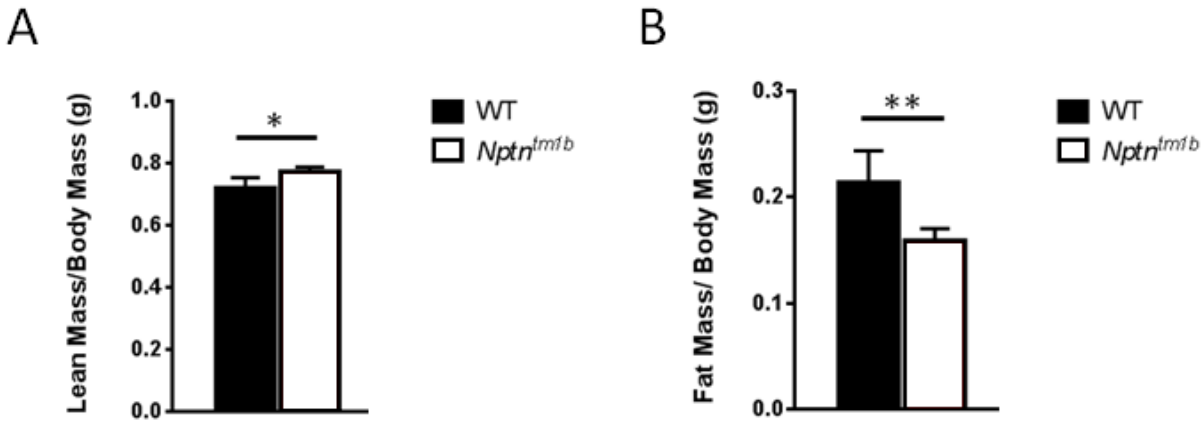

Figure 69. Male *Nptn*^{tm1b} mutant mice display a lean phenotype.

A) Male *Nptn*^{tm1b} mutant mice had a higher lean mass to body mass ratio, on average 0.05 – 0.1g higher than in control mice. p = 0.0027, *p=< 0.01.**B)** Male *Nptn*^{tm1b} mutant mice have a lower fat mass to body mass ratio, approximately 0.05g lower than that observed in WT littermates. p = 0.001, **p=<0.001. Statistical analysis: unpaired student's *t*-test (two-tailed) with Welch's correlation. n = 8 per genotype. Data shown as mean + S.E.M.

Nptn^{tm1b} mutant mice had a higher lean-mass-to-body-mass ratio than WT littermate controls (Figure 68A). Additionally, DEXA analysis identified that *Nptn*^{tm1b} mutant mice have significantly decreased fat mass relative to total body mass (Figure 69B). These results indicate that *Nptn*^{tm1b} mutant mice are leaner than WT littermate controls. The lean phenotype observed is unexpected, as previous studies in human populations have linked hearing loss with increased body mass index (BMI) and waist circumference (Fransen et al., 2008, Hwang et al., 2009). To my knowledge no studies have yet linked hearing loss with decreased fat mass or increased lean mass.

5.5. Discussion

My study of the *pitch* mutant has identified a critical role for Neuroplastin in auditory function, in particular the structure of the IHC ribbon synapse. In addition to the ear, ribbon synapses are critical for retinal function in the eye. As such, it is interesting that Neuroplastin is expressed in the rat retina, where it has been speculated to be required for retinal synaptogenesis (Kreutz et al., 2001, Hill et al., 1988). Unfortunately the genetic background of *pitch* did not allow for assessment of

visual ability. However, targeted ES cells were available as part of the IMPC project, which employs an inbred strain suitable for retinal electrophysiology studies. In addition to allowing retinal phenotyping, once generated the *Neuroplastin* knockout model would also enter the IMPC broad-based phenotyping pipeline, which covers many disease areas.

Several approaches were employed to investigate retinal structure and function in the absence of Neuroplastin. However, first I demonstrated that Np65 is localised to the OPL and IPL synaptic layers of the mouse retina, consistent with the reported rat data showing Np65 to be present at both ribbon (OPL) and conventional (IPL) synapses. Immunolabelling also identified the absence of Np65 protein in *pitch* mutant retina, which is expected in light of the inner ear data I have generated. Histological assessment of retinal structure did not reveal any obvious morphological differences between *pitch* mutant and wild type retina, with all three nuclear layers present. Additional immunolabelling studies, using the pre-synaptic marker RIBEYE, gave strong labelling in the OPL for both *pitch* mutant and wild type retina, suggesting the ribbon synapses are not affected. To ascertain the function of the retina, electroretinography (ERG) studies were undertaken for $Nptn^{tm1b}$ mutant and wild type mice. These studies identified a very mild visual processing defect in the $Nptn^{tm1b}$ mutant retina compared with wild type, but unlikely substantial enough to cause a visual deficit in these mice. I had hoped to ascertain whether Neuroplastin is an Usher (deaf-blindness) syndrome gene, but unfortunately the mouse is not a good model for this disease. Mouse models are available for each of the 10 reported human Usher genes and they all show hearing loss. However, to date only one model, *Ush2c*, also shows a visual deficit (Williams, 2008). In the case of *CIB2*, the recently identified gene for Ush1J, drosophila knock outs were used to model the visual phenotype, with Usher syndrome later confirmed in human populations (Riazuddin et al., 2012). The reason why the mouse is not a good model for the retinal dystrophy in Usher syndrome is unclear, but it has been suggested that anatomical differences may account for the lack of a retinal phenotype. It has been shown that USH1 proteins co-localized at membrane interfaces, between

microvillus-like calyceal processes and the outer segment basolateral region of the photoreceptor rod and cone cells, forming an adhesion belt. Mouse photoreceptors lack these calyceal processes and USH1 proteins do not localize to the outer segment interface. In humans, USH1 proteins form an adhesion belt around the basolateral region of the photoreceptor outer segment, and defects in this structure are suggested to cause the retinal degeneration in USH1 patients (Sahly et al., 2012).

Several Usher models including *Shaker-1* (*Ush1b*) and *Ames waltzer* (*Ush1f*) have shown increased a- and b-wave amplitudes by electroretinography, as reviewed by Williams (2008). However, *Nptn*^{tm1b} mutant mice only have a mildly increased a-wave amplitude. In addition, contrary to the findings in other Usher mutants the amplitude of the b-wave is mildly decreased in *Nptn*^{tm1b} mutant mice.

Usher proteins are reported to interact as part of a large 'Usher interactome', principally within the inner or outer segments of the photoreceptor cells, whereas my results suggest that Np65 likely functions at the synapse. Based on published data and the results gained from studying the *Nptn* mouse mutants, I believe it is unlikely that Neuroplastin is an Usher gene. However, our collaborators are screening their idiopathic Usher patients for *Neuroplastin* mutations, which will help to verify if it is an Usher gene.

In addition to hearing impairment, a vestibular deficit was noted in aged *pitch* mutant mice. Histological assessment of the vestibular apparatus identified that P90 head tilting *pitch* mutant mice lack otoconia in the saccule or utricle. Interestingly, otoconia are present in P90 non-head tilting *pitch* mutant mice, suggesting that otoconia loss underlies the vestibular deficit in head tilting mice. From studying the inner ear sections I was unable to establish whether otoconia have been resorbed or have become detached.

The vestibular sensory hair cells are similar to the cochlear sensory hair cells in that they have stereocilia, facilitate mechano-electrical transduction and signal to afferent neurons via ribbon synapses. It is possible that Neuroplastin functions at vestibular hair cell synapses in a similar way to how it functions at the synapses of cochlear hair cells. In addition, my results show progressive loss of cochlear hair cells in the absence of Neuroplastin. Therefore, if required at the vestibular synapse, it is possible that vestibular hair cells will also undergo progressive degeneration in the absence of Neuroplastin. Progressive loss of vestibular hair cells would certainly cause the late-onset head tilt phenotype, but explaining the otoconia loss is less obvious. Perhaps loss of vestibular hair cells leads to a reduction in volume or stability of the otolithic membrane, which eventually leads to otoconia becoming detached from the epithelium.

Two mouse models of otoconial degeneration have been reported. The gene has not been identified for one, but for *Ames waltzer* the mutation is in *Pcdh15,* which encodes a cell adhesion molecule - reviewed Hughes et al. (2006). Although expression of Protocadherin 15 and Np65 differ in the ear, *Ames waltzer* mice show progressive loss of the saccular neurosensory epithelia and demineralisation and fragmentation of the otoconia from P25, supporting the hypothesis that progressive degeneration leads to otoconial detachment or loss (Alagramam et al., 2005).

Further investigation is required to fully elaborate upon the vestibular phenotype of *pitch* mutant mice. Relevant studies would include ultrastructural and immunolabelling studies to assess degeneration of the vestibular hair cells and expression of Neuroplastin, respectively.

To date, no direct role for Neuroplastin in human disease, including neurologic disorders, has been established. However, there is evidence linking Neuroplastin to a number of pathophysiological conditions such as: schizophrenia, ischaemia and breast cancer.

The broad-based phenotyping of *Nptn*^{tm1b} mutant mice, undertaken as part of the IMPC programme, identified behavioural changes as observed in Open-field testing including: increased distance travelled; increased number of centre entries; decreased speed through the centre zone; and, reduced rest time (hyperactive). Although the increased distance and number of centre entries may be attributable to hyperactivity, decreased speed through the centre zone suggests reduced anxiety in *Nptn*^{tm1b} mutant mice. This result suggests that Neuroplastin may be a modifier of anxiety, increased anxiety is a known symptom of schizophrenia. Interestingly, Neuroplastin has been identified as a risk factor for schizophrenia in both rodent and human studies (Ouchi et al., 2005, Saito et al., 2006). In humans, chronic use of the psychotomimetic drug methamphetamine induces a psychotic state resembling schizophrenia, and administration of phencyclidine mimics both the positive and negative symptoms of schizophrenia. In two rat models for schizophrenia (administration of methamphetamine or phencyclidine) gene expression studies have shown that Neuroplastin, and related protein family member Basigin, are up-regulated. In addition, studies of schizophrenic patients have identified non-coding SNPs in the Neuroplastin gene locus, one exhibits increased frequency in schizophrenia, and one exhibits decreased frequency. The latter SNP was shown to significantly lower Neuroplastin transcription, thus suggesting lower Nptn transcription could lower the onset risk for schizophrenia. These data are consistent with the Open-field phenotypes observed for the Neuroplastin knockout mice.

Recently, a single nucleotide polymorphism (SNP) in the human Neuroplastin locus has been shown to be associated with reduced cortical thickness and impaired intellectual ability in adolescents (Desrivieres et al., 2014). It would be interesting to assess the cortical thickness of *Nptn*^{tm1b} and/or *Nptn*^{pitch} mice.

In addition to the behavioural changes, *Nptn*^{tm1b} mutant mice also show increased lean mass and reduced fat mass. However, given the hyperactivity phenotype identified by Open-field testing, it is

plausible that the reduced fat mass phenotype observed in *Nptn*^{tm1b} mutant mice may be simply explained by the increase activity observed. However, it would be good to generate a full metabolic profile of these mice, for example using the CLAMS system. This will measure activity, food intake, etc, and together with body composition data generated using Echo-MRI, it will be possible to ascertain the true extent of this potential phenotype.

To summarise, mutant models of Neuroplastin have identified that Nptn has a much wider contribution to mouse physiology than was initially identified in *pitch* mice, and further exploration of these models will expand our knowledge of more than just the auditory pathway.

Chapter 6. Discussion

The aim of this study was to characterise the mouse mutant model of early-onset sensorineural deafness, *pitch*. To do this I undertook comprehensive *in silico*, *in vitro*, *in vivo* and *ex vivo* analyses of *pitch*. These studies identified *Neuroplastin* as a novel deafness-related gene and establish a role for Np65 in auditory ribbon synapse formation and function. This is the first mammalian phenotype to be directly associated with a Neuroplastin mutation, and expands our knowledge of this cell adhesion molecule (CAM) in wider physiology.

Neuroplastin, together with Basigin and Embigin, form a distinct family of neural CAMs belonging to the immunoglobulin superfamily. Embigin has 2 extracellular Ig domains, whereas Basigin, like Neuroplastin, is expressed as 2 or 3 Ig domain-containing isoforms named Basigin-1 and -2, respectively (Beesley et al., 2014). As such, Basigin-2 and Np65 are both able to form homophilic interactions, whereas Embigin cannot. Embigin is the least studied member of the family, but it has been shown to be involved in neuromuscular synapse formation and plasticity (Lain et al., 2009). Basigin is the most studied member of the family and is reported to have important roles in fetal, neuronal, lymphocyte and extracellular matrix development (Iacono et al., 2007). Indeed Basigin is believed to have a role in several pathological conditions including heart disease, Alzheimer's, stroke and cancer (Iacono et al., 2007). Investigation of a Basigin knockout mouse model has shown that the majority of homozygous null embryos die around the time of implantation (Igakura et al., 1998). Some homozygous mice do survive to adulthood, but these are sterile (Igakura et al., 1998).In addition, Basigin knockout mice have impaired vision from the time of eye-opening, exhibiting normal retinal architecture, but having severely depressed ERG amplitudes (Ochrietor et al., 2002). This is followed by degeneration of the photoreceptor cells by 8 weeks of age (Ochrietor et al., 2001, Hori et al., 2000). Prior to this study, there have been no reports suggesting expression of this gene family in the ear, or links to auditory dysfunction reported in human or mouse studies. I have

established that Neuroplastin is both expressed and required within the ear, it would be interesting to determine if Basigin and Embigin are also expressed in the ear. I would initially use qRT-PCR to determine if these genes are expressed in the ear at transcript level. If they are found to be expressed, immunolabelling studies would be undertaken to assess the localisation of the proteins in the ear. Ultimately, I would hope to obtain or generate mutant mouse models for these genes and assess their auditory function. Although, given the embryonic lethality observed for the published Basigin knockout mice, a conditional knockout approach may prove more fruitful.

The data presented support the hypothesis that Np65 is critical for hearing and auditory ribbon synapse function. The major limitation of this study is the failure to identify the exact sub-cellular localisation of Np65 at the auditory synapse. Attempts to determine the localisation using immunogold labelling coupled to TEM, and a DAB labelling substitute, both failed. Two methods could be used to overcome this obstacle. One would be to generate additional antibodies to Np65, with the hope that one would work for immunogold labelling. The second would be to employ super-resolution microscopy of immunolabelled cochlear cryosections, using antibodies against Np65, RIBEYE (pre-synaptic marker) and GluR2 (post-synaptic marker). This technique provides single photon resolution and could establish if Np65 spans the synaptic cleft. Initial plans were made to allow this experiment with collaborators at the Micron Oxford Advanced Bioimaging Unit. However, due to difficulty breeding homozygous *pitch* animals I was not able to collect the samples required for this experiment.

Additionally, it would be interesting to investigate the auditory ribbon synapse of heterozygous *pitch* mice ($Nptn^{pitch/+}$). In $Nptn^{pitch/pitch}$ mice there is a mismatch of pre- and post-synaptic puncta ~35 – 45%, whereas in $Nptn^{+/+}$ mice only between 5 and 10% of puncta are mismatched. This result suggests there may be a threshold of synaptic mismatch above which auditory impairment becomes evident. Investigation of the ribbon synapse in $Nptn^{pitch/+}$ mice would determine if only having one

copy of functional Np65 leads to an intermediate degree of mismatching between that observed for *Nptn*$^{+/+}$ and *Nptn*$^{pitch/pitch}$ mice. If an intermediate level of mismatching is found it will give an indication of the matched threshold required to sustain the normal hearing function observed in the *Nptn*$^{pitch/+}$ mice.

In addition to the total number of matched/mismatched synapses, I also feel the possible morphological differences identified for the *Nptn*$^{pitch/pitch}$ matched ribbon synapses requires further exploration. To enable this, I would like to examine the morphology of the ribbon synapses and quantify their size and distribution using TEM microscopy of resin sections from the inner ears of *Nptn*$^{+/+}$ and *Nptn*$^{pitch/pitch}$ mice. In particular I would investigate the distance between pre- and post-synaptic markers to determine if synapses are less tightly coupled in the absence of Np65.

6.1. Np65 in the retina

Investigation of *Nptn* as a possible Usher gene was inconclusive in our knockout mouse model. There were some mild differences in the ERG responses observed between WT and *Nptn*^{tm1b} mice, but as mentioned previously known Usher genes do not cause retinitis pigmentosa in mouse models. However, given the severe auditory impairment observed in Nptn mutant models, and the high level of Np65 expression observed in the eye, it is plausible that Nptn will turn out to be an Usher gene.

To prove *Neuroplastin* is an Usher gene, mutations would need to be identified in human patients. Currently, our collaborators are screening this gene in Usher and non-syndromic deafness patients.

6.2. Neuroplastin in wider physiology

The IMPC phenotyping pipeline identified several phenotypes in *Nptn*$^{tm1b/tm1b}$ which were not previously identified in *pitch*. Of particular interest were the phenotypes identified by open field, suggesting that *Nptn*^{tm1b} knock out mice are hyperactive and less anxious, and the lean and fat mass phenotypes identified by DEXA.

The breadth of phenotypes identified in *Nptn*^{tm1b} knockout mice using the IMPC pipeline, in comparison to those identified in *Nptn*$^{pitch/pitch}$ demonstrate how valuable large-scale broad-based phenotyping projects, such as IMPC, are to expanding our knowledge of mammalian functional genomics. However, the identification of so many potential phenotypes begs the question as to what are the key biological roles/requirements of Neuroplastin?

To date the majority of studies into the function of Neuroplastin have been performed *in vitro,* thus the involvement of Neuroplastin in the whole system is less well characterised and many pathways and interactions are yet to be identified (Beesley et al., 2014). However, the association of SNPs in *NEUROPLASTIN* with changes in human cortical thickness and intelligence indicate that Neuroplastin is likely to regulate synaptic function and the neuronal network in humans, implying that previous *in vitro* and *ex vivo* research indicating the involvement of Neuroplastin in rat synapses is biologically relevant between species (Desrivieres et al., 2014, Beesley et al., 2014). Identification of Np55 as a biomarker in human breast cancer patients and speculation that Np55 may act through FGFR1 in the pathophysiology of the disease, suggests that Neuroplastin has a wider role throughout the human body than currently characterised in rodent models (Rodriguez-Pinto et al., 2009). It seems likely that the phenotypes identified by the IMPC phenotyping may hint at involvement of Neuroplastin in pathways and interactions that have yet to be characterised.

6.3. Whole study limitations

One limitation in this study was availability of *Nptn*$^{pitch/pitch}$ animals to perform experiments and there are several experiments I was unable to perform due to lack of mutant mice. Male *Nptn*$^{pitch/pitch}$ mice are infertile; therefore I was not able to arrange homozygous crosses. *Nptn*$^{pitch/pitch}$ females did produce offspring, so I was able to set up heterozygous x homozygous matings. However, *Nptn*$^{pitch/pitch}$ mothers littered less frequently, produced smaller litters, and pups had to be fostered

shortly after birth. If I were to continue this study, I would look to cross the *pitch* mutation onto a different background strain in hopes to improve fertility and increase litter sizes.

Another limitation of this study is n numbers within experiments. Adhering to the 3R's (reduction, replacement and refinement) experimental cohorts were designed to contain the minimum numbers to achieve statistical significance. However, this may mean that more subtle differences go undetected, and outliers can really affect the data. This is something I had to be extremely mindful of when analysing the data produced. This limitation is particularly evident in the IMPC screen, where for more invasive tests such as ABR; only 2 WT animals are used to create the baseline data. Comparisons can be made to WT animals from other cohorts, but this does not control for all of the variables that might occur.

Although there are limitations associated with working with mice, the benefits; such as close genetic identity with humans and short generation time, identify the mouse as the best organism for modelling auditory disease.

6.4. Conclusion

This study describes Np65 as an essential auditory protein, required for synaptic function at the auditory ribbon synapse, however Np65 was found to be non-essential for vision. This study also details several other phenotypes identified in *Nptn*^{tm1b} knock out mice, suggesting that Neuroplastin will have a wider role in the pathophysiology of disease.

Identification of *Neuroplastin* as a gene required for auditory function has several implications. As mutations in *Neuroplastin* have not yet been associated with deafness in human populations, *Neuroplastin* can now be screened as a potential candidate in unresolved deafness cases. Also, given the functional overlap between Neuroplastin and its fellow nCAMs Basigin and Embigin, the

identification of Neuroplastin as an auditory gene suggests that Basigin and Embigin may also be involved in the auditory pathway and are good candidates for further assessment.

The identification of Neuroplastin as a deafness-related gene and the requirement of Np65 for ribbon synapse function is an interesting discovery and paves the way for future investigation of similar proteins within the auditory system.

References

ACEVEDO-AROZENA, A., RICKETTS, T. & CORROCHANO, S. 2010. Deconstructing Gene Function through ENU Mutagenesis. *Encyclopedia of Life Sciences.* Chichester: John Wiley & Sons, Ltd.

ACEVEDO-AROZENA, A., WELLS, S., POTTER, P., KELLY, M., COX, R. D. & BROWN, S. D. 2008. ENU mutagenesis, a way forward to understand gene function. *Annu Rev Genomics Hum Genet,* 9**,** 49-69.

ACTION-ON-HEARING-LOSS. 2011. *Types and causes of hearing loss* [Online]. Available: http://www.actiononhearingloss.org.uk/your-hearing/about-deafness-and-hearing-loss/types-and-cause-of-hearing-loss/genetics.aspx [Accessed 01/06/2014 2014].

ADACHI, N., YOSHIDA, T., NIN, F., OGATA, G., YAMAGUCHI, S., SUZUKI, T., KOMUNE, S., HISA, Y., HIBINO, H. & KURACHI, Y. 2013. The mechanism underlying maintenance of the endocochlear potential by the K+ transport system in fibrocytes of the inner ear. *J Physiol,* 591**,** 4459-72.

ADATO, A., VREUGDE, S., JOENSUU, T., AVIDAN, N., HAMALAINEN, R., BELENKIY, O., OLENDER, T., BONNE-TAMIR, B., BEN-ASHER, E., ESPINOS, C., MILLAN, J. M., LEHESJOKI, A. E., FLANNERY, J. G., AVRAHAM, K. B., PIETROKOVSKI, S., SANKILA, E. M., BECKMANN, J. S. & LANCET, D. 2002. USH3A transcripts encode clarin-1, a four-transmembrane-domain protein with a possible role in sensory synapses. *Eur J Hum Genet,* 10**,** 339-50.

ADLER, J. & PARMRYD, I. 2010. Quantifying colocalization by correlation: the Pearson correlation coefficient is superior to the Mander's overlap coefficient. *Cytometry A,* 77**,** 733-42.

ADZHUBEI, I. A., SCHMIDT, S., PESHKIN, L., RAMENSKY, V. E., GERASIMOVA, A., BORK, P., KONDRASHOV, A. S. & SUNYAEV, S. R. 2010. A method and server for predicting damaging missense mutations. *Nat Methods,* 7**,** 248-9.

AHMED, Z. M., RIAZUDDIN, S., AHMAD, J., BERNSTEIN, S. L., GUO, Y., SABAR, M. F., SIEVING, P., RIAZUDDIN, S., GRIFFITH, A. J., FRIEDMAN, T. B., BELYANTSEVA, I. A. & WILCOX, E. R. 2003. PCDH15 is expressed in the neurosensory epithelium of the eye and ear and mutant alleles are responsible for both USH1F and DFNB23. *Human Molecular Genetics,* 12**,** 3215-3223.

ALAGRAMAM, K. N., STAHL, J. S., JONES, S. M., PAWLOWSKI, K. S. & WRIGHT, C. G. 2005. Characterization of vestibular dysfunction in the mouse model for Usher syndrome 1F. *J Assoc Res Otolaryngol,* 6**,** 106-18.

ALBERTS, B. 2008. *Molecular biology of the cell,* New York, Garland Science.

ALI MOSRATI, M., SCHRAUWEN, I., BEN SAIID, M., AIFA-HMANI, M., FRANSEN, E., MNEJA, M., GHORBEL, A., VAN CAMP, G. & MASMOUDI, S. 2013. Genome-wide analysis reveals a novel autosomal-recessive hearing loss locus DFNB80 on chromosome 2p16.1-p21. *J Hum Genet,* 58**,** 98-101.

ALLEN, E. K., CHEN, W. M., WEEKS, D. E., CHEN, F., HOU, X., MATTOS, J. L., MYCHALECKYJ, J. C., SEGADE, F., CASSELBRANT, M. L., MANDEL, E. M., FERRELL, R. E., RICH, S. S., DALY, K. A. & SALE, M. M. 2013. A genome-wide association study of chronic otitis media with effusion and recurrent otitis media identifies a novel susceptibility locus on chromosome 2. *J Assoc Res Otolaryngol,* 14**,** 791-800.

ANDO, M. & TAKEUCHI, S. 1999. Immunological identification of an inward rectifier K+ channel (Kir4.1) in the intermediate cell (melanocyte) of the cochlear stria vascularis of gerbils and rats. *Cell Tissue Res,* 298**,** 179-83.

ASHA. 2014. *Cochlear Implant Frequently Asked Questions* [Online]. Available: http://www.asha.org/public/hearing/Cochlear-Implant-Frequently-Asked-Questions/ [Accessed 06/06/2014 2014].

ASSAD, J. A., SHEPHERD, G. M. & COREY, D. P. 1991. Tip-link integrity and mechanical transduction in vertebrate hair cells. *Neuron,* 7**,** 985-94.

BALLING, R. 2001. ENU mutagenesis: analyzing gene function in mice. *Annu Rev Genomics Hum Genet,* 2**,** 463-92.

BANCROFT, J. D. & STEVENS, A. 1990. *Theory and practice of histological techniques,* Edinburgh ; New York, Churchill Livingstone.

BARCLAY, M., RYAN, A. F. & HOUSLEY, G. D. 2011. Type I vs type II spiral ganglion neurons exhibit differential survival and neuritogenesis during cochlear development. *Neural Dev,* 6**,** 33.

BEDELL, M. A., LARGAESPADA, D. A., JENKINS, N. A. & COPELAND, N. G. 1997. Mouse models of human disease. Part II: recent progress and future directions. *Genes Dev,* 11**,** 11-43.

BEESLEY, P. W., HERRERA-MOLINA, R., SMALLA, K. H. & SEIDENBECHER, C. 2014. The Neuroplastin adhesion molecules: key regulators of neuronal plasticity and synaptic function. *J Neurochem*.

BERNSTEIN, H. G., SMALLA, K. H., BOGERTS, B., GORDON-WEEKS, P. R., BEESLEY, P. W., GUNDELFINGER, E. D. & KREUTZ, M. R. 2006. The immunolocalization of the synaptic glycoprotein neuroplastin differs substantially between the human and the rodent brain. *Brain Res,* 1134**,** 107-12.

BIOON. 2014. *Eye and Retina* [Online]. Available: http://www.bioon.com/bioline/neurosci/course/eyeret.html [Accessed 10/07/2014].

BOLSHAKOV, K. V., TIKHONOV, D. B., GMIRO, V. E. & MAGAZANIK, L. G. 2000. Different arrangement of hydrophobic and nucleophilic components of channel binding sites in N-methyl-D-aspartate and AMPA receptors of rat brain is revealed by channel blockade. *Neurosci Lett,* 291**,** 101-4.

BOLZ, H., VON BREDERLOW, B., RAMIREZ, A., BRYDA, E. C., KUTSCHE, K., NOTHWANG, H. G., SEELIGER, M., CABRERA, M. D. S., VILA, M. C., MOLINA, O. P., GAL, A. & KUBISCH, C. 2001. Mutation of CDH23, encoding a new member of the cadherin gene family, causes Usher syndrome type 1D. *Nature Genetics,* 27**,** 108-112.

BONNET, C. & EL-AMRAOUI, A. 2012. Usher syndrome (sensorineural deafness and retinitis pigmentosa): pathogenesis, molecular diagnosis and therapeutic approaches. *Curr Opin Neurol,* 25**,** 42-9.

BROWN, A. C. 1874. The Sense of Rotation and the Anatomy and Physiology of the Semicircular Canals of the Internal Ear. *J Anat Physiol,* 8**,** 327-31.

BROWN, S. D., HARDISTY-HUGHES, R. E. & MBURU, P. 2008. Quiet as a mouse: dissecting the molecular and genetic basis of hearing. *Nat Rev Genet,* 9**,** 277-90.

BUCKBY, L. E., MUMMERY, R., CROMPTON, M. R., BEESLEY, P. W. & EMPSON, R. M. 2004. Comparison of neuroplastin and synaptic marker protein expression in acute and cultured organotypic hippocampal slices from rat. *Developmental Brain Research,* 150**,** 1-7.

BURDA, H. & BRANIS, M. 1988. Postnatal development of the organ of Corti in the wild house mouse, laboratory mouse, and their hybrid. *Hear Res,* 36**,** 97-105.

CAMPO, P., LATAYE, R., COSSEC, B. & PLACIDI, V. 1997. Toluene-induced hearing loss: a mid-frequency location of the cochlear lesions. *Neurotoxicol Teratol,* 19**,** 129-40.

CAROLA, R., HARLEY, J. P. & NOBACK, C. R. 1992. Human anatomy and physiology. 2nd ed. New York: McGraw-Hill.

CHANG, B., HAWES, N. L., HURD, R. E., DAVISSON, M. T., NUSINOWITZ, S. & HECKENLIVELY, J. R. 2002. Retinal degeneration mutants in the mouse. *Vision Res,* 42**,** 517-25.

CHEESEMAN, M. T., TYRER, H. E., WILLIAMS, D., HOUGH, T. A., PATHAK, P., ROMERO, M. R., HILTON, H., BALI, S., PARKER, A., VIZOR, L., PURNELL, T., VOWELL, K., WELLS, S., BHUTTA, M. F., POTTER, P. K. & BROWN, S. D. 2011. HIF-VEGF pathways are critical for chronic otitis media in Junbo and Jeff mouse mutants. *PLoS Genet,* 7**,** e1002336.

CHISOLM, T. H., ABRAMS, H. B. & MCARDLE, R. 2004. Short- and long-term outcomes of adult audiological rehabilitation. *Ear Hear,* 25**,** 464-77.

CHOI, Y., SIMS, G. E., MURPHY, S., MILLER, J. R. & CHAN, A. P. 2012. Predicting the Functional Effect of Amino Acid Substitutions and Indels. *PLoS One,* 7.

CHRISTENSEN, K., FREDERIKSEN, H. & HOFFMAN, H. J. 2001. Genetic and environmental influences on self-reported reduced hearing in the old and oldest old. *J Am Geriatr Soc,* 49**,** 1512-7.

COGHILL, E. L., HUGILL, A., PARKINSON, N., DAVISON, C., GLENISTER, P., CLEMENTS, S., HUNTER, J., COX, R. D. & BROWN, S. D. 2002. A gene-driven approach to the identification of ENU mutants in the mouse. *Nat Genet,* 30**,** 255-6.

DAUWERSE, J. G., DIXON, J., SELAND, S., RUIVENKAMP, C. A., VAN HAERINGEN, A., HOEFSLOOT, L. H., PETERS, D. J., BOERS, A. C., DAUMER-HAAS, C., MAIWALD, R., ZWEIER, C., KERR, B., COBO, A. M., TORAL, J. F., HOOGEBOOM, A. J., LOHMANN, D. R., HEHR, U., DIXON, M. J., BREUNING, M. H. & WIECZOREK, D. 2011. Mutations in genes encoding subunits of RNA polymerases I and III cause Treacher Collins syndrome. *Nat Genet,* 43**,** 20-2.

DAVIS, A., SMITH, P., FERGUSON, M., STEPHENS, D. & GIANOPOULOS, I. 2007. Acceptability, benefit and costs of early screening for hearing disability: a study of potential screening tests and models. *Health Technol Assess,* 11**,** 1-294.

DAVIS, R. I., AHROON, W. A. & HAMERNIK, R. P. 1989. The relation among hearing loss, sensory cell loss and tuning characteristics in the chinchilla. *Hear Res,* 41**,** 1-14.

DENOYELLE, F., WEIL, D., MAW, M. A., WILCOX, S. A., LENCH, N. J., ALLEN-POWELL, D. R., OSBORN, A. H., DAHL, H. H., MIDDLETON, A., HOUSEMAN, M. J., DODE, C., MARLIN, S., BOULILA-ELGAIED, A., GRATI, M., AYADI, H., BENARAB, S., BITOUN, P., LINA-GRANADE, G., GODET, J., MUSTAPHA, M., LOISELET, J., EL-ZIR, E., AUBOIS, A., JOANNARD, A., LEVILLIERS, J., GARABEDIAN, E. N., MUELLER, R. F., GARDNER, R. J., PETIT, C. & ET AL. 1997. Prelingual deafness: high prevalence of a 30delG mutation in the connexin 26 gene. *Hum Mol Genet,* 6**,** 2173-7.

DESRIVIERES, S., LOURDUSAMY, A., TAO, C., TORO, R., JIA, T., LOTH, E., MEDINA, L. M., KEPA, A., FERNANDES, A., RUGGERI, B., CARVALHO, F. M., COCKS, G., BANASCHEWSKI, T., BARKER, G. J., BOKDE, A. L., BUCHEL, C., CONROD, P. J., FLOR, H., HEINZ, A., GALLINAT, J., GARAVAN, H., GOWLAND, P., BRUHL, R., LAWRENCE, C., MANN, K., MARTINOT, M. L., NEES, F., LATHROP, M., POLINE, J. B., RIETSCHEL, M., THOMPSON, P., FAUTH-BUHLER, M., SMOLKA, M. N., PAUSOVA, Z., PAUS, T., FENG, J. & SCHUMANN, G. 2014. Single nucleotide polymorphism in the neuroplastin locus associates with cortical thickness and intellectual ability in adolescents. *Mol Psychiatry*.

DI PALMA, F., HOLME, R. H., BRYDA, E. C., BELYANTSEVA, I. A., PELLEGRINO, R., KACHAR, B., STEEL, K. P. & NOBEN-TRAUTH, K. 2001. Mutations in Cdh23, encoding a new type of cadherin, cause stereocilia disorganization in waltzer, the mouse model for Usher syndrome type 1D. *Nature Genetics,* 27**,** 103-107.

ECHTELER, S. M. 1992. Developmental segregation in the afferent projections to mammalian auditory hair cells. *Proc Natl Acad Sci U S A,* 89**,** 6324-7.

EMPSON, R. M., BUCKBY, L. E., KRAUS, M., BATES, K. J., CROMPTON, M. R., GUNDELFINGER, E. D. & BEESLEY, P. W. 2006. The cell adhesion molecule neuroplastin-65 inhibits hippocampal long-term potentiation via a mitogen-activated protein kinase p38-dependent reduction in surface expression of GluR1-containing glutamate receptors. *J Neurochem,* 99**,** 850-60.

EMSLIE-SMITH, D. & BELL, G. H. 1988. Textbook of physiology (BDS). 11th ed. Edinburgh ; New York: Churchill Livingstone.

ERKMAN, L., MCEVILLY, R. J., LUO, L., RYAN, A. K., HOOSHMAND, F., O'CONNELL, S. M., KEITHLEY, E. M., RAPAPORT, D. H., RYAN, A. F. & ROSENFELD, M. G. 1996. Role of transcription factors Brn-3.1 and Brn-3.2 in auditory and visual system development. *Nature,* 381**,** 603-6.

EVANS, D. G., SAINIO, M. & BASER, M. E. 2000. Neurofibromatosis type 2. *J Med Genet,* 37**,** 897-904.

FERREIRA, M. A. 2004. Linkage analysis: principles and methods for the analysis of human quantitative traits. *Twin Res,* 7**,** 513-30.

FETTIPLACE, R. & HACKNEY, C. M. 2006. The sensory and motor roles of auditory hair cells. *Nat Rev Neurosci,* 7**,** 19-29.

FLAGELLA, M., CLARKE, L. L., MILLER, M. L., ERWAY, L. C., GIANNELLA, R. A., ANDRINGA, A., GAWENIS, L. R., KRAMER, J., DUFFY, J. J., DOETSCHMAN, T., LORENZ, J. N., YAMOAH, E. N., CARDELL, E. L. & SHULL, G. E. 1999. Mice lacking the basolateral Na-K-2Cl cotransporter have impaired epithelial chloride secretion and are profoundly deaf. *J Biol Chem,* 274**,** 26946-55.

FLOCK, A. & CHEUNG, H. C. 1977. Actin filaments in sensory hairs of inner ear receptor cells. *J Cell Biol,* 75**,** 339-43.

FORGE, A. & WRIGHT, T. 2002. The molecular architecture of the inner ear. *Br Med Bull,* 63**,** 5-24.

FRANSEN, E., TOPSAKAL, V., HENDRICKX, J. J., VAN LAER, L., HUYGHE, J. R., VAN EYKEN, E., LEMKENS, N., HANNULA, S., MAKI-TORKKO, E., JENSEN, M., DEMEESTER, K., TROPITZSCH, A., BONACONSA, A., MAZZOLI, M., ESPESO, A., VERBRUGGEN, K., HUYGHE, J., HUYGEN, P. L., KUNST, S., MANNINEN, M., DIAZ-LACAVA, A., STEFFENS, M., WIENKER, T. F., PYYKKO, I., CREMERS, C. W., KREMER, H., DHOOGE, I., STEPHENS, D., ORZAN, E., PFISTER, M., BILLE, M., PARVING, A., SORRI, M., VAN DE HEYNING, P. & VAN CAMP, G. 2008. Occupational noise, smoking, and a high body mass index are risk factors for age-related hearing impairment and moderate alcohol consumption is protective: a European population-based multicenter study. *J Assoc Res Otolaryngol,* 9**,** 264-76; discussion 261-3.

FRIEDMAN, R. A., VAN LAER, L., HUENTELMAN, M. J., SHETH, S. S., VAN EYKEN, E., CORNEVEAUX, J. J., TEMBE, W. D., HALPERIN, R. F., THORBURN, A. Q., THYS, S., BONNEUX, S., FRANSEN, E., HUYGHE, J., PYYKKO, I., CREMERS, C. W., KREMER, H., DHOOGE, I., STEPHENS, D., ORZAN, E., PFISTER, M., BILLE, M., PARVING, A., SORRI, M., VAN DE HEYNING, P. H., MAKMURA, L., OHMEN, J. D., LINTHICUM, F. H., JR., FAYAD, J. N., PEARSON, J. V., CRAIG, D. W., STEPHAN, D. A. & VAN CAMP, G. 2009. GRM7 variants confer susceptibility to age-related hearing impairment. *Hum Mol Genet,* 18**,** 785-96.

FUCHS, P. 2002. The synaptic physiology of cochlear hair cells. *Audiol Neurootol,* 7**,** 40-4.

GELEOC, G. S., LENNAN, G. W., RICHARDSON, G. P. & KROS, C. J. 1997. A quantitative comparison of mechanoelectrical transduction in vestibular and auditory hair cells of neonatal mice. *Proc Biol Sci,* 264**,** 611-21.

GERNANDT, B. E. 1960. Handbook of physiology; a critical, comprehensive presentation of physiological knowledge and concepts. *In:* FIELD, J. (ed.) *Section 1: NEUROPHYSIOLOGY.* 1 ed. Washington: American Society of Physiology.

GIROTTO, G., PIRASTU, N., SORICE, R., BIINO, G., CAMPBELL, H., D'ADAMO, A. P., HASTIE, N. D., NUTILE, T., POLASEK, O., PORTAS, L., RUDAN, I., ULIVI, S., ZEMUNIK, T., WRIGHT, A. F., CIULLO, M., HAYWARD, C., PIRASTU, M. & GASPARINI, P. 2011. Hearing function and thresholds: a genome-wide association study in European isolated populations identifies new loci and pathways. *J Med Genet,* 48**,** 369-74.

GIROTTO, G., VUCKOVIC, D., BUNIELLO, A., LORENTE-CANOVAS, B., LEWIS, M., GASPARINI, P. & STEEL, K. P. 2014. Expression and replication studies to identify new candidate genes involved in normal hearing function. *PLoS One,* 9**,** e85352.

GLOWATZKI, E. & FUCHS, P. A. 2000. Cholinergic synaptic inhibition of inner hair cells in the neonatal mammalian cochlea. *Science,* 288**,** 2366-8.

GLUZMAN, Y. 1981. SV40-transformed simian cells support the replication of early SV40 mutants. *Cell,* 23**,** 175-82.

GOUDY, S., LOTT, D., CANADY, J. & SMITH, R. J. 2006. Conductive hearing loss and otopathology in cleft palate patients. *Otolaryngol Head Neck Surg,* 134**,** 946-8.

GREVERS, G. 2010. Challenges in reducing the burden of otitis media disease: an ENT perspective on improving management and prospects for prevention. *Int J Pediatr Otorhinolaryngol,* 74**,** 572-7.

GUILFORD, P., BEN ARAB, S., BLANCHARD, S., LEVILLIERS, J., WEISSENBACH, J., BELKAHIA, A. & PETIT, C. 1994. A non-syndrome form of neurosensory, recessive deafness maps to the pericentromeric region of chromosome 13q. *Nat Genet,* 6**,** 24-8.

HAIN, T. C. 2003. *Central Hearing Loss* [Online]. Available: http://www.dizziness-and-balance.com/disorders/hearing/cent_hearing.html [Accessed 06/07/2014 2014].

HAMRA, F. K. 2010. Gene targeting: Enter the rat. *Nature,* 467**,** 161-3.

HARDISTY-HUGHES, R. E., PARKER, A. & BROWN, S. D. 2010. A hearing and vestibular phenotyping pipeline to identify mouse mutants with hearing impairment. *Nat Protoc,* 5**,** 177-90.

HARDISTY-HUGHES, R. E., TATEOSSIAN, H., MORSE, S. A., ROMERO, M. R., MIDDLETON, A., TYMOWSKA-LALANNE, Z., HUNTER, A. J., CHEESEMAN, M. & BROWN, S. D. 2006. A mutation in the F-box gene, Fbxo11, causes otitis media in the Jeff mouse. *Hum Mol Genet,* 15**,** 3273-9.

HARDISTY, R. E., ERVEN, A., LOGAN, K., MORSE, S., GUIONAUD, S., SANCHO-OLIVER, S., HUNTER, A. J., BROWN, S. D. & STEEL, K. P. 2003. The deaf mouse mutant Jeff (Jf) is a single gene model of otitis media. *J Assoc Res Otolaryngol,* 4**,** 130-8.

HARRISON, T., GRAHAM, F. & WILLIAMS, J. 1977. Host-range mutants of adenovirus type 5 defective for growth in HeLa cells. *Virology,* 77**,** 319-29.

HEALTHY-HEARING. 2014. *Degrees of Hearing Loss* [Online]. Available: http://www.healthyhearing.com/content/faqs/Hearing-loss/Test/41775-Degrees-of-hearing-loss [Accessed 11/09/2014].

HEIDELBERGER, R., THORESON, W. B. & WITKOVSKY, P. 2005. Synaptic transmission at retinal ribbon synapses. *Prog Retin Eye Res,* 24**,** 682-720.

HELLIER, W. P., WAGSTAFF, S. A., O'LEARY, S. J. & SHEPHERD, R. K. 2002. Functional and morphological response of the stria vascularis following a sensorineural hearing loss. *Hear Res,* 172**,** 127-36.

HENDERSON, D., BIELEFELD, E. C., HARRIS, K. C. & HU, B. H. 2006. The role of oxidative stress in noise-induced hearing loss. *Ear Hear,* 27**,** 1-19.

HEQUEMBOURG, S. & LIBERMAN, M. C. 2001. Spiral ligament pathology: a major aspect of age-related cochlear degeneration in C57BL/6 mice. *J Assoc Res Otolaryngol,* 2**,** 118-29.

HERRERA-MOLINA, R., SARTO-JACKSON, I., MONTENEGRO-VENEGAS, C., HEINE, M., SMALLA, K. H., SEIDENBECHER, C. I., BEESLEY, P. W., GUNDELFINGER, E. D. & MONTAG, D. 2014. Structure of excitatory synapses and GABAA receptor localization at inhibitory synapses are regulated by neuroplastin-65. *J Biol Chem,* 289**,** 8973-88.

HIBINO, H. & KURACHI, Y. 2006. Molecular and physiological bases of the K+ circulation in the mammalian inner ear. *Physiology (Bethesda),* 21**,** 336-45.

HILL, I. E., SELKIRK, C. P., HAWKES, R. B. & BEESLEY, P. W. 1988. Characterization of novel glycoprotein components of synaptic membranes and postsynaptic densities, gp65 and gp55, with a monoclonal antibody. *Brain Res,* 461**,** 27-43.

HIRSCHHORN, J. N., LOHMUELLER, K., BYRNE, E. & HIRSCHHORN, K. 2002. A comprehensive review of genetic association studies. *Genet Med,* 4**,** 45-61.

HOELTER, S. M., DALKE, C., KALLNIK, M., BECKER, L., HORSCH, M., SCHREWE, A., FAVOR, J., KLOPSTOCK, T., BECKERS, J., IVANDIC, B., GAILUS-DURNER, V., FUCHS, H., HRABE DE ANGELIS, M., GRAW, J. & WURST, W. 2008. "Sighted C3H" mice--a tool for analysing the influence of vision on mouse behaviour? *Front Biosci,* 13**,** 5810-23.

HORI, K., KATAYAMA, N., KACHI, S., KONDO, M., KADOMATSU, K., USUKURA, J., MURAMATSU, T., MORI, S. & MIYAKE, Y. 2000. Retinal dysfunction in basigin deficiency. *Invest Ophthalmol Vis Sci,* 41**,** 3128-33.

HUDSPETH, A. J. 1989. How the ear's works work. *Nature,* 341**,** 397-404.

HUGHES, I., THALMANN, I., THALMANN, R. & ORNITZ, D. M. 2006. Mixing model systems: using zebrafish and mouse inner ear mutants and other organ systems to unravel the mystery of otoconial development. *Brain Res,* 1091**,** 58-74.

HUMES, L. E., GARNER, C. B., WILSON, D. L. & BARLOW, N. N. 2001. Hearing-aid outcome measured following one month of hearing aid use by the elderly. *J Speech Lang Hear Res,* 44**,** 469-86.

HWANG, J. H., WU, C. C., HSU, C. J., LIU, T. C. & YANG, W. S. 2009. Association of central obesity with the severity and audiometric configurations of age-related hearing impairment. *Obesity (Silver Spring),* 17**,** 1796-801.

IACONO, K. T., BROWN, A. L., GREENE, M. I. & SAOUAF, S. J. 2007. CD147 immunoglobulin superfamily receptor function and role in pathology. *Exp Mol Pathol,* 83**,** 283-95.

IGAKURA, T., KADOMATSU, K., KANAME, T., MURAMATSU, H., FAN, Q. W., MIYAUCHI, T., TOYAMA, Y., KUNO, N., YUASA, S., TAKAHASHI, M., SENDA, T., TAGUCHI, O., YAMAMURA, K., ARIMURA, K. & MURAMATSU, T. 1998. A null mutation in basigin, an immunoglobulin superfamily member, indicates its important roles in peri-implantation development and spermatogenesis. *Dev Biol,* 194**,** 152-65.

ISAACSON, J. E. & VORA, N. M. 2003. Differential diagnosis and treatment of hearing loss. *Am Fam Physician,* 68**,** 1125-32.

JACOBSON, S. G., CIDECIYAN, A. V., ALEMAN, T. S., SUMAROKA, A., ROMAN, A. J., GARDNER, L. M., PROSSER, H. M., MISHRA, M., BECH-HANSEN, N. T., HERRERA, W., SCHWARTZ, S. B., LIU, X. Z., KIMBERLING, W. J., STEEL, K. P. & WILLIAMS, D. S. 2008. Usher syndromes due to MYO7A, PCDH15, USH2A or GPR98 mutations share retinal disease mechanism. *Human Molecular Genetics,* 17**,** 2405-2415.

JAVITT, D. C. 2001. Management of negative symptoms of schizophrenia. *Curr Psychiatry Rep,* 3**,** 413-7.

JAWOREK, T. J., BHATTI, R., LATIEF, N., KHAN, S. N., RIAZUDDIN, S. & AHMED, Z. M. 2012. USH1K, a novel locus for type I Usher syndrome, maps to chromosome 10p11.21-q21.1. *J Hum Genet,* 57**,** 633-7.

JENTSCH, T. J. 2000. Neuronal KCNQ potassium channels: physiology and role in disease. *Nat Rev Neurosci,* 1**,** 21-30.

JERGER, S., JOHNSON, K. & LOISELLE, L. 1988. Pediatric central auditory dysfunction. Comparison of children with confirmed lesions versus suspected processing disorders. *Am J Otol,* 9 Suppl**,** 63-71.

JOENSUU, T., HAMALAINEN, R., YUAN, B., JOHNSON, C., TEGELBERG, S., GASPARINI, P., ZELANTE, L., PIRVOLA, U., PAKARINEN, L., LEHESJOKI, A. E., DE LA CHAPELLE, A. & SANKILA, E. M. 2001. Mutations in a novel gene with transmembrane domains underlie Usher syndrome type 3. *Am J Hum Genet,* 69**,** 673-84.

JOHNSON, K. R., LONGO-GUESS, C., GAGNON, L. H., YU, H. & ZHENG, Q. Y. 2008. A locus on distal chromosome 11 (ahl8) and its interaction with Cdh23 ahl underlie the early onset, age-related hearing loss of DBA/2J mice. *Genomics,* 92**,** 219-25.

JOHNSON, K. R., ZHENG, Q. Y. & ERWAY, L. C. 2000. A major gene affecting age-related hearing loss is common to at least ten inbred strains of mice. *Genomics,* 70**,** 171-80.

JOHNSON, S. L., WEDEMEYER, C., VETTER, D. E., ADACHI, R., HOLLEY, M. C., ELGOYHEN, A. B. & MARCOTTI, W. 2013. Cholinergic efferent synaptic transmission regulates the maturation of auditory hair cell ribbon synapses. *Open Biol,* 3**,** 130163.

JUSTICE, M. J., NOVEROSKE, J. K., WEBER, J. S., ZHENG, B. & BRADLEY, A. 1999. Mouse ENU mutagenesis. *Hum Mol Genet,* 8**,** 1955-63.

KALLBERG, M., WANG, H., WANG, S., PENG, J., WANG, Z., LU, H. & XU, J. 2012. Template-based protein structure modeling using the RaptorX web server. *Nat Protoc,* 7**,** 1511-22.

KHIMICH, D., NOUVIAN, R., PUJOL, R., TOM DIECK, S., EGNER, A., GUNDELFINGER, E. D. & MOSER, T. 2005. Hair cell synaptic ribbons are essential for synchronous auditory signalling. *Nature,* 434**,** 889-94.

KLEIN, J. O. 1994. Otitis media. *Clin Infect Dis,* 19**,** 823-33.

KREUTZ, M. R., LANGNAESE, K., DIETERICH, D. C., SEIDENBECHER, C. I., ZUSCHRATTER, W., BEESLEY, P. W. & GUNDELFINGER, E. D. 2001. Distribution of transcript and protein isoforms of the synaptic glycoprotein neuroplastin in rat retina. *Invest Ophthalmol Vis Sci,* 42**,** 1907-14.

KUHN, S., JOHNSON, S. L., FURNESS, D. N., CHEN, J., INGHAM, N., HILTON, J. M., STEFFES, G., LEWIS, M. A., ZAMPINI, V., HACKNEY, C. M., MASETTO, S., HOLLEY, M. C., STEEL, K. P. & MARCOTTI, W. 2011. miR-96 regulates the progression of differentiation in mammalian cochlear inner and outer hair cells. *Proc Natl Acad Sci U S A,* 108**,** 2355-60.

KUMAR, P., HENIKOFF, S. & NG, P. C. 2009. Predicting the effects of coding non-synonymous variants on protein function using the SIFT algorithm. *Nat Protoc,* 4**,** 1073-81.

LADAPO, J. A., NEUMANN, P. J., KEREN, R. & PROSSER, L. A. 2008. *NHS Newborn Hearing Screening Programme* [Online]. Available: http://www.nice.org.uk/guidance/ta166/resources/nhs-newborn-hearing-screening-program2 [Accessed 05/10/2014].

LAIN, E., CARNEJAC, S., ESCHER, P., WILSON, M. C., LOMO, T., GAJENDRAN, N. & BRENNER, H. R. 2009. A novel role for embigin to promote sprouting of motor nerve terminals at the neuromuscular junction. *J Biol Chem,* 284**,** 8930-9.

LANGNAESE, K., MUMMERY, R., GUNDELFINGER, E. D. & BEESLEY, P. W. 1998. Immunoglobulin superfamily members gp65 and gp55: tissue distribution of glycoforms. *FEBS Lett,* 429**,** 284-8.

LEMASURIER, M. & GILLESPIE, P. G. 2005. Hair-cell mechanotransduction and cochlear amplification. *Neuron,* 48**,** 403-15.

LENZI, D. & VON GERSDORFF, H. 2001. Structure suggests function: the case for synaptic ribbons as exocytotic nanomachines. *Bioessays,* 23**,** 831-40.

LIBERMAN, L. D., WANG, H. & LIBERMAN, M. C. 2011. Opposing gradients of ribbon size and AMPA receptor expression underlie sensitivity differences among cochlear-nerve/hair-cell synapses. *J Neurosci,* 31**,** 801-8.

LIBERMAN, M. C. 1982. The cochlear frequency map for the cat: labeling auditory-nerve fibers of known characteristic frequency. *J Acoust Soc Am,* 72**,** 1441-9.

LIBERMAN, M. C. & BEIL, D. G. 1979. Hair cell condition and auditory nerve response in normal and noise-damaged cochleas. *Acta Otolaryngol,* 88**,** 161-76.

LIM, D. J. 1986. Functional structure of the organ of Corti: a review. *Hear Res,* 22**,** 117-46.

LOCHER, H., DE GROOT, J. C., VAN IPEREN, L., HUISMAN, M. A., FRIJNS, J. H. & CHUVA DE SOUSA LOPES, S. M. 2014. Distribution and development of peripheral glial cells in the human fetal cochlea. *PLoS One,* 9**,** e88066.

LODISH, H. F. 2003. *Molecular cell biology,* New York, W.H. Freeman and Company.

MAGUPALLI, V. G., SCHWARZ, K., ALPADI, K., NATARAJAN, S., SEIGEL, G. M. & SCHMITZ, F. 2008. Multiple RIBEYE-RIBEYE interactions create a dynamic scaffold for the formation of synaptic ribbons. *J Neurosci,* 28**,** 7954-67.

MANOLIO, T. A. 2010. Genomewide association studies and assessment of the risk of disease. *N Engl J Med,* 363**,** 166-76.

MARCOTTI, W., JOHNSON, S. L., HOLLEY, M. C. & KROS, C. J. 2003. Developmental changes in the expression of potassium currents of embryonic, neonatal and mature mouse inner hair cells. *J Physiol,* 548**,** 383-400.

MARZBAN, H., KHANZADA, U., SHABIR, S., HAWKES, R., LANGNAESE, K., SMALLA, K. H., BOCKERS, T. M., GUNDELFINGER, E. D., GORDON-WEEKS, P. R. & BEESLEY, P. W. 2003. Expression of the immunoglobulin superfamily neuroplastin adhesion molecules in adult and developing mouse cerebellum and their localisation to parasagittal stripes. *J Comp Neurol,* 462**,** 286-301.

MATTHEWS, G. & FUCHS, P. 2010. The diverse roles of ribbon synapses in sensory neurotransmission. *Nat Rev Neurosci,* 11**,** 812-22.

MCDONALD, J. H. & DUNN, K. W. 2013. Statistical tests for measures of colocalization in biological microscopy. *J Microsc,* 252**,** 295-302.

MERCHANT, S. N., RAVICZ, M. E., PURIA, S., VOSS, S. E., WHITTEMORE, K. R., JR., PEAKE, W. T. & ROSOWSKI, J. J. 1997. Analysis of middle ear mechanics and application to diseased and reconstructed ears. *Am J Otol,* 18**,** 139-54.

MILLAN, J. M., ALLER, E., JAIJO, T., BLANCO-KELLY, F., GIMENEZ-PARDO, A. & AYUSO, C. 2011. An update on the genetics of usher syndrome. *J Ophthalmol,* 2011**,** 417217.

MOSER, T., NEEF, A. & KHIMICH, D. 2006. Mechanisms underlying the temporal precision of sound coding at the inner hair cell ribbon synapse. *J Physiol,* 576**,** 55-62.

MURAL, R. J., ADAMS, M. D., MYERS, E. W., SMITH, H. O., MIKLOS, G. L., WIDES, R., HALPERN, A., LI, P. W., SUTTON, G. G., NADEAU, J., SALZBERG, S. L., HOLT, R. A., KODIRA, C. D., LU, F., CHEN, L., DENG, Z., EVANGELISTA, C. C., GAN, W., HEIMAN, T. J., LI, J., LI, Z., MERKULOV, G. V., MILSHINA, N. V., NAIK, A. K., QI, R., SHUE, B. C., WANG, A., WANG, J., WANG, X., YAN, X., YE, J., YOOSEPH, S., ZHAO, Q., ZHENG, L., ZHU, S. C., BIDDICK, K., BOLANOS, R., DELCHER, A. L., DEW, I. M., FASULO, D., FLANIGAN, M. J., HUSON, D. H., KRAVITZ, S. A., MILLER, J. R., MOBARRY, C. M., REINERT, K., REMINGTON, K. A., ZHANG, Q., ZHENG, X. H., NUSSKERN, D. R., LAI, Z., LEI, Y., ZHONG, W., YAO, A., GUAN, P., JI, R. R., GU, Z., WANG, Z. Y., ZHONG, F., XIAO, C., CHIANG, C. C., YANDELL, M., WORTMAN, J. R., AMANATIDES, P. G., HLADUN, S. L., PRATTS, E. C., JOHNSON, J. E., DODSON, K. L., WOODFORD, K. J., EVANS, C. A., GROPMAN, B., RUSCH, D. B., VENTER, E., WANG, M., SMITH, T. J., HOUCK, J. T., TOMPKINS, D. E., HAYNES, C., JACOB, D., CHIN, S. H., ALLEN, D. R., DAHLKE, C. E., SANDERS, R., LI, K., LIU, X., LEVITSKY, A. A., MAJOROS, W. H., CHEN, Q., XIA, A. C., LOPEZ, J. R., DONNELLY, M. T., NEWMAN, M. H., GLODEK, A., KRAFT, C. L., NODELL, M., ALI, F., AN, H. J., BALDWIN-PITTS, D., BEESON, K. Y., CAI, S., et al. 2002. A comparison of whole-genome shotgun-derived mouse chromosome 16 and the human genome. *Science,* 296**,** 1661-71.

MURRAY, S. A., MORGAN, J. L., KANE, C., SHARMA, Y., HEFFNER, C. S., LAKE, J. & DONAHUE, L. R. 2010. Mouse gestation length is genetically determined. *PLoS One,* 5**,** e12418.

NEWMAN, C. W. & WEINSTEIN, B. E. 1988. The Hearing Handicap Inventory for the Elderly as a measure of hearing aid benefit. *Ear Hear,* 9**,** 81-5.

NIN, F., HIBINO, H., DOI, K., SUZUKI, T., HISA, Y. & KURACHI, Y. 2008. The endocochlear potential depends on two K+ diffusion potentials and an electrical barrier in the stria vascularis of the inner ear. *Proc Natl Acad Sci U S A,* 105**,** 1751-6.

NOUVIAN, R., BEUTNER, D., PARSONS, T. D. & MOSER, T. 2006. Structure and function of the hair cell ribbon synapse. *J Membr Biol,* 209**,** 153-65.

OCHRIETOR, J. D., MOROZ, T. M., KADOMATSU, K., MURAMATSU, T. & LINSER, P. J. 2001. Retinal degeneration following failed photoreceptor maturation in 5A11/basigin null mice. *Exp Eye Res,* 72**,** 467-77.

OCHRIETOR, J. D., MOROZ, T. P., CLAMP, M. F., TIMMERS, A. M., MURAMATSU, T. & LINSER, P. J. 2002. Inactivation of the Basigin gene impairs normal retinal development and maturation. *Vision Res,* 42**,** 447-53.

OHMEN, J., KANG, E. Y., LI, X., JOO, J. W., HORMOZDIARI, F., ZHENG, Q. Y., DAVIS, R. C., LUSIS, A. J., ESKIN, E. & FRIEDMAN, R. A. 2014. Genome-wide association study for age-related hearing loss (AHL) in the mouse: a meta-analysis. *J Assoc Res Otolaryngol,* 15**,** 335-52.

OTT, J., KAMATANI, Y. & LATHROP, M. 2011. Family-based designs for genome-wide association studies. *Nat Rev Genet,* 12**,** 465-74.

OUCHI, Y., KUBOTA, Y., KURAMASU, A., WATANABE, T. & ITO, C. 2005. Gene expression profiling in whole cerebral cortices of phencyclidine- or methamphetamine-treated rats. *Brain Res Mol Brain Res,* 140**,** 142-9.

OWCZAREK, S. & BEREZIN, V. 2012. Neuroplastin: cell adhesion molecule and signaling receptor. *Int J Biochem Cell Biol,* 44**,** 1-5.

OWCZAREK, S., KIRYUSHKO, D., LARSEN, M. H., KASTRUP, J. S., GAJHEDE, M., SANDI, C., BEREZIN, V., BOCK, E. & SOROKA, V. 2010. Neuroplastin-55 binds to and signals through the fibroblast growth factor receptor. *FASEB J,* 24**,** 1139-50.

OWCZAREK, S., SOROKA, V., KIRYUSHKO, D., LARSEN, M. H., YUAN, Q., SANDI, C., BEREZIN, V. & BOCK, E. 2011. Neuroplastin-65 and a mimetic peptide derived from its homophilic binding site modulate neuritogenesis and neuronal plasticity. *J Neurochem,* 117**,** 984-94.

PARADISE, J. L., BLUESTONE, C. D., COLBORN, D. K., BERNARD, B. S., SMITH, C. G., ROCKETTE, H. E. & KURS-LASKY, M. 1999. Adenoidectomy and adenotonsillectomy for recurrent acute otitis media: parallel randomized clinical trials in children not previously treated with tympanostomy tubes. *JAMA,* 282**,** 945-53.

PARKINSON, N., HARDISTY-HUGHES, R. E., TATEOSSIAN, H., TSAI, H. T., BROOKER, D., MORSE, S., LALANE, Z., MACKENZIE, F., FRAY, M., GLENISTER, P., WOODWARD, A. M., POLLEY, S., BARBARIC, I., DEAR, N., HOUGH, T. A., HUNTER, A. J., CHEESEMAN, M. T. & BROWN, S. D. 2006. Mutation at the Evi1 locus in Junbo mice causes susceptibility to otitis media. *PLoS Genet,* 2**,** e149.

PETIT, C. 2006. From deafness genes to hearing mechanisms: harmony and counterpoint. *Trends Mol Med,* 12**,** 57-64.

PFAFFL, M. W. 2001. A new mathematical model for relative quantification in real-time RT-PCR. *Nucleic Acids Research,* 29**,** e45.

POST, J. C., HILLER, N. L., NISTICO, L., STOODLEY, P. & EHRLICH, G. D. 2007. The role of biofilms in otolaryngologic infections: update 2007. *Curr Opin Otolaryngol Head Neck Surg,* 15**,** 347-51.

PROBST, F. J. & CAMPER, S. A. 1999. The role of mouse mutants in the identification of human hereditary hearing loss genes. *Hear Res,* 130**,** 1-6.

PUJOL, R., CARLIER, E. & LENOIR, M. 1980. Ontogenetic approach to inner and outer hair cell function. *Hear Res,* 2**,** 423-30.

PURVES, D. & WILLIAMS, S. M. 2001. Hair Cells and the Mechanoelectrical Transduction of Sound Waves. *Neuroscience.* 2nd ed. Sunderland, Mass.: Sinauer Associates.

QUWAILID, M. M., HUGILL, A., DEAR, N., VIZOR, L., WELLS, S., HORNER, E., FULLER, S., WEEDON, J., MCMATH, H., WOODMAN, P., EDWARDS, D., CAMPBELL, D., RODGER, S., CAREY, J., ROBERTS, A., GLENISTER, P., LALANNE, Z., PARKINSON, N., COGHILL, E. L., MCKEONE, R., COX, S., WILLAN, J., GREENFIELD, A., KEAYS, D., BRADY, S., SPURR, N., GRAY, I., HUNTER, J., BROWN, S. D. & COX, R. D. 2004. A gene-driven ENU-based approach to generating an allelic series in any gene. *Mamm Genome,* 15**,** 585-91.

RAJEWSKY, K., GU, H., KUHN, R., BETZ, U. A., MULLER, W., ROES, J. & SCHWENK, F. 1996. Conditional gene targeting. *J Clin Invest,* 98**,** 600-3.

RAPHAEL, Y. & ALTSCHULER, R. A. 2003. Structure and innervation of the cochlea. *Brain Res Bull,* 60**,** 397-422.

REHM, H. L. & MORTON, C. C. 1999. A new age in the genetics of deafness. *Genet Med,* 1**,** 295-302; quiz 303.

REICH, D. E., CARGILL, M., BOLK, S., IRELAND, J., SABETI, P. C., RICHTER, D. J., LAVERY, T., KOUYOUMJIAN, R., FARHADIAN, S. F., WARD, R. & LANDER, E. S. 2001. Linkage disequilibrium in the human genome. *Nature,* 411**,** 199-204.

RIAZUDDIN, S., BELYANTSEVA, I. A., GIESE, A. P., LEE, K., INDZHYKULIAN, A. A., NANDAMURI, S. P., YOUSAF, R., SINHA, G. P., LEE, S., TERRELL, D., HEGDE, R. S., ALI, R. A., ANWAR, S., ANDRADE-ELIZONDO, P. B., SIRMACI, A., PARISE, L. V., BASIT, S., WALI, A., AYUB, M., ANSAR, M.,

AHMAD, W., KHAN, S. N., AKRAM, J., TEKIN, M., COOK, T., BUSCHBECK, E. K., FROLENKOV, G. I., LEAL, S. M., FRIEDMAN, T. B. & AHMED, Z. M. 2012. Alterations of the CIB2 calcium- and integrin-binding protein cause Usher syndrome type 1J and nonsyndromic deafness DFNB48. *Nat Genet,* 44**,** 1265-71.

RODRIGUEZ-PINTO, D., SPARKOWSKI, J., KEOUGH, M. P., PHOENIX, K. N., VUMBACA, F., HAN, D. K., GUNDELFINGER, E. D., BEESLEY, P. & CLAFFEY, K. P. 2009. Identification of novel tumor antigens with patient-derived immune-selected antibodies. *Cancer Immunol Immunother,* 58**,** 221-34.

RYE, M. S., WARRINGTON, N. M., SCAMAN, E. S., VIJAYASEKARAN, S., COATES, H. L., ANDERSON, D., PENNELL, C. E., BLACKWELL, J. M. & JAMIESON, S. E. 2012. Genome-wide association study to identify the genetic determinants of otitis media susceptibility in childhood. *PLoS One,* 7**,** e48215.

SAFIEDDINE, S., EL-AMRAOUI, A. & PETIT, C. 2012. The auditory hair cell ribbon synapse: from assembly to function. *Annu Rev Neurosci,* 35**,** 509-28.

SAHLY, I., DUFOUR, E., SCHIETROMA, C., MICHEL, V., BAHLOUL, A., PERFETTINI, I., PEPERMANS, E., ESTIVALET, A., CARETTE, D., AGHAIE, A., EBERMANN, I., LELLI, A., IRIBARNE, M., HARDELIN, J. P., WEIL, D., SAHEL, J. A., EL-AMRAOUI, A. & PETIT, C. 2012. Localization of Usher 1 proteins to the photoreceptor calyceal processes, which are absent from mice. *J Cell Biol,* 199**,** 381-99.

SAITO, A., FUJIKURA-OUCHI, Y., KURAMASU, A., SHIMODA, K., AKIYAMA, K., MATSUOKA, H. & ITO, C. 2006. Association study of putative promoter polymorphisms in the neuroplastin gene and schizophrenia. *Neurosci Lett,* 411**,** 168-73.

SAMBROOK, J. & RUSSELL, D. W. 2001. *Molecular cloning : a laboratory manual,* Cold Spring Harbor, N.Y., Cold Spring Harbor Laboratory Press.

SCHEIBE, F. & HAUPT, H. 1985. Biochemical differences between perilymph, cerebrospinal fluid and blood plasma in the guinea pig. *Hear Res,* 17**,** 61-6.

SCHRAFF, S. A. 2008. Contemporary indications for ventilation tube placement. *Curr Opin Otolaryngol Head Neck Surg,* 16**,** 406-11.

SCHRODINGER, LLC 2010. The PyMOL Molecular Graphics System, Version 1.3r1.

SCHWANDER, M., KACHAR, B. & MULLER, U. 2010. Review series: The cell biology of hearing. *J Cell Biol,* 190**,** 9-20.

SCHWARZ, F. & AEBI, M. 2011. Mechanisms and principles of N-linked protein glycosylation. *Curr Opin Struct Biol,* 21**,** 576-82.

SCUDAMORE, C. L. C. 2014. *A Practical Guide to the Histology of the Mouse*, Wiley-Blackwell.

SHOTWELL, S. L., JACOBS, R. & HUDSPETH, A. J. 1981. Directional sensitivity of individual vertebrate hair cells to controlled deflection of their hair bundles. *Ann N Y Acad Sci,* 374**,** 1-10.

SILVER, L. M. 1995. *Mouse genetics : concepts and applications,* New York, Oxford University Press.

SINGER, J. H. & DIAMOND, J. S. 2006. Vesicle depletion and synaptic depression at a mammalian ribbon synapse. *J Neurophysiol,* 95**,** 3191-8.

SMALLA, K. H., MATTHIES, H., LANGNASE, K., SHABIR, S., BOCKERS, T. M., WYNEKEN, U., STAAK, S., KRUG, M., BEESLEY, P. W. & GUNDELFINGER, E. D. 2000. The synaptic glycoprotein neuroplastin is involved in long-term potentiation at hippocampal CA1 synapses. *Proc Natl Acad Sci U S A,* 97**,** 4327-32.

SMITH, R. J., BALE, J. F., JR. & WHITE, K. R. 2005. Sensorineural hearing loss in children. *Lancet,* 365**,** 879-90.

SPIDEN, S. L., BORTOLOZZI, M., DI LEVA, F., DE ANGELIS, M. H., FUCHS, H., LIM, D., ORTOLANO, S., INGHAM, N. J., BRINI, M., CARAFOLI, E., MAMMANO, F. & STEEL, K. P. 2008. The novel mouse mutation Oblivion inactivates the PMCA2 pump and causes progressive hearing loss. *PLoS Genet,* 4**,** e1000238.

STENFELT, S. 2006. Middle ear ossicles motion at hearing thresholds with air conduction and bone conduction stimulation. *J Acoust Soc Am,* 119**,** 2848-58.

STENFELT, S. & GOODE, R. L. 2005. Bone-conducted sound: physiological and clinical aspects. *Otol Neurotol,* 26**,** 1245-61.

STENFELT, S., PURIA, S., HATO, N. & GOODE, R. L. 2003. Basilar membrane and osseous spiral lamina motion in human cadavers with air and bone conduction stimuli. *Hear Res,* 181**,** 131-43.

TAKEUCHI, S., ANDO, M. & KAKIGI, A. 2000. Mechanism generating endocochlear potential: role played by intermediate cells in stria vascularis. *Biophys J,* 79**,** 2572-82.

TANNOUS, A., PISONI, G. B., HEBERT, D. N. & MOLINARI, M. 2014. N-linked sugar-regulated protein folding and quality control in the ER. *Semin Cell Dev Biol*.

THE-JACKSON-LABORATORY. 2014a. *Advantages of the Mouse as a Model Organism* [Online]. Available: http://research.jax.org/mousegenetics/advantages/advantages-of-mouse.html [Accessed 22/06/2014].

THE-JACKSON-LABORATORY. 2014b. *Mice Database: C3A.BLiA-Pde6b+/J* [Online]. Available: http://jaxmice.jax.org/strain/001912.html [Accessed 18th August 2014].

THE-TCS-COLLABORATION 1996. Positional cloning of a gene involved in the pathogenesis of Treacher Collins syndrome. The Treacher Collins Syndrome Collaborative Group. *Nat Genet,* 12**,** 130-6.

TORTORA, G. J. 1992. Principles of human anatomy. 6th ed. New York, NY: HarperCollins Publishers.

TORTORA, G. J. & GRABOWSKI, S. R. 1993. Principles of anatomy and physiology. 7th ed. New York: HarperCollinsCollege.

TWYMAN, R. 2003. *Linkage Analysis* [Online]. Available: http://genome.wellcome.ac.uk/doc_WTD020778.html [Accessed 3rd February 2015].

UHARI, M., MANTYSAARI, K. & NIEMELA, M. 1996. A meta-analytic review of the risk factors for acute otitis media. *Clin Infect Dis,* 22**,** 1079-83.

USUKURA, J. & YAMADA, E. 1987. Ultrastructure of the synaptic ribbons in photoreceptor cells of Rana catesbeiana revealed by freeze-etching and freeze-substitution. *Cell Tissue Res,* 247**,** 483-8.

VAHAVA, O., MORELL, R., LYNCH, E. D., WEISS, S., KAGAN, M. E., AHITUV, N., MORROW, J. E., LEE, M. K., SKVORAK, A. B., MORTON, C. C., BLUMENFELD, A., FRYDMAN, M., FRIEDMAN, T. B., KING, M. C. & AVRAHAM, K. B. 1998. Mutation in transcription factor POU4F3 associated with inherited progressive hearing loss in humans. *Science,* 279**,** 1950-4.

VAITHIANATHAN, T., AKMENTIN, W., HENRY, D. & MATTHEWS, G. 2013. The ribbon-associated protein C-terminal-binding protein 1 is not essential for the structure and function of retinal ribbon synapses. *Mol Vis,* 19**,** 917-26.

VAN CAMP, G. & SMITH, R. 2014. *Nonsyndromic Genes* [Online]. Available: http://hereditaryhearingloss.org [Accessed 10/07/2014 2014].

VAN DEN STEEN, P., RUDD, P. M., DWEK, R. A. & OPDENAKKER, G. 1998. Concepts and principles of O-linked glycosylation. *Crit Rev Biochem Mol Biol,* 33**,** 151-208.

VAN LAER, L., VAN EYKEN, E., FRANSEN, E., HUYGHE, J. R., TOPSAKAL, V., HENDRICKX, J. J., HANNULA, S., MAKI-TORKKO, E., JENSEN, M., DEMEESTER, K., BAUR, M., BONACONSA, A., MAZZOLI, M., ESPESO, A., VERBRUGGEN, K., HUYGHE, J., HUYGEN, P., KUNST, S., MANNINEN, M., KONINGS, A., DIAZ-LACAVA, A. N., STEFFENS, M., WIENKER, T. F., PYYKKO, I., CREMERS, C. W., KREMER, H., DHOOGE, I., STEPHENS, D., ORZAN, E., PFISTER, M., BILLE, M., PARVING, A., SORRI, M., VAN DE HEYNING, P. H. & VAN CAMP, G. 2008. The grainyhead like 2 gene (GRHL2), alias TFCP2L3, is associated with age-related hearing impairment. *Hum Mol Genet,* 17**,** 159-69.

VESKE, A., OEHLMANN, R., YOUNUS, F., MOHYUDDIN, A., MULLER-MYHSOK, B., MEHDI, S. Q. & GAL, A. 1996. Autosomal recessive non-syndromic deafness locus (DFNB8) maps on chromosome 21q22 in a large consanguineous kindred from Pakistan. *Hum Mol Genet,* 5**,** 165-8.

VOGEL, C. & MARCOTTE, E. M. 2012. Insights into the regulation of protein abundance from proteomic and transcriptomic analyses. *Nature Reviews Genetics,* 13**,** 227-232.

VON GERSDORFF, H., VARDI, E., MATTHEWS, G. & STERLING, P. 1996. Evidence that vesicles on the synaptic ribbon of retinal bipolar neurons can be rapidly released. *Neuron,* 16**,** 1221-7.

VOSSEN, R. H., ATEN, E., ROOS, A. & DEN DUNNEN, J. T. 2009. High-resolution melting analysis (HRMA): more than just sequence variant screening. *Hum Mutat,* 30**,** 860-6.

WADE, C. M. & DALY, M. J. 2005. Genetic variation in laboratory mice. *Nat Genet,* 37**,** 1175-80.

WALSH, M. K. & LICHTMAN, J. W. 2003. In vivo time-lapse imaging of synaptic takeover associated with naturally occurring synapse elimination. *Neuron,* 37**,** 67-73.

WILLIAMS, D. S. 2008. Usher syndrome: animal models, retinal function of Usher proteins, and prospects for gene therapy. *Vision Res,* 48**,** 433-41.

WILSON, M. C., KRAUS, M., MARZBAN, H., SARNA, J. R., WANG, Y., HAWKES, R., HALESTRAP, A. P. & BEESLEY, P. W. 2013. The Neuroplastin Adhesion Molecules Are Accessory Proteins That Chaperone the Monocarboxylate Transporter MCT2 to the Neuronal Cell Surface. *PLoS One,* 8**,** e78654.

YOON, Y. S., YOON, Y. J. & LEE, E. J. 2014. Incidentally detected middle ear osteoma: two cases reports and literature review. *Am J Otolaryngol,* 35**,** 524-8.

ZDEBIK, A. A. 2009. Statins and fibrate target ClC-1 - from side effects to CLC pharmacology. *Br J Pharmacol,* 156**,** 1204-5.

ZHAI, R. G. & BELLEN, H. J. 2004. The architecture of the active zone in the presynaptic nerve terminal. *Physiology (Bethesda),* 19**,** 262-70.

ZHENG, Q. Y., DING, D., YU, H., SALVI, R. J. & JOHNSON, K. R. 2009. A locus on distal chromosome 10 (ahl4) affecting age-related hearing loss in A/J mice. *Neurobiol Aging,* 30**,** 1693-705.

S1. Raw click box data from G3 pedigrees aged 7 – 8 weeks

Mouse ID	Sex	DOB	Date tested	Age at Test	Startle response (0,1 or 2)
PEDV/66.1a	F	22-Aug-07	10-Oct-07	49	2
PEDV/66.1b	F	22-Aug-07	10-Oct-07	49	2
PEDV/66.1c	F	22-Aug-07	10-Oct-07	49	2
PEDV/66.1d	F	22-Aug-07	10-Oct-07	49	2
PEDV/66.1e	F	22-Aug-07	10-Oct-07	49	2
PEDV/66.1f	F	22-Aug-07	10-Oct-07	49	0.5
PEDV/66.1g	F	22-Aug-07	10-Oct-07	49	2
PEDV/66.1h	F	22-Aug-07	10-Oct-07	49	2
PEDV/66.1i	F	22-Aug-07	10-Oct-07	49	2
PEDV/66.1j	M	22-Aug-07	10-Oct-07	49	0.5
PEDV/66.1k	M	22-Aug-07	10-Oct-07	49	2
PEDV/66.1l	M	22-Aug-07	10-Oct-07	49	2
PEDV/66.1m	M	22-Aug-07	10-Oct-07	49	0.5
PEDV/66.1n	M	22-Aug-07	10-Oct-07	49	2
PEDV/66.1o	M	22-Aug-07	10-Oct-07	49	2
PEDV/66.1p	M	22-Aug-07	10-Oct-07	49	2
PEDV/66.2a	F	14-Sep-07	01-Nov-07	48	0.5
PEDV/66.2b	F	14-Sep-07	01-Nov-07	48	2
PEDV/66.2c	F	14-Sep-07	01-Nov-07	48	2
PEDV/66.2d	M	14-Sep-07	01-Nov-07	48	2
PEDV/66.2e	M	14-Sep-07	01-Nov-07	48	2
PEDV/66.2f	M	14-Sep-07	01-Nov-07	48	2
PEDV/66.3a	F	16-Sep-07	01-Nov-07	46	2
PEDV/66.3b	F	16-Sep-07	01-Nov-07	46	2
PEDV/66.3c	F	16-Sep-07	01-Nov-07	46	2
PEDV/66.3d	M	16-Sep-07	01-Nov-07	46	2
PEDV/66.3e	M	16-Sep-07	01-Nov-07	46	2
PEDV/66.3f	M	16-Sep-07	01-Nov-07	46	2
PEDV/66.3g	M	16-Sep-07	01-Nov-07	46	0.5
PEDV/66.3h	M	16-Sep-07	01-Nov-07	46	2
PEDV/66.3i	M	16-Sep-07	01-Nov-07	46	2
PEDV/66.4a	F	08-Oct-07	28-Nov-07	51	2
PEDV/66.4b	F	08-Oct-07	28-Nov-07	51	2
PEDV/66.4c	F	08-Oct-07	28-Nov-07	51	2
PEDV/66.4d	F	08-Oct-07	28-Nov-07	51	2
PEDV/66.4e	F	08-Oct-07	28-Nov-07	51	2
PEDV/66.4f	M	08-Oct-07	28-Nov-07	51	1
PEDV/66.4g	M	08-Oct-07	28-Nov-07	51	2
PEDV/66.4h	M	08-Oct-07	28-Nov-07	51	2
PEDV/66.4i	M	08-Oct-07	28-Nov-07	51	2
PEDV/66.4j	M	08-Oct-07	28-Nov-07	51	2
PEDV/66.5a	F	09-Oct-07	28-Nov-07	50	2
PEDV/66.5b	F	09-Oct-07	28-Nov-07	50	2
PEDV/66.5c	F	09-Oct-07	28-Nov-07	50	2
PEDV/66.5d	F	09-Oct-07	28-Nov-07	50	2
PEDV/66.5e	M	09-Oct-07	28-Nov-07	50	2
PEDV/66.5f	M	09-Oct-07	28-Nov-07	50	2
PEDV/66.5g	M	09-Oct-07	28-Nov-07	50	1
PEDV/66.5h	M	09-Oct-07	28-Nov-07	50	2
PEDV/66.6a	F	31-Oct-07	20-Dec-07	50	2
PEDV/66.6b	F	31-Oct-07	20-Dec-07	50	2
PEDV/66.6c	F	31-Oct-07	20-Dec-07	50	2
PEDV/66.6d	F	31-Oct-07	20-Dec-07	50	0.5
PEDV/66.6e	F	31-Oct-07	20-Dec-07	50	2
PEDV/66.6f	M	31-Oct-07	20-Dec-07	50	2
PEDV/66.6g	M	31-Oct-07	20-Dec-07	50	2
PEDV/66.6h	M	31-Oct-07	20-Dec-07	50	2
PEDV/66.7a	F	02-Nov-07	20-Dec-07	48	2
PEDV/66.7b	F	02-Nov-07	20-Dec-07	48	0.5
PEDV/66.7c	F	02-Nov-07	20-Dec-07	48	0.5
PEDV/66.4j	M	08-Oct-07	28-Nov-07	51	2
PEDV/66.5a	F	09-Oct-07	28-Nov-07	50	2
PEDV/66.5b	F	09-Oct-07	28-Nov-07	50	2
PEDV/66.5c	F	09-Oct-07	28-Nov-07	50	2
PEDV/66.5d	F	09-Oct-07	28-Nov-07	50	2
PEDV/66.5e	M	09-Oct-07	28-Nov-07	50	2
PEDV/66.5f	M	09-Oct-07	28-Nov-07	50	2
PEDV/66.5g	M	09-Oct-07	28-Nov-07	50	1
PEDV/66.5h	M	09-Oct-07	28-Nov-07	50	2
PEDV/66.6a	F	31-Oct-07	20-Dec-07	50	2
PEDV/66.6b	F	31-Oct-07	20-Dec-07	50	2
PEDV/66.6c	F	31-Oct-07	20-Dec-07	50	2
PEDV/66.6d	F	31-Oct-07	20-Dec-07	50	0.5
PEDV/66.6e	F	31-Oct-07	20-Dec-07	50	2
PEDV/66.6f	M	31-Oct-07	20-Dec-07	50	2
PEDV/66.6g	M	31-Oct-07	20-Dec-07	50	2
PEDV/66.6h	M	31-Oct-07	20-Dec-07	50	2
PEDV/66.7a	F	02-Nov-07	20-Dec-07	48	2
PEDV/66.7b	F	02-Nov-07	20-Dec-07	48	0.5
PEDV/66.7c	F	02-Nov-07	20-Dec-07	48	0.5
PEDV/66.7d	F	02-Nov-07	20-Dec-07	48	2
PEDV/66.7e	F	02-Nov-07	20-Dec-07	48	2
PEDV/66.7f	F	02-Nov-07	20-Dec-07	48	2
PEDV/66.7g	F	02-Nov-07	20-Dec-07	48	2
PEDV/66.7h	F	02-Nov-07	20-Dec-07	48	1
PEDV/66.7i	M	02-Nov-07	20-Dec-07	48	2
PEDV/66.7j	M	02-Nov-07	20-Dec-07	48	2
PEDV/66.7k	M	02-Nov-07	20-Dec-07	48	1
PEDV/66.8a	F	24-Nov-07	10-Jan-08	47	2
PEDV/66.8b	F	24-Nov-07	10-Jan-08	47	2
PEDV/66.8c	F	24-Nov-07	10-Jan-08	47	2
PEDV/66.9a	F	26-Nov-07	17-Jan-08	52	2
PEDV/66.9b	F	26-Nov-07	17-Jan-08	52	2
PEDV/66.9c	F	26-Nov-07	17-Jan-08	52	2
PEDV/66.9d	F	26-Nov-07	17-Jan-08	52	2
PEDV/66.9e	F	26-Nov-07	17-Jan-08	52	0.5
PEDV/66.9f	F	26-Nov-07	17-Jan-08	52	0.5
PEDV/66.9g	F	26-Nov-07	17-Jan-08	52	0.5
PEDV/66.9h	M	26-Nov-07	17-Jan-08	52	0.5
PEDV/66.9i	M	26-Nov-07	17-Jan-08	52	2
PEDV/66.9j	M	26-Nov-07	17-Jan-08	52	2
PEDV/66.9k	M	26-Nov-07	17-Jan-08	52	2
PEDV/66.10a	F	03-Jan-08	18-Feb-08	46	2
PEDV/66.10b	M	03-Jan-08	18-Feb-08	46	2
PEDV/66.10c	M	03-Jan-08	18-Feb-08	46	2
PEDV/66.10d	M	03-Jan-08	18-Feb-08	46	2
PEDV/66.11a	M	08-Jan-08	28-Feb-08	51	2
PEDV/66.11b	M	08-Jan-08	28-Feb-08	51	2
PEDV/66.11d	F	08-Jan-08	28-Feb-08	51	0.5
PEDV/66.11e	F	08-Jan-08	28-Feb-08	51	2
PEDV/66.11f	F	08-Jan-08	28-Feb-08	51	0.5

S2. Raw click box data from G5 pedigrees

Mouse ID	Sex	DOB	Date tested	Age at Test	Startle response
					0,1 or 2
PITCH/1.1a	F	02-Jul-08	23-Jul-08	21	2
PITCH/1.1b	F	02-Jul-08	23-Jul-08	21	2
PITCH/1.1c	F	02-Jul-08	23-Jul-08	21	2
PITCH/1.1d	F	02-Jul-08	23-Jul-08	21	2
PITCH/1.1e	F	02-Jul-08	23-Jul-08	21	0
PITCH/1.1f	M	02-Jul-08	23-Jul-08	21	0
PITCH/1.1g	M	02-Jul-08	23-Jul-08	21	2
PITCH/1.1h	M	02-Jul-08	23-Jul-08	21	2
PITCH/2.1a	F	02-Jul-08	24-Jul-08	22	2
PITCH/2.1b	F	02-Jul-08	24-Jul-08	22	0
PITCH/2.1c	F	02-Jul-08	24-Jul-08	22	2
PITCH/2.1d	F	02-Jul-08	24-Jul-08	22	0
PITCH/2.1e	F	02-Jul-08	24-Jul-08	22	2
PITCH/2.1f	F	02-Jul-08	23-Jul-08	21	2
PITCH/2.1g	F	02-Jul-08	23-Jul-08	21	2
PITCH/2.1h	F	02-Jul-08	23-Jul-08	21	2
PITCH/2.1i	M	02-Jul-08	23-Jul-08	21	2
PITCH/2.1j	M	02-Jul-08	23-Jul-08	21	0
PITCH/2.1k	M	02-Jul-08	23-Jul-08	21	2
PITCH/2.1l	M	02-Jul-08	23-Jul-08	21	2
PITCH/2.1m	M	02-Jul-08	23-Jul-08	21	2
PITCH/2.1n	M	02-Jul-08	23-Jul-08	21	2
PITCH/2.1o	M	02-Jul-08	23-Jul-08	21	1
PITCH/2.1p	M	02-Jul-08	23-Jul-08	21	0
PITCH/2.1q	M	02-Jul-08	23-Jul-08	21	2
PITCH/2.1r	M	02-Jul-08	23-Jul-08	21	2
PITCH/1.2a	F	04-Jul-08	23-Jul-08	19	2
PITCH/1.2b	F	04-Jul-08	24-Jul-08	20	2
PITCH/1.2c	F	04-Jul-08	24-Jul-08	20	2
PITCH/1.2d	F	04-Jul-08	24-Jul-08	20	0
PITCH/1.2e	F	04-Jul-08	24-Jul-08	20	2
PITCH/1.2f	F	04-Jul-08	24-Jul-08	20	2
PITCH/1.2g	F	04-Jul-08	24-Jul-08	20	2
PITCH/1.2h	M	04-Jul-08	23-Jul-08	19	2
PITCH/1.2i	M	04-Jul-08	23-Jul-08	19	2
PITCH/3.1a	F	04-Jul-08	23-Jul-08	19	2
PITCH/3.1b	F	04-Jul-08	23-Jul-08	19	2
PITCH/3.1c	F	04-Jul-08	23-Jul-08	19	2

Mouse ID	Sex	DOB	Date tested	Age at Test	Startle response
					0,1 or 2
PITCH/3.1d	F	04-Jul-08	23-Jul-08	19	2
PITCH/3.1e	M	04-Jul-08	23-Jul-08	19	2
PITCH/3.1f	M	04-Jul-08	23-Jul-08	19	0
PITCH/3.1g	M	04-Jul-08	23-Jul-08	19	2
PITCH/3.1h	M	04-Jul-08	23-Jul-08	19	2
PITCH/3.1i	M	04-Jul-08	23-Jul-08	19	2
PITCH/3.1j	M	04-Jul-08	23-Jul-08	19	0
PITCH/3.1k	M	04-Jul-08	23-Jul-08	19	2
PITCH/3.1l	M	04-Jul-08	23-Jul-08	19	0
PITCH/4.1a	F	05-Jul-08	24-Jul-08	19	2
PITCH/4.1b	M	05-Jul-08	24-Jul-08	19	2
PITCH/4.1c	M	05-Jul-08	24-Jul-08	19	2
PITCH/4.1d	M	05-Jul-08	24-Jul-08	19	2
PITCH/4.1e	M	05-Jul-08	24-Jul-08	19	2
PITCH/4.1f	M	05-Jul-08	24-Jul-08	19	2
PITCH/4.1g	M	05-Jul-08	24-Jul-08	19	2
PITCH/4.1h	M	05-Jul-08	24-Jul-08	19	2
PITCH/4.1i	M	05-Jul-08	24-Jul-08	19	2
PITCH/4.1j	M	05-Jul-08	24-Jul-08	19	2
PITCH/4.2a	F	17-Jul-08	07-Aug-08	21	2
PITCH/4.2b	F	17-Jul-08	07-Aug-08	21	2
PITCH/4.2c	F	17-Jul-08	07-Aug-08	21	2
PITCH/4.2d	F	17-Jul-08	07-Aug-08	21	2
PITCH/4.2e	F	17-Jul-08	07-Aug-08	21	2
PITCH/4.2f	F	17-Jul-08	07-Aug-08	21	2
PITCH/3.2a	F	23-Jul-08	21-Aug-08	29	2
PITCH/3.2b	F	23-Jul-08	21-Aug-08	29	2
PITCH/3.2c	F	23-Jul-08	21-Aug-08	29	2
PITCH/3.2d	M	23-Jul-08	21-Aug-08	29	2
PITCH/3.2e	M	23-Jul-08	21-Aug-08	29	0
PITCH/3.2f	M	23-Jul-08	21-Aug-08	29	2
PITCH/3.2g	M	23-Jul-08	21-Aug-08	29	0
PITCH/3.2h	M	23-Jul-08	21-Aug-08	29	2
PITCH/1.3a	F	25-Jul-08	21-Aug-08	27	2
PITCH/1.3b	F	25-Jul-08	21-Aug-08	27	2
PITCH/1.3c	F	25-Jul-08	21-Aug-08	27	2
PITCH/1.3d	F	25-Jul-08	21-Aug-08	27	0
PITCH/1.3e	F	25-Jul-08	21-Aug-08	27	2

Mouse ID	Sex	DOB	Date tested	Age at Test	Startle response
					0,1 or 2
PITCH/1.3f	F	25-Jul-08	21-Aug-08	27	2
PITCH/1.3g	F	25-Jul-08	21-Aug-08	27	2
PITCH/1.3h	F	25-Jul-08	21-Aug-08	27	2
PITCH/1.3i	M	25-Jul-08	21-Aug-08	27	2
PITCH/1.3j	M	25-Jul-08	21-Aug-08	27	2
PITCH/1.3k	M	25-Jul-08	21-Aug-08	27	2
PITCH/1.3l	M	25-Jul-08	21-Aug-08	27	2
PITCH/1.3m	M	25-Jul-08	21-Aug-08	27	2
PITCH/1.3n	M	25-Jul-08	21-Aug-08	27	2
PITCH/1.3o	M	25-Jul-08	21-Aug-08	27	0
PITCH/1.3p	M	25-Jul-08	21-Aug-08	27	2
PITCH/2.2a	F	27-Jul-08	21-Aug-08	25	0
PITCH/2.2b	F	27-Jul-08	21-Aug-08	25	0
PITCH/2.2c	F	27-Jul-08	21-Aug-08	25	2
PITCH/2.2d	F	27-Jul-08	21-Aug-08	25	2
PITCH/2.2e	F	27-Jul-08	21-Aug-08	25	2
PITCH/2.2f	M	27-Jul-08	21-Aug-08	25	2
PITCH/2.2g	M	27-Jul-08	21-Aug-08	25	2
PITCH/4.3a	F	30-Jul-08	21-Aug-08	22	0
PITCH/4.3b	F	30-Jul-08	21-Aug-08	22	2
PITCH/4.3c	M	30-Jul-08	21-Aug-08	22	2
PITCH/4.3d	M	30-Jul-08	21-Aug-08	22	2
PITCH/2.3a	F	31-Jul-08	21-Aug-08	21	2
PITCH/2.3b	F	31-Jul-08	21-Aug-08	21	2
PITCH/2.3c	F	31-Jul-08	21-Aug-08	21	2
PITCH/2.3d	M	31-Jul-08	21-Aug-08	21	0
PITCH/2.3e	M	31-Jul-08	21-Aug-08	21	2
PITCH/2.3f	M	31-Jul-08	21-Aug-08	21	0
PITCH/2.3g	M	31-Jul-08	21-Aug-08	21	2
PITCH/2.3h	M	31-Jul-08	21-Aug-08	21	2
PITCH/5.1a	F	05-Aug-08	28-Aug-08	23	2
PITCH/5.1b	M	05-Aug-08	28-Aug-08	23	2
PITCH/4.4a	F	06-Aug-08	28-Aug-08	22	2
PITCH/4.4b	F	06-Aug-08	28-Aug-08	22	2
PITCH/4.4c	F	06-Aug-08	28-Aug-08	22	2
PITCH/4.4d	F	06-Aug-08	28-Aug-08	22	2
PITCH/4.4e	F	06-Aug-08	28-Aug-08	22	2
PITCH/4.4f	F	06-Aug-08	28-Aug-08	22	2

Mouse ID	Sex	DOB	Date tested	Age at Test	Startle response
					0,1 or 2
PITCH/4.4g	M	06-Aug-08	28-Aug-08	22	2
PITCH/4.4h	M	06-Aug-08	28-Aug-08	22	2
PITCH/4.4i	M	06-Aug-08	28-Aug-08	22	0
PITCH/6.1a	F	06-Aug-08	28-Aug-08	22	0
PITCH/6.1b	M	06-Aug-08	28-Aug-08	22	2
PITCH/6.2a	F	11-Aug-08	04-Sep-08	24	0
PITCH/6.2b	F	11-Aug-08	04-Sep-08	24	2
PITCH/6.2c	M	11-Aug-08	04-Sep-08	24	2
PITCH/6.2d	M	11-Aug-08	04-Sep-08	24	2
PITCH/5.2a	F	12-Aug-08	04-Sep-08	23	2
PITCH/5.2b	F	12-Aug-08	04-Sep-08	23	2
PITCH/5.2c	F	12-Aug-08	04-Sep-08	23	0
PITCH/5.2d	M	12-Aug-08	04-Sep-08	23	2
PITCH/5.2e	M	12-Aug-08	04-Sep-08	23	2
PITCH/5.2f	M	12-Aug-08	04-Sep-08	23	2
PITCH/5.2g	M	12-Aug-08	04-Sep-08	23	2
PITCH/5.2h	M	12-Aug-08	04-Sep-08	23	0
PITCH/5.2i	M	12-Aug-08	04-Sep-08	23	2
PITCH/1.5a	F	21-Aug-08	18-Sep-08	28	0
PITCH/1.5b	F	21-Aug-08	18-Sep-08	28	0
PITCH/1.5c	F	21-Aug-08	18-Sep-08	28	0
PITCH/1.5d	F	21-Aug-08	18-Sep-08	28	2
PITCH/1.5e	F	21-Aug-08	18-Sep-08	28	2
PITCH/1.5f	F	21-Aug-08	18-Sep-08	28	0
PITCH/1.5g	M	21-Aug-08	25-Sep-08	35	0
PITCH/1.5h	M	21-Aug-08	25-Sep-08	35	0
PITCH/1.5i	M	21-Aug-08	25-Sep-08	35	0
PITCH/1.5j	M	21-Aug-08	25-Sep-08	35	2
PITCH/2.5a	F	26-Aug-08	18-Sep-08	23	0
PITCH/2.5b	F	26-Aug-08	18-Sep-08	23	2
PITCH/2.5c	F	26-Aug-08	18-Sep-08	23	2
PITCH/2.5d	F	26-Aug-08	18-Sep-08	23	2
PITCH/2.5e	F	26-Aug-08	18-Sep-08	23	2
PITCH/2.5f	F	26-Aug-08	18-Sep-08	23	2
PITCH/2.5g	F	26-Aug-08	18-Sep-08	23	2
PITCH/2.5h	M	26-Aug-08	18-Sep-08	23	0
PITCH/2.5i	M	26-Aug-08	18-Sep-08	23	0
PITCH/2.5j	M	26-Aug-08	18-Sep-08	23	0

Mouse ID	Sex	DOB	Date tested	Age at Test	Startle response 0,1 or 2
PITCH/3.5a	F	31-Aug-08	18-Sep-08	18	2
PITCH/3.5b	F	31-Aug-08	18-Sep-08	18	2
PITCH/3.5c	F	31-Aug-08	18-Sep-08	18	2
PITCH/3.5d	M	31-Aug-08	18-Sep-08	18	0
PITCH/3.5e	M	31-Aug-08	18-Sep-08	18	2
PITCH/3.5f	M	31-Aug-08	18-Sep-08	18	2
PITCH/3.5g	M	31-Aug-08	18-Sep-08	18	2
PITCH/3.6a	F	04-Sep-08	25-Sep-08	21	0.5
PITCH/3.6b	F	04-Sep-08	25-Sep-08	21	0
PITCH/3.6c	F	04-Sep-08	25-Sep-08	21	2
PITCH/3.6d	F	04-Sep-08	25-Sep-08	21	2
PITCH/3.6e	F	04-Sep-08	25-Sep-08	21	2
PITCH/3.6f	M	04-Sep-08	25-Sep-08	21	2
PITCH/3.6g	M	04-Sep-08	25-Sep-08	21	2
PITCH/3.6h	M	04-Sep-08	25-Sep-08	21	2
PITCH/3.6i	M	04-Sep-08	25-Sep-08	21	2
PITCH/6.3a	F	08-Sep-08	02-Oct-08	24	2
PITCH/6.3c	M	08-Sep-08	02-Oct-08	24	0
PITCH/6.3d	M	08-Sep-08	02-Oct-08	24	2
PITCH/4.7a	F	11-Sep-08	02-Oct-08	21	2
PITCH/4.7b	M	11-Sep-08	02-Oct-08	21	0
PITCH/4.7c	M	11-Sep-08	02-Oct-08	21	2
PITCH/4.7d	M	11-Sep-08	02-Oct-08	21	1
PITCH/1.6a	F	11-Sep-08	02-Oct-08	21	2
PITCH/1.6b	F	11-Sep-08	02-Oct-08	21	2
PITCH/1.6c	F	11-Sep-08	02-Oct-08	21	2
PITCH/1.6d	F	11-Sep-08	02-Oct-08	21	2
PITCH/1.6e	M	11-Sep-08	02-Oct-08	21	0
PITCH/1.6f	M	11-Sep-08	02-Oct-08	21	0
PITCH/1.6g	M	11-Sep-08	02-Oct-08	21	0
PITCH/1.6h	M	11-Sep-08	02-Oct-08	21	2
PITCH/1.6i	M	11-Sep-08	02-Oct-08	21	2
PITCH/1.6j	M	11-Sep-08	02-Oct-08	21	2
PITCH/1.6k	M	11-Sep-08	02-Oct-08	21	2
PITCH/6.4a	F	16-Sep-08	10-Oct-08	24	2
PITCH/6.4b	M	16-Sep-08	10-Oct-08	24	2
PITCH/6.4c	M	16-Sep-08	10-Oct-08	24	2
PITCH/6.4d	M	16-Sep-08	10-Oct-08	24	2
PITCH/6.4e	M	16-Sep-08	10-Oct-08	24	2
PITCH/5.3a	F	16-Sep-08	03-Nov-08	48	0
PITCH/5.3b	F	16-Sep-08	03-Nov-08	48	2
PITCH/5.3c	F	16-Sep-08	03-Nov-08	48	2
PITCH/5.3d	F	16-Sep-08	03-Nov-08	48	2
PITCH/5.3e	F	16-Sep-08	03-Nov-08	48	2
PITCH/5.3f	F	16-Sep-08	10-Oct-08	24	2
PITCH/5.3g	F	16-Sep-08	10-Oct-08	24	2
PITCH/5.3h	M	16-Sep-08	10-Oct-08	24	1
PITCH/5.3i	M	16-Sep-08	10-Oct-08	24	2
PITCH/5.3j	M	16-Sep-08	10-Oct-08	24	2
PITCH/5.3l	M	16-Sep-08	10-Oct-08	24	1
PITCH/5.4a	M	22-Sep-08	15-Oct-08	23	2
PITCH/5.4b	M	22-Sep-08	15-Oct-08	23	2
PITCH/5.4c	M	22-Sep-08	15-Oct-08	23	2
PITCH/5.4d	M	22-Sep-08	15-Oct-08	23	2
PITCH/5.4e	M	22-Sep-08	15-Oct-08	23	2
PITCH/5.4f	M	22-Sep-08	15-Oct-08	23	2
PITCH/6.5a	F	28-Sep-08	03-Nov-08	36	2
PITCH/6.5b	M	28-Sep-08	28-Oct-08	30	2
PITCH/6.6a	M	05-Oct-08	28-Oct-08	23	2
PITCH/6.6b	M	05-Oct-08	28-Oct-08	23	2
PITCH/6.6c	M	05-Oct-08	28-Oct-08	23	2
PITCH/6.6d	M	05-Oct-08	28-Oct-08	23	2
PITCH/5.5a	F	07-Oct-08	28-Oct-08	21	2
PITCH/5.5b	F	07-Oct-08	28-Oct-08	21	2
PITCH/5.5c	M	07-Oct-08	28-Oct-08	21	2
PITCH/5.5d	M	07-Oct-08	28-Oct-08	21	0
PITCH/5.6a	F	28-Oct-08	20-Nov-08	23	2
PITCH/5.6b	F	28-Oct-08	20-Nov-08	23	2
PITCH/5.6c	F	28-Oct-08	20-Nov-08	23	2
PITCH/5.6d	F	28-Oct-08	20-Nov-08	23	2
PITCH/5.6e	F	28-Oct-08	20-Nov-08	23	2
PITCH/5.6f	F	28-Oct-08	20-Nov-08	23	2
PITCH/5.6g	F	28-Oct-08	20-Nov-08	23	2
PITCH/5.6h	F	28-Oct-08	20-Nov-08	23	2
PITCH/5.6i	M	28-Oct-08	20-Nov-08	23	2
PITCH/5.6j	M	28-Oct-08	20-Nov-08	23	2
PITCH/5.6k	M	28-Oct-08	20-Nov-08	23	2
PITCH/5.6l	M	28-Oct-08	20-Nov-08	23	2
PITCH/5.6m	M	28-Oct-08	20-Nov-08	23	0
PITCH/5.6n	M	28-Oct-08	20-Nov-08	23	2
PITCH/5.6o	M	28-Oct-08	20-Nov-08	23	1
PITCH/5.6p	M	28-Oct-08	20-Nov-08	23	1
PITCH/5.6q	M	28-Oct-08	20-Nov-08	23	0
PITCH/6.7a	F	05-Nov-08	26-Nov-08	21	0
PITCH/6.7b	F	05-Nov-08	26-Nov-08	21	2
PITCH/6.7c	F	05-Nov-08	26-Nov-08	21	2
PITCH/6.7d	F	05-Nov-08	26-Nov-08	21	2
PITCH/6.7e	F	05-Nov-08	26-Nov-08	21	2
PITCH/6.7f	M	05-Nov-08	26-Nov-08	21	0
PITCH/6.7g	M	05-Nov-08	26-Nov-08	21	2
PITCH/6.7h	M	05-Nov-08	26-Nov-08	21	2
PITCH/6.7i	M	05-Nov-08	26-Nov-08	21	2
PITCH/6.7j	M	05-Nov-08	26-Nov-08	21	2
PITCH/6.8a	F	09-Nov-08	11-Dec-08	32	2
PITCH/6.8b	F	09-Nov-08	11-Dec-08	32	2
PITCH/6.8c	M	09-Nov-08	11-Dec-08	32	2
PITCH/6.8d	M	09-Nov-08	11-Dec-08	32	2
PITCH/6.8e	M	09-Nov-08	11-Dec-08	32	2
PITCH/6.8f	M	09-Nov-08	11-Dec-08	32	2
PITCH/6.8g	M	09-Nov-08	11-Dec-08	32	2
PITCH/5.7a	F	20-Nov-08	11-Dec-08	21	2
PITCH/5.7b	F	20-Nov-08	11-Dec-08	21	2
PITCH/5.7c	F	20-Nov-08	11-Dec-08	21	2
PITCH/5.7d	F	20-Nov-08	11-Dec-08	21	0
PITCH/5.7e	F	20-Nov-08	11-Dec-08	21	0
PITCH/5.7f	M	20-Nov-08	11-Dec-08	21	2
PITCH/5.7g	M	20-Nov-08	11-Dec-08	21	0
PITCH/5.7h	M	20-Nov-08	11-Dec-08	21	2
PITCH/5.7i	M	20-Nov-08	11-Dec-08	21	2
PITCH/5.7j	M	20-Nov-08	11-Dec-08	21	2
PITCH/6.9a	M	27-Nov-08	18-Dec-08	21	2
PITCH/6.9b	M	27-Nov-08	18-Dec-08	21	2
PITCH/6.10a	F	03-Dec-08	15-Jan-09	43	2
PITCH/6.10b	F	03-Dec-08	15-Jan-09	43	2
PITCH/6.10c	F	03-Dec-08	15-Jan-09	43	2
PITCH/6.10d	F	03-Dec-08	15-Jan-09	43	2
PITCH/6.10e	F	03-Dec-08	15-Jan-09	43	2
PITCH/6.10f	F	03-Dec-08	15-Jan-09	43	2
PITCH/6.10g	M	03-Dec-08	15-Jan-09	43	0
PITCH/5.8a	F	06-Dec-08	15-Jan-09	40	0
PITCH/5.8b	F	06-Dec-08	15-Jan-09	40	2
PITCH/5.8c	M	06-Dec-08	15-Jan-09	40	2
PITCH/5.8d	M	06-Dec-08	15-Jan-09	40	2
PITCH/5.9a	F	12-Dec-08	15-Jan-09	34	2
PITCH/5.9b	F	12-Dec-08	15-Jan-09	34	0
PITCH/5.9c	F	12-Dec-08	15-Jan-09	34	2
PITCH/5.9d	F	12-Dec-08	15-Jan-09	34	2
PITCH/5.9e	F	12-Dec-08	15-Jan-09	34	2
PITCH/5.9f	F	12-Dec-08	15-Jan-09	34	1
PITCH/5.9g	F	12-Dec-08	15-Jan-09	34	0
PITCH/5.9h	M	12-Dec-08	15-Jan-09	34	0
PITCH/5.9i	M	12-Dec-08	15-Jan-09	34	0
PITCH/5.9j	M	12-Dec-08	15-Jan-09	34	2
PITCH/5.9k	M	12-Dec-08	15-Jan-09	34	2
PITCH/6.12a	F	01-Jan-09	23-Feb-09	53	2
PITCH/6.12b	F	01-Jan-09	23-Feb-09	53	1
PITCH/6.12c	F	01-Jan-09	23-Feb-09	53	0
PITCH/6.12d	F	01-Jan-09	23-Feb-09	53	2
PITCH/5.11a	F	21-Jan-09	23-Feb-09	33	0
PITCH/5.11b	F	21-Jan-09	23-Feb-09	33	2
PITCH/5.11c	F	21-Jan-09	23-Feb-09	33	2
PITCH/5.11d	F	21-Jan-09	23-Feb-09	33	2
PITCH/5.11e	F	21-Jan-09	23-Feb-09	33	2
PITCH/5.11f	M	21-Jan-09	23-Feb-09	33	0
PITCH/5.11g	M	21-Jan-09	23-Feb-09	33	1
PITCH/5.11h	M	21-Jan-09	23-Feb-09	33	2
PITCH/5.11i	M	21-Jan-09	23-Feb-09	33	1
PITCH/5.11j	M	21-Jan-09	23-Feb-09	33	2
PITCH/5.11k	M	21-Jan-09	23-Feb-09	33	2
PITCH/6.13a	F	06-Feb-09	13-Mar-09	35	2
PITCH/6.13b	M	06-Feb-09	13-Mar-09	35	2
PITCH/5.12a	F	28-Feb-09	06-Apr-09	37	2
PITCH/5.12b	F	28-Feb-09	06-Apr-09	37	2
PITCH/5.12c	M	28-Feb-09	06-Apr-09	37	0
PITCH/5.12d	M	28-Feb-09	06-Apr-09	37	2
PITCH/5.12e	M	28-Feb-09	06-Apr-09	37	2
PITCH/5.12f	M	28-Feb-09	06-Apr-09	37	2
PITCH/5.13a	F	05-Mar-09	06-Apr-09	32	2
PITCH/5.13b	M	05-Mar-09	06-Apr-09	32	2
PITCH/5.13c	M	05-Mar-09	06-Apr-09	32	2

S3. Vestibular observations in the G5 pedigree

Mouse ID	Sex	DOB	Assessment Date	Age at Test (Days)	Startle response 0,1 or 2	Vestibular phenotypes
PITCH/1.1a	F	02-Jul-08	23-Jul-08	21	2	No head tilt or curling.
PITCH/1.1b	F	02-Jul-08	23-Jul-08	21	2	No head tilt or curling.
PITCH/1.1c	F	02-Jul-08	23-Jul-08	21	2	No head tilt or curling.
PITCH/1.1d	F	02-Jul-08	23-Jul-08	21	2	No head tilt or curling.
PITCH/1.1e	F	02-Jul-08	23-Jul-08	21	0	No head tilt or curling.
PITCH/1.1f	M	02-Jul-08	23-Jul-08	21	0	No head tilt or curling.
PITCH/1.1g	M	02-Jul-08	23-Jul-08	21	2	No head tilt or curling.
PITCH/1.1h	M	02-Jul-08	23-Jul-08	21	2	No head tilt or curling.
PITCH/4.7b	M	11-Sep-08	02-Oct-08	21	0	Curling, Slight HT, R Down
PITCH/4.7c	M	11-Sep-08	02-Oct-08	21	2	No head tilt or curling.
PITCH/4.7d	M	11-Sep-08	02-Oct-08	21	1	No head tilt or curling.
PITCH/1.6e	M	11-Sep-08	02-Oct-08	21	0	No head tilt or curling.
PITCH/1.6f	M	11-Sep-08	02-Oct-08	21	0	No head tilt or curling.
PITCH/1.6g	M	11-Sep-08	02-Oct-08	21	0	No head tilt or curling.
PITCH/1.6h	M	11-Sep-08	02-Oct-08	21	2	No head tilt or curling.
PITCH/1.6i	M	11-Sep-08	02-Oct-08	21	2	No head tilt or curling.
PITCH/1.6j	M	11-Sep-08	02-Oct-08	21	2	No head tilt or curling.
PITCH/1.6k	M	11-Sep-08	02-Oct-08	21	2	No head tilt or curling.
PITCH/5.7d	F	20-Nov-08	11-Dec-08	21	0	No head tilt or curling.
PITCH/5.7e	F	20-Nov-08	11-Dec-08	21	0	No head tilt or curling.
PITCH/6.3c	M	08-Sep-08	02-Oct-08	24	0	Curling. No head tilt.
PITCH/6.3d	M	08-Sep-08	02-Oct-08	24	2	No head tilt or curling.
PITCH/6.4a	F	16-Sep-08	10-Oct-08	24	2	No head tilt or curling.
PITCH/6.4b	M	16-Sep-08	10-Oct-08	24	2	No head tilt or curling.
PITCH/6.4c	M	16-Sep-08	10-Oct-08	24	2	No head tilt or curling.
PITCH/6.4d	M	16-Sep-08	10-Oct-08	24	2	No head tilt or curling.
PITCH/6.4e	M	16-Sep-08	10-Oct-08	24	2	No head tilt or curling.
PITCH/3.5d	M	31-Aug-08	26-Sep-08	26	0	No head tilt or curling.
PITCH/1.2d	F	04-Jul-08	31-Jul-08	27	0	No head tilt or curling.
PITCH/3.1f	M	04-Jul-08	31-Jul-08	27	0	No head tilt or curling.
PITCH/3.6a	F	04-Sep-08	02-Oct-08	28	0.5	No head tilt or curling.
PITCH/3.6b	F	04-Sep-08	02-Oct-08	28	0	No head tilt or curling.
PITCH/4.4i	M	06-Aug-08	05-Sep-08	30	0	No head tilt or curling.
PITCH/2.5a	F	26-Aug-08	26-Sep-08	31	0	No head tilt or curling.
PITCH/2.5h	M	26-Aug-08	26-Sep-08	31	0	Curling. No head tilt.
PITCH/2.5i	M	26-Aug-08	26-Sep-08	31	0	Curling. No head tilt.
PITCH/2.5j	M	26-Aug-08	26-Sep-08	31	0	No head tilt or curling.
PITCH/3.5d	M	31-Aug-08	02-Oct-08	32	0	No head tilt or curling.
PITCH/1.3d	F	25-Jul-08	27-Aug-08	33	0	No head tilt or curling.
PITCH/1.2d	F	04-Jul-08	07-Aug-08	34	0	No head tilt or curling.
PITCH/3.1f	M	04-Jul-08	07-Aug-08	34	0	No head tilt or curling.
PITCH/6.13b	M	06-Feb-09	13-Mar-09	35	2	No head tilt or curling.
PITCH/1.5c	F	21-Aug-08	26-Sep-08	36	0	No head tilt or curling.
PITCH/1.6e	M	11-Sep-08	17-Oct-08	36	0	No head tilt or curling.
PITCH/1.6f	M	11-Sep-08	17-Oct-08	36	0	No head tilt or curling.
PITCH/1.6g	M	11-Sep-08	17-Oct-08	36	0	No head tilt or curling.
PITCH/2.5a	F	26-Aug-08	02-Oct-08	37	0	No head tilt or curling.
PITCH/2.5h	M	26-Aug-08	02-Oct-08	37	0	Curling. No head tilt.
PITCH/2.5i	M	26-Aug-08	02-Oct-08	37	0	Curling. No head tilt.
PITCH/2.5j	M	26-Aug-08	02-Oct-08	37	0	No head tilt or curling.
PITCH/5.12a	F	28-Feb-09	06-Apr-09	37	2	No head tilt or curling.
PITCH/5.12b	F	28-Feb-09	06-Apr-09	37	2	No head tilt or curling.
PITCH/6.3c	M	08-Sep-08	17-Oct-08	39	0	No head tilt or curling.
PITCH/1.3d	F	25-Jul-08	05-Sep-08	42	0	No head tilt or curling.
PITCH/1.5c	F	21-Aug-08	02-Oct-08	42	0	No head tilt or curling.
PITCH/1.5h	M	21-Aug-08	02-Oct-08	42	0	No head tilt or curling.
PITCH/3.6a	F	04-Sep-08	17-Oct-08	43	0.5	No head tilt or curling.
PITCH/3.6b	F	04-Sep-08	17-Oct-08	43	0	No head tilt or curling.
PITCH/4.4i	M	06-Aug-08	19-Sep-08	44	0	No head tilt or curling.
PITCH/1.2d	F	04-Jul-08	20-Aug-08	47	0	No head tilt or curling.
PITCH/3.1f	M	04-Jul-08	20-Aug-08	47	0	No head tilt or curling.
PITCH/3.5d	M	31-Aug-08	17-Oct-08	47	0	No head tilt or curling.
PITCH/4.4i	M	06-Aug-08	26-Sep-08	51	0	No head tilt or curling.
PITCH/5.11i	M	21-Jan-09	13-Mar-09	51	1	No head tilt or curling.
PITCH/2.5a	F	26-Aug-08	17-Oct-08	52	0	No head tilt or curling.
PITCH/2.5h	M	26-Aug-08	17-Oct-08	52	0	Curling. No head tilt.
PITCH/2.5i	M	26-Aug-08	17-Oct-08	52	0	Curling. No head tilt.
PITCH/2.5j	M	26-Aug-08	17-Oct-08	52	0	No head tilt or curling.
PITCH/1.2d	F	04-Jul-08	27-Aug-08	54	0	No head tilt or curling.
PITCH/3.1f	M	04-Jul-08	27-Aug-08	54	0	No head tilt or curling.
PITCH/2.1a	F	02-Jul-08	26-Aug-08	55	2	No head tilt or curling.
PITCH/2.1b	F	02-Jul-08	26-Aug-08	55	0	No head tilt or curling.
PITCH/2.1c	F	02-Jul-08	26-Aug-08	55	2	No head tilt or curling.
PITCH/2.1d	F	02-Jul-08	26-Aug-08	55	0	No head tilt or curling.
PITCH/2.1e	F	02-Jul-08	26-Aug-08	55	2	No head tilt or curling.
PITCH/2.1f	F	02-Jul-08	26-Aug-08	55	2	No head tilt or curling.

Mouse ID	Sex	DOB	Assessment Date	Age at Test (Days)	Startle response 0,1 or 2	Vestibular phenotypes
PITCH/2.1g	F	02-Jul-08	26-Aug-08	55	2	No head tilt or curling.
PITCH/2.1h	F	02-Jul-08	26-Aug-08	55	2	No head tilt or curling.
PITCH/2.1i	M	02-Jul-08	26-Aug-08	55	0	No head tilt or curling.
PITCH/2.1j	M	02-Jul-08	26-Aug-08	55	0	No head tilt or curling.
PITCH/2.1k	M	02-Jul-08	26-Aug-08	55	2	No head tilt or curling.
PITCH/2.1l	M	02-Jul-08	26-Aug-08	55	2	No head tilt or curling.
PITCH/2.1m	M	02-Jul-08	26-Aug-08	55	2	No head tilt or curling.
PITCH/2.1n	M	02-Jul-08	26-Aug-08	55	0	No head tilt or curling.
PITCH/2.1o	M	02-Jul-08	26-Aug-08	55	1	No head tilt or curling.
PITCH/2.1p	M	02-Jul-08	26-Aug-08	55	0	No head tilt or curling.
PITCH/2.1q	M	02-Jul-08	26-Aug-08	55	2	No head tilt or curling.
PITCH/2.1r	M	02-Jul-08	26-Aug-08	55	2	No head tilt or curling.
PITCH/1.3d	F	25-Jul-08	19-Sep-08	56	0	No head tilt or curling.
PITCH/4.4i	M	06-Aug-08	02-Oct-08	57	0	No head tilt or curling.
PITCH/1.5c	F	21-Aug-08	17-Oct-08	57	0	No head tilt or curling.
PITCH/1.5h	M	21-Aug-08	17-Oct-08	57	0	No head tilt or curling.
PITCH/6.13a	F	06-Feb-09	06-Apr-09	59	2	No head tilt or curling.
PITCH/5.9f	F	12-Dec-08	12-Feb-09	62	0	No head tilt or curling.
PITCH/5.9g	F	12-Dec-08	12-Feb-09	62	0	Slight Curling reflex when suspended
PITCH/1.2d	F	04-Jul-08	05-Sep-08	63	0	No head tilt or curling.
PITCH/3.1f	M	04-Jul-08	05-Sep-08	63	0	No head tilt or curling.
PITCH/1.3d	F	25-Jul-08	26-Sep-08	63	0	No head tilt or curling.
PITCH/1.3d	F	25-Jul-08	02-Oct-08	69	0	No head tilt or curling.
PITCH/4.4i	M	06-Aug-08	17-Oct-08	72	0	No head tilt or curling.
PITCH/5.11a	F	21-Jan-09	06-Apr-09	75	0	Slight Curling reflex when suspended.
PITCH/5.11b	F	21-Jan-09	06-Apr-09	75	2	No head tilt or curling.
PITCH/5.11c	F	21-Jan-09	06-Apr-09	75	2	No head tilt or curling.
PITCH/5.11d	F	21-Jan-09	06-Apr-09	75	2	No head tilt or curling.
PITCH/5.11e	F	21-Jan-09	06-Apr-09	75	2	No head tilt or curling.
PITCH/5.11f	M	21-Jan-09	06-Apr-09	75	0	No head tilt or curling.
PITCH/5.11g	M	21-Jan-09	06-Apr-09	75	2	No head tilt or curling.
PITCH/5.11h	M	21-Jan-09	06-Apr-09	75	2	No head tilt or curling.
PITCH/5.11j	M	21-Jan-09	06-Apr-09	75	2	No head tilt or curling.
PITCH/5.13a	F	05-Mar-09	20-May-09	76	2	No head tilt or curling.
PITCH/5.13b	M	05-Mar-09	20-May-09	76	2	No head tilt or curling.
PITCH/5.13c	M	05-Mar-09	20-May-09	76	2	No head tilt or curling.
PITCH/1.2d	F	04-Jul-08	19-Sep-08	77	0	No head tilt or curling.
PITCH/3.1f	M	04-Jul-08	19-Sep-08	77	0	No head tilt or curling.
PITCH/1.6e	M	11-Sep-08	27-Nov-08	77	0	No head tilt or curling.
PITCH/1.6f	M	11-Sep-08	27-Nov-08	77	0	No head tilt or curling.
PITCH/1.6g	M	11-Sep-08	27-Nov-08	77	0	No head tilt or curling.
PITCH/6.3c	M	08-Sep-08	27-Nov-08	80	0	No head tilt or curling.
PITCH/5.12c	M	28-Feb-09	20-May-09	81	0	Slight head tilt to the right. Clasping of limbs when suspended.
PITCH/5.12d	M	28-Feb-09	20-May-09	81	2	No head tilt or curling.
PITCH/5.12e	M	28-Feb-09	20-May-09	81	2	No head tilt or curling.
PITCH/5.12f	M	28-Feb-09	20-May-09	81	2	No head tilt or curling.
PITCH/6.9a	M	27-Nov-08	18-Feb-09	83	2	No head tilt or curling.
PITCH/6.9b	M	27-Nov-08	18-Feb-09	83	2	No head tilt or curling.
PITCH/1.2d	F	04-Jul-08	26-Sep-08	84	0	No head tilt or curling.
PITCH/3.1f	M	04-Jul-08	26-Sep-08	84	0	No head tilt or curling.
PITCH/1.3d	F	25-Jul-08	17-Oct-08	84	0	No head tilt or curling.
PITCH/3.5d	M	31-Aug-08	27-Nov-08	88	0	No head tilt or curling.
PITCH/5.7f	M	20-Nov-08	18-Feb-09	90	0	Curling.
PITCH/5.7g	M	20-Nov-08	18-Feb-09	90	0	Curling. Head tilt to the right.
PITCH/5.7h	M	20-Nov-08	18-Feb-09	90	0	Curling. Head tilt to the left.
PITCH/5.7i	M	20-Nov-08	18-Feb-09	90	2	No head tilt or curling.
PITCH/5.7j	M	20-Nov-08	18-Feb-09	90	2	No head tilt or curling.
PITCH/2.5a	F	26-Aug-08	27-Nov-08	93	0	No head tilt or curling.
PITCH/2.5h	M	26-Aug-08	27-Nov-08	93	0	Curling. No head tilt.
PITCH/2.5i	M	26-Aug-08	27-Nov-08	93	0	Curling. No head tilt.
PITCH/2.5j	M	26-Aug-08	27-Nov-08	93	0	No head tilt or curling.
PITCH/6.12a	F	01-Jan-09	06-Apr-09	95	2	No head tilt or curling.
PITCH/6.12b	F	01-Jan-09	06-Apr-09	95	0	Curling. No head tilt.
PITCH/6.12c	F	01-Jan-09	06-Apr-09	95	0	Slight curling. No head tilt.
PITCH/6.12d	F	01-Jan-09	06-Apr-09	95	2	No head tilt or curling.
PITCH/1.5c	F	21-Aug-08	27-Nov-08	98	0	No head tilt or curling.
PITCH/6.8a	F	09-Nov-08	18-Feb-09	101	2	No head tilt or curling.
PITCH/6.8b	F	09-Nov-08	18-Feb-09	101	2	No head tilt or curling.
PITCH/6.8c	M	09-Nov-08	18-Feb-09	101	2	No head tilt or curling.
PITCH/6.8d	M	09-Nov-08	18-Feb-09	101	2	No head tilt or curling.
PITCH/6.8e	M	09-Nov-08	18-Feb-09	101	2	No head tilt or curling.
PITCH/6.8f	M	09-Nov-08	18-Feb-09	101	2	No head tilt or curling.
PITCH/6.8g	M	09-Nov-08	18-Feb-09	101	2	No head tilt or curling.
PITCH/1.2d	F	04-Jul-08	17-Oct-08	105	0	No head tilt or curling.
PITCH/3.1f	M	04-Jul-08	17-Oct-08	105	0	No head tilt or curling.
PITCH/6.7a	F	05-Nov-08	18-Feb-09	105	0	Curling. Slight head tilt to the left side.
PITCH/6.7b	F	05-Nov-08	18-Feb-09	105	2	No head tilt or curling.
PITCH/6.7c	F	05-Nov-08	18-Feb-09	105	2	No head tilt or curling.
PITCH/6.7d	F	05-Nov-08	18-Feb-09	105	2	No head tilt or curling.
PITCH/6.7e	F	05-Nov-08	18-Feb-09	105	2	No head tilt or curling.
PITCH/6.7f	M	05-Nov-08	18-Feb-09	105	0	No head tilt or curling.
PITCH/6.7g	M	05-Nov-08	18-Feb-09	105	2	No head tilt or curling.
PITCH/6.7h	M	05-Nov-08	18-Feb-09	105	2	No head tilt or curling.
PITCH/6.7i	M	05-Nov-08	18-Feb-09	105	2	No head tilt or curling.
PITCH/6.7j	M	05-Nov-08	18-Feb-09	105	2	No head tilt or curling.
PITCH/4.4i	M	06-Aug-08	27-Nov-08	113	0	Slight head tilt to the left.
PITCH/4.4i	M	06-Aug-08	27-Nov-08	113	0	Head tilt to the left, normal reach. No circling.
PITCH/5.6a	F	28-Oct-08	18-Feb-09	113	2	No head tilt or curling.

Mouse ID	Sex	DOB	Assessment Date	Age at Test (Days)	Startle response 0,1 or 2	Vestibular phenotypes
PITCH/5.6b	F	28-Oct-08	18-Feb-09	113	2	No head tilt or curling.
PITCH/5.6c	F	28-Oct-08	18-Feb-09	113	2	No head tilt or curling.
PITCH/5.6d	F	28-Oct-08	18-Feb-09	113	2	No head tilt or curling.
PITCH/5.6e	F	28-Oct-08	18-Feb-09	113	2	No head tilt or curling.
PITCH/5.6f	F	28-Oct-08	18-Feb-09	113	1	No head tilt or curling.
PITCH/5.6g	F	28-Oct-08	18-Feb-09	113	2	No head tilt or curling.
PITCH/5.6h	F	28-Oct-08	18-Feb-09	113	2	No head tilt or curling.
PITCH/5.6i	M	28-Oct-08	18-Feb-09	113	1	No head tilt or curling.
PITCH/5.6j	M	28-Oct-08	18-Feb-09	113	0.5	No head tilt or curling.
PITCH/5.6k	M	28-Oct-08	18-Feb-09	113	2	No head tilt or curling.
PITCH/5.6l	M	28-Oct-08	18-Feb-09	113	2	No head tilt or curling.
PITCH/5.6m	M	28-Oct-08	18-Feb-09	113	0	No head tilt or curling.
PITCH/5.6n	M	28-Oct-08	18-Feb-09	113	2	No head tilt or curling.
PITCH/5.6o	M	28-Oct-08	18-Feb-09	113	2	No head tilt or curling.
PITCH/5.6p	M	28-Oct-08	18-Feb-09	113	2	No head tilt or curling.
PITCH/5.6q	M	28-Oct-08	18-Feb-09	113	0	Slight curling.
PITCH/5.9a	F	12-Dec-08	06-Apr-09	115	2	No head tilt or curling.
PITCH/5.9b	F	12-Dec-08	06-Apr-09	115	0	Head tilt to the left.
PITCH/5.9c	F	12-Dec-08	06-Apr-09	115	2	No head tilt or curling.
PITCH/5.9d	F	12-Dec-08	06-Apr-09	115	2	No head tilt or curling.
PITCH/5.9e	F	12-Dec-08	06-Apr-09	115	2	No head tilt or curling.
PITCH/5.9h	M	12-Dec-08	06-Apr-09	115	0	No head tilt. Curling.
PITCH/5.9i	M	12-Dec-08	06-Apr-09	115	0	No head tilt. Curling.
PITCH/5.9j	M	12-Dec-08	06-Apr-09	115	2	No head tilt or curling.
PITCH/5.9k	M	12-Dec-08	06-Apr-09	115	2	No head tilt or curling.
PITCH/5.8a	F	06-Dec-08	06-Apr-09	121	0	Head tilt to the left. Curling.
PITCH/5.8b	F	06-Dec-08	06-Apr-09	121	2	No head tilt or curling.
PITCH/5.8c	M	06-Dec-08	06-Apr-09	121	2	No head tilt or curling.
PITCH/5.8d	M	06-Dec-08	06-Apr-09	121	2	No head tilt or curling.
PITCH/6.10a	F	03-Dec-08	06-Apr-09	124	2	No head tilt or curling.
PITCH/6.10b	F	03-Dec-08	06-Apr-09	124	2	No head tilt or curling.
PITCH/6.10c	F	03-Dec-08	06-Apr-09	124	2	No head tilt or curling.
PITCH/6.10d	F	03-Dec-08	06-Apr-09	124	2	No head tilt or curling.
PITCH/6.10e	F	03-Dec-08	06-Apr-09	124	2	No head tilt or curling.
PITCH/6.10f	F	03-Dec-08	06-Apr-09	124	2	No head tilt or curling.
PITCH/6.10g	M	03-Dec-08	06-Apr-09	124	0	Head tilt to the left. Curling.
PITCH/1.3d	F	25-Jul-08	27-Nov-08	125	0	Slight head tilt to right, curling.
PITCH/5.5a	F	07-Oct-08	12-Feb-09	128	2	No head tilt or curling.
PITCH/5.5b	F	07-Oct-08	12-Feb-09	128	2	No head tilt or curling.
PITCH/5.5c	M	07-Oct-08	12-Feb-09	128	2	No head tilt or curling.
PITCH/5.5d	M	07-Oct-08	12-Feb-09	128	0	No head tilt or curling.
PITCH/6.3c	M	08-Sep-08	16-Jan-09	130	0	No head tilt or curling.
PITCH/6.6a	M	05-Oct-08	12-Feb-09	130	2	No head tilt or curling.

Mouse ID	Sex	DOB	Assessment Date	Age at Test (Days)	Startle response 0,1 or 2	Vestibular phenotypes
PITCH/6.6b	M	05-Oct-08	12-Feb-09	130	2	No head tilt or curling.
PITCH/6.6c	M	05-Oct-08	12-Feb-09	130	2	No head tilt or curling.
PITCH/6.6d	M	05-Oct-08	12-Feb-09	130	2	No head tilt or curling.
PITCH/3.5d	M	31-Aug-08	15-Jan-09	137	0	Slight head tilt to the right.
PITCH/6.5a	F	28-Sep-08	12-Feb-09	137	2	No head tilt or curling.
PITCH/6.5b	M	28-Sep-08	12-Feb-09	137	2	No head tilt or curling.
PITCH/5.3a	F	16-Sep-08	27-Nov-08	141	0	No head tilt or curling.
PITCH/5.3a	F	16-Sep-08	04-Feb-09	141	0	No head tilt or curling.
PITCH/5.3b	F	16-Sep-08	04-Feb-09	141	2	No head tilt or curling.
PITCH/5.3c	F	16-Sep-08	04-Feb-09	141	2	No head tilt or curling.
PITCH/5.3d	F	16-Sep-08	04-Feb-09	141	2	No head tilt or curling.
PITCH/5.3e	F	16-Sep-08	04-Feb-09	141	2	No head tilt or curling.
PITCH/2.5a	F	26-Aug-08	15-Jan-09	142	0	Slight curling. Head tilt to the right.
PITCH/2.5h	M	26-Aug-08	15-Jan-09	142	0	Curling. No head tilt.
PITCH/2.5i	M	26-Aug-08	15-Jan-09	142	0	Curling. No head tilt.
PITCH/2.5j	M	26-Aug-08	15-Jan-09	142	0	Slight curling.
PITCH/5.4b	M	22-Sep-08	12-Feb-09	143	2	No head tilt or curling.
PITCH/5.4c	M	22-Sep-08	12-Feb-09	143	2	No head tilt or curling.
PITCH/5.4d	M	22-Sep-08	12-Feb-09	143	2	No head tilt or curling.
PITCH/5.4e	M	22-Sep-08	12-Feb-09	143	2	No head tilt or curling.
PITCH/5.4f	M	22-Sep-08	12-Feb-09	143	2	No head tilt or curling.
PITCH/1.2d	F	04-Jul-08	27-Nov-08	146	0	Slight head tilt towards the right.
PITCH/3.1f	M	04-Jul-08	27-Nov-08	146	0	No head tilt or curling.
PITCH/1.5c	F	21-Aug-08	15-Jan-09	147	0	Slight head tilt to the left.
PITCH/5.3h	M	16-Sep-08	12-Feb-09	149	2	No head tilt or curling.
PITCH/5.3i	M	16-Sep-08	12-Feb-09	149	2	No head tilt or curling.
PITCH/5.3j	M	16-Sep-08	12-Feb-09	149	2	No head tilt or curling.
PITCH/5.3l	M	16-Sep-08	12-Feb-09	149	2	No head tilt or curling.
PITCH/3.6d	F	04-Sep-08	04-Feb-09	153	2	No head tilt or curling.
PITCH/3.6e	F	04-Sep-08	04-Feb-09	153	2	No head tilt or curling.
PITCH/4.7d	M	11-Sep-08	12-Feb-09	154	1	No head tilt or curling.
PITCH/1.6b	F	11-Sep-08	12-Feb-09	154	2	No head tilt or curling.
PITCH/1.6c	F	11-Sep-08	12-Feb-09	154	2	No head tilt or curling.
PITCH/1.6d	F	11-Sep-08	12-Feb-09	154	2	No head tilt or curling.
PITCH/3.5d	M	31-Aug-08	04-Feb-09	157	0	Curling. Head tilt to the right. Had a seizure after assessment.
PITCH/3.5e	M	31-Aug-08	04-Feb-09	157	2	No head tilt or curling.
PITCH/3.5f	M	31-Aug-08	04-Feb-09	157	2	No head tilt or curling.
PITCH/3.5g	M	31-Aug-08	04-Feb-09	157	2	No head tilt or curling.
PITCH/2.5c	F	26-Aug-08	04-Feb-09	162	2	No head tilt or curling.
PITCH/2.5d	F	26-Aug-08	04-Feb-09	162	2	No head tilt or curling.
PITCH/2.5e	F	26-Aug-08	04-Feb-09	162	1	No head tilt or curling.
PITCH/2.5h	M	26-Aug-08	04-Feb-09	162	0	Slight Curling, head tilt to the right.
PITCH/2.5i	M	26-Aug-08	04-Feb-09	162	0	Curling. Head tilt to the right.

Mouse ID	Sex	DOB	Assessment Date	Age at Test (Days)	Startle response 0,1 or 2	Vestibular phenotypes
PITCH/2.5j	M	26-Aug-08	04-Feb-09	162	0	Curling, No head tilt.
PITCH/1.3d	F	25-Jul-08	15-Jan-09	174	0	Head tilt to the right, curling to the left when body suspended.
PITCH/1.5h	M	21-Aug-08	18-Feb-09	181	0	Curling, strong head tilt down to the left (ear touching ground).
PITCH/2.3g	M	31-Jul-08	04-Feb-09	188	2	No head tilt or curling.
PITCH/2.3h	M	31-Jul-08	04-Feb-09	188	2	No head tilt or curling.
PITCH/1.3a	F	25-Jul-08	04-Feb-09	194	2	No head tilt or curling.
PITCH/1.3b	F	25-Jul-08	04-Feb-09	194	2	No head tilt or curling.
PITCH/1.3c	F	25-Jul-08	04-Feb-09	194	2	No head tilt or curling.
PITCH/1.3d	F	25-Jul-08	04-Feb-09	194	0	Head tilt to the right, curling. Very slow righting reflex.
PITCH/1.2d	F	04-Jul-08	15-Jan-09	195	0	Head tilt worsened towards the right.
PITCH/3.1f	M	04-Jul-08	15-Jan-09	195	0	Curling phenotype. Unable to reach to grab cage bars. No head tilt.
PITCH/3.6a	F	04-Sep-08	18-Mar-09	195	0.5	Extreme head tilt to the left.
PITCH/3.2d	M	23-Jul-08	04-Feb-09	196	2	No head tilt or curling.
PITCH/3.2e	M	23-Jul-08	04-Feb-09	196	0	Curling. Head tilt to the left.
PITCH/3.2f	M	23-Jul-08	04-Feb-09	196	2	No head tilt or curling.
PITCH/3.2g	M	23-Jul-08	04-Feb-09	196	0	Curling. Head tilt to the left.
PITCH/3.2h	M	23-Jul-08	04-Feb-09	196	2	No head tilt or curling.
PITCH/4.2f	F	17-Jul-08	19-Feb-09	217	2	No head tilt or curling.
PITCH/1.2a	F	04-Jul-08	19-Feb-09	230	2	No head tilt or curling.
PITCH/1.2b	F	04-Jul-08	19-Feb-09	230	2	No head tilt or curling.
PITCH/1.2c	F	04-Jul-08	19-Feb-09	230	2	No head tilt or curling.
PITCH/1.2d	F	04-Jul-08	19-Feb-09	230	0	Slight Curling, head tilt to the right.
PITCH/1.2e	F	04-Jul-08	19-Feb-09	230	2	No head tilt or curling.
PITCH/1.2f	F	04-Jul-08	19-Feb-09	230	1.5	No head tilt or curling.
PITCH/1.2g	F	04-Jul-08	19-Feb-09	230	2	No head tilt or curling.
PITCH/1.2h	M	04-Jul-08	19-Feb-09	230	2	No head tilt or curling.
PITCH/1.2i	M	04-Jul-08	19-Feb-09	230	2	No head tilt or curling.
PITCH/3.1a	F	04-Jul-08	19-Feb-09	230	2	No head tilt or curling.
PITCH/3.1b	F	04-Jul-08	19-Feb-09	230	1.5	No head tilt or curling.
PITCH/3.1c	F	04-Jul-08	19-Feb-09	230	2	No head tilt or curling.
PITCH/3.1d	F	04-Jul-08	19-Feb-09	230	2	No head tilt or curling.
PITCH/3.1e	M	04-Jul-08	19-Feb-09	230	2	No head tilt or curling.
PITCH/3.1f	M	04-Jul-08	19-Feb-09	230	0	Curling. Head tilt to the left. Slightly Smaller Testes.
PITCH/3.1g	M	04-Jul-08	19-Feb-09	230	2	No head tilt or curling.
PITCH/3.1h	M	04-Jul-08	19-Feb-09	230	2	No head tilt or curling.
PITCH/3.1j	M	04-Jul-08	19-Feb-09	230	0	Head tilt to the right. Curling.
PITCH/3.1k	M	04-Jul-08	19-Feb-09	230	2	No head tilt or curling.
PITCH/3.1l	M	04-Jul-08	19-Feb-09	230	0	No curling. Head tilt to the left.

S4. Swim-test phenotyping of select animals from the G5 pedigree

Mouse ID	Generation	Sex	DOB	Date of Test	Age at Test (Days)	Startle response	Swim phenotype
						0,1 or 2	
PITCH/1.2b	G5	F	04-Jul-08	19-Feb-09	230	2	Swims Normally
PITCH/1.2c	G5	F	04-Jul-08	19-Feb-09	230	2	Swims Normally
PITCH/1.2d	G5	F	04-Jul-08	19-Feb-09	230	0	Bad Swim - Circles, no flagella motion in tail, swims on one side.
PITCH/1.2e	G5	F	04-Jul-08	19-Feb-09	230	2	Swims Normally
PITCH/1.2f	G5	F	04-Jul-08	19-Feb-09	230	1.5	Swims Normally
PITCH/1.2g	G5	F	04-Jul-08	19-Feb-09	230	2	Swims Normally
PITCH/1.2h	G5	M	04-Jul-08	19-Feb-09	230	2	Swims Normally
PITCH/1.2i	G5	M	04-Jul-08	19-Feb-09	230	2	Swims Normally
PITCH/3.1a	G5	F	04-Jul-08	19-Feb-09	230	2	Swims Normally
PITCH/3.1b	G5	F	04-Jul-08	19-Feb-09	230	1.5	Swims Normally
PITCH/3.1c	G5	F	04-Jul-08	19-Feb-09	230	2	Swims Normally
PITCH/3.1d	G5	F	04-Jul-08	19-Feb-09	230	2	Swims Normally
PITCH/3.1e	G5	M	04-Jul-08	19-Feb-09	230	2	Swims Normally
PITCH/3.1f	G5	M	04-Jul-08	19-Feb-09	230	0	Bad Swim - Lies on left side
PITCH/3.1g	G5	M	04-Jul-08	19-Feb-09	230	2	Swims Normally
PITCH/3.1h	G5	M	04-Jul-08	19-Feb-09	230	2	Swims Normally
PITCH/3.1j	G5	M	04-Jul-08	19-Feb-09	230	0	Bad Swim - Circles on one side
PITCH/3.1k	G5	M	04-Jul-08	19-Feb-09	230	2	Swims Normally
PITCH/3.1l	G5	M	04-Jul-08	19-Feb-09	230	0	Bad Swim - lies on one side
PITCH/4.2f	G5	F	17-Jul-08	19-Feb-09	217	2	Swims Normally
PITCH/6.10e	G5	F	03-Dec-08	13-Mar-09	100	2	Normal Swim
PITCH/6.10f	G5	F	03-Dec-08	13-Mar-09	100	2	Normal Swim
PITCH/6.10g	G5	M	03-Dec-08	13-Mar-09	100	0	Poor Swim - Floats hunched up. Circles.
PITCH/5.8a	G5	F	06-Dec-08	13-Mar-09	97	0	OK Swim but lists to the right hand side. Erratic limb movement. Circling
PITCH/5.8b	G5	F	06-Dec-08	13-Mar-09	97	2	Normal Swim
PITCH/5.8c	G5	M	06-Dec-08	13-Mar-09	97	2	Normal Swim
PITCH/5.8d	G5	M	06-Dec-08	13-Mar-09	97	2	Normal Swim

Mouse ID	Generation	Sex	DOB	Date of Test	Age at Test (Days)	Startle response	Swim phenotype
						0,1 or 2	
PITCH/5.9a	G5	F	12-Dec-08	13-Mar-09	91	2	Normal Swim
PITCH/5.9b	G5	F	12-Dec-08	13-Mar-09	91	0	OK Swim but tilted to the left side and circling, slow to start, floats.
PITCH/5.9c	G5	F	12-Dec-08	13-Mar-09	91	2	Normal Swim
PITCH/5.9d	G5	F	12-Dec-08	13-Mar-09	91	2	Normal Swim
PITCH/5.9e	G5	F	12-Dec-08	13-Mar-09	91	2	Normal Swim
PITCH/5.9f	G5	F	12-Dec-08	13-Mar-09	91	0	Normal Swim
PITCH/5.9g	G5	F	12-Dec-08	13-Mar-09	91	0	Slight Curling
PITCH/5.9h	G5	M	12-Dec-08	13-Mar-09	91	0	Poor Swim. Slow to start, floats, left side down on swim. No Head tilt.
PITCH/5.9i	G5	M	12-Dec-08	13-Mar-09	91	0	Poor Swim. Slow to start, floats, lists to one side and then the other. No Head tilt.
PITCH/5.9j	G5	M	12-Dec-08	13-Mar-09	91	2	Normal Swim
PITCH/5.9k	G5	M	12-Dec-08	13-Mar-09	91	2	Normal Swim
PITCH/6.12a	G5	F	01-Jan-09	13-Mar-09	71	2	Normal Swim
PITCH/6.12b	G5	F	01-Jan-09	13-Mar-09	71	0	OK Swim but circling and listing, left side down. No head tilt.
PITCH/6.12c	G5	F	01-Jan-09	13-Mar-09	71	0	OK Swim but listing, left side down. No head tilt.
PITCH/6.12d	G5	F	01-Jan-09	13-Mar-09	71	2	Normal Swim
PITCH/5.11f	G5	M	21-Jan-09	13-Mar-09	75	0	Pretty Good Swim but slow to start, slightly down to the left side. No head tilt.
PITCH/5.11g	G5	M	21-Jan-09	13-Mar-09	75	2	Pretty good swim, slightly down the right.
PITCH/5.11h	G5	M	21-Jan-09	13-Mar-09	75	2	Normal Swim
PITCH/5.11i	G5	M	21-Jan-09	13-Mar-09	51	1	Normal Swim
PITCH/5.11j	G5	M	21-Jan-09	13-Mar-09	75	2	Normal Swim

S5. Western blot to analyse Np65-cMyc protein expression and processing

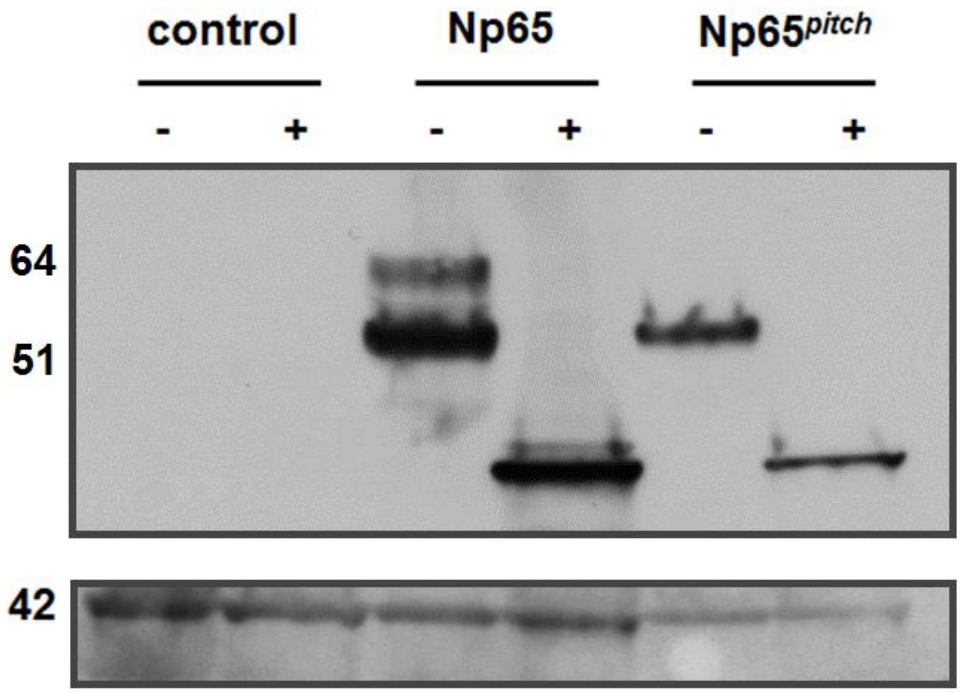

***pitch* affects post-translational modification of Nptn.** Np65 full length protein is approximately 40kDa when deglycosylated (Langnaese et al., 1998). The cMyc- tag has a low molecular mass (approximately 1.2kDa) therefore, only marginally increases the full length Np65 protein mass to approximately 42kDa. In lysates treated with PNGaseF (**+**) a deglycosylated band can be observed at around 42kDa in both WT and *pitch* Np65-cMyc, indicating that *pitch* does not affect the production of full-length protein. In untreated lysates (**-**) both WT and Np65-cMyc have an intermediate protein band at approximately 55kDa, however only the WT displays a "mature" glycosylation band above this at around 65kDa. This result indicates that *pitch* prevents full glycosylation of Nptn. Control samples show no immunoreactivity, confirming antibody specificity. This result supports the data obtained using the Np55-EGFP and Np65-EGFP vectors, indicating that the tags do not affect post-translational modification of the protein. Re-probing of the stripped blot using a primary antibody against beta-actin confirms protein levels are similar between samples.

S6. Subcellular localisation studies

S6.1. GM130 co-labelling of Np65-EGFP transfected HEK293 cells

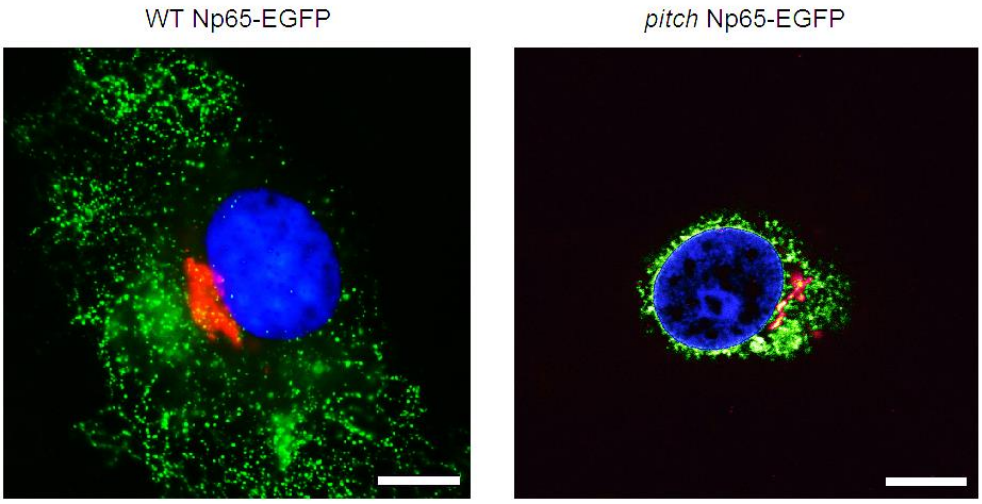

***pitch* Np65-EGFP is not retained in the golgi membrane.** The images demonstrate the expression of WT Np65-EGFP and *pitch* mutant Np65-EGFP (green) in HEK293 cells, co-labelled with DAPI a nuclear marker (blue) and GM130, a golgi marker (red). Np65-EGFP extends throughout the cytoplasm in WT Np65-EGFP transfected cells, however when transfected with *pitch* Np65-EGFP, cells show protein retention close to the nucleus. Co-labelling with GM130 does not show co-expression with Np65-EGFP, indicating that the golgi apparatus is not the site of retention for *pitch* protein.

S6. 2. Co-labelling of Np55-EGFP transfected HEK293 cells with PDI, shows retention of *pitch* protein in the ER

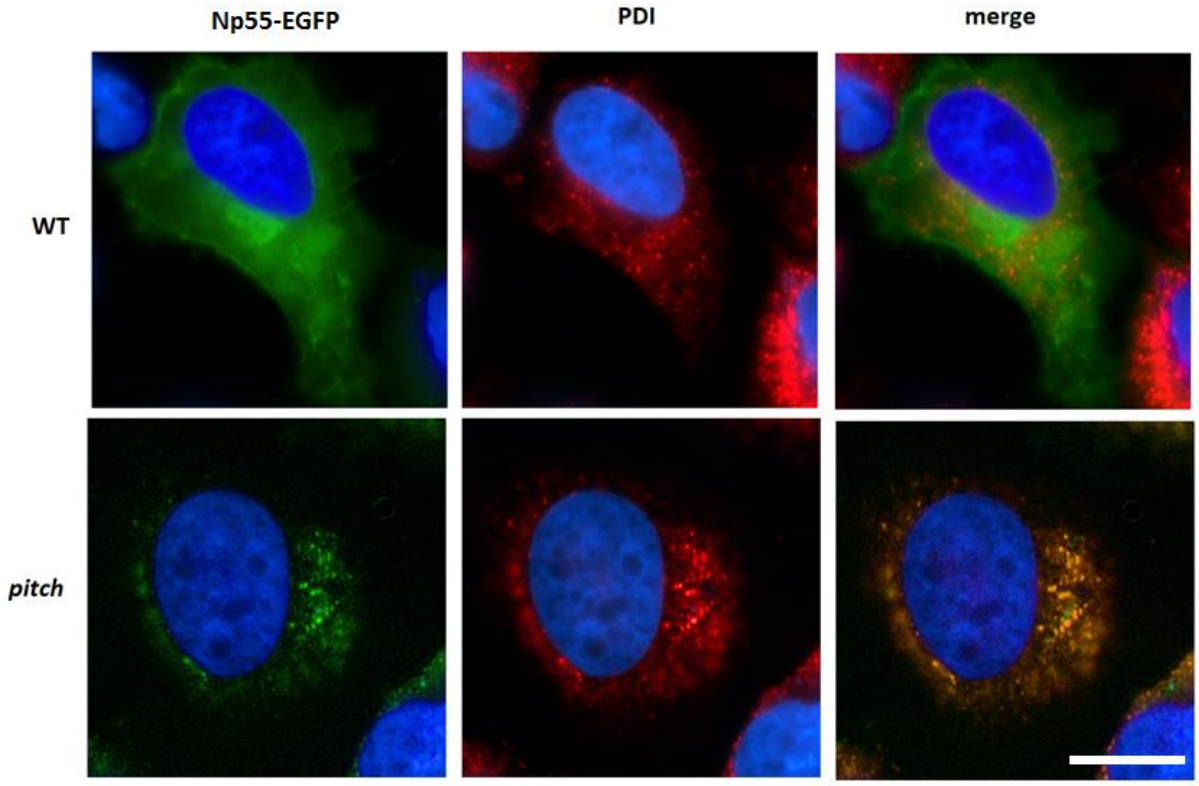

***pitch* Np55-eGFP is retained in the endoplasmic reticulum.** These images demonstrate expression of WT Np55-eGFP in HEK293 cells, co-labelled with DAPI a nuclear marker (blue) and the ER marker PDI (red). *pitch* Np65-EGFP is retained close to the nucleus and does not extend throughout the cytoplasm or to the cell surface. The *pitch* Np55-EGFP (green) signal and the PDI (red) signal are co-expressed in the cell, as indicated by the overlap of signal which appears yellow/orange in the merged image. This data identifies that *pitch* Np55 is retained in the ER and supports the data obtained using the Np65-EGFP vector. Scale bar = 10µM.

S6.3. No difference in expression is detected between Np65-EGFP and Np65-cMyc tagged vectors

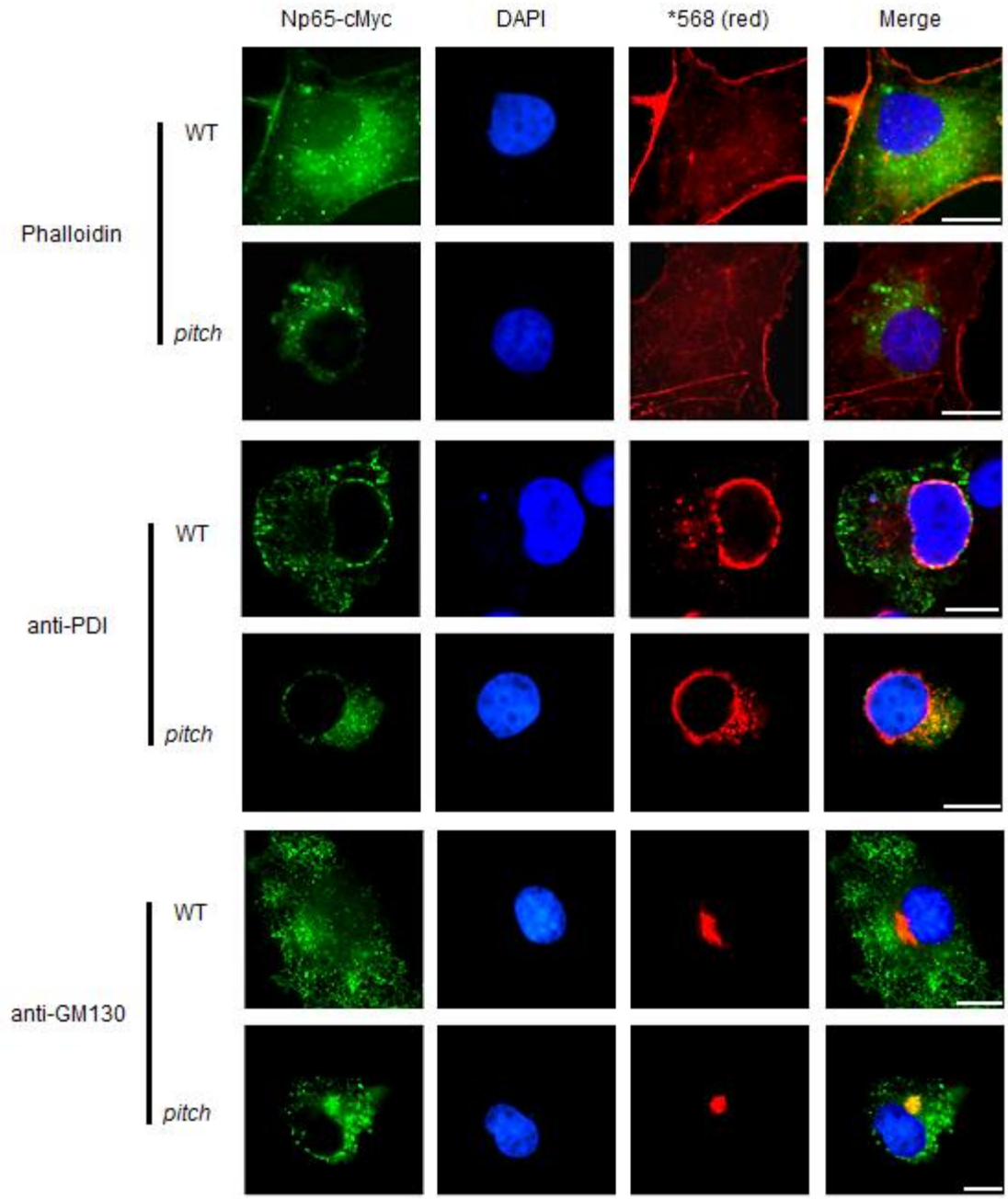

WT and *pitch* Np65-cMyc show identical expression to WT and Np65-EGFP vectors when transfected into HEK293 cells. WT and *pitch* Np65-cMyc (green) were transfected into HEK293 cells and co-labelled with DAPI a nuclear marker (blue), Phalloidin (*red, top two rows) to demark the actin cytoskeleton, PDI (*red, middle two rows) an ER marker and GM130 (*red, bottoms two rows) a golgi membrane marker. Labelling with phalloidin indicated that WT Np65-cMyc extended throughout the cytoplasm and to the cell membrane. *Pitch* Np65-cMyc was retained close to the nucleus and labelling with anti-PDI identified co-expression of the red and green signals, indicating that *pitch* Np65-cMyc was retained within the ER. This data supports the observations made in HEK293 cells transfected with Np65-EGFP vectors, indicating that the EGFP- and cMyc-tags do not affect subcellular localisation.

S7. Primers for screening the MRC Harwell ENU archive for Nptn mutants

The following primer pairs were used to perform Lightscanner PCR screening of the Harwell ENU archive:

Exon 1: Forward: 5'-TGC CTC CCT CGT TCA CT-3'

Reverse: 5'- CTC TGG TTG CCA GAG CC-3'

Exon 2: Forward: 5'- TCT GAT TGG CCT GTC ACT -3'

Reverse: 5'-GTCATTGGGCCACCTCTAAA-3'

Exon 3: Forward: 5'- CAGGCCAGGGCTACAAA-3'

Reverse: 5'-AATGTGAATTGCTAATGATGAAGGATTAT-3'

Exon 4: Forward: 5'-TTGCCTTCTGTTGCCCA-3'

Reverse: 5'-AACAGTCATTCAGAGTAAAGAAGTA-3'

Exon5: Forward: 5'-AGTAGGTAAGACCTTTGGTATCTTAG-3'

Reverse: 5'-GATGTCTGAACCTCTTCAGGAA-3'

Exon 6: Forward: 5'-TAGCTTATCTACTCTGACCTGC-3'

Reverse: 5'-AATACCCAAGGAACCAACC-3'